eman ta zabal zazu
Universidad del País Vasco
Euskal Herriko Unibertsitatea
CSIC
Consejo Superior de Investigaciones Científicas
Instituto Biofisika Institutua
eman ta zabal zazu
Universidad del País Vasco
Euskal Herriko Unibertsitatea

In vitro characterization of *LDLR*, *PCSK9* and *APOB* variants as a tool to understand molecular aspects of familial hypercholesterolemia and improving genetic diagnosis.

Asier Benito Vicente

Doctoral Thesis 2018

Universidad del País Vasco Euskal Herriko Unibertsitatea

CSIC

Instituto Biofisika Institutua

Universidad del País Vasco Euskal Herriko Unibertsitatea

In vitro characterization of *LDLR, PCSK9* and *APOB* variants as a tool to understand molecular aspects of familial hypercholesterolemia and to improve genetic diagnosis

LDLR, PCSK9 eta *APOB* aldaeren *in vitro* karakterizazioa, familia-hiperkolesterolemiaren aspektu molekularrak ulertzeko eta diagnosi genetikoa hobetzeko tresna giza

Tesis Doctoral para optar al grado de Doctor, presentada por:

Asier Benito Vicente

2018

Directores de Tesis:

Dr. César Martín Plágaro

Dra. Helena Ostolaza Etxabe

Table of contents

2. Metodologia esperimentala

2.1 Metodologia esperimental orokorra

2.2 LDLR proteinaren analisian erabilitako fluoreszentzia metodologiaren balioztapena. Erabilitako metodologia espezifikoa

2.3 LDLR analisi bateraturako erabilietako metodologia espezifikoa

2.3.1 Ikerketaren partehartzaileak

2.3.2 Lipido-profila

2.3.3 Segregazio-analisia

2.3.4 Analisi molekularra

2.3.5 in silico analisiak

2.3.6 c.-13A>G, c.818-3C>G, eta c.1706-10G>A aldaeren balioztapen funtzionala

2.3.7 Aldaera ezberdinen mutagenesi guneratua

2.3.8 LDLR proteinaren in vitro adierazpena

2.3.9 Western plapaketa bidezko analisia

2.3.10 Fluxu-zitometria bidezko LDLR aldaeren aktibitatearen neurketa

2.3.11 Mikroskopia konfokala

2.3.11 p.(Arg406Trp) aldaeraren birziklapen zinetikak

2.3.12 Lipido-profilen analisi estatistikoa

2.4 PCSK9 aldaeren analisian erabilitako metodologia espezifikoa

2.4.1 Mutagenesi guneratua

2.4.2 PCSK9 adierazpenaren Western plapaketa bidezko analisia

2.4.3 PCSK9 proteinaren purifikazioa

2.4.5 LDL-FITC barneraketa PCSK9-ren presentzian

2.4.6 LDLR ektodomeinuaren nikel afinitate bidezko purifikazioa

2.4.7 ELISA bidezko PCSK9-LDLR arteko afinitatearen determinazioa

2.4.8 Western plapaketa bidezko erretikulu endoplasmatiko PCSK9-aren determinazioa

4.9 PCSK9-ren kokapenaren analisia mikroskopia konfokala erabiliz

2.4.10 L8 eta L11 PCSK9-peptido seinaleen ΔGapp-aren kalkulua

2.4.11 PCSK9 basatia eta L8 eta L11 peptido seinaleen aldaeren egitura

2.5 ApoB partikulen analisian erabilitako material eta metodo espezifikoak

2.5.1 Lipoproteinen purifikazioa, markaketa eta karakterizazio biokimikoa

2.5.2 DLS bidezko LDL tamainaren determinazioa

2.5.3 Mikroskopia elektroniko bidezko tamainaren determinazioa

2.5.4 Infragorri-espektroskopia bidezko

2.5.4.2 Infragorri-espektroskopia bidezko neurketak

2.5.4.3 Infragorri-espektroen analisia

2.5.5 LDL lotura eta barneraketa linfozitoetan

2.5.6 LDL barneraketa HepG2 zeluletan

2.1.1 U937 zelulen bikoizketa-tasaren determinazioa

3. LDLR aldaeren karakterizazio funtzionala/ Functional characterization of LDLR variants

3.1 LDLR-ren karakterizazio funtzionala burutzeko fluoreszentzian oinarritutako metodologien baliogarritasuna

3.1.1 Sarrera

3.1.2 Emaitzak

3.1.2.1 In Silico analisia

3.1.2.2 Western plapaketa bidezko LDLR aldaera ezberdinen adierazpena CHO-ldlΔ7 zeluletan

3.1.2.3 ^{125}I-LDL-ren barneraketa, degradazioa eta LDL-FITC-aren barneraketa LDLR basatiarekin transfektatutako CHO-ldlΔ7 zeluletan

3.1.2.4 LDLR aldaera ezberdinekin tranfektatutako CHO-ldlΔ7 zelulen ^{125}I-LDL-ren barneraketa, degradazioa eta LDL-FITC-aren barneraketa

3.1.2.5 LDLR aldaera ezberdinekin tranfektatutako CHO-ldlΔ7 zelulen LDL-FITC-aren lotura

3.1.2.6 Fluxu zitometria bidezko LDLR aldaera ezberdinen adierazpena-mailaren determinazioa CHO-ldlΔ7 zeluletan

3.1.2.7 LDLR aldaera ezberdinen zelula-barneko kokapena eta mutazioen klasifikazioa

3.1.3 Eztabaida

Annex 2: miR-27b modulates insulin resistance in hepatocytes by targeting insulin receptor and repressing insulin signaling pathway

6.1 Introduction

6.2 Materials and Methods

6.2.1 Bioinformatics

6.2.2 Cell culture

6.2.3 In vitro miRNA transfections

6.2.4 RNA isolation and quantitative PCR analysis

6.2.5 Western blot analysis

6.2.6 Mice studies

6.2.6.1 miR-27b overexpression studies in mice

6.2.6.2 miR-27b inhibition studies

6.3 Results

6.3.1 Identification of miR-27b as a potential regulator of the insulin signaling pathway

6.3.2 miR-27b regulates hepatic INSR in Huh7 cells

6.3.3 miR-27b regulates hepatic INSR in vivo in wild type mice

6.4 Discussion

ABBREVIATIONS

ΔG_{app}	Apparent Gibson´s free energy
AAV	Adeno-associated virus
ABCA1	ATP-binding cassette sub-family A member 1
ABCB4	ATP-binding cassette sub-family B member 4
ABCG1	ATP-binding cassette sub-family G member 1
ABCG5	ATP-binding cassette sub-family G member 5
ABCG8	ATP-binding cassette sub-family G member 8
ACAT	Acetyl-CoA Acetyltransferase
ADH	Autosomic dominant hypercholesterolemia
AEBSF	4-(2-aminoethyl)benzenesulfonyl fluoride hydrochloride
AGO	Argonaute **protein**
AKT	serine/threonine-protein kinase
ApoA I	Apolipoprotein AI
ApoAII	Apolipoprotein AII
ApoAIV	Apolipoprotein AIV
ApoAV	Apolipoprotein AV
ApoB100	Apolipoprotein B100
ApoB48	Apolipoprotein B48
ApoCIII	Apolipoprotein CIII
ApoE	Apolipoprotein E
BSEP/ABCB11	ATP-binding cassette sub-family B member 11
cDNA	Complementary DNA
CE	Cholesterol ester

CETP	Cholesteryl ester transfer protein
CM	Chylomicron
CNV	Copy number variation
COPII	Coat complex protein II
CRAC	Cholesterol Recognition/interaction Amino acid Consensus sequence
Cryo-EM	Cryo Electron microscopy
CTD	C-terminal domain
CVD	Cardiovascular disease
DGCR8	DiGeorge syndrome critical region gene 8
DLCM	Duch Lipid Clinic Network
DLS	Dynamic light scattering
DMII/T2DM	Type 2 diabetes mellitus
DNA	Deoxyribonucleic acid
EC_{50}	Half maximal effective concentration
ED	Ecto-domain
EGF	Epidermal growth factor
ER	Endoplasmic Reticulum
FBS	Fetal bovine serum
FFA	Free fatty acid
FH	Familial hypercholesterolemia
FITC	Fluorescein isothiocyanate
FOXO1	Forkhead box protein O1
GOF	Gain of function
GSK3β	Glycogen synthase kinase 3 beta
HDL	High density lipoprotein
HeFH	Heterozygous familial hypercholesterolemia

HFD	High fat diet
HL	Hepatic lipase
HoFH	Homozygous familial hypercholesterolemia
IDL	Intermediate density lipoprotein
IDOL	Inducible degrader of LDLR
INSR	Insulin receptor
IR	Infra red
IRS	Insulin receptor substrate
I-TASSER	I terative Threading ASSEmbly Refinement
LCAT	Lecithin–cholesterol acyltransferase
LDL	Low density lipoprotein
LDL-C	LDL colesterol
LDLR	Low density lipoprotein receptor
LDLRAP1	Low Density Lipoprotein Receptor Adaptor Protein 1
LIPA	Lysosomal acid lipase
LNA	Locked nucleic acid
LOF	Loss of function
LPL	Lipoprotein lipase
LRP	LDLR related protein
LXR	Liver X receptors
MAF	Minor allele frequency
MEDPED	Make Early Diagnosis to Prevent Early Death
miRNA	Micro RNA
mRNA	Messenger RNA
MTP	Microsomal triglyceride transfer protein
MVA	Mevalonate

NGS	Next generation sequencing
NPC1	Niemann-Pick disease, type C1
NPC1L1	Niemann-Pick C1-Like 1
NPC2	Niemann-Pick disease, type C2
NS	Nephrotic syndrome
NS-EM	Negative stain electron microscopy
PBS	Phosphate buffered saline
PCR	Polymerase chain reaction
PCSK9	Proprotein convertase subtilisin kexin 9
pre-miRNA	Precursor miRNA
pri-miRNA	Primary miRNA
qRT-PCR	Quantitative real time PCR
RCT	Reverse cholesterol transport
RISC	RNA-induced silencing complex
RNA	Ribonucleic acid
SBRG	Simon Broome Register Group
SCAP	SREBP cleavage-activating protein
SDS	Sodium dodecyl sulfate
SNP	Single nucleotide polymorphism
SP	Signal peptide
SR	Scavenger receptor
SR-BI	Scavenger receptor class B type 1
SREBP	Sterol regulatory element-binding protein
STAP1	Signal-transducing adaptor protein 1
TBST	Tris buffered saline
TG	Triglyceride

TRPB	TAR RNA binding protein
VLDL	Very low density lipoprotein
VSMC	Vascular smooth muscle cell
WHO	World Health Organization
WT	Wild Type

Chapter 1

Introduction

Publications extracted from this chapter:

1. **Benito-Vicente A**, Uribe KB, Jebari S, Galicia-Garcia U, Ostolaza H, Martin M. Familial Hypercholesterolemia: The Most Frequent Cholesterol Metabolism Disorder Caused Disease. Int J Mol Sci. 1;19(11). pii: E3426. doi: 10.3390/ijms19113426 (2018)

1.1 Cholesterol

Cholesterol was first isolated from gallstones in 1789 during the French Revolution and since then has been extensively studied. Nowadays, much information about its structure, function and implication in disease development is available [1].

Cholesterol is an essential component of cell barrier formation and cell signaling transduction [23] that regulates membrane fluidity and interacts with other lipids and proteins [4]. In addition, cholesterol affects the biophysical properties of the membrane by increasing lipid lateral order and membrane packaging and decreasing membrane fluidity and consequently membrane permeability [5]. Cholesterol can also regulate the function of many proteins, directly by interacting with them [4] or indirectly by its effects on membrane fluidity. Among cholesterol interacting proteins are proteins accepting cholesterol as a substrate (Acyl-CoA acyl-transferase (ACAT)) [6], proteins that need cholesterol-rich environments to effectively interact with the membrane (cholesterol-dependent cytolysins) [7], proteins with sterol binding domains (cleavage-activating protein (SCAP)) or hydroxymethylglutaryl-CoA reductase (HMG-CoA reductase)) [89], proteins with cholesterol recognition amino acids consensus' (CRAC) domain and many others [10].

Cholesterol is also the precursor of many steroid molecules as bile salts, steroid hormones and vitamins. Bile salts are synthesized in the liver and are used as highly effective detergents that allow lipid solubilization [11,12]. In the case of hormones, cholesterol is the precursor of five major classes of steroid hormones: progestagens, glucocorticoids, mineralocorticoids, androgens and estrogens [12]. Vitamin D is also a cholesterol derived molecule with a remarkable importance in calcium and phosphorus metabolism [13].

The complex functions mediated by cholesterol together with its role as precursor and its participation in metabolism pathways require a coordinated input and output regulation to achieve cholesterol homeostasis. This is of significant importance in order to avoid detrimental over-accumulation and abnormal deposition of cholesterol within the body that prevent diseases caused by a failure in cholesterol metabolism.

1.2. Cholesterol metabolism.

1.2.1. Cholesterol synthesis

Cell cholesterol is mainly acquired from two sources: dietary cholesterol [14] or intracellular synthesized cholesterol [15]. Almost all tissues have the ability to *de novo* synthesize cholesterol*;* however, the liver produces the majority of total body cholesterol [1617]. *De novo* synthesis is a tightly regulated process where several proteins have an important role depending on the specific requirements. Hence, when intracellular cholesterol levels exceed physiologic

need, sterol regulatory element- binding proteins (SREBPs) in the endoplasmic reticulum (ER) are inhibited. SREBPs are dedicated sterol sensors in the cell [18] and their activation promotes HMG-CoA reductase transcription (the limiting enzyme of the cholesterol synthesis) and concomitantly activates mevalonate (MVA) pathway to increase intracellular cholesterol synthesis. Cholesterol is synthesized in the ER in a 19 step process, then is secreted to the cytoplasm [19] where becomes available and can be distributed or stored as cholesterol esters (CEs) in lipid droplets after its esterification by ACAT [6].

1.2.2. Cholesterol absorption

Dietary cholesterol absorption is the second source of cholesterol in the body after *de novo* synthetized cholesterol [20]. Cholesterol, free fatty acids (FFA) and triglycerides are the main lipids coming from the diet and are absorbed in the intestine [21]. Cholesterol absorption by the enterocytes is not an efficient process and for a correct uptake, cholesterol must be emulsified by bile acids. Bile acid emulsification generates cholesterol-bile acid micelles that can be delivered to the intestine. There, intestinal lipases hydrolyze cholesterol esters to free cholesterol that is taken up by the enterocytes through Niemann-Pick C1-like 1 (NPC1L1) protein [22]. NPC1L1 has a cholesterol-binding site in its N-terminal domain exposed to the extracellular space and a C-terminal domain bound to the membrane. Free cholesterol interaction with NPC1L1 N-terminal domain, promotes a rearrangement in the intracellular domain of the protein that releases the YVNXXF-containing region from the membrane to the cytosol. Once in the cytosol, Numb, a clathrin adaptor protein, binds and promotes the internalization of the cholesterol-NPC1L1-Numb complex by clathrin-coated pits (Figure 1.1 A and B) [22,23].

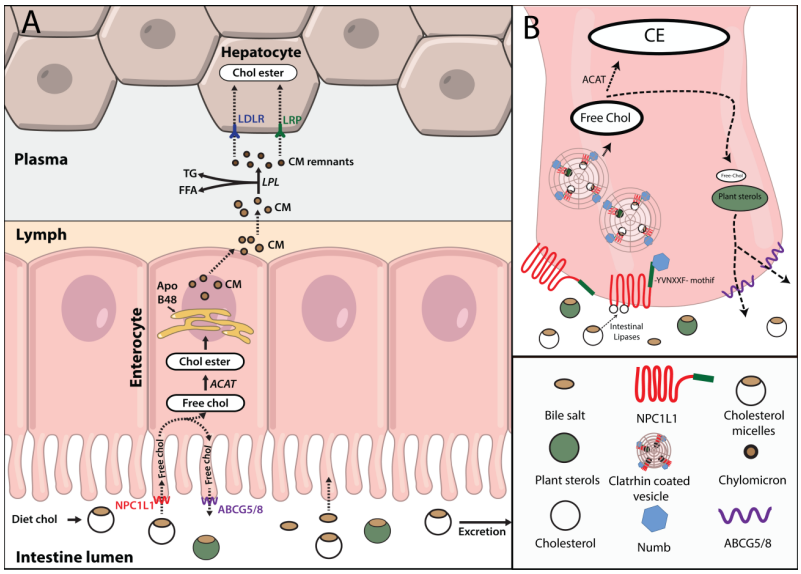

Figure 1.1. Dietary cholesterol absorption A) Diet cholesterol forms micelles in complex with bile acids and travels across the intestinal lumen where it is hydrolyzed and taken up by NPC1L1 in the enterocyte membrane. Internalized cholesterol can either be transported back to the intestinal lumen

through ABCG5/8 along with plant sterols or esterified by ACAT. Esterified cholesterol within other lipids is incorporated into chylomicrons (CM) and secreted to the lymph. Once in the lymph they are drained to the plasma whereby means oflipoprotein lipase (LPL) activity lose their triglycerides and become in chylomicron remnants that are finally taken up by the liver by LDLR or LRPs. **B)** Free cholesterol binds NPC1L1 and promotes its conformational change. This conformational change allows binding of Numb adaptor protein to YVNXXF motif and promotes its internalization in clathrin coated pits.

Once internalized, free cholesterol is delivered to ER where it is either transported back to the intestinal lumen via sterolins (ABCG5/8) or is re-esterified by ACAT. Re-esterified cholesterol can be stored in lipid droplets or be directly packaged together with triglycerides in apolipoprotein B48 (ApoB48) containing lipoproteins (chylomicrons) [24]. Contrary to ACAT, ABCG5/8 have high affinity for plant sterols. Along with ACAT, ABCG5/8 are responsible for the reduced absorption of the plant derived sterols. Indeed mutations in *ABCG5/8* genes lead to an accumulation of plant sterols in the body, mainly sitosterol, causing a disease condition called sitosterolemia [25].

Chylomicrons (CM) are lipoproteins exclusively generated in the intestine during fasting; these particles contain ApoB48, a truncated form of ApoB100 that is produced by an alternative mRNA editing which determines the metabolic role of the chylomicron [26]. In the lipoprotein assembly process IT is essential the activity of the microsomal triglyceride transfer protein (MTP) [21]. Chylomicrons also contain a large variety of APOlipoproteins such as ApoA-I, ApoA-II, ApoA-IV, ApoA-V, ApoC-I, ApoC-II, ApoC-III or Apo-E that are incorporated during chylomicron biogenesis or acquired from other circulating lipoproteins [27]. Newly synthesized chylomicrons are secreted into the lymph and transported through the lymphatic system [28] to the thoracic duct where the chylomicron -rich lymph is drained into the bloodstream at the left subclavian vein [29]. Then, blood circulating chylomicrons interact with lipoprotein lipases (LPL) of peripheral tissues, primarily adipose and muscle tissue, where LPL is highly expressed [30]. ApoC-II of chylomicrons activates LPL leading to the hydrolysis of triglycerides[3132]. The released FFAs are actively taken up by adipocytes and muscle cells through fatty acid transporters and CD36. Hydrolysis of FFAs from chylomicrons results in smaller particles enriched in cholesterol esters that transfer ApoA and ApoC to other lipoproteins (basically high density lipoproteins (HDL)) and acquire ApoE [33]. Finally, chylomicron remnants are cleared from the plasma by the liver due to interaction of ApoE with Low density lipoprotein receptor (LDLR) and other LDLR related proteins (LRP) (Figure 1.2) [34].

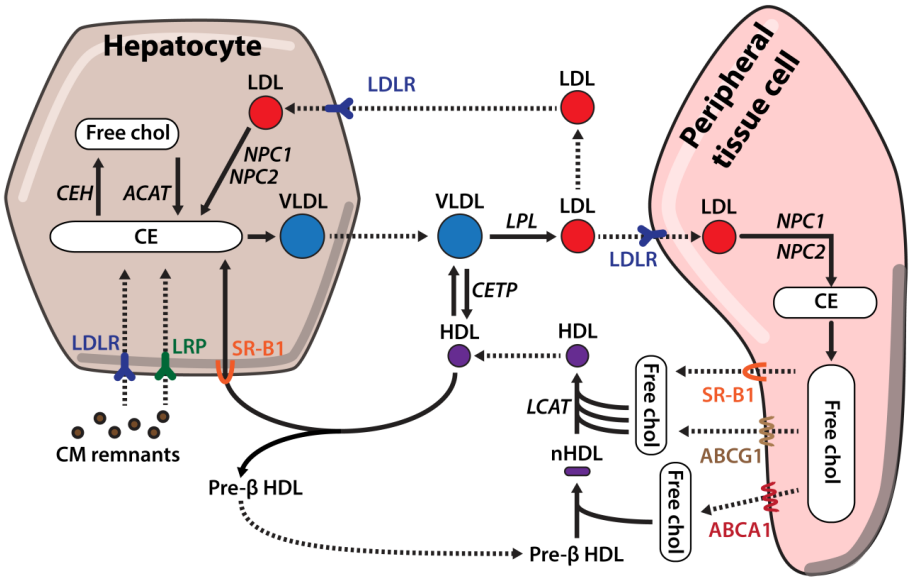

Figure 1.2. Molecular regulation of lipoprotein metabolism. Cholesterol is secreted from the liver to peripheral tissues in triglyceride rich lipoproteins, VLDLs. Once in the bloodstream, VLDLs are transformed into cholesterol rich LDL particles by interaction with different proteins, such as LPL, or exchange of lipids and apolipoproteins with HDLs. LDL particles are taken up by peripheral tissue cells through LDLR. Excess cholesterol from peripheral tissues is packageed in HDL lipoproteins for it clearance. First, free cholesterol is transferred to lipid poor pre-β HDL through ABCA1. Second, this first cholesterol loading changes HDL conformation and allows its interaction with ABCG1 and SR-B1 transporters that along with LCAT produce mature HDL particles that are transported back to the liver for their clearance.

1.2.3. Hepatic cholesterol efflux

The liver is the primary organ regulating cholesterol homeostasis and plays a key role in cholesterol synthesis [16], lipoprotein synthesis and secretion [35], lipoprotein clearance [36] and cholesterol excretion among other processes [37]. Cholesterol is secreted from the liver in triglyceride-rich lipoproteins known as Very Low Density Lipoproteins (VLDL). Regulation of VLDL synthesis and secretion is extremely well coordinated as they are critical for cholesterol distribution. VLDL synthesis is a two-step process that starts with the translocation of nascent apoB100 across the ER membrane of the hepatocytes and becomes lipidated by MTP [38]. If apoB100 is not well lipidated due to low triglyceride concentration or a failure in the process, the apolipoprotein is directed for degradation [39]. In a second step, partially lipidated VLDL particles are transported to the Golgi in vesicles containing coat protein complex II (COPII) [40]. Once in the Golgi they acquire apoA1 and apoE apolipoproteins and get further lipidated [41]. Finally, mature VLDL particles are secreted into the bloodstream and transport lipids to peripheral tissues[42].

High level secretion of VLDL by the liver can eventually be translated into high low density lipoprotein (LDL) levels in plasma and an enhanced cardiovascular risk [43]. On the other hand, an impaired VLDL secretion leads to lipid accumulation in the liver which can be the

starting step of fatty liver disease, therefore both processes need to be well coordinated and regulated [43,44].

1.2.4. Cholesterol influx

Apart from *de novo* synthesized cholesterol, cells obtain cholesterol from the uptake of plasma lipoproteins through LDL receptor (LDLR) pathway[14]. In plasma, triglycerides from VLDL are removed by the action of LPLs and produce VLDL remnants also known as intermediate density lipoproteins (IDL). Additional IDLs processing by hepatic lipases (HL) together with exchange of lipids and apolipoproteins with HDLs leads to low density lipoproteins (LDL) formation. LDLs are mainly composed by cholesterol esters and apoB-100 and they are the main cholesterol carriers of the body. They deliver cholesterol from liver to peripheral tissues where they bind LDLR and are endocytosed in clathrin coated pits[45]. Once LDL binds LDLR, LDL receptor adaptor protein 1 (LDLRAP1) recognizes the NPXY motif in the cytoplasmic tail of the LDLR and allows clustering of LDLR into clathrin-coated pits[46]. LDLR-LDL complex is delivered to endocytic compartment where due to pH acidification LDLR dissociates from LDL and is recycled back to the membrane due to pH dependent conformational change (Figure 1.3 A). Dissociation of LDL from LDLR in the endosome is a key process that enables receptor recycling while LDL-cholesterol is hydrolyzed in the lysosome due to lysosomal lipase action to release free cholesterol[47 4849]. Finally, free cholesterol is transferred from lysosomes to the ER by the action of Niemann-Pick type C1/C2 (NPC1/NPC2) proteins [50].

1.2.4.1. Cholesterol influx regulation

LDLR-mediated cholesterol internalization is a tightly regulated process with several checkpoints both at the transcriptional and post-transcriptional level [18,51,52]. On one hand SREBP-2, an inactive sterol regulatory element located in the ER, is activated at high intracellular cholesterol levels and translocates into the nucleus thus promoting *LDLR* transcription [18,53]. On the other hand proprotein convertase subtilisin/kexin 9 (PCSK9) [54] and IDOL, an inducible degrader of the LDLR, regulate LDLR at the membrane level by impairing the recycling of LDLR and promoting its degradation[55].

PCSK9 is the ninth member of the convertase protein family that is synthesized as a proprotein and requires an autocatalytic cleavage to become mature [56]. The result of the cleave is a N-terminal prodomain that remains bound to the catalytic domain and inhibits convertase function[57]. Mature PCSK9 is secreted to the extracellular medium where it binds epidermal grow factor A (EGF-A) domain of the LDLR and the complex is internalized by clathrin-mediated endocytosis. Upon endosome acidification, affinity of PCSK9 to LDLR increases thus impairing the required conformational change of LDLR for recycling. The non-dissociated PCSK9-LDLR complex is then delivered to the lysosome[5859].

IDOL, like PCSK9, regulates LDLR pathway post-transcriptionally. IDOL is an E3 ubiquitin ligase that mediates ubiquitination and degradation of LDLR[60]. IDOL expression is induced by oxysterols, generated due to high intracellular cholesterol concentration; activated cholesterol sensing nuclear receptors (LXRs) enhances IDOL expression along with genes involved in reverse cholesterol transport (RCT)[61]. The up-regulation of IDOL promotes ubiquitination of the cytoplasmic tail of the LDLR and its subsequent degradation [51,60].

Additionally, epigenetics and post-translational modifications of LDLR are important for LDLR mediated lipoprotein uptake [62–64]. For instance, microRNAs (miRNAs) have an active role in modulating efficiently LDLR expression. miRNAs are small single stranded non-coding RNAs with the ability to inhibit mRNA translation. They are synthesized as 70-100 nucleotide pri-miRNA which are sequentially modified by Drosha and Dicer endonucleases to produce mature miRNAs [65]. The mature miRNAs are about 20 nucleotide long molecules that are incorporated into RNA-induced silencing complex (RISC) to target mRNAs for their translational repression [66]. Many studies have shown that miRNAs are important regulators of the LDLR dependent LDL uptake. Indeed, miR-27b [67], miR-27a [68], miR-148a [69] and miR-128-1 [64] among other miRNAs are able to directly bind the 3´UTR of the LDLR mRNA and selectively degrade it.

1.2.5. Reverse cholesterol transport (RCT)

RCT is a tightly controlled mechanism by which the body is able to excrete the excess of cholesterol from peripheral tissues through the liver to the feces [70]. In this process, ApoA-1 containing HDLs are the mayor cholesterol acceptor from extra-hepatic tissues and the main responsible for cholesterol excess clearance [71].

RCT begins by interaction of ApoA-1 lipid free particles (pre-β HDL) with the ATP-binding cassette transporter A1 (ABCA1) in the plasma membrane which promotes free-cholesterol efflux from the endocytic compartment [71]. Lipidation of pre-β HDL induces conformational changes within the lipoprotein that adopts a discoid shape thus becoming a nascent-HDL. Free cholesterol is then esterified by Lecithin–cholesterol acyltransferase (LCAT) generating spherical mature HDL with a CE core[72]. In addition to ABCA1, the mature HDLs can interact with other cholesterol transporters such as ATP-binding cassette subfamily G member 1 (ABCG1) or Scavenger receptor class B type 1 (SR-B1) enhancing free-cholesterol efflux from peripheral tissues and increasing HDL particles size[72733 6]. Passive cholesterol transport from cell membranes to nascent HDL also contributes to cholesterol loading of the lipoprotein [74]. Once HDLs are fully lipidated, they are transported to the liver where CEs are selectively removed by SR-B1 for their excretion into bile (Figure 1.2) [36].

Interactions between different lipoproteins are also common during RCT. Mature HDL exchange both, proteins and lipids with other lipoproteins in plasma. CEs are transferred from

the core of the mature HDL to VLDL by the action of cholesterol ester transfer protein (CETP) and receives triglycerides in exchange[75]. As a consequence, VLDL remnants are generated and converted to LDL that can either be removed by LDLR in extra-hepatic tissues or by the liver for excretion into bile[76].

1.2.6. Bile acid excretion

Cholesterol excretion into bile is the last step in cholesterol elimination[76]. Bile acids are key modulators of cholesterol homeostasis and the main component of the bile. As mentioned before, they are essential for diet cholesterol emulsification and absorption and they also participate in the excretion of cholesterol leftovers from the liver [77]. Bile acids are primarily synthesized from cholesterol in the liver through a complex pathway strongly regulated by a feedback mechanism[78]. Once synthesized, they are pumped out by ABCB11 (also known as bile salt export pump (BSEP)) and promote secretion of phospholipids and cholesterol to the canalicular plasma, leading to micelle formation [37]. Cholesterol transport to the bile is mainly enhanced by ABCG5/8 heterodimer[7980] and requires phospholipids because they are a critical component for micelle formation. Indeed, defective phospholipid transport by ABCB4 (historically named multi-drug resistance P-glycoprotein 2(MDR2)) almost completely eliminates cholesterol secretion[81] . Finally the micelles are stored within the gallbladder and released into the intestinal lumen after food ingestion-produced stimuli [82].

In summary, cholesterol metabolism is a complex mechanism with many factors involved that requires a high level of coordination. Cholesterol absorption in the enterocytes, lipoprotein transport, cholesterol uptake in peripheral tissues and cholesterol excretion in the liver are tightly controlled processes that allow a correct balance of cholesterol in the organism. Hence, deregulation of these processes or mutation affecting proteins involved in these pathways can be disease causing. Mutations that alter LDL metabolism are the most frequent defects leading to a cholesterol metabolism derived disease denominated familial hypercholesterolemia.

1.3. Familial Hypercholesterolemia

Familial hypercholesterolemia (FH) is a common inherited autosomal co-dominant disorder primarily characterized by high plasma levels of low-density lipoprotein cholesterol (LDL-C) due to its reduced catabolism [14]. If untreated, exposure to high LDL-C levels during lifetime increases atherosclerotic plaque development and premature cardiovascular disease risk [83].

FH prevalence in its heterozygous form (HeFH) has traditionally been considered to be approximately 1:500. However, frequency can vary between 1:200 and 1:300 depending on which criteria are used to define FH (mutation only, LDL-C threshold only, clinical score or a combination of factors) and the studied populations [84]. Regarding the homozygous form of the

disease (HoFH), the prevalence has traditionally been estimated in 1:1,000,000 but recent studies have revealed a prevalence upwards to 1 in 300,000 [84].

1.3.1. Genetics of FH

Cholesterol metabolism and its distribution is a complex system in which many proteins and pathways are involved. LDL catabolism is one of the key points in this process and any defect in its function by any of the proteins involved can lead to FH. The major determinants of FH are *LDLR*, accounting for 80-85% of FH cases, *apoB100*, causing 5-10% of the cases, *PCSK9* 2% of the cases and *LDL receptor adaptor protein 1* (*LDLRAP1*) accounting for less than 1% of the cases [85]. Mutations in *APOE* [86], *signal transducing adaptor family member 1* (*STAP1*) [87], *lysosomal acid lipase* (*LIPA*) [47], *ABCG5* or *ABCG8* [88] genes can also generate a FH like phenotype but its frequency is very low in all of the cases.

1.3.1.1. *LDLR*

LDLR with more than 3000 variants already reported (Clin Var database [89]) is one of the key genes responsible of FH development [49]. LDLR removes LDL from plasma circulation (Figure 1.3 A) and malfunctioning of LDLR is commonly associated with high levels of circulating LDL-C. Many different *LDLR* variants have been described as pathogenic, including large-scale DNA copy number variation (CNV), insertion and deletions, nonsense and missense mutations and splicing mutations [859091]. CNV, nonsense and splicing mutations are commonly associated with higher LDL-C levels [49929394] than missense mutations. LDLR mutations can affect at different steps of the LDL uptake system and thus can be classified depending on their phenotypic behavior as: class 1 mutants are characterized by a null protein synthesis; class 2 mutants are partially or completely retained in the endoplasmic reticulum (Figure 1.3 B); class 3 mutants have a binding defect and are not able to properly interact with apoB apolipoprotein (Figure 1.3 C); class 4 mutants have an impaired endocytosis (Figure 1.3 D) and finally class 5 mutants affect the recycle mechanism and LDLR cannot be recycle bact to the membrane (Figure 1.3 E)

1.3.1.2. *APOB*

Mutations in *APOB* are a second cause of FH with a phenotype known as familial defective APOB [85]. Mutations in *APOB* gene were first detected in the highly conserved receptor binding-site (exons 26 and 29) [95] leading to deficient binding to LDLR. Recently some studies have also described new variants out from the consensus binding site of the APOB [96], these variants have been functionally characterized and classified as pathogenic indicating that LDLR-LDL binding could be more dynamic than expected [48]. APOB pathogenic variants are associated with lower LDL-C levels than those observed with *LDLR* pathogenic variants (Figure 1.3 F).

1.3.1.3. *PCSK9*

PCSK9 variants started to be described in the early 2000s when PCSK9 locus was mapped [54]. These variants can either be loss of function (LOF) variants, generating less functional proteins or gain of function variants (GOF) producing more active proteins [97]. GOF variants are associated with increased LDL-C levels as they enhances degradation of LDLR extracellularly due to increased affinity (Figure 1.3 G) or intracellularly while it is been transported to the membrane [98]. Both mechanisms lead to a reduced expression of LDLR resulting in plasma LDL accumulation. To date, more than 30 GOF PCSK9 variants have been reported; most of them missense mutations located all around the 3 domains of PCSK9 [97]. Different mechanisms underlying the increased activity, including increased transcription, altered autocatalysis or enhanced binding ability for the receptor have been described [97]. LOF mutations are less common than GOF mutations and are associated with lower LDL-C levels and reduced cardiovascular disease [99].

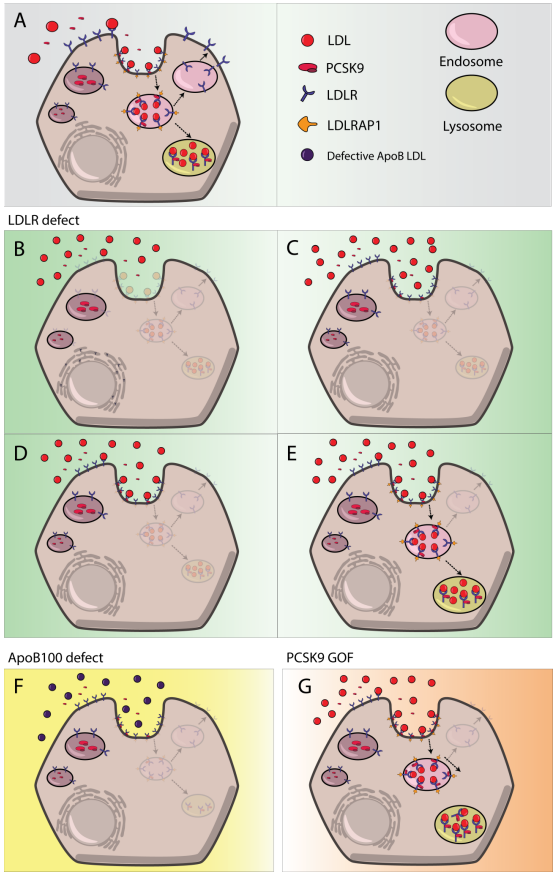

Figure 1.3. LDLR, ApoB100 and PCSK9 defects producing FH. A) LDL uptake process by LDLR; B) class 2 LDLR mutants, LDLR retention in the ER: C) Class 3 mutants, no LDL-LDLR binding; D) class 4 mutants, impaired LDL-LDLR complex internalization; E) class 5 mutants, recycling defect; F) defective ApoB-100 derived impaired LDL-LDLR binding; G) PCSK9 gain of function mutant.

1.3.1.4. *LDLRAP1*

LDLRAP1 mutations constitute the fourth most common protein defects among LDLR cycle proteins and cause autosomal recessive hypercholesterolaemia [100]. Pathogenic mutations in both alleles of the gene impair LDLR-LDL complex internalization. A dysfunctional LDLRAP1 does not allow proper clathrin-coated endosome formation and inhibits LDL uptake thus increasing plasma LDL-C accumulation [101102].

1.3.2. Second generation FH

High cholesterol levels are frequently associated to genes or processes related with cholesterol trafficking but sometimes they can be a consequence of other diseases or environmental factors. Mutations in *ABCG5* or *ABCG8* genes cause sitosterolemia, in which patients present increased LDL-C levels, some characteristic FH phenotype features and higher cardiovascular risk, alike FH [103104]. The main cause of this manifestation is plant-sterol accumulation, therefore its treatment consist on administration of sterol absorption inhibitors instead of a statin treatment [25]. Nephrotic syndrome (NS) is also associated with an increased cholesterol and triglyceride accumulation. Patients with acute NS have marked proteinuria that generates an increased synthesis of lipoproteins in the liver [105106]. Liver failure [107], hypothyroidism [108] or cholestasis are other diseases associated with higher levels of plasma cholesterol and an increased risk of cardiovascular disease [109].

1.3.3. FH implication in cardiovascular disease

FH is characterized by abnormally increased levels of LDL-C, which promotes early atherosclerosis development[84]. Atherosclerosis is the underlying cause of cardiovascular disease, increasing the risk of heart attack, stroke and peripheral vascular disease [110]. In FH patients, accumulated plasma LDL-C particles and VLDL remnants cross the endothelial lining of the arteries and get retained in the subendothelial compartment where they become oxidized [111]. This lipid accumulation is enhanced in places where the endoplasmic barrier and the junction between endothelial cells are weaker, mainly in arterial curves and branches where a disturbed blood flow causes higher stress [112]. Endothelial cells increase the secretion of different adhesion and chemoattractant molecules in response to oxidized particle stimuli thus generating monocyte recruitment and trans-endothelial cell migration [113]. Once in the subendothelial space, monocytes differentiate to proinflamatory macrophages and start to internalize modified lipoproteins through a non-regulated variety of scavenger receptors (SRs) [114]. The excess of cholesterol in macrophages induces foam cell formation and enhances their proinflamatory fate by promoting migration of vascular smooth muscle cells (VSMC) and proliferation of those macrophages already present in the intima. Finally, activated VSMC start the production of the fibrous cap, an extracellular matrix composed primarily of collagen,

elastin and proteoglycans [115]. As atherosclerosis progresses, the necrotic core, covered by the fibrous cap, increases in size as a consequence of increased macrophage death and impaired efferocytosis. This process reduces the diameter of the arteries causing lumen occlusion; furthermore, at this stage, pro-inflamatory cells present in the plaque start to secrete matrix metalloproteinases that degrade the extracellular matrix of the fibrous cap favoring the rupture of the plaque and increasing the risk of heart attack and peripheral vascular disease[116,117] (Figure 1.4).

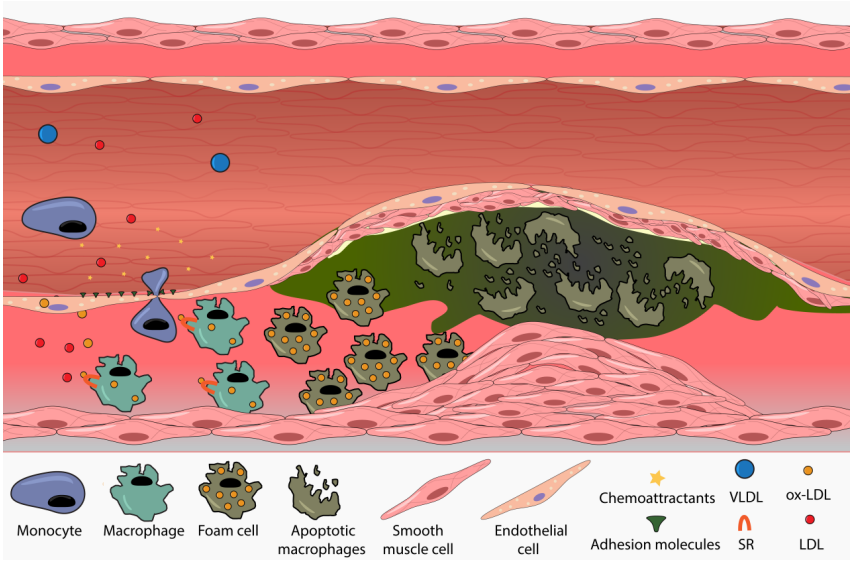

Figure 1.4. Atherome plaque development. Accumulated LDL particles cross endothelial barrier and get oxidized in subendothelial space. Lipoprotein oxidation activates endothelial cells that increase the synthesis and secretion of chemoattractants and adhesion molecules promoting monocyte recruitment and transedothelial migration. Once at sub-endothelial compartments they are differentiated into machrophages and start to internalize ox-LDL through a non regulated SR-B1 scavenger receptor. Cholesterol excess in macrophages induces foam cell formation and promotes SVMC migration and fibrous cap synthesis. Finally, due to increased macrophage death and impaired efferocytosis, the size of the plaque increases and the diameter of the artery is reduced.

1.3.4. FH diagnosis

Different guidelines are available for FH diagnosis. Among them, Simon Broome Register Group (SBRG)[118], Make Early Diagnosis to Prevent Early Death (MEDPED)[119] and Duch Lipid Clinic Network (DLCM)[85] are the most extended ones. All the guidelines share common criteria with small differences in the threshold and, combination of factors needed for a definitive FH diagnosis including physical symptoms (tendinous xanthomata and arcus cornealis if under 45 years old), plasma cholesterol levels (if are over 330 mg/dL is a definite diagnose), familial history of FH, clinical history of the patient and DNA analysis.

1.3.5. Evolution of lipid lowering therapies

High cholesterol levels do not have any direct symptoms so many people usually ignore that they suffer FH. Typically, 200 mg/dL total cholesterol and 100 mg/dL LDL-C are considered threshold values over from which the risk of suffering CVD increases dramatically[120]. Therefore, prevention and treatment of FH is critical. Nowadays, statins constitute the gold standard treatment of FH but historically other drugs or drug-combination have been commonly used. Additionally, statin treatment in some cases of HeFH and in HoFH only show promising results if combined with other cholesterol lowering therapies [121122].

1.3.5.1. Statins

Statins are the main cholesterol-lowering drug nowadays. They were discovered in the early 70s by Akira Endo but not commercially available until 1986 when lovastatin was commercialized as the first HMG-CoA reductase inhibitor [123]. Statins inhibit HMG-CoA and the downstream metabolite production of mevalonate pathway. As a consequence, intracellular cholesterol production highly decreases. Indirectly, statins increase LDL and even VLDL clearance from the plasma due to overexpression of LDLR in the liver and peripheral tissues [123]. The most potent statins; Rosuvastatin, Atorvastatin and Sinvastatin can also reduce LDL levels in HoFH patients probably because of lower LDL-C production in the liver [124]. Although high efficacy and safety of the statins has been demonstrated, long-term high-dose treatments studies have revealed some adverse effects in some individuals,. The most common ones are the statin-associated muscle symptoms as muscle pain or weakness [125]. The influence of statins on the development of type II diabetes mellitus (DMII) is also under study. Indeed, high dose statin treatment has been implicated in the development of DMII [126]. Several adverse effects on hepatic, renal or even cognitive function should not be discarded [127].

1.3.5.2. Niacin

Niacin, also called vitamin B3 or nicotinic acid, was the first lipid-modifying drug used for the treatment of FH. Niacin reduces FFA mobilization from adipose tissue by inhibiting its protein lipase system. Therefore, the reduced FFA availability in liver impairs synthesis of cholesterol and triglyceride containing particles. The common side effects of niacin are vasodilatation and elevation of hepatic enzymes[128].

1.3.5.3. Bile acid sequestrants

Bile acid sequestrants were introduced in the market in 1975[129]. These molecules form insoluble complexes with bile acid-cholesterol micelles thus avoiding capture by enterocytes and consequently the micelles are excreted[130]. Because enterocyte-liver cholesterol transit is partially inhibited, liver cholesterol levels are reduced so LDL and VLDL secretion is reduced and consequently their bloodstream concentration [131]. They are proven to reduce both cardiovascular events and derived mortality however; they are usually not well tolerated. Indeed, they interfere with absorption of some fat-soluble vitamins and also with bile acids

reabsorption that, in normal condition, are almost entirely reabsorbed. They are not useful in cases of HoFH with null receptor function[132].

1.3.5.4. Ezetimibe

Ezetimibe is a selective cholesterol absorption inhibitor that blocks the uptake of cholesterol. It inhibits NPC1L1 both at enterocyte lumen and hepatobiliary interface affecting cholesterol but not trygliceride or fat-soluble vitamin absorption [133]. The inhibition of cholesterol absorption in the intestine results in a reduced chylomicron formation and secretion in addition to bile cholesterol reabsorption inhibition. The sum of these effects leads to a depletion of cholesterol stores in the hepatocytes. Reduced cholesterol content in the liver favors LDLR expression as well as reduced VLDL generation resulting in lower LDL-C in plasma [134].

1.3.5.5. Human monoclonal anti-PCSK9 antibodies

Human monoclonal anti-PCSK9 antibodies have been demonstrated to lower LDL-C levels efficiently and reduce CVD especially in high risk patients [135]. Their use is recommended when neither statins nor ezetimide is able to reduce cholesterol under recommended levels [136]. Currently, two different monoclonal antibodies are available, alirocumab and evolovumab. Both are Human IgG subtypes that bind circulating PCSK9 and inhibit their binding to LDLR leading to a PCSK9 deficiency-like condition [137]. The absence of functional PCSK9 enhances LDLR recycling and its availability in the membranes thus favoring LDL clearance from the plasma. While anti-PCSK9 antibodies have low side effects and high efficacy in comparison with other drugs, the high cost of the therapy remains a barrier for more widespread implementation of anti-PCSK9 treatments [137].

1.3.5.6. Other treatments

Recently some drugs affecting lipoprotein synthesis have been introduced. Lomitapide is a MTP inhibitor, a protein responsible for the assembly of lipids onto the proteins both in hepatocytes and enterocytes. Mipomersen is an antisense oligonucleotide that binds apoB mRNA reducing VLDL and LDL generation in the liver. Both drugs have been associated with many side effects and their use is not recommended except in cases of HoFH or very high cardiovascular risk [138].

Lipoprotein apheresis (LA) is a therapeutic tool normally used in extremely high-risk patients where other therapies have not worked or appear to be not effective. HoFH is a clear example where LA is recommended [139,140]. Usually HoFH patients with no LDLR expression have residual response to statin treatment and monoclonal antibodies against PCSK9 are rarely effective. In those cases, with a really high risk of CVD and poor prognosis LA therapy should be started [139]. LA is only recommended when other lipid lowering drugs are ineffective due to its high cost and time consuming. In fact, the accessibility to LA is reduced to a few countries [129].

To date, statins are the main used cholesterol-reducing drug, both due to their high efficacy and low cost[136]. They are recommended as first treatment option and only statin-intolerant patients and patients under statin treatment not achieving recommended LDL-C values, the use of other drugs should be suggested. In cases in which statins have low effect, they are usually combined with ezetamibe, PCSK9 inhibitors or both with promising results [136]. In HoFH with non LDLR function, MTP inhibitors or apoB inhibiting oligonucleotides are appropriate the choice to reduce LDLR levels assuming their low tolerability and high cost [137].

1.3.6. Nutraceuticals in FH

Nutraceuticals are natural lipid regulating products recommended in combination with the previously described therapies for management of different dyslipidemias [141]. Nutraceuticals are able to affect at different steps of cholesterol metabolism and can improve the effects of the different cholesterol reducing therapies. Plant sterols and green tea are able to reduce dietary cholesterol absorption [142,143], berberine (extracted from a variety of plants) inhibits PCSK9 action [144,145] and monacolins, present in red yeast rice, share structural similarities with statins and inhibit intracellular cholesterol synthesis [146].

1.3.7. Current FH situation

As mentioned before, untreated FH increases 13 fold the risk of CVD[147]. Sustained high plasma cholesterol levels induce lipoprotein oxidation and infiltration through endothelial barrier enhancing and accelerating progression of atherosclerotic plaque. Nowadays many high efficacy cholesterol-reducing therapies are available and their efficacies have been probed [137]. However, the main issue in FH treatment is the underdiagnose of this disease. In most countries, less than 1% of the population has been diagnosed and only in The Netherlands have diagnosed more than 50% of their population. In Spain for example, the diagnose condition is reduced to the 6% of the population [85148]. Taking in account that the estimated prevalence of the disease is 1:200-1:300 and global numbers reveal less than 1% of diagnosed population, there are about 24 and 36 million of FH individuals with non definitive FH diagnose and high risk of premature CVD.

Historically, HeFH has been clinically diagnosed based on LDL-C levels, tendon xanthomas, or familial history of coronary artery disease. This kind of diagnosis was able to detect the most severe cases of HeFH and HoFH but, many mild FH phenotypes were not identified. Through improvements in understanding of FH and the development of new generation sequencing techniques, FH mutations causing mild FH phenotypes are now more easily detected. Combinations of both genetic testing and clinical criteria have enabled detection

of mild FH phenotype patients and identification of patients with clinical FH and without mutation in FH generating classical genes [148,149]

Differences in LDL-C levels between FH causing mutation carriers with non-carriers vary with age. At young ages, the differences in LDL-C levels are higher than in people over 55 years old, so differences in LDL-C accumulation are set up mainly in early stages of the disease underlying the importance of an early diagnosis and treatment of the FH [150]. Moreover, early treatment of the disease makes possible an efficient low dose statin treatment instead of high dose treatments required in cases where the FH is diagnosed later in life, thus side effects derived from aggressive statin use are avoided [127].

1.3.8. Functional studies as a complement to genetic testing

Genetic testing is proven to be the best mechanism for a correct early FH diagnosis. However, because the great majority of the variants are not functionally characterized, genetic testing must be complemented to provide an accurate and definitive diagnose [151]. Cosegregation studies, functional studies or a combination of both are good alternatives to complement genetic studies. Cosegregation studies unlike functional studies have the limitation of clinical data availability and alteration carrier number [152]. Functional studies instead can be performed in any research laboratory and not only give information about the pathogenicity but also about the disease causing mechanism of the different mutations [48,49,153,154].

References

1. Maxfield, F. R. & Tabas, I. Role of cholesterol and lipid organization in disease. *Nature* **438,** 612–621 (2005).

2. Cherezov, V. *et al.* High-Resolution Crystal Structure of an Engineered Human 2-Adrenergic G Protein-Coupled Receptor. *Science (80-.).* **318,** 1258–1265 (2007).

3. Ikonen, E. Cellular cholesterol trafficking and compartmentalization. *Nat. Rev. Mol. Cell Biol.* **9,** 125–138 (2008).

4. Grouleff, J., Irudayam, S. J., Skeby, K. K. & Schiøtt, B. The influence of cholesterol on membrane protein structure, function, and dynamics studied by molecular dynamics simulations. *Biochim. Biophys. Acta - Biomembr.* **1848,** 1783–1795 (2015).

5. Yang, S.-T., Kreutzberger, A. J. B., Lee, J., Kiessling, V. & Tamm, L. K. The role of cholesterol in membrane fusion. *Chem. Phys. Lipids* **199,** 136–143 (2016).

6. Rogers, M. A. *et al.* Acyl-CoA:cholesterol acyltransferases (ACATs/SOATs): Enzymes with multiple sterols as substrates and as activators. *J. Steroid Biochem. Mol. Biol.* **151,** 102–107 (2015).

7. Christie, M. P., Johnstone, B. A., Tweten, R. K., Parker, M. W. & Morton, C. J. Cholesterol-dependent cytolysins: from water-soluble state to membrane pore. *Biophys. Rev.* (2018). doi:10.1007/s12551-018-0448-x

8. Gao, Y., Zhou, Y., Goldstein, J. L., Brown, M. S. & Radhakrishnan, A. Cholesterol-induced conformational changes in the sterolsensing domain of the Scap protein suggest feedback mechanism to control cholesterol synthesis. *J. Biol. Chem.* **292,** 8729–8737 (2017).

9. Theesfeld, C. L., Pourmand, D., Davis, T., Garza, R. M. & Hampton, R. Y. The sterol-sensing domain (SSD) directly mediates signal-regulated endoplasmic reticulum-associated degradation (ERAD) of 3-hydroxy-3- methylglutaryl (HMG)-CoA reductase isozyme Hmg2. *J. Biol. Chem.* **286,** 26298–26307 (2011).

10. Di Scala, C. *et al. Relevance of CARC and CRAC Cholesterol-Recognition Motifs in the Nicotinic Acetylcholine Receptor and Other Membrane-Bound Receptors*. *Current Topics in Membranes* **80,** (Elsevier Inc., 2017).

11. Russell, D. W. The Enzymes, Regulation, and Genetics of Bile Acid Synthesis. *Annu. Rev. Biochem.* **72,** 137–174 (2003).

12. Midzak, A. & Papadopoulos, V. Binding domain-driven intracellular trafficking of sterols for synthesis of steroid hormones, bile acids and oxysterols. *Traffic* **15,** 895–914 (2014).

13. Wang, T. J. Vitamin D and Cardiovascular Disease. *Annu. Rev. Med.* **67,** 261–272 (2016).

14. Brown, M. & Goldstein, J. A receptor-mediated pathway for cholesterol homeostasis. *Science (80-.).* **232,** 34–47 (1986).

15. Bloch, K. Sterol molecule: structure, biosynthesis, and function. *Steroids* **57,** 378–383 (1992).

16. Dietschy, J. M., Turley, S. D. & Spady, D. K. Role of liver in the maintenance of cholesterol and low density lipoprotein homeostasis in different animal species, including humans. *J. Lipid Res.* **34,** 1637–1659 (1993).

17. Goedeke, L. & Fernández-Hernando, C. Regulation of cholesterol homeostasis. *Cell. Mol. Life Sci.* **69,** 915–930 (2012).

18. Horton, J. D., Goldstein, J. L. & Brown, M. S. SREBPs: activators of the complete program of cholesterol and fatty acid synthesis in the liver. *J. Clin. Invest.* **109,** 1125–1131 (2002).

19. Fears, R. The contribution of the cholesterol biosynthetic pathway to intermediary metabolism and cell function. *Biochem. J.* **199,** 1–7 (1981).

20. Goldstein, J. L. & Brown, M. S. The LDL Receptor. *Arterioscler. Thromb. Vasc. Biol.* **29,** 431–438 (2009).

21. Hussain, M. M. Intestinal lipid absorption and lipoprotein formation. *Curr. Opin. Lipidol.* **25,** 200–206 (2014).

22. Betters, J. L. & Yu, L. NPC1L1 and cholesterol transport. *FEBS Lett.* **584,** 2740–2747 (2010).

23. Li, P. S. *et al.* The clathrin adaptor Numb regulates intestinal cholesterol absorption through dynamic interaction with NPC1L1. *Nat. Med.* **20,** 80–86 (2014).

24. Dash, S., Xiao, C., Morgantini, C. & Lewis, G. F. New Insights into the Regulation of Chylomicron Production. *Annu. Rev. Nutr.* **35,** 265–294 (2015).

25. Yoo, E. Sitosterolemia : a review and update of pathophysiology , clinical spectrum , diagnosis , and management. *Ann Pediatr Endocrinol Metab.* **21,** 7–14 (2016).

26. Marcel, Y. L. *et al.* Mapping of human apolipoprotein B antigenic determinants. *Arteriosclerosis* **7,** 166–75 (1987).

27. Julve, J., Martín-Campos, J. M., Escolà-Gil, J. C. & Blanco-Vaca, F. Chylomicrons: Advances in biology, pathology, laboratory testing, and therapeutics. *Clin. Chim. Acta* **455,** 134–148 (2016).

28. Dixon, J. B. Mechanisms of chylomicron uptake into lacteals. *Ann. N. Y. Acad. Sci.* **1207,** 52–57 (2010).

29. Randolph, G. J. & Miller, N. E. Lymphatic transport of high-density lipoproteins and chylomicrons. *J. Clin. Invest.* **124,** 929–935 (2014).

30. Olivecrona, G. Role of lipoprotein lipase in lipid metabolism. *Current Opinion in Lipidology* **27,** 233–241 (2016).

31. Wolska, A. *et al.* Apolipoprotein C-II: New findings related to genetics, biochemistry, and role in triglyceride metabolism. *Atherosclerosis* (2017). doi:10.1016/j.atherosclerosis.2017.10.025

32. Dallinga-Thie, G. M. *et al.* The metabolism of triglyceride-rich lipoproteins revisited: New players, new insight. *Atherosclerosis* **211,** 1–8 (2010).

33. Heeren, J. Apolipoprotein E Recycling: Implications for Dyslipidemia and Atherosclerosis. *Arterioscler. Thromb. Vasc. Biol.* **26,** 442–448 (2005).

34. Frazier-Wood, A. C. *et al.* The association between LRP-1 variants and chylomicron uptake after a high fat meal. *Nutr. Metab. Cardiovasc. Dis.* **23,** 1154–1158 (2013).

35. Thompson, G. R., Naoumova, R. P. & Watts, G. F. Role of cholesterol in regulating apolipoprotein B secretion by the liver. *J. Lipid Res.* **37,** 439–447 (1996).

36. Ganesan, L. P. *et al.* Scavenger receptor B1, the HDL receptor, is expressed abundantly in liver sinusoidal endothelial cells. *Sci. Rep.* **6,** 1–13 (2016).

37. Oude Elferink, R. P. & Groen, a K. Mechanisms of biliary lipid secretion and their role in lipid homeostasis. *Semin. Liver Dis.* **20,** 293–305 (2000).

38. Sirtori, C. R., Pavanello, C. & Bertolini, S. Microsomal transfer protein (MTP) inhibition—a novel approach to the treatment of homozygous hypercholesterolemia. *Ann. Med.* **46,** 464–474 (2014).

39. Olofsson, S. O. & Borén, J. Apolipoprotein B secretory regulation by degradation. *Arterioscler. Thromb. Vasc. Biol.* **32,** 1334–1338 (2012).

40. Wang, Y. *et al.* Mea6 controls VLDL transport through the coordinated regulation of COPII assembly. *Cell Res.* **26,** 787–804 (2016).

41. Hossain, T., Riad, A., Siddiqi, S., Parthasarathy, S. & Siddiqi, S. A. Mature VLDL triggers the biogenesis of a distinct vesicle from the trans -Golgi network for its export to the plasma membrane. *Biochem. J.* **459,** 47–58 (2014).

42. Doonan, L. M., Fisher, E. A. & Brodsky, J. L. Can modulators of apolipoproteinB biogenesis serve as an alternate target for cholesterol-lowering drugs? *Biochim. Biophys. Acta - Mol. Cell Biol. Lipids* **1863,** 762–771 (2018).

43. Tiwari, S. & Siddiqi, S. A. Intracellular trafficking and secretion of VLDL. *Arterioscler. Thromb. Vasc. Biol.* **32,** 1079–1086 (2012).

44. Nassir, F., Adewole, O. L., Brunt, E. M. & Abumrad, N. A. CD36 deletion reduces VLDL secretion, modulates liver prostaglandins, and exacerbates hepatic steatosis in ob/ob mice. *J. Lipid Res.* **54,** 2988–2997 (2013).

45. Etxebarria, A. *et al.* Activity-associated effect of LDL receptor missense variants located in the cysteine-rich repeats. *Atherosclerosis* **238,** 304–312 (2015).

46. Soufi, M., Rust, S., Walter, M. & Schaefer, J. R. A combined LDL receptor/LDL receptor adaptor protein 1 mutation as the cause for severe familial hypercholesterolemia. *Gene* **521,** 200–203 (2013).

47. Reiner, Ž. *et al.* Lysosomal acid lipase deficiency - An under-recognized cause of dyslipidaemia and liver dysfunction. *Atherosclerosis* **235,** 21–30 (2014).

48. Fernández-Higuero, J. A. *et al.* Structural changes induced by acidic pH in human apolipoprotein B-100. *Sci. Rep.* **6,** 1–10 (2016).

49. Etxebarria, A. *et al.* Functional characterization and classification of frequent low-density lipoprotein receptor variants. *Hum. Mutat.* **36,** 129–141 (2015).

50. Yu, X.-H. *et al.* NPC1, intracellular cholesterol trafficking and atherosclerosis. *Clin. Chim. Acta* **429,** 69–75 (2014).

51. Zhang, L., Reue, K., Fong, L. G., Young, S. G. & Tontonoz, P. Feedback Regulation of Cholesterol Uptake by the LXR-IDOL-LDLR Axis. *Arterioscler. Thromb. Vasc. Biol.* **32,** 2541–2546 (2012).

52. Lopez, D. PCSK9: An enigmatic protease. *Biochim. Biophys. Acta - Mol. Cell Biol. Lipids* **1781,** 184–191 (2008).

53. Horton, J. D. *et al.* Combined analysis of oligonucleotide microarray data from transgenic and knockout mice identifies direct SREBP target genes. *Proc. Natl. Acad. Sci.* **100,** 12027–12032 (2003).

54. Abifadel, M. *et al.* Mutations in PCSK9 cause autosomal dominant hypercholesterolemia. *Nat. Genet.* **34,** 154–156 (2003).

55. Zelcer, N., Hong, C., Boyadjian, R. & Tontonoz, P. LXR Regulates Cholesterol Uptake Through Idol-Dependent Ubiquitination of the LDL Receptor. *Science (80-.).* **325,** 100–104 (2009).

56. Wierød, L., Cameron, J., Strøm, T. B. & Leren, T. P. Studies of the autoinhibitory

segment comprising residues 31-60 of the prodomain of PCSK9: Possible implications for the mechanism underlying gain-of-function mutations. *Mol. Genet. Metab. reports* **9,** 86–93 (2016).

57. Luna Saavedra, Y. G., Zhang, J. & Seidah, N. G. PCSK9 Prosegment Chimera as Novel Inhibitors of LDLR Degradation. *PLoS One* **8,** (2013).

58. Schroeder, C. I. *et al.* Design and Synthesis of Truncated EGF-A Peptides that Restore LDL-R Recycling in the Presence of PCSK9 In Vitro. *Chem. Biol.* **21,** 284–294 (2014).

59. Gu, H., Adijiang, A., Mah, M. & Zhang, D. Characterization of the role of EGF-A of low density lipoprotein receptor in PCSK9 binding. *J. Lipid Res.* **54,** 3345–3357 (2013).

60. Wang, B. & Tontonoz, P. Liver X receptors in lipid signalling and membrane homeostasis. *Nat. Rev. Endocrinol.* **14,** 452–463 (2018).

61. Tontonoz, P. & Mangelsdorf, D. J. Liver X Receptor Signaling Pathways in Cardiovascular Disease. *Mol. Endocrinol.* **17,** 985–993 (2003).

62. Wang, S. *et al.* Site-specific O-glycosylation of members of the low-density lipoprotein receptor superfamily enhances ligand interactions. *J. Biol. Chem.* **293,** 7408–7422 (2018).

63. Goedeke, L., Wagschal, A., Fernández-Hernando, C. & Näär, A. M. miRNA regulation of LDL-cholesterol metabolism. *Biochim. Biophys. Acta - Mol. Cell Biol. Lipids* **1861,** 2047–2052 (2016).

64. Wagschal, A. *et al.* Genome-wide identification of microRNAs regulating cholesterol and triglyceride homeostasis. *Nat. Med.* **21,** 1290–1297 (2015).

65. Ha, M. & Kim, V. N. Regulation of microRNA biogenesis. *Nat. Rev. Mol. Cell Biol.* **15,** 509–524 (2014).

66. Romero-Cordoba, S. L., Salido-Guadarrama, I., Rodriguez-Dorantes, M. & Hidalgo-Miranda, A. miRNA biogenesis: Biological impact in the development of cancer. *Cancer Biol. Ther.* **15,** 1444–1455 (2014).

67. Goedeke, L. *et al.* miR-27b inhibits LDLR and ABCA1 expression but does not influence plasma and hepatic lipid levels in mice. *Atherosclerosis* **243,** 499–509 (2015).

68. Alvarez, M. L., Khosroheidari, M., Eddy, E. & Done, S. C. MicroRNA-27a decreases the level and efficiency of the LDL receptor and contributes to the dysregulation of

cholesterol homeostasis. *Atherosclerosis* **242,** 595–604 (2015).

69. Goedeke, L. *et al.* MicroRNA-148a regulates LDL receptor and ABCA1 expression to control circulating lipoprotein levels. *Nat. Med.* **21,** 1280–1288 (2015).

70. Favari, E. *et al.* in *Handbook of experimental pharmacology* **224,** 181–206 (2015).

71. Wang, S. & Smith, J. D. ABCA1 and nascent HDL biogenesis. *BioFactors* **40,** 547–554 (2014).

72. Zannis, V. I., Chroni, A. & Krieger, M. Role of apoA-I, ABCA1, LCAT, and SR-BI in the biogenesis of HDL. *Journal of Molecular Medicine* **84,** 276–294 (2006).

73. Terasaka, N. *et al.* ATP-binding cassette transporter G1 and high-density lipoprotein promote endothelial NO synthesis through a decrease in the interaction of caveolin-1 and endothelial NO synthase. *Arterioscler. Thromb. Vasc. Biol.* **30,** 2219–2225 (2010).

74. Gillard, B. K., Rosales, C., Xu, B., Jr, A. M. G. & Pownall, H. J. Rethinking reverse cholesterol transport and dysfunctional high-density lipoproteins. 849–856 (2018).

75. Wang, X. *et al.* The therapeutic potential of CETP inhibitors: a patent review. *Expert Opin. Ther. Pat.* **28,** 331–340 (2018).

76. Dikkers, A. & Tietge, U. J. F. Biliary cholesterol secretion: More than a simple ABC. *World J. Gastroenterol.* **16,** 5936–5945 (2010).

77. Halilbasic, E., Claudel, T. & Trauner, M. Bile acid transporters and regulatory nuclear receptors in the liver and beyond. *J. Hepatol.* **58,** 155–168 (2013).

78. Norlin, M. & Wikvall, K. Enzymes in the Conversion of Cholesterol into Bile Acids. *Curr. Mol. Med.* **7,** 199–218 (2007).

79. Yu, X. H. *et al.* ABCG5/ABCG8 in cholesterol excretion and atherosclerosis. *Clin. Chim. Acta* **428,** 82–88 (2014).

80. Bonamassa, B. & Moschetta, A. Atherosclerosis: Lessons from LXR and the intestine. *Trends Endocrinol. Metab.* **24,** 120–128 (2013).

81. Gordo-Gilart, R., Andueza, S., Hierro, L., Jara, P. & Alvarez, L. Functional Rescue of Trafficking-Impaired ABCB4 Mutants by Chemical Chaperones. *PLoS One* **11,** e0150098 (2016).

82. Cohen, D. E. Balancing cholesterol synthesis and absorption in the gastrointestinal tract.

J. Clin. Lipidol. **2,** 1–5 (2008).

83. Ference, B. A. *et al.* Low-density lipoproteins cause atherosclerotic cardiovascular disease. 1. Evidence from genetic, epidemiologic, and clinical studies. A consensus statement fromthe European Atherosclerosis Society Consensus Panel. *Eur. Heart J.* **38,** 2459–2472 (2017).

84. Vallejo-Vaz, A. J. *et al.* Pooling and expanding registries of familial hypercholesterolaemia to assess gaps in care and improve disease management and outcomes: Rationale and design of the global EAS Familial Hypercholesterolaemia Studies Collaboration. *Atheroscler. Suppl.* **22,** 1–32 (2016).

85. Nordestgaard, B. G. *et al.* Familial hypercholesterolaemia is underdiagnosed and undertreated in the general population: Guidance for clinicians to prevent coronary heart disease. *Eur. Heart J.* **34,** 3478–3490 (2013).

86. Cenarro, A. *et al.* The p.Leu167del mutation in APOE gene causes autosomal dominant hypercholesterolemia by down-regulation of LDL receptor expression in hepatocytes. *J. Clin. Endocrinol. Metab.* **101,** 2113–2121 (2016).

87. Fouchier, S. W. *et al.* Mutations in STAP1 are associated with autosomal dominant hypercholesterolemia. *Circ. Res.* **115,** 552–555 (2014).

88. Rios, J., Stein, E., Shendure, J., Hobbs, H. H. & Cohen, J. C. Identification by whole-genome resequencing of gene defect responsible for severe hypercholesterolemia. *Hum. Mol. Genet.* **19,** 4313–4318 (2010).

89. Landrum, M. J. *et al.* ClinVar: public archive of interpretations of clinically relevant variants. *Nucleic Acids Res.* **44,** D862–D868 (2016).

90. Defesche, J. C. *et al.* Familial hypercholesterolaemia. *Nat. Rev. Dis. Prim.* **3,** 17093 (2017).

91. Iacocca, M. A. & Hegele, R. A. Role of DNA copy number variation in dyslipidemias. *Curr. Opin. Lipidol.* **29,** 125–132 (2018).

92. Etxebarria, A. *et al.* Functional characterization of splicing and ligand-binding domain variants in the LDL receptor. *Hum. Mutat.* **33,** 232–243 (2012).

93. Ho, C. K. M., Musa, F. R., Bell, C. & Walker, S. W. LDLR gene synonymous mutation c.1813C>T results in mRNA splicing variation in a kindred with familial hypercholesterolaemia. *Ann. Clin. Biochem.* **52,** 680–684 (2015).

94. Holla, Ø. L., Kulseth, M. A., Berge, K. E., Leren, T. P. & Ranheim, T. Nonsense-mediated decay of human LDL receptor mRNA. *Scand. J. Clin. Lab. Invest.* **69,** 409–417 (2009).

95. Alves, A. C. *et al.* Further evidence of novel APOB mutations as a cause of Familial Hypercholesterolaemia. *Atherosclerosis* (2018). doi:10.1016/j.atherosclerosis.2018.06.819

96. Alves, A. C. atarina, Etxebarria, A., Soutar, A. K. atherine, Martin, C. & Bourbon, M. Novel functional APOB mutations outside LDL-binding region causing familial hypercholesterolaemia. *Hum. Mol. Genet.* **23,** 1817–1828 (2014).

97. Dron, J. S. & Hegele, R. A. Complexity of mechanisms among human proprotein convertase subtilisin-kexin type 9 variants. *Curr. Opin. Lipidol.* **28,** 161–169 (2017).

98. Mousavi, S. A., Berge, K. E. & Leren, T. P. The unique role of proprotein convertase subtilisin/kexin 9 in cholesterol homeostasis. *J. Intern. Med.* **266,** 507–519 (2009).

99. Cohen, J. C., Boerwinkle, E., Mosley, T. H. & Hobbs, H. H. Sequence variations in PCSK9, low LDL, and protection against coronary heart disease. *N. Engl. J. Med.* **354,** 1264–72 (2006).

100. Berberich, A. J. & Hegele, R. A. The complex molecular genetics of familial hypercholesterolaemia. *Nat. Rev. Cardiol.* **250,** (2018).

101. Soutar, A. K. & Naoumova, R. P. Mechanisms of disease: Genetic causes of familial hypercholesterolemia. *Nat. Clin. Pract. Cardiovasc. Med.* **4,** 214–225 (2007).

102. Quagliarini, F. *et al.* Autosomal recessive hypercholesterolemia in Spanish kindred due to a large deletion in the ARH gene. *Mol. Genet. Metab.* **92,** 243–248 (2007).

103. Tada, H., Nomura, A., Yamagishi, M. & Kawashiri, M. aki. First case of sitosterolemia caused by double heterozygous mutations in ABCG5 and ABCG8 genes. *J. Clin. Lipidol.* (2018). doi:10.1016/j.jacl.2018.06.003

104. Wang, W. *et al.* A case of sitosterolemia misdiagnosed as familial hypercholesterolemia: A 4-year follow-up. *J. Clin. Lipidol.* **12,** 236–239 (2018).

105. Muso, E. Beneficial effect of LDL-apheresis in refractory nephrotic syndrome. *Clinical and Experimental Nephrology* **18,** 286–290 (2014).

106. Agrawal, S., Zaritsky, J. J., Fornoni, A. & Smoyer, W. E. Dyslipidaemia in nephrotic

syndrome: mechanisms and treatment. *Nat. Rev. Nephrol.* **14,** 57–70 (2017).

107. Chrostek, L. *et al.* The effect of the severity of liver cirrhosis on the level of lipids and lipoproteins. *Clin. Exp. Med.* **14,** 417–421 (2014).

108. Rizos, C. V, Elisaf, M. S. & Liberopoulos, E. N. Effects of thyroid dysfunction on lipid profile. *Open Cardiovasc. Med. J.* **5,** 76–84 (2011).

109. Nemes, K., Åberg, F., Gylling, H. & Isoniemi, H. Cholesterol metabolism in cholestatic liver disease and liver transplantation: From molecular mechanisms to clinical implications. *World J. Hepatol.* **8,** 924 (2016).

110. Mozaffarian, D. *et al. Heart disease and stroke statistics-2015 update : A report from the American Heart Association*. *Circulation* **131,** (2015).

111. Schwenke, D. C. & Carew, T. E. Initiation of atherosclerotic lesions in cholesterol-fed rabbits. II. Selective retention of LDL vs. selective increases in LDL permeability in susceptible sites of arteries. *Arteriosclerosis* **9,** 908–18 (1989).

112. Davies, P. F. Flow-mediated endothelial mechanotransduction. *Physiol. Rev.* **75,** 519–560 (1995).

113. Galkina, E. & Ley, K. Vascular adhesion molecules in atherosclerosis. *Arterioscler. Thromb. Vasc. Biol.* **27,** 2292–2301 (2007).

114. Moore, K. J. & Freeman, M. W. Scavenger receptors in atherosclerosis: Beyond lipid uptake. *Arterioscler. Thromb. Vasc. Biol.* **26,** 1702–1711 (2006).

115. Libby, P. Changing concepts of atherogenesis. *J. Intern. Med.* **247,** 349–358 (2000).

116. Heusch, G. *et al.* Cardiovascular remodelling in coronary artery disease and heart failure. *Lancet* **383,** 1933–1943 (2014).

117. Bench, T. J., Jeremias, A. & Brown, D. L. Matrix metalloproteinase inhibition with tetracyclines for the treatment of coronary artery disease. *Pharmacol. Res.* **64,** 561–566 (2011).

118. Scientific Steering Committe on behalf of the Simon Broome Register Group. Risk of fatal coronary heart disease in familial hypercholesterolaemia. *BMJ* **303,** 893–896 (1991).

119. Williams, R. R. *et al.* Diagnosing heterozygous familial hypercholesterolemia using new practical criteria validated by molecular genetics. *Am. J. Cardiol.* **72,** 171–176 (1993).

120. Ito, M. K. & Watts, G. F. Challenges in the Diagnosis and Treatment of Homozygous Familial Hypercholesterolemia. *Drugs* **75,** 1715–1724 (2015).

121. Gagné, C., Gaudet, D. & Bruckert, E. Efficacy and safety of ezetimibe coadministered with atorvastatin or simvastatin in patients with homozygous familial hypercholesterolemia. *Circulation* **105,** 2469–2475 (2002).

122. Raal, F. J. *et al.* Mipomersen, an apolipoprotein B synthesis inhibitor, for lowering of LDL cholesterol concentrations in patients with homozygous familial hypercholesterolaemia: a randomised, double-blind, placebo-controlled trial. *Lancet* **375,** 998–1006 (2010).

123. ENDO, A. A historical perspective on the discovery of statins. *Proc. Japan Acad. Ser. B* **86,** 484–493 (2010).

124. Marais, A. D. *et al.* A dose-titration and comparative study of rosuvastatin and atorvastatin in patients with homozygous familial hypercholesterolaemia. *Atherosclerosis* **197,** 400–406 (2008).

125. Stroes, E. S. *et al.* Statin-associated muscle symptoms: impact on statin therapy - European Atherosclerosis Society Consensus Panel Statement on Assessment, Aetiology and Management. *Eur. Heart J.* **36,** 1012–1022 (2015).

126. Sattar, N., Preiss, D. & Murray, H. M. Statins and risk of incident diabetes: A collaborative meta-analysis of randomised statin trials. *Rev. Port. Cardiol.* **29,** 1077–1078 (2010).

127. Mach, F. *et al.* Adverse effects of statin therapy: perception vs. the evidence – focus on glucose homeostasis, cognitive, renal and hepatic function, haemorrhagic stroke and cataract. *Eur. Heart J.* **0,** 1–18 (2018).

128. Gille, A., Bodor, E. T., Ahmed, K. & Offermanns, S. Nicotinic Acid: Pharmacological Effects and Mechanisms of Action. *Annu. Rev. Pharmacol. Toxicol.* **48,** 79–106 (2008).

129. Julius, U. History of lipidology and lipoprotein apheresis. *Atheroscler. Suppl.* **30,** 1–8 (2017).

130. Chang, Y. & Robidoux, J. Dyslipidemia management update. *Curr. Opin. Pharmacol.* **33,** 47–55 (2017).

131. Scaldaferri, F., Pizzoferrato, M., Ponziani, F. R., Gasbarrini, G. & Gasbarrini, A. Use and indications of cholestyramine and bile acid sequestrants. *Intern. Emerg. Med.* **8,**

205–210 (2013).

132. Davidson, M. H. A systematic review of bile acid sequestrant therapy in children with familial hypercholesterolemia. *J. Clin. Lipidol.* **5,** 76–81 (2011).

133. Altmann, S. W. Niemann-Pick C1 Like 1 Protein Is Critical for Intestinal Cholesterol Absorption. *Science (80-.).* **303,** 1201–1204 (2004).

134. Temel, R. E. *et al.* Hepatic Niemann-Pick C1-like 1 regulates biliary cholesterol concentration and is a target of ezetimibe. *J. Clin. Invest.* **117,** 1968–1978 (2007).

135. Rosenson, R. S., Hegele, R. A., Fazio, S. & Cannon, C. P. The Evolving Future of PCSK9 Inhibitors. *J. Am. Coll. Cardiol.* **72,** 314–329 (2018).

136. Robinson, J. G. *et al.* Determining When to Add Nonstatin Therapy. *J. Am. Coll. Cardiol.* **68,** 2412–2421 (2016).

137. Zodda, D., Giammona, R. & Schifilliti, S. Treatment Strategy for Dyslipidemia in Cardiovascular Disease Prevention: Focus on Old and New Drugs. *Pharmacy* **6,** 10 (2018).

138. Polychronopoulos, G. & Tziomalos, K. Novel treatment options for the management of heterozygous familial hypercholesterolemia. *Expert Rev. Clin. Pharmacol.* **10,** 1375–1381 (2017).

139. Thompson, G. R. *et al.* Severe hypercholesterolaemia: Therapeutic goals and eligibility criteria for LDL apheresis in Europe. *Curr. Opin. Lipidol.* **21,** 492–498 (2010).

140. Julius, U. Current Role of Lipoprotein Apheresis in the Treatment of High-Risk Patients. *J. Cardiovasc. Dev. Dis.* **5,** (2018).

141. Catapano, A. L. *et al.* ESC / EAS Guidelines for the management of dyslipidaemias The Task Force for the management of dyslipidaemias of the European Society of Cardiology (ESC) and the European Atherosclerosis Society (EAS) , . **217,** 3–46 (2011).

142. Gylling, H. *et al.* Plant sterols and plant stanols in the management of dyslipidaemia and prevention of cardiovascular disease qq. **232,** 346–360 (2014).

143. Shishikura, Y., Khokhar, S. & Murray, B. S. Effects of tea polyphenols on emulsification of olive oil in a small intestine model system. *J. Agric. Food Chem.* **54,** 1906–1913 (2006).

144. Cameron, J., Ranheim, T., Kulseth, M. A., Leren, T. P. & Berge, K. E. Berberine decreases PCSK9 expression in HepG2 cells. **201,** 266–273 (2008).

145. Li, H. *et al.* Hepatocyte Nuclear Factor 1α Plays a Critical Role in PCSK9 Gene Transcription and Regulation by the Natural Hypocholesterolemic Compound Berberine. *J. Biol. Chem.* **284,** 28885–28895 (2009).

146. Chen, C., Yang, J., Uang, Y. & Lin, C. Improved dissolution rate and oral bioavailability of lovastatin in red yeast rice products. *Int. J. Pharm.* **444,** 18–24 (2013).

147. Steering, S. & Register, B. Mortality in treated heterozygous familial hypercholesterolaemia: implications for clinical management. Scientific Steering Committee on behalf of the Simon Broome Register Group. *Atherosclerosis* **142,** 105–12 (1999).

148. Palacios, L. *et al.* Molecular characterization of familial hypercholesterolemia in Spain. *Atherosclerosis* **221,** 137–142 (2012).

149. Civeira, F. *et al.* Comparison of Genetic Versus Clinical Diagnosis in Familial Hypercholesterolemia. *Am. J. Cardiol.* **102,** (2008).

150. Starr, B. *et al.* Development of sensitive and specific age- and gender- specific low-density lipoprotein cholesterol cutoffs for diagnosis of first-degree relatives with familial hypercholesterolaemia in cascade testing. **46,** 791–803 (2008).

151. Benito-Vicente, A. *et al.* The importance of an integrated analysis of clinical, molecular, and functional data for the genetic diagnosis of familial hypercholesterolemia. *Genet. Med.* **17,** 980–988 (2015).

152. Huijgen, R., Kindt, I., Defesche, J. C. & Kastelein, J. J. P. Cardiovascular risk in relation to functionality of sequence variants in the gene coding for the low-density lipoprotein receptor: A study among 29 365 individuals tested for 64 specific low-density lipoprotein-receptor sequence variants. *Eur. Heart J.* **33,** 2325–2330 (2012).

153. Strøm, T. B., Tveten, K. & Leren, T. P. PCSK9 acts as a chaperone for the LDL receptor in the endoplasmic reticulum. *Biochem. J.* **457,** 99–105 (2014).

154. Benito-Vicente, A. *et al.* Validation of LDLr Activity as a Tool to Improve Genetic Diagnosis of Familial Hypercholesterolemia: A Retrospective on Functional Characterization of LDLr Variants. *Int. J. Mol. Sci.* **19,** 1676 (2018).

General objectives

FH is the most serious commonly inherited metabolic disease and, with an estimated frequency of 1:200 - 1:250, remains severely underdiagnosed. Autosomal dominant mutations in *LDLR*, *APOB*, and *PCSK9* genes account for most of the FH cases and although genetic testing can contribute to patients' benefit, only the identification of functional FH-causing mutation provides a definitive diagnosis. To date, there have been described more than 2,500 genetic *LDLR* variants*, 376 APOB variants of uncertain* significance, and 46 *PCSK9* variants. Since the great majority of them do not have functional studies, identification of the pathogenic variants causing FH is priority, as it would provide a definitive diagnosis, which is essential to improve patient prognosis.

Therefore, **the main objective of the present work has been to develop a reliable assay for the functional characterization and assignment of LDLR class type mutation of LDLR variants**.

Specific objectives:

- Functional characterization and classification of *LDLR* variants.
- Functional characterization of *PCSK9* variants.
- To study the effect caused by the insertion of two leucines (p.Leu22_Leu23dup) in the leucine stretch of the PCSK9 signal peptide on protein activity.
- Functional characterization of *APOB* variants.

Chapter 2 / 2. Atala

Metodologia esperimentalak

2.1 Metodologia esperimental orokorra

2.1.1 Gene-aldaera ezberdinen izendapena

DNA osagarriaren numerazioa Human Genome Variant Socity esandakoaren arabera agertzen da non c.1 nukleotidoa ATG hasiera kodoiaren adeninari dagokio[1,2]. LDLR sekuentzia ezberdinen analisirako NM_000527.4 erreferentzia sekuentzia erabili da eta PCSK9 sekuentzia ezberdinen analisirako NM_174936.3 erreferentzia.

2.1.2 Mutagenesi guneratua

Aldaera ezberdinak kodetzen dituzten plasmidoak sortzeko 2.1 taulan aipatzen diren oligonukleotido ezberdinak erabili dira. Mutazio ezberdinak, *LDLR* (NM_000527.4) edo *PCSK9* (NM_174936.3) kodetzen dituzten sekuentziak adierazpen bektorreak XXX taulan agertzen diren bektoreetan sartu dira mutagenesi guneratua erabiliz. Mutagenesi guneratua aurrera eramateko Agilent konpainiako Quick Change Lighting mutagenesis sistema erabili da produktuak ekarritako argibideak jarraituz. Nukleotidoaren aldaketa egokia polimerasaren kate-erreakzio (PCR, ingelestik *Polimerase Chain Reaction*) bidez ziurtatu da eta murrizte-entzimen bidez *LDLR*-aren osotasuna egiaztatu da.

2.1.3 *In silico* analisia

Proteina mutante ezberdienen efektua sarrera libreko software bitartez aurreikusi egin da hurrengo sofwerrak erabiliz: PolyPhen-2 [3], Sorting Tolerant From Intolerant (SIFT) [4], Consensus Deleteriousness core of missense SNVs (Condel) [5], Mutation taster [6], Grantham Score [7] eta PhyloP [8]. Polyphen softwareak 3 kategori ezberdinetan banatzen ditu aldaera ezberdinak, ¨Probably damaging¨, ¨Posibly Damaging¨ edo ¨Benign¨. SIFT eta CONDEL programak aminoazido aldaketak ¨Deleterious¨edo¨Neutral¨ kategorietan ezberdintzen dituzte kaltegarriak edo efektu gabekoak diren arabera. Mutation Taster porgramak ¨Disease Causing¨ edo ¨Polymorphism¨

terminoen barruan multzokatzen ditu. Granthan programak ordea aminoazido aldaketa bakoitzari balio bat ematen dio kontserbakorra (0-50), nahiko kontserbakorra (50-100), nahiko erradikala (100-150) edo erradikala (≥150) den arabera. Azkenik, PhyloP (phlylogenetic p-value) programak -14.1-etik 6.4-ra doan eskala baten arabera klasifikatzen ditu aldatzen diren nukleotidoak (zenbaki handienak espezie arteko kontserbazio maila altuena duten nukleotidoak izanik). RNAren moztu-itsaste guneetan aurkitzen diren aldaeretan ordea funtzio galera aurreikusteko software ezberdinak erabili behar izan dira, hala nola Splice-Site Predictor (Splice Port) [9], Neural Network Splice Site Prediction Tool (NNSSP) [10], and Neural Network Predictions of Splice Sites in Humans (NerGen2)[11].

2.1 Taula. Gure taldeak aztertutako LDLR eta PCSK9 aldaerak eta hauek sintetizatzeko erabilitako hazleak.

gene originala	Plasmidoa	Aldaera	Erabilitako oligonuklotidoa*
LDLR	pcDNA3	c.135C>G p.(Cys46Gly)	Fw: 5'-TACAAGTGGGTCG**G**GATGGCAGCGC-3' Rv: 5'-GCGCTGCCATCG**C**CGACCCACTTGTA-3'
LDLR	pcDNA3	c.226G>T p.(Gly76Trp)	Kindly provided by Mafalda Bourbon
LDLR	pcDNA3	c. 292G>A (p.Gly98Ser)	Kindly provided by Luya Wang
LDLR	pcDNA3	c.346T>C (p.Cys116Arg)	Fw: 5´GGACGAGTTTCGC**C**GCCACGATGGGA 3´ Rw: 5´TCCCATCGTGGC**G**GCGAAACTCGTCC 3´
LDLR	pcDNA3	c.464G>A (p.Cys155Tyr)	Fw: 5´ CGCCAGCTTCCAGT**A**CAACAGCTCCACC 3´ Rw: 5´ GGTGGAGCTGTTGT**T**ACTGGAAGCTGGCG 3´
LDLR	pcDNA3	c.502G>A (p.Asp168Asn)	Fw: 5´ 5´CTGTGGGCCTGC**A**ACAACGACCCCG 3´ Rw: 5´CGGGGTCGTTGT**T**GCAGGCCCACAG 3´
LDLR	pcDNA3	c.514G>A (p.Asp172Asn)	Fw: 5´GCGACAACGACCCC**A**ACTGCGAAGATGG 3´ Rw: 5´CCATCTTCGCAG**T**TGGGGTCGTTGTCGC 3´
LDLR	pcDNA3	c.769C>T (p.Arg257Trp)	Fw: 5´GCCGGCAGTGTGAC**T**GGGAATATGACTGC 3´ Rw: 5´GCAGTCATATTCCC**A**GTCACACTGCCGGC 3´
LDLR	pcDNA3	c.806G>A (p.Gly269Asp)	Kindly provided by Mafalda Bourbon
LDLR	pcDNA3	c.829G>A (p.Glu277Lys)	Kindly provided by Mafalda Bourbon
LDLR	pcDNA3	c.862G>A (p.Glu288Lys)	Kindly provided by Mafalda Bourbon
LDLR	pcDNA3	c. 890A>C (p.Asn297Thr)	Kindly provided by Luya Wang
LDLR	pcDNA3	c.895G>A (p.Ala299Thr)	Kindly provided by Mafalda Bourbon
LDLR	pcDNA3	c.898A>G (p.Arg300Gly)	Fw: 5´CTGCAACATGGCT**G**GAGACTGCCGGG 3´ Rw: 5´CCCGGCAGTCTC**C**AGCCATGTTGCAG 3´
LDLR	pcDNA3	c.902A>G (p.Asp301Gly)	Fw: 5´ACATGGCTAGAG**G**CTGCCGGGACTGG 3´ Rw: 5´CCAGTCCCGGCAG**C**CTCTAGCCATGT 3´
LDLR	pcDNA3	c.1216C>T (p.Arg406Trp)	Kindly provided by Mafalda Bourbon
LDLR	pcDNA3	c.1246C>T (p.Arg416Trp)	Fw: 5´GATGACGCTGGAC**T**GGAGCGAGTACACC 3´ Rw: 5´ GGTGTACTCGCTCC**A**GTCCAGCGTCATC 3´
LDLR	pcDNA3	c.1285G>C (p.Val429Leu)	Kindly provided by Mafalda Bourbon
LDLR	pcDNA3	c.1322T>C (p.Ile441Thr)	Kindly provided by Mafalda Bourbon
LDLR	pcDNA3	c.1336 C>G (p.Leu446Val)	Fw: 5' GAATCTACTGGTCTGAC**G**TGTCCCAGAGAATGATC 3' Rw: 5' GATCATTCTCTGGGACA**C**GTCAGACCAGTAGATTC 3'
LDLR	pcDNA3	c.1361C>A (p.Thr454Asn)	Fw: 5´ GAATGATCTGCAGCAA**C**CAGCTTGACAGAGCC 3´ Rw: 5´ GGCTCTGTCAAGCTGG**T**TGCTGCAGATCATTC 3´
LDLR	pcDNA3	c.1468T>C (p.Trp490Arg)	Fw: 5´ CACAGCAACATCTAC**C**GGACCGACTCTGTCC3´ Rw: 5´ GGACAGAGTCGGTCC**G**GTAGATGTTGCTGTG3´
LDLR	pcDNA3	c.1633G>T (p.Gly545Trp)	Kindly provided by Mafalda Bourbon
LDLR	pcDNA3	c.1723G>T (p.Leu575Phe)	Kindly provided by Luya Wang
LDLR	pcDNA3	c.1729T>G (p.Trp577Gly)	Fw: 5´ GTGGCCGCCTCTAC**G**GGGTTGACTCC 3´ Rw: 5´ GGAGTCAACCC**C**GTAGAGGCGGCCAC 3´
LDLR	pcDNA3	c.1744C>T (p.Leu582Phe)	Kindly provided by Luya Wang
LDLR	pcDNA3	c.1942T >C (p.Ser648Pro)	Kindly provided by Mafalda Bourbon
LDLR	pcDNA3	c.2053C>T (p.Pro685Ser)	Kindly provided by Mafalda Bourbon
LDLR	pcDNA3	c.2475C>A (p.Asn825Lys)	Fw: 5´ GCATCAACTTTGACAA**A**CCCGTCTATCAGAAGACC 3´ Rw: 5´ GGTCTTCTGATAGACGGG**T**TTGTCAAAGTTGATGC 3´
LDLR	pcDNA3	c.2575G>A (p.Val859Met)	Kindly provided by Mafalda Bourbon
EC-LDLR-His	pcDNA3	LDLR Δ789-860	Kindly provided by proffesor Leren
PCSK9	pCMV-PCSK9-FLAG	--	kindly provided by Prof. Horton
PCSK9	pCMV-PCSK9-FLAG	c.60_65dupGCTGCT	Fw: 5´ GCTGCTGCT**GCTGCT**GCTGCTGCTGCTCCTGG 3´ Rw: 5´ CCAGGAGCAGCAGC**AGCAGC**AGCAGCAGCAGC 3´
PCSK9	pCMV-PCSK9-FLAG	c.63_65delGCT	Fw: 5´ CCACTGCTGCTGCTGCTGCTGCTCCTGG 3´ Rw: 5´ CCAGGAGCAGCAGCAGCAGCAGTGG 3´
PCSK9	pCMV-PCSK9-FLAG	C.185C>A(p.Ala62Asp)	Kindly provided by Mafalda Bourbon
PCSK9	pCMV-PCSK9-FLAG	c.991C > G (p.Pro331Ala)	Fw: 5' CCAGCCTCAGCT**G**CCGAGGTCATCAC 3' Rw: 5' GTGATGACCTCGG**C**AGCTGAGGCTGG 3'
PCSK9	pCMV-PCSK9-FLAG	c.1069C > T (p.Arg357Cys)	Kindly provided by Giuliana Di Taranto
PCSK9	pCMV-PCSK9-FLAG	c.1120G>T (p.Asp374Pro)	Fw: 5´GGTGCCTCCAGC**T**ACTGCAGCACCTG3´ Rw: 5´CAGGTGCTGCAGTA**G**CTGGAGGCACC3´
PCSK9	pCMV-PCSK9-FLAG	c.1399C > G (p.Pro467Ala)	Kindly provided by Mafalda Bourbon
PCSK9	pCMV-PCSK9-FLAG	c.1496A > G (p.Arg499His)	Fw: 5' GGCGGGGCGAGC**A**CATGGAGGCCCAAG 3' Rw: 5' CTTGGGCCTCCATG**T**GCTCGCCCCGCC 3'
PCSK9	pCMV-PCSK9-FLAG	c.1906A > C (p.Ser636Arg)	Fw: 5' CTGACTGGCTGC**C**GTGCCCTCCCTG 3' Rw: 5' CAGGGAGGGCAC**G**GCAGCCAGTCAG 3'
PCSK9	pCMV-PCSK9-FLAG	c.1928A > G (p.His643Arg)	Fw: 5' CTGGGACCTCCC**G**CGTCCTGGGGGC 3' Rw: 5' GCCCCCAGGACG**C**GGGAGGTCCCAG 3'

*aldatutako nukleotidoa letra beltzez agertzen da

2.1.4 Zelula eukariotoen hazkuntza

HepG2 zelulak giza hepatoma zeluletatik abiatuz sortutako zelulak dira. Zelulak "Flask" oinarriari itsatsita hazten dira, DMEM medioan (Low glucose 1 g/L, GE, Healthcare, EEUU). DMEM medioari inaktibatutako

%10 (b/b) idi-umeki seruma (FBS, ingelesetik *fetal bovine serum*) (Lonza, Belgika), 100 U/mL penizilina, 100 µg/mL estreptomizina eta 4 mM glutamina (Invitrogen, USA) gehitu zaizkio. Zelula hauek 37 °C-tan eta % 5-ko CO_2-dun atmosferan hazi dira.

Huh7 zelulak giza hepatoma zeluletatik abiatuz sortutako zelulak dira. Zelulak "Flask" oinarriari itsatsita hazten dira, DMEM medioan (Low glucose 1 g/L, GE, Healthcare, EEUU). DMEM medioari inaktibatutako %10 (b/b) FBS (Lonza, Belgika), 100 U/mL penizilina, 100 µg/mL estreptomizina eta 4 mM glutamina (Pen Strep Glutamine, Invitrogen) gehitu zaizkio. Zelula hauek 37 °C-tan eta % 5-ko CO_2-dun atmosferan hazi dira.

CHO-*ldl*Δ7 hamster obulutegietatik isolatutako fibroblastoak dira. 1981. urtean Monty Kriegerrek isolatu zituen lehenengo aldiz[12]. Zelula hauen berezitasun nabarmenena LDLR kodetzeko ezintasuna da eta ondorioz LDLR aldaeren karakterizazio funtzionala egiteko zelula oso aproposak dira. Zelulak "Flask" oinarriari itsatsita hazten dira, HAM´s-F12 medioan (Nutirent mixture F-12 HAM, Sigma-Aldrich, EEUU). Hams-F12 medioari inaktibatutako %10 (b/b) FBS (Lonza, Belgika), 100 U/mL penizilina, 100 µg/mL estreptomizina eta 4 mM glutamina (Pen Strep Glutamine, Invitrogen) gehitu zaizkio. Zelula hauek 37 °C-tan eta % 5-ko CO_2-dun atmosferan hazi dira.

U937 zelulak, giza linfoma batetik abiatuta sortu diren zelulak dira. Zelula hauek RPMI medioan hazten dira zeinari inaktibatutako %10 (b/b) FBS (Lonza, Belgika), 100 U/mL penizilina, 100 µg/mL estreptomizina eta 4 mM glutamina (Pen Strep Glutamine, Invitrogen) gehitzen zaizkio. Zelula hauek ez daukate 3-ketoredukatasa entzima aktibitatea eta ondorioz ez dira kolesterol propioa sintetizatzeko kapazak. Zelula hauek 37 °C-tan eta % 5-ko CO_2-dun atmosferan hazi dira.

HEK 293 zelulak, giza enbrioi jatorrizko giltzurrun zelulen transformazioz sortutakoak dira. HEK293 zelulak hazteko % 10 FBS eta % 1

penizilina/estreptomizina-dun DMEM medioan inkubatu dira 37 °C-tan % 5-ko CO_2-dun atmosferan. Zelula hauek bere metabolismo azkarraren ondorioz hautatu dira.

2.1.5 Erabilitako transfekzio sistemak

2.*1.5.1 Kaltzio fosfato bidezko transfekzio iragankorra*

Transfekzioa baino 4 ordu lehenago, zelulak antibiotikorik gabeko medioan diluitzen dira transfekzio egunean zelulek % 40 inguruko baterakuntza izan dezaten. Transfekzioa egiterakoan, saiodi batean, transfekatatu nahi den putzuari dagokion 250 mM $CaCl_2$ bolumena eta transfektatu nahi diren plasmidoak gehitzen dira. Ondoren pipeta baten laguntzaz tantaka-tantaka giro tenperaturan dagoen HBS 2x (50 mM HEPES, 1,5 mM Na_2HPO_4 eta 140 mM NaCl pH 7,05-ra doituta) gehitu da saiodira, aldi berean nahasketa mugitzen den bitartean osagai guztien banaketa homogeneoa lortzeko. Nahasketa minutu batez giro tenperaturan inkubatu ondoren putzura gehitu da kontu handiz, zelulak ez daitezen plakatik desitsatsi. 24 orduko inkubazioaren ondoren transfekzio soluzioa kendu eta zelulei antibiotikodun hazkuntza medio berria gehitzen zaie.

2.1.5.1.1 HEK293 zelulen transfekzio egonkorrak

Zelulak kaltzio kloruroz transfektatu ostean 24 orduz utzi dira transfekziodun medioa. 24 orduak pasatu eta gero, DMEM medioei plasmidoek daukaten erresistentziaren aurkako antibiotikoa gehitu zaie, gure kasuan, genetizina (sc-29065A, Santa Cruz) 0.5mg/ml-ko kontzentrazioan erabili da. Zelula hauei pase ezberdinak eman zaizkie genetizinadun medio honetan zelula heriotza tasa 0 inguruan egon arte. Momentu honetan zelula guztiak era egonkorrean trasnfektatuta daudela esan daiteke.

2.1.5.2 Lipofektamina bidezko transfekzio iragankorra

Lipofektamina transfekzio teknikak, positiboki kargatutako liposometan oinarrituta daude. Hauek, negatiboki kargatutako zelula mintzekin efizientzia handiz elkarrekiten dute eta endozitosi bidez barneratzen dira.

Transfekzioa egiterakoan, saiodi batean, transfekatatu nahi den putzuari dagokion lipofektamina bolumena eta transfektatu nahi diren plasmidoak gehitzen dira. Zelulak % 50-eko konfluentziara ailegatzen direnean Opti-Mem medioan diluitzen dira. 24 orduren ostean Lipofektamina-DNA mixak prestatzen dira eta zelula medioei gehitzen zaizkie. 6 orduren ostean Opti-Mem medio honi % 5 FBS gehitzen zaio zelulen biziraupen tasa hobetzeko eta 48 orduz uzten dira inkubatzen adierazpen maila maximoa lortu arte.

2.2 **Taula.** Erabilitako lipofektamina kantitatea plakaren arabera.

		24 well	6 well
Seed cells	Cells	50.000 cells	300.000 cells
Lipofectamine mix	Opti-MEM Medium	25 µl	150 µl
	Lipofectamine LTX Reagent	1 µl	5 µl
DNA mix	Opti-MEM Medium	25 µl	150 µl
	Plus Reaent	1 µl	5 µl
	Diluted DNA	1 µg	5 µg
	Dilute DNA mix into Lipofectamine 1:1 ratio		
	DNA -lipid complex per well	50 µl	300 µl

2.1.6 Alderantzizko transkripzio-polimerasaren kate-erreakzio kuantitatiboa

Alderantzizko transkripzio-polimerasaren kate-erreakzio kuantitatiboa (qRT-PCR, ingelesetik *Quantitative reverse transcriptase polymerase chain reaction*) proteina ezberdinen RNA mezulari maila neurtzeko erabili da. Zelula ezberdinen RNA TRIZOL erreaktiboa (Invitrogen) erabiliz erauzi egin da. DNA osagarria (cDNA, ingelesetik *complemtary DNA*) Affinity Script qRT-PCR cDNA sintesi kit-a (Stratagene, Agilent Technologies, USA) erabiliz sintetizatu egin da RNA 1µg batetik abiatuta eta produktuak ekarritako argibideak jarraituz. Polimerasa kate-erreakzio kuantitatiboa (qPCR, ingelesetik *Quantitative polymerase chain reaction*) Brilliant-III Ultra Fast SYBR qPCR-a erabiliz egin da lagin bakoitza hiru biderrez errepikatuz. Intereseko genearen cDNA-kantitatea jatorrizko cDNA kantitate totalarekiko normalizatzeko adierazpen egonkorreko *GAPDH* genea erabili da. *qPCR erreakzioak Applied Biosystem 7900HT Fast Real-Time PCR*

System aparatuan egin dira. Erabilitako programak 10 minutuko inkubazio bat dauka 95°C-tan 40 zikloz jarraitua, ziklo hauetan laginak 95°C arte berotzen dira 15 segundoz segituan minutu bat usteko 60°C-tan. Gene bakoitza amplifikatzeko erabili diren hazleak 2.3 taulan ageri dira.

2.3 Taula. *Gene ezberdinen RNA mezularia anplifikatzeko erabilitako hazleak.*

Gene	Forward Primer Sequence (5' -> 3')	Reverse Primer Sequence (5' -
LDLR	CATGTTCCAGTATGACTCCACTC	CATGTTCCAGTATGACTCCACTC
PCSK9	ACGTCGAGGCGCTCATGGTT	TGGCAGCGGCCACCAGGA
GAPDH	GGAGCGAGATCCCTCCAAAAT	GGCTGTTGTCATACTTCTCATGG

2.1.7 Western plapaketa bidezko analisia

Transfektatu eta 48 ordu pasa ondoren, zelulen medioa kendu eta 300 µl liseriketa medioaz (50 mM Tris–HCl, pH 7.5, 125 mM NaCl, 1% Nonidet P-40, 5.3 mM NaF, 1.5 mM NaP, 1 mM orthovanadate, 1 mg/ml protease inhibitor cocktail (Roche), and 0.25 mg/ml Pefabloc, 4-(2-aminoethyl)-benzenesulfonyl fluoride hydrochloride (AEBSF; Roche) ordezkatu da. Liseritutako zelula jalkinak western plakaketa bidezko analisi semi-kuantitatibo bat burutzeko prestatu dira. Horretarako proteinen kontzentrazioa neurtu da eta pisu molekularraren arabera sodio dodezil sulfatozko poliakrilamidazko elekroforesi gelak erabiliz (SDS-PAGE) banatu dira. Nitrozelulozazko mintzak ordubetez inkubatu dira blokeo soluzioan (TBST + % 5 esne gaingabetua) lotura inezpezifikoak ekiditeko eta antigorputz primarioekin inkubatu dira 16 orduz 4℃-tan. 3 TBST garbiketa egin ostean, mintza HRP- (ingelesetik, horseradish peroxidase) konjugatutako antigorputz sekundarioarekin ordu batez giro tenperaturan inkubatu dira. proteinen detekzioa ECL-Plus Western plapaketarako erreaktibo kimioluminiszentearekin (Pierce Biotechnology, Rockford, IL, USA) inkubatu da eta bistaratzea ChemiDoc XRS-a (Bio-Rad, Hercules, CA, USA) erabiliz burutu da Quantitiy One Basic 4.4.0 software-a (Bio-Rad) erabiliz banda ezberdinen intentsitatea neurtzeko. Antigorputzen kontzentrazioak, kontzentrazio-seinale proportzional bat eta seinale ez-

espezifiko gutxien agertzeko optimizatu dira. Erabilitako antigorputzak 2.4 taulan ageri dira.

2.4 Taula: Western plapaketan erabilitako antigorputz zerrenda

Ab	Merkataritzaetxe	Erreferentzia	Mw (KDa)	Diluzioa	Inkubazioa	
					Debora	Tenperatura
LDL Receptor Polyclonal Antibody*	Cayman	10007665	120/160	1:500	16 ordu	4°C
GAPDH Antibody	Santa Cruz	SC-47724	35.8	1:1000	16 ordu	4°C
PCSK9 Polyclonal Antibody	Cayman	10240	74/63	1:1000	16 ordu	4°C
DYKDDDDK Tag Antibody (L5)	Thermo	MA1-142	--	1:1000	16 ordu	4°C
Anti-Calreticulin antibody	Abcam	ab39818	48	1:1000	16 ordu	4°C
Anti-rabbit IgG, HRP-linked Antibody	Cell Signaling	7074	--	1:2000	1 ordu	25°C
Anti-mouse IgG, HRP-linked Antibody	Cell Signaling	7076	--	1:2000	1 ordu	25°C
Anti-rat IgG, HRP-linked Antibody	Cell Signaling	7077	--	1:2000	1 ordu	25°C

*LDLR western plapaketetan erabilitako tanpoi indargetzaileek 2 mM $CaCl_2$ daukate

2.1.8 LDL purifikazioa

Dentsitate baxuko proteinak eta dentsitate oso baxuko proteinak pazienteei ateratako odoletik banatu dira. Horretarako lehenbizi EDTA hodietan ateratako odola 30 minutuz 12,000 x g-tan zentrifugatu da odoleko seruma eta zelulak banatu ahal izateko. Odol serumetik LDL-k edo VLDL-k beste proteinetatik banatzeko KBr erabiliz bi faseko gradiente bat sortzen da. Beheko fasean seruma *jartzen* da (LDL-aren kasuan KBr gehituko zaio 1.21 g/ml dentsitatera heldu arte) eta goiko fasean PBS indargetzailea. Laginak 244,500 x g-ko abiaduran zentrifugatzen dira 19 orduz eta 4°C-tan. Bukatzeko LDL edo VLDL-ei dagokien bandak berreskuratzen dira (2.1 Irudia).

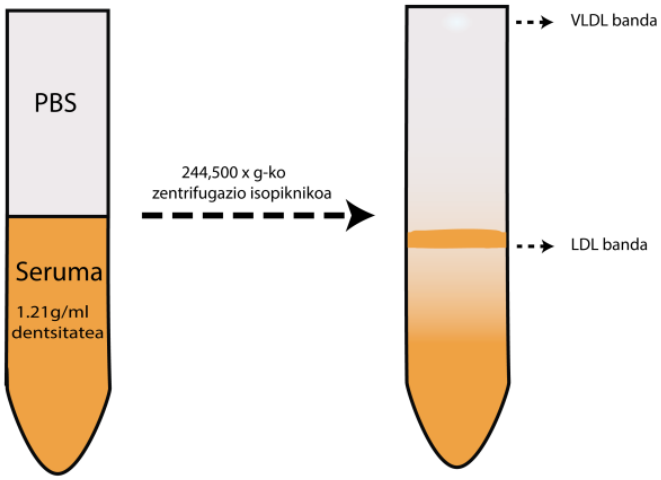

2.1 Irudia. LDL purifikazioa zentrifugazio isopikniko baten bitartez.

2.1.9 FITC bidezko lipoproteinaren markaketa

LDL partikulak FITC fluoroforoa (ingelesatik (ingelesetik, Fluorescein isothiocyanate) erabiliz markatu dira aurretiaz deskribatutako metodologia jarraituz [13]. Laburki, 0.1M Na_2HPO_4 (pH=9) indargetzailean dagoen LDL ml bakoitzeko (1mg/ml) 10µl FITC (1.8mg/ml, dimetil solfoxidoan disolbatua) nahastu zaizkio. Nahastea 2 orduz irabiatu da giro tenperaturan. Lotu ez den fluoroforo soberakina kentzeko LDL-ak PBS-an orekatutako sephadex G25 gel iragazpen zutabe batetik pasatu dira. Lagin guztien proteina kontzentrazioa behi serumaren albumina (BSA, ingelesetik, *Bovine Serum Albumin*) estandar moduan erabiliz neurtu da, Pierce BCA proteina neurketa metodoa erabiliz (Pierce BCA protein assay, Pierce).

2.1.10 Fluxu-zitometria

Fluxu-zitometria zelulen analisirako parametro anitzeko teknika da. Bertan, aztertu behar diren partikulen esekidura (gehienetan zelulak) banan bana alienatuta laser batetik pasarazten dira. Laserrak zelulekin talka egitean informazioa ematen duten seinale desberdinak igortzen ditu, argiaren dispertsioarengatik eta fluoreszentzia igorpenarengatik. Zelula bakoitzetik detektatzen diren parametroak hauek dira:

- Argiaren dispertsio frontala (ingelesez “foward scatter”, FSC): Partikulak duen tamainarekiko proportzionala den parametroa da.

- Angelu zuzeneko dispertsioa (ingelesez “Side Scatter” SSC): zelulak duen barne konplexutasunarekiko proportzionala da
- Fluoreszentzi intentsitatea uhin luzera desberdinetan: Zelulak saioan jasan duen markaketa edo fluorokromoaren araberakoa izango da

2.1.10.1 Fluxu-zitometria bidezko LDLR adierazpena

Esperimentua bukatutakoan, zelulak 3 aldiz garbitu dira PBS %1-BSA indargetzailearekin, 10 minutuz fixatu dira %4 paraformaldehidoan, berriro garbitu eta ordu batez blokeatzen jarri dira giro tenperaturan %5 FBS-dun garbiketa tampoian. Hartzailearen detekziorako LDLR-ren aurkako antigorputzarekin (1:100; 5mg/L; Progen Biotechnik GmbH, Cat No. 61087) inkubatu dira 4 ºC-tan gau osoz. Hurrengo pausuan 3 garbiketa berri egin dira eta arratoiaren aurkako Alexa Fluor 488 floroforoarekin konjugatutako antigorputz sekundarioarekin (1:200; Molecular Probes; Cat No. A-11001) inkubatu dira, ordu batez, giro tenperaturan. LDLR-ren aurkako antigorputzaren funtzionamendu egokia eta espezifizitatea bermatzeko, LDLR basatia kodetzen duen plasmidoaz edo plasmido utz batez transfekatutako CHO-*ldl*Δ7 zelulak erabili dira. Saio guztiak hiru bider errepikatu dira eta 10.000 zelulen intentsitatea neurtu da lagin bakoitzeko Fascalibur Fluxu zitometroa erabiliz eta zitometroak ekarritako argibideak jarraituz aurretiaz deskribatu den moduan [14]. Grafikoetan datuak LDLR basatian lortutako maximoarekiko portzentaje moduan irudikatzen dira.

2.1.10.2 Fluxu-zitometria bidezko LDLR-LDL lotura-tasaren kuantifikazioa

Esperimentutan erabilitako zelulak 2 orduz inkubatu dira 4°C-tan LDLR eta LDL-FITC partikulen arteko lotura-tasa zehazteko. LDL-FITC inkubazioaren ostean zelulak hiru aldiz garbitu dira PBS-%1-BSA indargetzailea erabiliz, 10 minutuz %4 paraformaldehidoan fixatu dira eta berriro garbitu dira PBS-%1-BSA indargetzailean. Fluoreszentzia intentsitateak fluxu zitometria bidez neurtu dira, Fascalibur Fluxu zitometroa erabiliz eta zitometroak ekarritako argibideak jarraituz aurretiaz deskribatu

den moduan [14]. Saio guztiak hiru bider errepikatu dira eta 10.000 zelulen intentsitatea neurtu da lagin bakoitzeko. Grafikoan datuak LDLR basatian lortutako maximoarekiko portzentaje moduan irudikatzen dira.

2.1.10.3 Fluxu-zitometria bidezko LDL barneraketa-tasaren kuantifikazioa

Esperimentuan erabilitako zelulak 4 orduz inkubatu dira 37°C-tan LDL-FITC partikulen barneraketa-tasa zehazteko. LDL-FITC inkubazioaren ostean zelulak hiru aldiz garbitu dira PBS-%1-BSA indargetzailea erabiliz, 10 minutuz %4 paraformaldehidoan fixatu dira eta berriro garbitu dira PBS-%1-BSA indargetzailean. Barneratutako LDL-FITC partikulen seinalea neurtzeko eta kanpoan lotuta geratu diren partikulek igortzen dutenetik bereizteko, Trypan blue disoluzioa (Sigma-Aldrich, Steinheim, Germany) erabili da, %0.2 bukaera kontzentrazioan[15]. Konposatu honek, FITC-aren seinalea iraungipen dinamiko bidez deuseztatzeko gaitasuna dauka beti eta molekula fluoreszentearekin elkarrekintza fisiko bat badu. Trypan blue konposatua, ez da kapaza bizirik dauden zelulen mintzak zeharkatzeko. Hori dela eta, kanpotik botaz gero, soilik kanpoan dagoen FITC-a iraungitu ahal izango du, ondorioz, barneratutako FITC seinalea, detektatuko den seinale bakarra izango da. Fluoreszentzia intentsitateak fluxu zitometria bidez neurtu dira, Fascalibur Fluxu zitometroa erabiliz eta zitometroak ekarritako argibideak jarraituz aurretiaz deskribatu den moduan [14]. Saio guztiak hiru bider errepikatu dira eta 10.000 zelulen intentsitatea neurtu da lagin bakoitzeko. Grafikoan datuak LDLR basatian lortutako maximoarekiko portzentaje moduan irudikatzen dira.

2.1.10.4 Fluxu-zitometrian erabilitako analisi estatistikoa

Lagin guztietarako ageri diren emaitzak gutxienez hiru saio ezberdinen emaitzen ondorio dira. Emaitzak esperimentu ezberdinen batez besteko moduan ageri dira ± desbiderapen estandarra (S.D., ingelesetik *standar desviation*). Esanguratasun estatistikoa Student testa ($p \leq 0.05$) erabiliz zehaztu da.

2.1.11 Mikroskopia konfokala

Mikroskopia konfokala, PCSK9, LDL eta LDLR proteinen barne kokapena eta haien arteko elkarrekintzak ikusteko erabili da. Horretarako, zelula ezberdinak estalki gainean 24 putzuko plaketan hazi dira. Esperimentuaren araberako transfekzio eta tratamendu ezberdinak egin ostean, zelulak PBS %1-BSA indargetzailearekin garbitu dira 3 aldiz ondoren 10 minutuz fixatzeko %4 paraformaldehido soluzioan. Proteinen barne kokalekua ikuskatzeko zelulak %1 Triton X-100 detergentearekin zulatu dira. Triton X-100 edo %4 paraformaldehido soberakinak kentzeko 3 garbiketa berri egin dira PBS %1-BSA soluzio indargetzailearekin. Antigorputz ezberdinen inkubazioekin hasi baino lehen zelulak %5 FBS-dun garbiketa tampoian inkubatu dira ordu batez giro tenperaturan lotura inespezifikoak ekiditeko. Proteina ezberdinak markatzeko, zelulak gau osoan zehar 4°C-tan utzi dira antigoputz primarioekin. Horren ostean, antigorputz sekundario ezberdinekin inkubatu dira ordu batez giro tenperaturan proteina ezberdinak detektatu ahal izateko. Azkenik, zelulak Dapi-rekin (Merck, 268298) 10 minutuz inkubatu dira zelulen nukleoak bereizteko. Irudiak IX 81 mikroskopio konfokala (Olympus) erabiliz lortu dira eta Flueview v.50 softwarearekin aztertu dira. Mikroskopi konfokala burutzeko erabilitako antigorputzak 2.5 taulan ageri dira.

2.5 Taula. Mikroskopia konfokalean erabilitako antigorputz zerrenda.

Ab	Merkataritzaetxe	Erreferentzia	Mw (KDa)	Diluzioa	Inkubazioa		Jatorria
					Debora	Tenperatura	
mouse mAB anti-LDLR	Progen Biotechnik	61087	120/160	1:100	16 ordu	4ºC	Sagua
Anti-Apolipoprotein B	Abcam	ab2073	550	1:100	16 ordu	4ºC	Sagua
PCSK9 Polyclonal Antibody	Cayman	10240	74/63	1:100	16 ordu	4ºC	Untzia
DYKDDDDK Tag Antibody (L5)	Thermo	MA1-142	--	1:100	16 ordu	4ºC	Arratoia
Anti-Calreticulin antibody	Abcam	ab18457	48	1:100	16 ordu	4ºC	Oiloa
Anti-GM130 antibody [EP892Y]	Abcam	ab52649	130	1:100	16 ordu	4ºC	Untzia
Anti-LAMP2 antibody	Cell Signaling	ab13524	100	1:100	16 ordu	4ºC	Arratoia
Alexa Fluor 488 Rabbit Anti-Mouse	Life Technologies	A-11058	--	1:200	1 ordu	25ºC	--
Texas Red Goat Anti-Mouse	Life Technologies	T-862	--	1:200	1 ordu	25ºC	--
Alexa Fluor 633 Rabbit Anti-Mouse	Life Technologies	A-21052	--	1:200	1 ordu	25ºC	--
Alexa Fluor 488 Goat Anti-Chicken	Life Technologies	A-11039	--	1:200	1 ordu	25ºC	--
Alexa Fluor 488 Goat Anti-Rat	Life Technologies	A-21212	--	1:200	1 ordu	25ºC	--
Alexa Fluor 594 chicken Anti-Rat	Life Technologies	A-21571	--	1:200	1 ordu	25ºC	--
Alexa Fluor 488 Goat Anti-Rabbit	Life Technologies	A-11008	--	1:200	1 ordu	25ºC	--
Texas Red Goat Anti-Rabbit	Life Technologies	T-2767	--	1:200	1 ordu	25ºC	--
Alexa Fluor 633 Goat Anti-Mouse	Life Technologies	A-21070	--	1:200	1 ordu	25ºC	--

2.2 LDLR proteinaren analisian erabilitako fluoreszentzia metodologiaren balioztapena. Erabilitako metodologia espezifikoa

2.2.1 Mutagenesi guneratua eta *in silico* analisak

p.(Val429Leu), p.(Trp490Arg), p.(Ser648Pro), p.(Pro685Ser) eta p.(Val859Met) *LDLR* aldaeren mutagenesi guneratua eta *in silico* analisiak 2.1.2 eta 2.1.3 ataletan zehazten den metodologia jarraituz burutu dira.

2.2.2 LDLR proteinaren *in vitro* adierazpena

LDLR-a espresatzen ez duten CHO- *ldl*Δ7 zelulak , 24 zein 6 putzuko plaketan hazi dira Ham´s F-12 medioan. Zelula hauek LDLR aldaera ezberdinak dauzkaten plasmidoekin transfektatu dira Lipofectamine LTX eta Plus Reagent (Invitrogen) transfekzio sistema erabiliz eta 48 orduz utzi dira kultibo medioan LDLR-aren espresio-maila maximoa lortu arte.

2.2.3 Western plapaketa bidezko proteinen detekzioa

LDLR basatiaz zein LDLR aldaera ezberdinekin transfektatutako CHO-*ldl*Δ7 zelulak 6 putzutako plaketan hazi dira ($0.5x10^6$ zelula/putzuko). Transfektatu eta 48 ordu pasa ondoren, zelulen medioa kendu eta 300 µl liseriketa medioz ordezkatu da. Proteina ezberdinak SDS-PAGE elektroforesi bidez banatu dira eta ondoren western plapaketa bidez detektatu dira 2.1.7 atalean zehazten den moduan. LDLR eta GAPDH proteinak hauen aurkako antigorputz espezifikoekin detektatu dira.

2.2.4 Alderantzizko transkripzio-polimerasaren kate-erreakzio kuantitatiboa

LDLR aldaera ezberdinekin transfektatutako CHO-*ldl*Δ7 qRT-PCR analisia burutu da. Horretarako, CHO-*ldl*Δ7 zelulak ($0.5x10^6$ zelula/putzuko) 6 putzuko plaketan hazi eta lehen azaldu den moduan transfektatuak izan dira. 48 ordu pasa ostean zelulen RNAa TRIZOL erreaktiboa (Invitrogen) erabiliz erauzi da eta 2.1.6 atalean zehazten de prozedura jarraituz RNA kopurua kuantifikatu da.

2.2.5 ^{125}I-LDL-ren barneraketa eta degradazioa

LDLR basatiaz zein LDLR aldaera ezberdinekin transfektatutako CHO-*ldl*Δ7 zelulek daukaten katabolismoa zehazteko, ^{125}I bidez markatutako LDL-k erabili dira aurretiaz deskribatutako metodologia jarraituz [1617]. Laburki, LDLR aldaera ezberdinak espresatzen dituzten CHO-*ldl*Δ7 zelulak 12 putzuko plaketan hazi dira ($2x10^5$ zelula/putzuko) hauen ^{125}I-LDL barneraketa (barneratutakoa gehi lotutakoa) eta degradazio ahalmena determinatzeko. LDLR adierazpen maximoa lortzeko, bigarren egunean zelulei medioa aldatu eta 12 orduz lipido gabeko seruma (LPDS, ingelesetik, *Lipid Deficent Serum*) eta esterol ezberdinak (90 µg/ml kolesterola eta 9 µg/ml 25(OH)-kolesterola) dituen medioan hazi dira. Hirugarren egunean zelulak garbitu eta 37°C-tan 4 orduz %5 LPDS medioan eta ^{125}I-LDL kontzentrazio ezberdinekin inkubatu dira. LDL barneraketak, 37°C-tan neurtua, barneratutako LDL eta lotutakoaren batura adierazten du. ^{125}I-LDL barneraketa eta degradazio maximoak zelulei atxikitutako erradioaktibitatea (barneraketa) edo medioan aurkitzen den erradioaktibitatea (degradazioa) neurtuz kalkulatu dira. ^{125}I-LDL kontzentrazio bakoitzarentzako barneraketa zein degradazio baloreak, markatu gabeko LDL-ren ausentzian eta presentzian (1mg/ml) agertzen den seinale ezberdintasuna kontuan izanik kalkulatu dira [18,19]. Grafikoan agertzen diren baloreak ehuneko moduan irudikatu dira maximoa LDLR basatiak 4 orduko inkubazioaren ostean daukan erradioaktibitate balioa izanik. Saioak hiru aldiz errepikatu dira lagin bakoitzeko.

2.2.6 LDLR-ren aktibitatearen neurketa fluxu zitometria bidez

LDLR basatiaz zein LDLR aldaera ezberdinekin transfektatutako CHO-*ldl*Δ7 zelulak 24 putzutako plaketan hazi dira (50.000 zelula/putzuko). Lipofektaminarekin transfektatu eta 48 ordu geroago hartzaile ezberdinek LDL-FITC lotzeko eta barneratzeko duten ahalmena neurtu da 2.1.9.2 eta 2.1.9.3 ataletan azaltzen den moduan.

2.2.6 Fluxu-zitometria bidezko LDLR adierazpenaren kuantifikazioa

LDLR basatiaz zein LDLR aldaera ezberdinekin transfektatutako CHO-*ldl*Δ7 zelulak 24 putzutako plaketan hazi dira (50.000 zelula/putzuko). Transfektatu eta 48 ordu pasa ondoren 2.9.1.1 atalean aipatzen den metodologia erabili da LDLR basatia eta bere aldaeren adierazpena kuantifikatzeko.

2.2.7 Mikroskopia Konfokala

Mikroskopia konfokala azterketa ezberdinetarako etabili da, batetik, LDLR-ren adierazpena eta kokapena determinatzeko konkretuki hartzaile basatia eta honen aldaerak erretikuku endoplasmatikoan (ER, ingelesetik, *Endoplasmic Reticulum*) atxikituta geratzen diren ikusteko, zehazki. Bestetik LDLR-ren eta LDL-ren arteko lotura determinatzeko. Horretarako, LDLR basatiaz zein LDLR aldaera ezberdinekin transfektatutako CHO-*ldl*Δ7 zelulak estalki gainean hazi dira 24 putzutako plaketan (50.000 zelula/putzuko). Transfekzioa bukatu eta 48 ordu pasa ostean 2.1.10 atalean agertzen den metodologia jarraitu da. Erretikuluarekin kolokalizazioa detektatzeko zelulak permeabilizatu egin dira, ez ordea LDLR eta LDL mintz lotura ikusteko.

2.3 LDLR analisi bateraturako erabilietako metodologia espezifikoa

2.3.1 Ikerketaren partehartzaileak

HF ikerketan parte hartu duten Portugaleko 135 pertsonen datu fenotipiko/genotipikoak aurkezten dira. Lana burutzeko ezinbestekoak diren partehartzaile guztien adostasun informatua, borondatezko partehartzea, eta konfidentzialtasuna bermatu dira. Bestalde, erabilitako protokolo eta datu-base guztiek behar diren komiteen (National Institute of Health Ethical Commitee and National Data Protection Commitee eta Research Ethics Committee from the University of the Basque Country (Comité de Ética en la Investigación y la Práctica Docente de la Universidad del País Vasco/Euskal Herriko Unibertsitatea, CEID/IIEB)) onarpena daukate.

2.3.2 Lipido-profila

Partehartzaileen odola gau osoko barau-aldiaren ostean atera da. Determinatu diren parametroak, kolesterol totala, LDL-tan aurkitzen den kolesterola (LDL-C), HDL-tan, triglizerido, apoA1, apoB eta lipoproteina(a) mailak zehaztu dira. Horretarako analisi entzimatiko eta antigorputzetan oinarritutako metodologia ezberdinak erabili dira.

Partehartzaile guztietarako LDL-C pertzentilak kalkulatu dira bakoitzaren adin eta sexuari egokituz. Portugaleko populazioan dagoen informazio-falta dela eta, pertzentilen kalkulua egin ahal izateko espainiar populazioaren balioak erreferentzia

moduan erabili dira[20]. Partehartzaile batzuen kasuan ikerketa hasteko unean dagoeneko tratamendupean zeuden, kasu hauetan LDL-C balioak kalkulatzerakoan zuzenketa faktore ezberdinak erabili dira tratamenduaren arabera. Estatinen tratamendurako %30-ko murrizketa faktore bat erabili da (LDL-C x 1.3); estatina eta ezetimibe konbinatzen dituzten tratamenduetan ordea % 50-ko murrizketa faktore bat erabili da (LDL-C x 1.5)[21,22].

2.3.3 Segregazio-analisia

Familia bakoitzerako LDLR aldaerak HF-rekin daukan kosegregazioa ikertu da. Kosegregazio balioak honela adierazi dira: "aldaera-eramaileak/ erasarritako partehartzaile totala" edo "aldaera eramaileak/ erazarri gabeko totala" moduan adierazi dira, non "erasarritako partehartzaile totala" (75-eko pertzentiletik gora) FH duten senitarteko guztien kopuruari dagokio eta "erasarri gabeko totala" (75-eko pertzentiletik behera) lipido-maila normala duten senitarteko guztien kopuruari dagokio.

2.3.4 Analisi molekularra

HF-ren diagnostiko genetikoa burutzeko *APOB* (26. eta 29. exoi zatiak), *LDLR* (DNA-ren berrantolaketa handiak barne) eta *PCSK9* geneak ikertu dira [23].

2.3.5 *in silico* analisiak

in silico analisiak 2.1.3 ataletan zehazten den metodologia jarraituz burutu dira.

2.3.6 c.-13A>G, c.818-3C>G, eta c.1706-10G>A aldaeren balioztapen funtzionala

Aldaera hauek dauzkaten partehartzaileen RNA mezularia (mRNA) hauen odoleko zelula mononuklearretatik erauzi da. Aldaeren funtzionaltasuna Bourbon eta lankideak deskribatutako protokoloa jarraituz burutu dira [24,25].

2.3.7 Aldaera ezberdinen mutagenesi guneratua

p.(Gly76Trp), p.(Arg406Trp), p.(Ile441Thr), p.(Gly545Trp), p.(Cys698Phe) LDLR aldaeren mutagenesi guneratua 2.1.2 atalean zehazten den metodologia jarraituz burutu dira.

2.3.8 LDLR proteinaren *in vitro* adierazpena

LDLR-a espresatzen ez duten CHO- *ldl*Δ7 zelulak , 24 zein 6 putzuko plaketan hazi dira Ham´s F-12 medioan. Zelula hauek LDLR aldaera ezberdinak dauzkaten plasmidoekin transfektatu dira Lipofectamine LTX and Plus Reagent (Invitrogen) transfekzio sistema erabiliz eta 48 orduz utzi dira kultibo-medioan LDLR-ren espresio maila maximoa lortu arte.

2.3.9 Western plapaketa bidezko analisia

LDLR basatiaz zein LDLR aldaera ezberdinekin transfektatutako CHO-*ldl*Δ7 zelulak 6 putzutako plaketan hazi dira ($0.5x10^6$ zelula/putzuko). Transfektatu eta 48 ordu pasa ondoren, zelulen medioa kendu eta 300µl liseriketa medioagatik (50 mM Tris–HCl, pH 7.5, 125 mM NaCl, 1% Nonidet P-40, 5.3 mM NaF, 1.5 mM NaP, 1 mM orthovanadate, 1 mg/ml protease inhibitor cocktail (Roche), and 0.25 mg/ml Pefabloc, 4-(2-aminoethyl)-benzenesulfonyl fluoride hydrochloride (AEBSF; Roche) ordezkatu da. Proteina ezberdinak SDS-PAGE elektroforesi bidez banatu dira lehenbizi eta ondoren western plapaketa bidez detektatu dira 2.1.7 atalean zehazten den moduan. LDLR eta GAPDH proteinak hauen aurkako antigorputz espezifikoekin detektatu dira.

2.3.10 Fluxu-zitometria bidezko LDLR aldaeren aktibitatearen neurketa

LDLR-ren aktibitatea neurtzeko, hartzailearen mintz adierazpena, LDL-a lotzeko gaitasuna eta LDL barneraketa parametroak neurtu dira fluxu-zitometria erabiliz. Horretarako zelulak 24 putzutako plaketan erein dira (50.000 zelula/putzuko) eta lipofektamina erreaktiboarekin transfektatu dira (2.5.2). 48 orduren ostean 2.1.9.1, 2.1.9.2 eta 2.1.9.3 ataletan agertzen den metodologia jarraituz, LDLR adierazpena, LDL lotura eta LDL barneraketa parametroak neurtu dira.

2.3.11 Mikroskopia konfokala

Mikroskopia konfokala LDLR-ren adierazpena eta kokapena analizatzeko erabili da, konkretuki hartzaile basatia eta honen aldaerak erretikuku endoplasmatikoan atxikituta geratzen diren detektatzeko. Horretarako, aurretiaz aldaera ezberdinekin transfektatutako CHO-*ldl*Δ7 zelulak estalki gainean hazi dira 24 putzutako plaketan (50.000 zelula/putzuko). Transfekzioa bukatu eta 48 ordu pasa ostean 2.1.10 atalean agertzen den metodologia jarraitu da. Erretikuluarekin kolokalizazioa determinatzeko permeabilizatu dira.

2.3.11 p.(Arg406Trp) aldaeraren birziklapen zinetikak

LDL hartzailearen birziklapen-mekanismoaren funtzionaltasuna konprobatzeko bi esperimentu mota egin dira. Batetik, LDLRren adierazpena konprobatu da denboran zehar markatu gabeko LDL-aren presentzian, eta bestetik, pH ezberdinetan LDL-LDLR konplexuaren askapen-tasa neurtu da. Lehenengo esperimentua burutzeko, aldaera ezberdinekin transfektatutako CHO- *ldl*Δ7 zelulak markatu gabeko 20 µg/µl LDL-kin denbora ezberdinetan inkubatu ostean LDLR adierazpena konprobatu da fluxu-zitometria bidez. Hurrengo esperimentuan aurretiaz transfektatutako CHO- *ldl*Δ7 zelulak 20 µg/µl LDL-FITC-rekin inkubatu dira 30 minutuz pH ezberdinetan eta 0.4 M sakarosaren presentzian. pH bakoitzean lotutako LDL kopurua fluxu zitometria bidez neurtu da 2.1.9.2 atalean deskribatutako metodologia jarraituz.

2.3.12 Lipido-profilen analisi estatistikoa

Lipido-profilen analisi estatistikoa SPSS softwarea erabiliz burutu da (version 17.0 for Windows; SPSS, Chicago, IL). Parametro kualitatiboen frekuentziak c^2 testa erabiliz kalkulatu dira. Bere partez, parametro kuantitaboen bataz besteko baloreak Student T testa edo bariantzen analisiaren bidez konparatu dira. Bestalde, medianen baloreak Mann-Whitney edo Kruskal Wallis testak erabiliz kalkulatu dira.

2.4 PCSK9 aldaeren analisian erabilitako metodologia espezifikoa

2.4.1 Mutagenesi guneratua

c.60_65dupGCTGCT, c.63_65delGCT, p.(Ala62Asp), p.(Pro331Ala), p.(Arg357Cys), p.(Asp374Pro), p.(Pro467Ala), p.(Arg499His), p.(Ser636Arg), eta p.(His643Arg) PCSK9 aldaeren mutagenesi guneratua 2.3 ataletan zehazten den metodologia jarraituz burutu da.

2.4.2 PCSK9 adierazpenaren Western plapaketa bidezko analisia

PCSK9 basatiaz zein PCSK9 aldaera ezberdinekin transfektatutako HEK293 zelulak 6 putzutako plaketan hazi dira ($0.5x10^6$ zelula/putzuko). Zelulen transfekzioak 2.1.5.2 atalean zehazten den moduan egin dira lipofektamina erreaktiboa erabiliz. Transfektatu eta 48 ordu pasa ondoren, zelulen medioa berreskuratu da medioan jariatu den PCSK9 kopurua neurtzeko eta zelulak 2.1.7 atalean zehazten den medioarekin lisatu dira zelula barruko PCSK9-aren prozesamendua determinatzeko. PCSK9 eta GAPDH proteinak hauen aurkako antigorputz espezifikoekin detektatu dira.

2.4.3 PCSK9 proteinaren purifikazioa

HEK293 zelulak "Flask T75" ontzien oinarriari itsatsita hazten dira DMEM medioan. Beharrezko konfluentzian daudenean kaltzio kloruro metodoaz transfektatzen dira (2.1.5.1) eta genetizinaz baliatuz zelula-lerro egonkor bat sortu da PCSK9 aldaera bakoitzerako. PCSK9 purifikazio bakoitzeko, 5 "Flask T75" erabiltzen dira. Zelulak % 80-ko baterakuntzara ailegatzean antibiotiko eta serum gabeko Opti-MEM medioan jartzen dira eta hiru egunez 37°C-tan uzten dira. Hirugarren egunean zelula-medioak berreskuratu eta zentrifugatu egiten dira zelula hilak kentzeko. Errendimendu altuko purifikazioa lortzeko, zelula-medioak nikeldun erretxinarekin (GE, ref: 17-5318-01) inkubatzen dira 2 orduz 4°C-tan. Ondoren erretxina garbitzen da 20 mM imidazola duen soluzio indargetzaile (300 mM NaCl, 50 mM Na_2HPO_4, 50 mM NaH_2PO_4, 1 mM $MgCl_2$, pH=8, % 10 glizerol) batekin, eta azkenik, 500 mM imidazol duen soluzio indargetzaile berdinarekin proteinak eluitzen dira. Purifikatutako PCSK9-a Tris-HCl 150 mM NaCl eta 10% glizerol, pH 8.0 soluzioan gordetzen da -80°C-tan.

2.4.4 LDLR proteinaren *in vitro* adierazpena PCSK9-ren presentzian

PCSK9 basatiaz zein PCSK9 aldaera ezberdinekin transfektatutako HepG2 eta HEK293 zelulak 24 putzutako plaketan hazi dira (50.000 zelula/putzuko). Transfektatu eta 48 ordu pasa ondoren 2.9.1 atalean aipatzen den metodologia erabili da PCSK9 ezberdinen presentzian LDLR basatiaren adierazpena determinatzeko. Bestalde, transfektatu gabeko HepG2 zelulak 2 orduz inkubatu dira purifikatutako 2 μg/ml PCSK9 ezberdinekin eta ondoren LDLR-ren adierazpena neurtu da PCSK9-aren kanpo-efektua ikusteko.

2.4.5 LDL-FITC barneraketa PCSK9-ren presentzian

PCSK9 basatiaz zein PCSK9 aldaera ezberdinekin transfektatutako HepG2 eta HEK293 zelulak 24 putzutako plaketan hazi dira (50.000 zelula/putzuko). Transfektatu eta 48 ordu pasa ondoren 2.1.9.3 atalean aipatzen den metodologia erabili da LDL-FITC barneraketa neurtzeko PCSK9 ezberdinen presentzian. Bestalde, transfektatu gabeko HepG2 zelulak 2 orduz inkubatu dira purifikatutako 2 μg/ml PCSK9 ezberdinekin eta ondoren LDL-FITC barneraketa neurtu da PCSK9-aren kanpo-efektua ikusteko.

2.4.6 LDLR ektodomeinuaren nikel afinitate bidezko purifikazioa

HEK293 zelulak "Flask T75" oinarriari itsatsita hazten dira DMEM medioan. Beharrezko konfluentzian daudenean kaltzio kloruro metodoaz transfektatzen dira LDLR-ektodomeinua kodetzen duen plasmido batez (2.1.5.1) eta genetizinaz baliatuz LDLR-ektodomeinua adierazten duen zelula lerro egonkor bat sortu da. Purifikazio bakoitzeko, 5 "Flask T75" erabiltzen dira. Zelulak % 80-ko konfluentziara ailegatzean antibiotiko eta serum gabeko Opti-MEM medioan jartzen dira eta hiru egunez 37°C-tan uzten dira. Hirugarren egunean zelula medioak berreskuratu eta zentrifugatu egiten dira zelula hilak kentzeko. Errendimendu altuko purifikazioa lortzeko zelula medioak nikel erretxinarekin (GE, ref: 17-5318-01) inkubatzen dira 2 orduz 4°C-tan. Ondoren erretxina garbitzen da 20 mM imidazola duen soluzio indargetzaile (300mM NaCl, 50mM Na_2HPO_4, 50mM NaH_2PO_4, 1mM $MgCl_2$, % 0.01 Brij-35, pH=7.5, % 10 glizerol) batekin eta azkenik 500 mM imidazola duen soluzio indargetzaile berdinarekin proteinak eluitzen dira. Purifikatutako PCSK9-a Tris-HCl 150 mM NaCl eta 10% glycerol, pH 8.0 soluzioan gorde da -80°C-tan.

2.4.7 ELISA bidezko PCSK9-LDLR arteko afinitatearen determinazioa

LDLR-ren ektodomeinua espresatzen duten HEK293 zelulak 96 putzutako plaketara itsasten utzi dira A soluzioan (10 mM Tris-HCl, pH 7.5, 50 mM NaCl, 2 mM $CaCl_2$)4°C-tan gau osoan zehar Hurrengo egunean plakak ordu batez % 5 BSA duen A soluzio indargetzailearekin blokeatzen dira eta 2 orduz PCSK9 aldaera ezberdinekin inkubatzen dira giro tenperaturan. Plakak hiru aldiz garbitu eta antigorputz primario (mouse monoclonal anti-DDK, clone OTI4C5, Origene, USA) eta sekundarioekin (peroxidase-conjugated horse anti-mouse. Cell Signalling, USA) inkubatzen dira giro tenperaturan. Antigorputz sekundarioaren inkubazioa bukatu ostean azken garbiketa bat egiten da eta 50 µl 2,2´-Azino-bis(3-ethilbenzothioazoline-6-sulfonic acid) substratua erabiliz (Sigma-Aldrich, MO, USA) antigorputzen detekzioa burutzen da. Konposatu honek peroxidasaren aktibitatearen ondorioz koloredun produktu batean bihurtzen da 405 nm-tan neurtu daitekeena. Kolorearen agerpenak linealtasuna mantentzen du eta 30-60 minutu tartean neurtzen da. Zuzenean lortutako balioak zuzendu egiten dira lotura inespezifikoak eta lotura maximoak ematen dituzten balioen kenketa eginez. EC_{50} afinitate- balioak bost parametrotako ekuazio logistikoak erabiliz kalkulatu dira SigmaPlot softwarea erabiliz.

2.4.8 Western plapaketa bidezko erretikulu endoplasmatiko PCSK9-aren determinazioa

PCSK9 aldaera ezberdinekin egonkorki transfektatutako HEK293 zelulak % 80-ko konfluentziara ailegatzean antibiotiko eta serum gabeko Opti-MEM medioan jartzen dira eta bi egunez 37°C-tan uzten dira. 48 orduak pasa ostean zelulak homogenizazio soluzioan jartzen dira (8.5 mM Tris-HCl, 4.25 mM KCl, 110 mM NaCl, 8.5 mM triethanolamina, 210 mM sakarosa, 1 mM EDTA, pH=7.4) eta 25 G-ko xiringa batetik pasatuz mekanikoki apurtzen dira. Behin zelulak apurtu direnean 500 x g-tan zentrifugatzen dira 10 minutuz 4°C-tan nukleoak eta apurtu gabeko zelulak kentzeko. Ondoren, gain-jalkina [% 0-26 (p/b)] iodixanol gradiente baten gainean jarri eta 280.000 x g-tan zentrifugatzen da 115 minutuz. Azkenik, frakzio ezberdinak berreskuratzen dira, eta erretikulua eta PCSK9 ezberdinak aztertzen dira western plapaketa bidez. Erretikulua eta PCSK9 detektatzeko kalrretikulina eta DDK-ren aurkako antigorputzak erabili dira.

2.4.9 PCSK9-ren kokapenaren analisia mikroskopia konfokala erabiliz

LDLR eta PCSK9 proteinen kokapen zelularra analizatzeko mikroskopia konfokala erabili da, konkretuki erretikuku endoplasmatikoan atxikituta geratzen diren ikusteko. Horretarako, aurretiaz aldaera ezberdinekin transfektatutako HEK293 zelulak estalki gainean hazi dira 24 putzutako plaketan (50.000 zelula/putzuko). Transfekzioa bukatu eta 48 ordu pasa ostean 2.1.10 atalean agertzen den metodologia jarraitu da.

2.4.10 L8 eta L11 PCSK9-peptido seinaleen ΔGapp-aren kalkulua

Aminoazido ezberdinak gehitzea edo kentzeak peptido seinaleen itxurazko energia askeari (ΔGapp) eragiten diote. Izan ere, aminoazido hidrofobikoak gehitzean, hidrofobizitate eta elizitate mailari eragiten diote eta ondorioz energia librea aldatzen dute. http://dgpred.cbr.su.se/ softwarea erabiliz, peptido bakoitzarentzako energia librea eta hidrofobizitatea kalkulatu dira.

2.4.11 PCSK9 basatia eta L8 eta L11 peptido seinaleen aldaeren egitura

Peptido ezberdinen hidrofobizitatea Kite-Doolittle formula erabiliz kalkulatu da ExPASy programa erabiliz. Proteinaren egiturak homologia bidez lortu dira Iterative Threading Assembly Refinement (I-TASSER) programa erabiliz eta antzerako sekuentziak molde giaa erabiliz.

2.5 ApoB partikulen analisian erabilitako material eta metodo espezifikoak

2.5.1 Lipoproteinen purifikazioa, markaketa eta karakterizazio biokimikoa

LDL partikulak 2.1.8 atalean deskribatu den moduan purifikatu dira. Lipoproteinen konposaketa determinatzeko teknika ezberdinak erabili dira. Proteina totala kuantifikatzeko Lowry-ren teknika erabili da eta triglizerido (erreferentzia 11529) eta kolesterol (erreferentzia 11505) kontzentrazioak BioSystem enpresak komerzializatzen dituen kit ezberdinen bidez kalkulatu dira. LDL-en funtzionaltasuna fluxu zitometria bidez determinatzeko FITC fluorofororekin markatu dira partikulak 2.1.9 atalean zehazten den moduan. Partikulen aktibitate ezberdinak konparatu ahal izateko datuak tratatu dira fluoreszentzia/partikula erratioa erabili da.

2.5.2 DLS bidezko LDL tamainaren determinazioa

Markatu gabeko 1 mg/ml LDL partikulen tamainak argi dispertsio dinamiko (ingelesetik, *dynamic light scattering* (DLS)) bidez determinatu egin dira Nano-S Zetasizer (Malvern Instruments UK) aparatua erabiliz. DLS-ak argiaren dispertsioak denboran zehar duen aldakortasuna neurtzen du puntu zehatz batean (173°). Zenbat eta aldakortasuna handiagoa izan partikulak txikiagoak izango dira hauen mugimendua partikula handiena baino handiagoa baita. Laginen dispertsioa 25 neurritako hiru tanda eginez kalkulatu dira. Neurketa guztiak soluzio eta tenperatura berdinak mantenduz egin dira. Tamaina-datu egokiak lortzeko datu gordinak medioaren biskositate eta honen errefrakzio-indize balioez zuzendu dira. Datuen analisiak Zetazizer softwarearekin egin dira.

2.5.3 Mikroskopia elektroniko bidezko tamainaren determinazioa

Markatu gabeko LDL partikulak (100 µg/ml) mikroskopia elektroniko bidez analizatu dira. Euskarriaren eta partikulen arteko kontrastea hobetzeko, partikulen tindaketa negatibo deritzon teknika erabiltzen da. LDL-ak tindatzeko lehenbizi kobrezko euskarri batean immobilizatzen dira eta ondoren uranilo azetato soluzioarekin tindatzen dira.

Azkenik ur desionizatuarekin garbitu eta lehortzen uzten dira. Partikulen tamaina kalkulatzeko Feret-en diametroa determinatu da Image-J softwarea erabiliz. LDL mota bakoitzeko 1600 partikulen diametroak neurtu dira.

2.5.4 Infragorri-espektroskopia bidezko

2.5.4.1 LDL laginen prestaketa

Markatu gabeko LDL partikulak infragorri-espektroskopia bidez neurtzeko D_2O-an eta pH ezberdinetan prestaturiko PBS soluzioetan disolbatu dira (pH 7.4-tik pH 5-era, 0.5 unitaeko tarteekin). H_2O-D_2O aldaketa egokia izan dela zihurtatzeko, H-O loturak ematen duen bandaren desagerpena jarraitu da infragorri bidez. Soluzio egokian jarri ostean, LDL laginak kontzentratu egin dira 10 mg/ml-ko kontzentrazioa lortu arte.

2.5.4.2 Infragorri-espektroskopia bidezko neurketak

Lagin ezberdinen neurketak MCT detektorea duen Nicolet Nexus 5700 espektrometroan egin dira. Lagin guztiak 20°C-tan neurtu dira eta espektroa bakoitza 370 interferogramen datuak batazbestekotuz lortzen da. Espektro bakoitzaren ebazpena 2 cm^{-1} koa da.

2.5.4.3 Infragorri-espektroen analisia

Proteinari dagokion informazioa 1600-1700cm^{-1} tartean kokatzen den amida I banda aztertuz lortu da tarte honetan lotura peptidikoan dauden C=O loturei buruzko informazioa bai dago. Informazio hau lotura hauen bibrazioetatik lortzen da, ezen bibrazio motaren arabera C=O lotura hau egitura sekundario batean edo bestean aurkituko da. Espektroen zarata murrizteko, laginak neurtu aurretik pH ezberdineko soluzio indargetzaeileen infragorri espektroak jaso egin dira, eta gero lagin bakoitzari bere bakground espektroa kendu zaio. Bestetik, laserrak denboran zehar izan dezakeen intentsitate aldaketek datuetan eraginik izan ez dazaten, amida banda guztiak normalizatu egin dira. Banda osoa egitura sekundarioei dagozkien banda ezberdinetan banatzeko Fernadez-Higuero eta lankideak deskribatzen duten metodologia jarraitu da[28]. ApoB-ren egitura sekundario bakoitza hurrengo uhin luzeretan neurtu da[29]: α -helizea (1656 cm^{-1}), β -orria (1631 cm^{-1}), β -bira (1668 and 1680 cm^{-1}) eta ez egituratutako parteak (1645 cm^{-1}). 1617 cm^{-1}-tan agertzen den banda lipidoan barneratutatko beta egiturei dagokie.

2.5.5 LDL lotura eta barneraketa linfozitoetan

LDL aldaera bakoitzaren funtzionaltasuna egiaztatzeko LDLR lotzeko gaitasuna eta giza-linfozitoek LDL hauek barneratzeko duten ahalmena fluxu-zitometria bidez konprobatu da. Horretarako, giza linfozitoak 72 orduz hazi dira lipido gabeko serumean eta CD3/CD28-dun partikula magnetikoen presentzian LDLR adierazpen maximoa lortzeko. LDL lotura eta LDL barneraketa determinatzeko fluxu-zitometria erabili da 2.1.10.2 eta 2.1.10.3 ataletan deskribatzen den metodologia jarraituz.

2.5.6 LDL barneraketa HepG2 zeluletan

HepG2 zelulak 24 putzuko plaketan eta DMEM (%10 FBS eta antibiotikoekin) medioan hazi dira. LDL barneraketa era egokian neurtzeko, zelulak lipido gabeko serum medioan jarri dira 24 orduz LDLR adierazpen maximoa lortzeko. LDL-FITC partikulen barneraketa kuantifikatzeko 2.1.10.3 ataletan deskribatzen den metodologia jarraitu da.

2.5.7 U937 zelulen bikoizketa-tasaren determinazioa

U937 zelulak 96 putzutako plaketan hazi dira ($1x10^5$ zelula/putzuko) 24 orduz. Zelulen bikoizketa-tasa determinatzeko 24 orduz lipido gabeko serum RPMI medioan jarri dira. Azkenik, LDL mota bakoitzeko 2 µg/ml gehitu dira eta 48 orduz utzi dira 37 °C-tan % 5-ko CO_2-dun atmosferan. Bikoizketa-tasa CellTiter 96wAQueous Non-Radioactive Cell Proliferation Assay sistema erabiliz kalkulatu da aurretiaz deskribatutako metodologia jarraituz[30]. Bikoizketa-tasaren kalkulua LDL gabeko U937 zelulen hazkuntza tasarekiko erlatibizatuz kalkulatu da.

Erreferentziak

1. Den Dunnen, J. T. & Antonarakis, S. E. Mutation nomenclature extensions and suggestions to describe complex mutations: A discussion. *Hum. Mutat.* **15,** 7–12 (2000).

2. Taschner, P. E. M. & den Dunnen, J. T. Describing structural changes by extending HGVS sequence variation nomenclature. *Hum. Mutat.* **32,** 507–511 (2011).

3. Adzhubei, I. A. *et al.* A method and server for predicting damaging missense mutations. *Nat. Methods* **7,** 248–9 (2010).

4. Ng, P. C. SIFT: predicting amino acid changes that affect protein function. *Nucleic Acids Res.* **31,** 3812–3814 (2003).

5. González-Pérez, A. & López-Bigas, N. Improving the assessment of the outcome of nonsynonymous SNVs with a consensus deleteriousness score, Condel. *Am. J. Hum. Genet.* **88,** 440–449 (2011).

6. Schwarz, J. M., Rödelsperger, C., Schuelke, M. & Seelow, D. MutationTaster evaluates disease-causing potential of sequence alterations. *Nat. Methods* **7,** 575–576 (2010).

7. Grantham, R. Amino Acid Difference Formula to Help Explain Protein Evolution Amino Acid Difference Formula to Help Explain Protein Evolution. *Science (80-.).* **185,** 862–864 (1974).

8. Pollard, K. S., Hubisz, M. J., Rosenbloom, K. R. & Siepel, A. Detection of nonneutral substitution rates on mammalian phylogenies. *Genome Res.* **20,** 110–121 (2010).

9. Dogan, R. I., Getoor, L., Wilbur, W. J. & Mount, S. M. SplicePort--An interactive splice-site analysis tool. *Nucleic Acids Res.* **35,** W285–W291 (2007).

10. REESE, M. G., EECKMAN, F. H., KULP, D. & HAUSSLER, D. Improved Splice Site Detection in Genie. *J. Comput. Biol.* **4,** 311–323 (1997).

11. Hebsgaard, S. M. *et al.* Splice site prediction in Arabidopsis thaliana pre-mRNA by combining local and global sequence information. *Nucleic Acids Res.* **24,** 3439–52 (1996).

12. Krieger, M., Brown, M. S. & Goldstein, J. L. Isolation of Chinese hamster cell mutants defective in the receptor-mediated endocytosis of low density lipoprotein. *J. Mol. Biol.* **150,** 167–184 (1981).

13. Dardik, R. *et al.* Homocysteine and oxidized low density lipoprotein enhanced platelet adhesion to endothelial cells under flow conditions: distinct mechanisms of thrombogenic modulation. *Thromb. Haemost.* **83,** 338–44 (2000).

14. Etxebarria, A. *et al.* Functional characterization of splicing and ligand-binding domain variants in the LDL receptor. *Hum. Mutat.* **33,** 232–243 (2012).

15. Hed, J., Hallden, G., Johansson, S. G. & Larsson, P. The use of fluorescence quenching in flow cytofluorometry to measure the attachment and ingestion phases in phagocytosis in peripheral blood without prior cell separation. *J. Immunol. Methods* **101,** 119–25 (1987).

16. KNIGHT, B. L. & SOUTAR, A. K. Changes in the Metabolism of Modified and Unmodified Low-Density Lipoproteins during the Maturation of Cultured Blood Monocyte-Macrophages from Normal and Homozygous Familial Hypercholesterolaemic Subjects. *Eur. J. Biochem.* **125,** 407–413 (1982).

17. Goldstein, J. L. & Brown, M. S. Binding and degradation of low density lipoproteins by cultured human fibroblasts. *J. Biol. Chem.* **249,** 5153–5162 (1974).

18. Sun, X. M., Patel, D. D., Knight, B. L. & Soutar, A. K. Comparison of the genetic defect with LDL-receptor activity in cultured cells from patients with a clinical diagnosis of heterozygous familial hypercholesterolemia. The Familial Hypercholesterolaemia Regression Study Group. *Arterioscler. Thromb. Vasc. Biol.* **17,** 3092–101 (1997).

19. Soutar, A. K., Knight, B. L. & Patel, D. D. Identification of a point mutation in growth factor repeat C of the low density lipoprotein-receptor gene in a patient with homozygous familial hypercholesterolemia that affects ligand binding and intracellular movement of receptors. *Proc. Natl. Acad. Sci. U. S. A.* **86,** 4166–4170 (1989).

20. Gómez-Gerique, J. A. *et al.* [Lipid profile of the Spanish population: the DRECE (diet and risk of cardiovascular disease in Spain) study. DRECE study group]. *Med. Clin. (Barc).* **113,** 730–5 (1999).

21. Rato, Q. Terapêutica farmacológica das dislipidemias. *rev port cardiol* 49–66 (2010).

22. Lange, L. A. *et al.* Whole-Exome Sequencing Identifies Rare and Low-Frequency Coding Variants Associated with LDL Cholesterol. *Am. J. Hum. Genet.* **94,** 233–245 (2014).

23. Bourbon, M., Alves, A. C., Medeiros, A. M., Silva, S. & Soutar, A. K. Familial hypercholesterolaemia in Portugal. *Atherosclerosis* **196,** 633–642 (2008).

24. Bourbon, M. *et al.* Genetic diagnosis of familial hypercholesterolaemia: the importance of functional analysis of potential splice-site mutations. *J. Med. Genet.* **46,** 352–357 (2009).

25. Medeiros, A. M., Alves, A. C., Francisco, V. & Bourbon, M. Update of the Portuguese Familial Hypercholesterolaemia Study. *Atherosclerosis* **212,** 553–558 (2010).

26. Etxebarria, A. *et al.* Advantages and versatility of fluorescence-based methodology to characterize the functionality of LDLR and class mutation assignment. *PLoS One* **9,** (2014).

27. Etxebarria, A. *et al.* Functional characterization and classification of frequent low-density lipoprotein receptor variants. *Hum. Mutat.* **36,** 129–141 (2015).

28. Fernández-Higuero, J. A. *et al.* Structural changes induced by acidic pH in human apolipoprotein B-100. *Sci. Rep.* **6,** 1–10 (2016).

29. Bañuelos, S., Arrondo, J. L., Goñi, F. M. & Pifat, G. Surface-core relationships in human low density lipoprotein as studied by infrared spectroscopy. *J. Biol. Chem.* **270,** 9192–6 (1995).

30. Alves, A. C. atarina, Etxebarria, A., Soutar, A. K. atherine, Martin, C. & Bourbon, M. Novel functional APOB mutations outside LDL-binding region causing familial hypercholesterolaemia. *Hum. Mol. Genet.* **23,** 1817–1828 (2014).

Chapter 3/ 3. Atala

LDLR aldaeren karakterizazio funtzionala/ Functional characterization of LDLR variants

Publications extracted from this chapter/ Atal honetan agertzen diren emaitzetatik publikatutako artikuluak:

1. Benito-Vicente, A., H. Siddiqi, K. B. Uribe, S. Jebari, U. Galicia-Garcia, A. Larrea-Sebal, M. Stef, H. Ostolaza, L. Palacios, and C. Martin. 2018. "P.(Asp47Asn) and p.(Thr62Met): Non Deleterious LDL Receptor Missense Variants Functionally Characterized in Vitro." Scientific Reports 8(1): 16614.

2. Benito-Vicente, A., K. B. Uribe, H. Siddiqi, S. Jebari, U. Galicia-Garcia, A. Larrea-Sebal, A. Cenarro, M. Stef, H. Ostolaza, F. Civeira, L. Palacios, and C. Martin. 2018. "Replacement of Cysteine at Position 46 in the First Cysteine-Rich Repeat of the LDL Receptor Impairs Apolipoprotein Recognition" edited by P. Aspichueta. PLOS ONE 13(10):e0204771.

3. Asier Benito-Vicente, Ana Catarina Alves, Aitor Etxebarria, Ana Medeiros Medeiros, Cesar Martin, and Mafalda Bourbon. 2015. "The Importance of an Integrated Analysis of Clinical, Molecular, and Functional Data for the Genetic Diagnosis of Familial Hypercholesterolemia." Genetics in Medicine 17(12):980–88.

4. Asier Benito-Vicente, Kepa Uribe, Shifa Jebari, Unai Galicia-Garcia, Helena Ostolaza, and Cesar Martin. 2018. "Validation of LDLR Activity as a Tool to Improve Genetic Diagnosis of Familial Hypercholesterolemia: A Retrospective on Functional Characterization of LDLR Variants." International Journal of Molecular Sciences 19(6):1676.

5. Etxebarria, A., A. Benito-Vicente, M. Stef, H. Ostolaza, L. Palacios, and C. Martin. 2015. "Activity-Associated Effect of LDL Receptor Missense Variants Located in the Cysteine-Rich Repeats." Atherosclerosis 238(2):304–12.

6. Aitor Etxebarria, Asier Benito-Vicente, Ana C. Alves, Helena Ostolaza, Mafalda Bourbon, and Cesar Martin. 2014. “Advantages and Versatility of Fluorescence-Based Methodology to Characterize the Functionality of LDLR and Class Mutation Assignment.” PLoS ONE 9(11).

7. Aitor Etxebarria, Asier Benito-Vicente, Lourdes Palacios, Marianne Stef, Ana Cenarro, Fernando Civeira, Helena Ostolaza, and Cesar Martin. 2015. “Functional Characterization and Classification of Frequent Low-Density Lipoprotein Receptor Variants.” Human Mutation 36(1):129–41.

8. Jiang Long, Asier Benito-Vicente, Ling Tang, Aitor Etxebarria, Wei Cui, Kepa B. Uribe, Xiao Dong Pan, Helena Ostolaza, Shi Wei Yang, Yu Jie Zhou, Cesar Martin, and Lu Ya Wang. 2017. “Analysis of LDLR Variants from Homozygous FH Patients Carrying Multiple Mutations in the LDLR Gene.” Atherosclerosis 263:163–70.

9. Jiang Long, Wen-Feng Wu, Li-Yuan Sun, Pan-Pan Chen, Wei Wang, Asier Benito-Vicente, Fan Zhang, Xiao-Dong Pan, Wei Cui, Shi-Wei Yang, Yu-Jie Zhou, Cesar Martin, and Lu-Ya Wang. 2016. “The Use of Targeted Exome Sequencing in Genetic Diagnosis of Young Patients with Severe Hypercholesterolemia.” Scientific Reports 6(1):36823.

3.1 LDLR-ren karakterizazio funtzionala burutzeko fluoreszentzian oinarritutako metodologien baliogarritasuna

3.1.1 Sarrera

Familia-hiperkolesterolemia (FH; MIM #143890) lipidoen metabolismoarekin erlazionatuta dagoen gaixotasun bat da eta hauen artean karakterizatu izan den lehenengoa. Bere mekanismoa gaixotasun kardiobaskularrarekin zuzenki lotuta dago eta bere berezitasunen artean, dentsitate baxuko lipoproteina-mailaren (LDL, ingelestik *Low Density Lipoprotein*) emendapena, tendoi xantomen agerpena, ehun periferikoetan ematen diren kolesterol-metaketak eta aterosklerosiaren garapena daude, hauek, gaixotasun kardiobaskularraren agerpen goiztiarra bultzatzen dute[1]. FH heterozigozian zein homozigozian egon daiteke, hauen prebalentzia 1:500 eta 1:1.000.000 izanik hurrenez hurren[2]. FH-ren kausa nagusia LDL hartzailean (LDLR, ingelesetik *Low Density Lipoprotein Receptor* ; MIM #606945) gertatzen diren mutazioak dira. Hartzaile honen eginkizun nagusia plasman dauden LDL partikulak barneratzea izanik, mutazio hauek plasman dauden LDL-en metaketa bultzatzen dute.

Gaur egun arte, 1300 mutazio ezberdin baino gehiago deskribatu dira munduan[3], hala ere, hartzailearen aktibitatean mutazio hauek dauzkaten efektuak kasu gehienetan ez daude deskribatuak. Mutazioa hauek, LDLR-aren funtzionamenduari nola eragiten dioten arabera boat talde edo "klase" ezberdinetan bana daitezke: lehenengo klasekoetan ez dago LDLRren sintesirik [4]; bigarren klasean, LDLR-a erretikulu endolasmatikoan partzialki (2b) edo erabat (2a) blokeatuta geratzen da[5]; hirugarren klasean, LDL eta LDLR-aren arteko lotura akasdun bat ematen da[6]; laugarren klaseko mutazioek klatrina-besikulen bidezko barneraketa oztopatzen dute [7,8], eta azkenik bostgarren klaseko mutazioek LDLR-aren birziklapen akasduna eragiten dute[9]. Gaixotasun honen diagnostiko definitibo ahalik eta berme handienarekin egin ahal izateko bai LDLRren funtzionaltasuna, zein mutazio klasea zein den fidagarritasunez berretsi beharko lirateke.

2008an argitaratutako ikerketa batean, 443 LDLR aldaera ezberdinen *in silico* analisia burutu zen eta hauetatik % 89-a hartzailearen funtzio galera bat aurreikusi zen [10]. Datu hauek ordea, kontuz begiratu behar dira *in silico* analisi hauek dauzkaten mugak direla eta [11]. Gaur egun, LDLRren aktibitate-galera balioztatzeko, balioztapen funtzionala egin beharra dago, akats gabeko diagnostiko fidagarri eta egokia posible izan dadin eta honen arabera arrisku kardiobaskularra murrizteko tratamendu egokia jarraitu ahal izateko. FH-aren diagnostiko goiztiar egokia burutzea bereziki garrantzitsua da gaixotasuna pairatzen duten pertsona

gazteetan. Hauek, ez dituzte FH-ak dituen efektu bereizgarriak garatu eta ondorioz tratamendu egokiarekin gaixotasun kardiobaskularraren progresioa laster eragotzi daiteke. Gaur egun LDLR-aren *ex vivo* funtzionaltasuna determinatzeko erabiltzen diren teknikak erradioaktibitatean edo fluxu zitometrian oinarrituta daude. Erradioaktibitatearen kasuan ^{125}I bidez markatutako LDL partikulak erabiltzen dira; fluxu-zitometrian ordea, (FITC) (*Fluorescein Isothiocyanate*) sunda fluoreszente bidez markaturiko LDL partikulak erabiltzen dira[6,12–17]. Bi metodologiak era berean erabiltzen dira, bata edo bestearen erabilera ikerlariaren irizpide edo laborategian dagoen ohituraren arabera erabakitzen delarik.

Bi teknika hauek LDLR hartzailearen funtzionaltasuna neurtzeko daukaten sentsibilitatea, erreproduzigarritasuna eta dauzkaten prozedura-arazoak alderatzeko bi laborategi ezberdinen artean analisi konparatibo bat burutu da. Horretarako, ^{125}I erabiliz lortutako datuak [11] LDL-FITC partikulekin lortutako datuekin konparatu dira. Horretaz gain, FITC bidez markatutako partikulen erabilgarritasuna eta fluxu zitometriak LDLR-aren funtzionaltasuna determinatzeko izan dezaketen baliogarritasuna aztertu dira, baita fluoreszentzian oinarritutako neurketek LDLR mutazioak zein klasetakoak diren definitzeko izan dezaketen abantaila posibleak ere. Bi laborategietan hurrengo plasmidoekin transfektatutako CHO-*ldl*Δ7 zelulak erabili dira: LDLR basatia (wt, ingelesetik *wild type*), p.Val429Leu (c.1285G>C), p.Trp490Arg (c.1468T>C), p.Ser648Pro (c.1942T>C), p.Pro685Ser (c.2053C>T) and p.Val859Met (c.2575G>A). LDLRren kokapen zelularra determinatzeko mikroskopia konfokala erabili da, baita mutazio bakoitza zein klasetakoa den zehaztu ahal izateko.

3.1.2 Emaitzak

3.1.2.1 In Silico analisia

Software ezberdinekin lortutako emaitzak 3.1 taulan ageri dira.

3.1 Taula. Software ezberdinekin lortutako LDLR aldaeren patogenizitate emaitzak

		Pathogenicity prediction					
cDNA	Protein	phyloP	Grantham score	SIFT	Polyphen-2	Mutation Taster	CONDEL
c.1285G>C	p.Val429Leu	3.84	Conservative	Tolerated	Benign	Disease Causing	Neutral
c.1468T>C	p.Trp490Arg	4.48	Moderate radical	Deleterious	Probably	Disease Causing	Deleterious
c.1942T>C	p.Ser648Pro	0.93	Moderate	Deleterious	Probably	Polymorphism	Neutral
c.2053C>T	p.Pro685Ser	5.72	Moderate	Deleterious	Probably	Disease Causing	Deleterious
c.2575G>A	p.Val859Met	−0.76	Conservative	Deleterious	Probably	Polymorphism	Deleterious

3.1.2.2 Western plapaketa bidezko LDLR aldaera ezberdinen adierazpena CHO-*ldl*Δ7 zeluletan

LDLR basati eta aldaera ezberdinekin transfektatutako hartzaile adierazpena western plapaketa eta qRT-PCR tekniken bidez testatu egin zen. 1A Irudian erakusten den moduan, LDLR helduari dagokion proteina-banda soilik LDLR basati eta p.Val859Met aldaeran ageri da (3.1A irudia, 3. eta 4. kaleak). P.Val429Leu eta p.Trp490Arg aldaerei dagokienez, soilik hartzaile heldu-gabeari dagokion banda ikus daiteke (3.1A irudia, 2. eta 7. kaleak). pSer648Pro eta p.Pro685Ser aldaeretan ordea bai hartzaile helduari dagokion banda bai hartzaile heldu-gabeari dagozkien bandak ikus daitezke, hartzaile helduari dagozkien banda LDLR basatiaren kasuan agertzen den bandaren intentsitatea baino baxuagoa izanik (3.1 A irudia, 5. eta 6. kaleak). Kale bakoitzean dagoen proteina-kantitatea banden dentsitateen analisia eginez kuantifikatu zen GAPDH proteina zitosolikoa barne kontrol moduan erabiliz (3.1B irudia). LDLR ezberdinak adierazten dituzten zelulaen RNA mezulari (mRNA) maila neurtzeko, qRT-PCR teknika erabili da. mRNA-ren erauzketa material eta metodoetan zehazten den protokoloa jarraituz egin da. 3.1C irudian erakusten den moduan, LDLR ezberdinen mRNA adierazpenak (GAPDH-aren mezulariarekin normalizatuta) LDLR basatiaren oso parekoak dira.

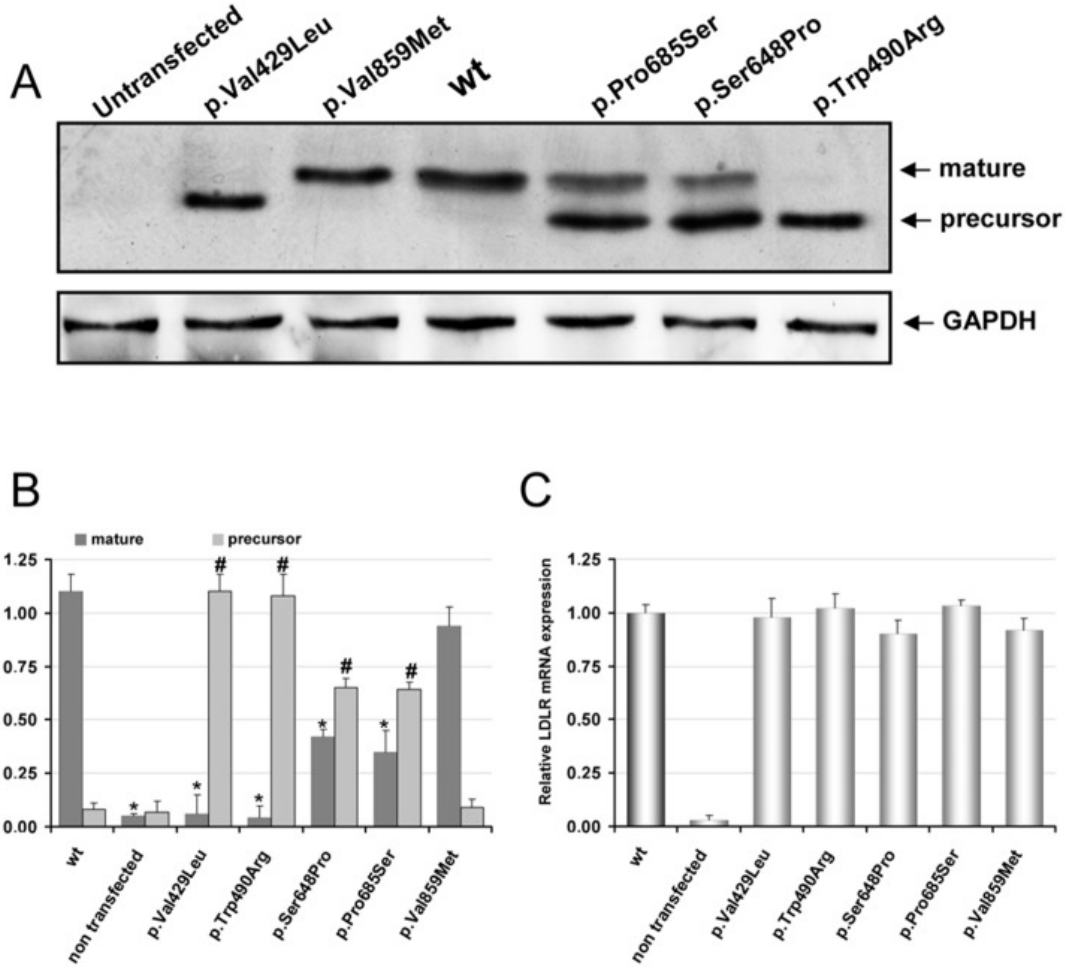

3.1 Irudia. Proteina eta mRNA adierazpena LDLR eta LDLR aldaera ezberdinekin transfekatauriko CHO-*ldl*Δ7 zeluletan. Zelulak aldaera ezberdinak kodetzeen dituzten plasmidoekin transfektatu ziren, proteina 48 orduz adierazten utzi zen eta (A) Proteinaren adierazpena Western plapaketa bidez, (B) hartzaile helduari eta hartzaile heldugabeari dagokien banden intentsitate erlatiboa 160 kDa eta 130 kDa banden intentsitatea GAPDH-ari dagokion bandarekiko ratioa eginez kalkulatu ziren, (C) LDLR-ren RNA mezulari maila GAPDH proteinarekiko erlatibizatua. A irudian 3 esperimentu independenteetan lortutako emaitza adierazgarria irudikatzen da. B eta C irudietan errore barrak hiru esperimentu independenteen arteko desbideratze estandarra adierazten dute. Emaitzen esangura maila student-en t proba erabiliz kalkulatu da. Student-en t proba *p<0,05; #p<0,005 aldaera basatiarekiko kalkultatua.

3.1.2.3 ^{125}I-LDL-ren barneraketa, degradazioa eta LDL-FITC-aren barneraketa LDLR basatiarekin transfektatutako CHO-*ldl*Δ7 zeluletan

Esperimentu hauetan LDLR basatia adierazten duten CHO-*ldl*Δ7 zelulak erabili ziren. Batetik, ^{125}I-LDL-k espezifikoki barneratzeko zein degradatzeko zelula hauek duten gaitasuna aztertu zen eta bestetik, LDL-FITC-ak espezifikoki barneratzeko duten gaitasuna.. Horretarako, transsfektaturiko CHO-*ldl*Δ7 zelulak bi metodoen bidez markaturiko LDL partikulekin inkubatu ziren, material eta metodoetan zehazten den moduan [11]. 3.2 irudian agertzen den moduan LDLR-ren aktibitate maximoa 10µg/ml LDL-tik aurrerako kontzentrazioekin lortu zen bai partikula erradiaktiboekin, zein partikula fluoreszenteekin. Horretaz gain, bi tekniken bidez lortutako balioak estatistikoki esanguratsuak izan ziren 1µg/ml-tik aurrera, 3.2 A eta 3.2 B grafikoetan partikula erradioaktiboentzako irudikatzen den moduan eta 3.2 C grafikoan partikula fluoreszenteentzako. Emaitza hauen arabera, bi teknika hauen sentsibilitatea eta detekzio- tartea oso antzekoak direla esan daiteke.

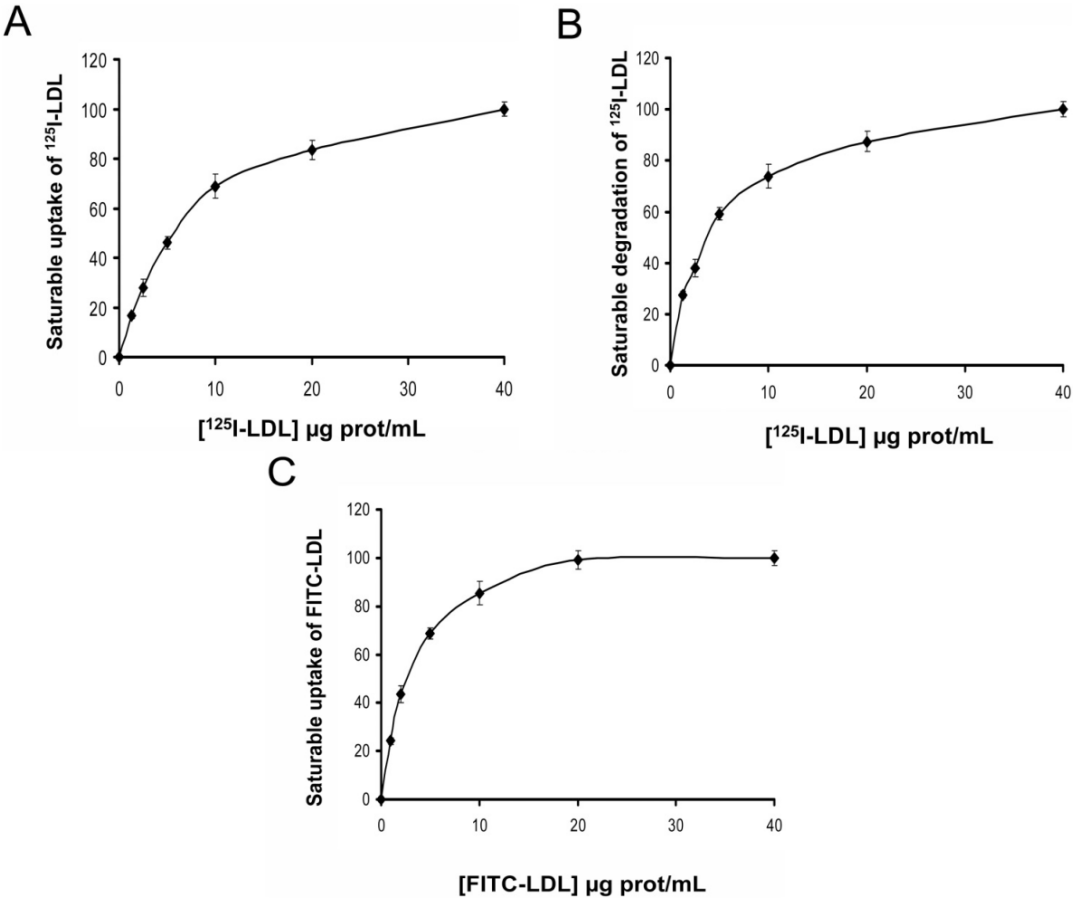

3.2 Irudia. Markatutako LDL partikulekin lortutako barneraketa eta degradazio maximoak LDLR basatiarekin transfektaturiko CHO-*ldl*Δ7 zeluletan. (A) ^{125}I-LDL-ren barneraketa maximoa, (B) ^{125}I-LDL-ren degradazio maximoa, (C) FITC-LDL-ren barneraketa maximoa. ^{125}I-LDL-ren barneraketa (lotutakoa gehi barneratutakoa) eta degradazioaren analisirako CHO-*ldl*Δ7 zelulak LDLR-ren aldaera basatiarekin transfektatu dira eta 4 orduz inkubatu dira 37°C-tan ^{125}I-LDL kontzentrazio ezberdinekin. LDL-FITC-aren barneraketaren analisiaren kasuan LDLR aldaera basatiarekin transfektatutako CHO-*ldl*Δ7 zelulak 4 orduz inkubatu dira 37°C-tan LDL-FITC kontzentrazio ezberdinekin material eta metodoetan azaltzen den moduan. 10.000 zelulen fluoreszentzia kuantifikatu da Fascalibur fluxu zitometroan eta emandako balioak material eta metodoetan zehazten den moduan kalkulatu dira. Esperimentu bakoitzaren hiru erreplika biologiko eta hiru erreplika tekniko gin dira. Emaitzen esangura maila student-en t proba erabiliz kalkulatu egin da.

3.1.2.4 LDLR aldaera ezberdinekin tranfektatutako CHO-*ldl*Δ7 zelulen ^{125}I-LDL-ren barneraketa, degradazioa eta LDL-FITC-aren barneraketa

LDLR basatia edo p.(Val859Met) , p.(Val429Leu), (p.Trp490Arg), p.(Ser648Pro), p.(Pro685Ser) aldaera ezberdinak kodetzen dituzten CHO-*ldl*Δ7 zelulen LDL barneratzeko ahalmena, Anne Katherine Soutar eta Cesar Martin-en laborategietan testatu zen da. Horretarako, transfektatutako zelulak laborategi bakoitzean erradiaktiboki edo fluoreszenteki markatutako 20µg/ml LDL-ekin inkubatu ziren 4 orduz 37°C-tan material eta metodoetan zehazten den moduan. p.Val429Leu eta p. Trp490Arg aldaerak adierazten dituzten CHO-*ldl*Δ7

zelulak ez zuten inolako ^{125}I-LDL barneraketarik edo degradaziorik aurkeztu (3.3A eta 3.3B irudiak) eta LDLR-FITC-aren barneraketari dagokionez, ez zuten inolako ezberdintasunik erakutsi transfektatu gabeko CHO-ldlΔ7 zelulekin alderatzean (3.3C irudia). p.Ser648Pro eta p.Pro685Ser aldaerak espresatzen dituzten zeluletan ordea, 125I-LDL-ren barneraketa eta degradazioa %32 eta %56-koak izan ziren hurrenez hurren LDLR basatia espresatzen duten zelulekin alderatuz, LDL-FITC-ren barneraketa %26 eta %52-koa izanik (3.3A eta 3.3C irudiak). Azkenik, p.(Val859Met) aldaerak LDLR basatiak zeukan aktibitate berdina aurkeztu zuen, bai LDL erradioaktiboa zein fluoreszentea erabiliz.

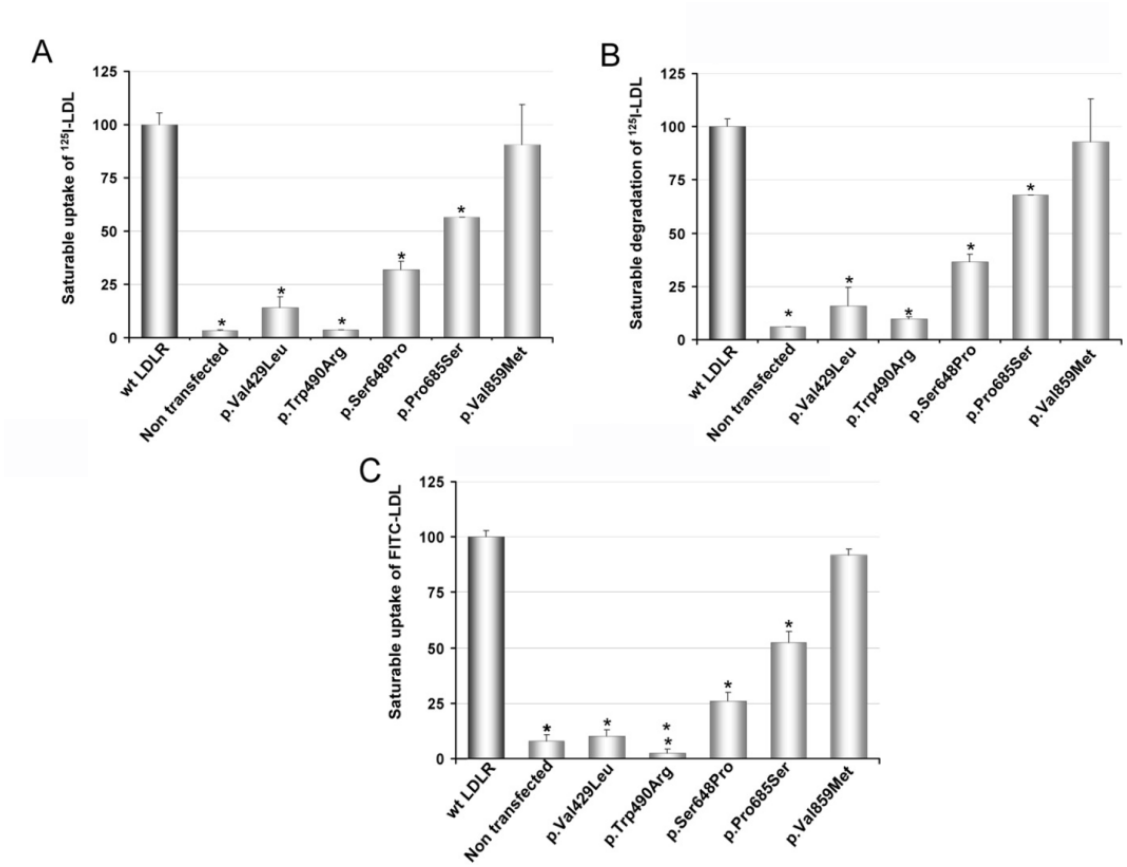

3.3 Irudia. Erradiaktiboki markaturiko LDL-k erabiliz lortutako barneraketa eta degradazio maila LDLR aldaera ezberdinekin transfektatutako CHO-*ldl*Δ7 zeluletan. A) ^{125}I-LDL-ren barneraketA, (B) ^{125}I-LDL-ren degradazio, (C) FITC-LDL-ren barneraketa. . ^{125}I-LDL-ren barneraketa (lotutakoa gehi barneratutakoa) eta degradazioaren analisirako CHO-*ldl*Δ7 zelulak LDLR-ren aldaera ezberdinekin transfektatu dira eta 4 orduz inkubatu dira 37°C-tan ^{125}I-LDL apolipoproteinarekin. LDL-FITC-aren barneraketaren analisiaren kasuan LDLR aldaera ezberdinekin transfektatutako CHO-*ldl*Δ7 zelulak 4 orduz inkubatu dira 20 µg/ml LDL-FITC-rekin 37°C-tan. 10,000 zelulen fluoreszentzia kuantifikatu da Fascalibur fluxu zitometroan eta emandako balioak material eta metodoetan zehazten den moduan kalkulatu dira. Esperimentu bakoitzaren hiru erreplika biologiko eta hiru erreplika tekniko egin dira. Emaitzen esangura maila student-en t proba erabiliz kalkulatu egin da, *p<0.001 LDLR basatiarekin alderatuz.

3.1.2.5 LDLR aldaera ezberdinekin tranfektatutako CHO-*ldl*Δ7 zelulen LDL-FITC-aren lotura

Behatutako LDL-ren barneraketa ezberdintasunak LDL barneraketa prozesuan sortutako akats baten ondorio edo LDL eta LDLR-ren arteko lortura akastun baten ondorio izan zitezken argitzeko, LDL-FITC eta LDLR arteko baturaren efizientzia LDLR aldaera bakoitzarentzako testatu zen fluxu- zitometria erabiliz. Zelulak 4 orduz inkubatu ziren 4°C tan 20μg/ml LDL-FITC-rekin materiak eta metodoetan zehazten den moduan. 20 μg/ml-ko kontzentrazioa aukeratu zen 10 μg/ml-tik aurrera saturazio-mailan bait gaude (3.4 irudia). 5A irudian erakusten den moduan, , p.(Val429Leu), p.(Trp490Arg), p.(Ser648Pro) eta p.(Pro685Ser) aldaerek, LDLR basatiak baino batura- gaitasun txikiagoa erakutsi zuten (LDLR basatia: 100±5, p.(Val429Leu): 22±4, p.(Trp490Arg): 5.8±5, p.(Ser648Pro): 48±5 eta p.(Pro685Ser): 45±3). p.(Val859Met) aldaerak ordea, LDLR basatiaren antzeko balioak erakutsi zituen (LDLR basatia: 100±5, p.(Val859Met): 95.3±3, p>0.26).

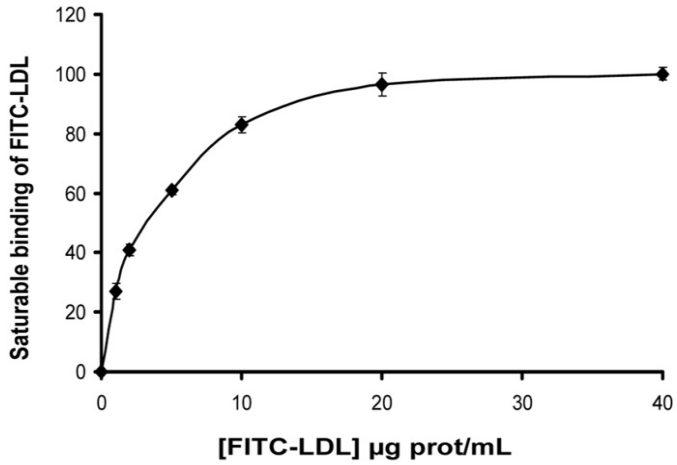

3.4 irudia. LDL-FITC-aren lotura maximoa LDLR basatiarekin transfektaturiko CHO-*ldl*Δ7 zeluletan. LDL-FITC-aren lotura zehazteko, LDLR aldaera basatiarekin transfektatutako CHO-*ldl*Δ7 zelulak 4 orduz inkubatu dira 4°C-tan LDL-FITC kontzentrazio ezberdinekin material eta metodoetan azaltzen den moduan. 10,000 zelulen fluoreszentzia kuantifikatu da Fascalibur fluxu zitometroan eta emandako balioak material eta metodoetan zehazten den moduan kalkulatu dira. Esperimentu bakoitzaren hiru erreplika biologiko eta hiru erreplika tekniko egin dira. Emaitzen esangura maila student-en t proba erabiliz kalkulatu egin da.

3.1.2.6 Fluxu zitometria bidezko LDLR aldaera ezberdinen adierazpena-mailaren determinazioa CHO-*ldl*Δ7 zeluletan

Mintzeko LDLR- adierazpena fluxu-zitometria bidez analizatu zen (3.5B irudia). p.(Val859Met) aldaeraren kasuan, mintzean detektatutako hartzaile-kopurua LDLR basatian detektatutakoaren

oso antzekoa izan zen (LDLR basatia: 100±2, p.(Val859Met): 91±4, p>0.15) (3.5B irudia). p.Ser648Pro eta p.Pro685Ser aldaerenen kasuan aldiz hartzaile basatiarekin lortutako balioen %50-aren ingurukoa izan zen (p.(Ser648Pro): 41±6 eta p.(Pro685Ser): 51±7). p.(Val429Leu) eta p.(Trp490Arg)-ren kasuan, ez zen hartzailearen inolako adierazpenik detektatu zelula mintzetan, lotura eta barneraketarekin gertatu moduan (3.3C eta 3.5A irudiak).

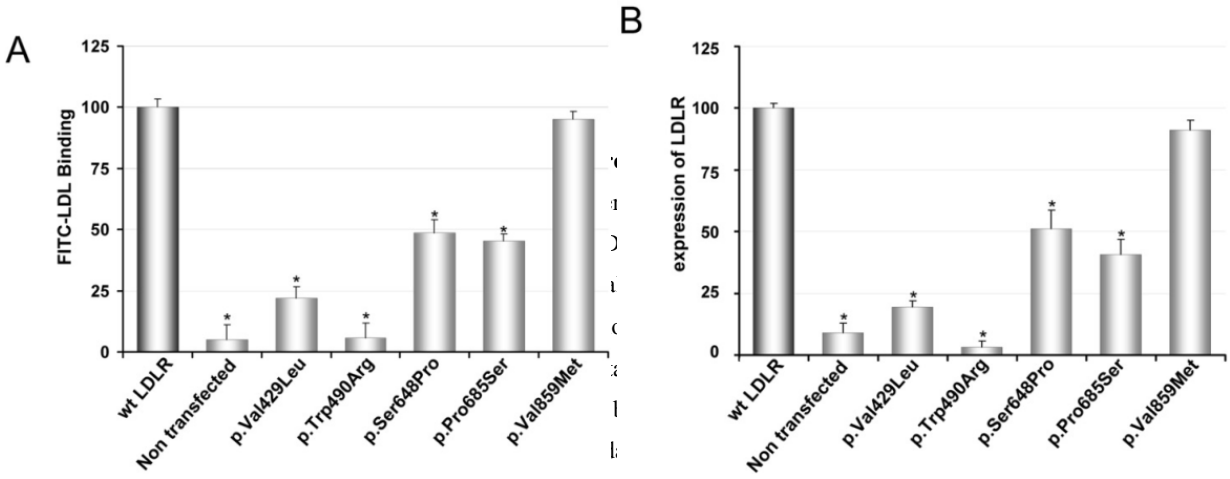

3.1.2.7 LDLR aldaera ezberdinen zelula-barneko kokapena eta mutazioen klasifikazioa

LDLR-ren adierazpena eta honen lokalizazioa aztertzeko mikroskopia konfokala erabili zen, batetik, zitometriaz eta western plapaketa bidez lortutako datuak baieztatzeko eta bestetik, aldaera ezberdinen mutazioak klase edo kategoria ezberdinetan sailkatzeko. Horretarako, LDLR basatia zein aldaera ezberdinak adierazten dituzten zelulak 4 orduz inkubatu ziren LDL partikulekin. LDL eta LDLR-ren kokapen zelularra determinatzeko hauen aurkako antigorputzekin inkubatu ziren zelulak. Texas Red eta FITC fluoroforoekin konjugatutako antigorputz sekundarioak LDLR eta LDL partikulak detektatzeko erabili ziren hurrenez hurren. 3.6 Irudian agertzen den moduan p.(Ser648Pro) eta p.(Pro685Ser) aldaerek hartzaile adierazpen-maila baxuagoa erakutsi zuten,p.(Val429Leu) eta p.(Trp490Arg) aldaerek berriz ez zuten inolako adierazpenik erakutsi. Bestalde, p.(Val859Met) aldaerak LDLR basatiak daukan adierazpen-maila berdina erakutsi zuen, zitometrian lortutako datuekin bat datorrena.

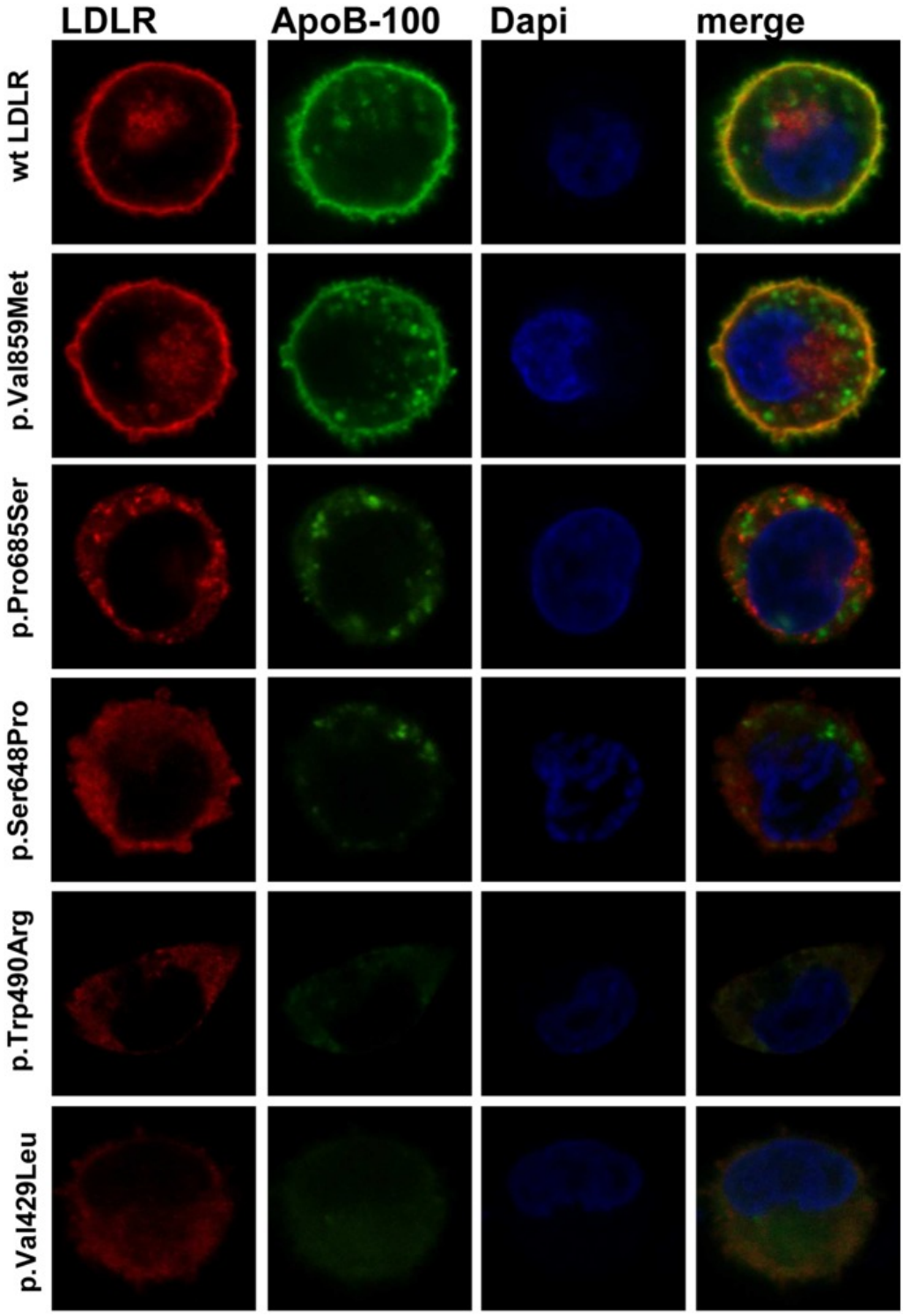

3.6 Irudia. LDLR aldaera ezberdinen mintz adierazpena CHO-*ldl*Δ7 zeluletan. Mintzeko hartzaile adierazpena eta LDL barneraketa detektatzeko mikroskopia konfokala erabili zen. Bai LDLR zein apoB proteinak markatzeko, hauen aurkako antigorputzak erabili dira. Texas Red eta alexa 488 bidez markatutako antigorputz sekundarioak LDLR eta apoB proteinak detektatzeko erabili dira hurrenez hurren. Nukleoak detektatzeko Dapi moleuka erabili da. Irudi bakoitzak baldintza horretarako zelula adierazgarri bat erakusten du.

Adierazpen- mailaz aparte, LDLR aldaera ezberdinen kokapen zelularra analizatu zen baita ere aldaera bakoitza dagoeneko finkatuta dauden klaseetan modu fidagarrian sailkatu ahal izateko. Horretarako zelulak erretikulu endoplasmatikoaren markatzaile espezifikoa den kalretikulinaren aurkako antigorputzekin inkubatu ziren (3.7 Irudia). p.(Val429Leu) eta p.(Trp490Arg) aldaeren kasuan hartzailea eta kalretikulinaren erabateko kolokalizazioak bi aldaera hauek 2a klasean sailkarazten ditu, izan ere hartzaile guztia erretikuluan metatuta geratzen baita bere mintzerainoko garraioa ekidinez. p.(Ser648Pro) eta p.(Pro685Ser) aldaeren kasuan, mikroskopio konfokalez lortutako irudien arabera hartzailea erretikuluan partzialki blokeatuta gelditzen da, eta ondorioz aldaera hauek 2b klasean sailkatuko lirateke

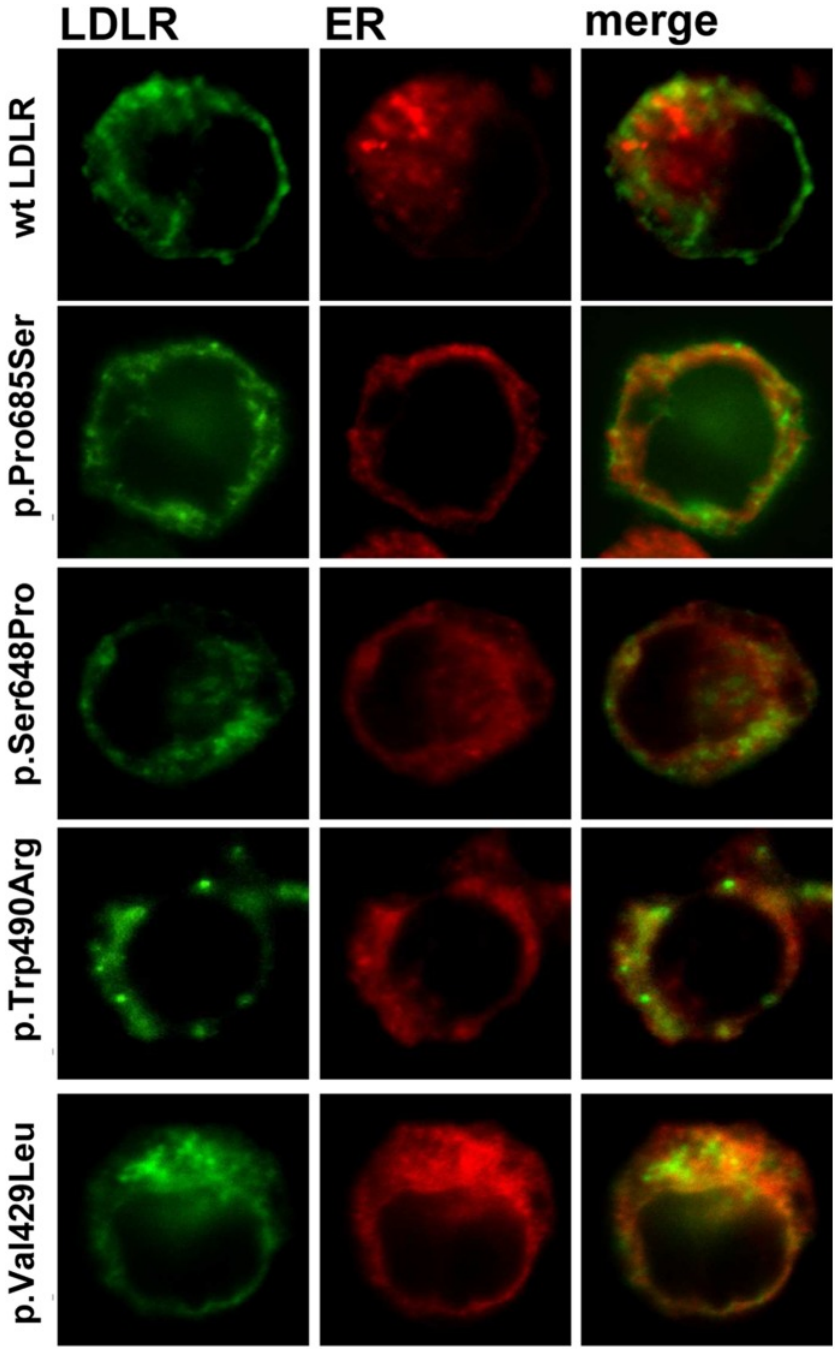

3.7 Irudia. LDLR aldaera ezberdinen zelula-barneko kokapem eta erretikulu endoplasmatikoarekiko kolokalizazioa CHO-*ldl*Δ7 zeluletan. Erretikulu endoplasmatikoaren eta LDLR-ren arteko kolokalizazioa LDLR aldaera ezberdinekin transfektatutako CHO-*ldl*Δ7 zeluletan. Bai LDLR bai kalretikulina proteinak markatzeko, hauen aurkako antigorputzak erabili dira. Texas Red eta alexa 488 bidez markatutako antigorputz sekundarioak kalretikulina eta LDLR proteinak detektatzeko erabili dira hurrenez hurren. Nukleoak detektatzeko Dapi moleuka erabili da. Irudi bakoitzak baldintza horretarako zelula adierazgarri bat erakusten du.

Trp490aminoazidoa, YWTD errepikapenean kokatzen da eta inguruko aminoazido apolarrekin elkarrekintza ezberdinak mantentzen ditu. Triptofano honen ordezkapenakarginina batengatik (3.8A irudiak), elkarrekintza hauen apurketa suposatzen du beta kupelaren tolesdura egokia oztopatuz. p.(Val429Leu) aldaeraren kasuan 3.8B irudian erakusten den bezala, balina, leuzina aminoazidoaz ordezkatzerakoan, beta orriaren tolesdura galarazten da. Bi aldaera hauetan ikusten diren efektu hauek azaldu lezakete hartzaile molekula guztiak erretikuluan blokeatuta gelditzea . 2b klasean ematen den atxikipen partziala bai p.(Ser648Pro) zein p.(Pro685Ser) aldaeretan, aminoazido aldaketek sortutako egitura aldaketen ondorio izan daiteke (3.8C eta 83.D irudiak). Ser64 aminoazidoa beta kupelaren lehenengo beta orrian kokatzen da. Aminoazido hau prolina batez ordezkatzerakoan bi prolina jarraian egongo lirateke eta honek beta kupelaren egitura desegonkortu dezake (3.8C irudia). Pro685 aminoazidoa, Epidermal Growth Factor(EGF)-C domienuaren tolesdurarako aminoazido gakoa da, Val529 eta Tyr532 aminoazidoekin elkarrekintza hidrofobikoak sortzen bait ditu [18]. Prolina honen ordezkapenak serina batez, 3.8D irudian azaltzen den moduan, elkarrekintza hauek apurtuko lituzke, aldaketak sortzen duen polaritate aldaketaren ondorioz..

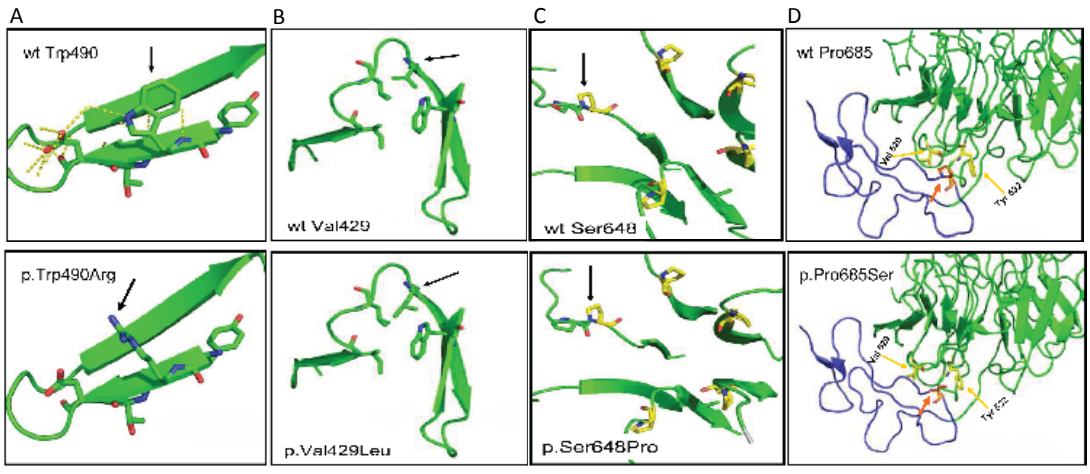

3.8 Irudia. A) Beta kupelean dauden YWTD errepikapenetan kokatutako triptofanoek proteina zati honek daukan horri egitura mantentzea baimentzen du. Triptofano hauek elkarrekintza hidrofobiko ezberdinak mantentzen dituzte inguruko aminoazidoekin, gainera, hidrogeno zubiak sortzen dituzte ondoan aurkitzen diren aspartikoekin, bi elkarrekintza hauek proteinaren zati honetan horri egitura mantentzea ahalbidetzen

dute. Trp490-ren ordezkapena Asn baten bidez lotura hidrofobikoak desegiten ditu. B) Val429 eta inguruko aminoazidoen egitura. Val429 proteina zati honen egituratze egokia baimentzen du elkarrekintza hidrofobikoen bidez. Leuzinak eta balinak ezaugarri kimiko nahiko antzeko dituzte, ezberdintasun garrantzitsuena tamaina izanik zeina egituraren toleste egokia oztopatu dezake. C) Beta kupela egituratzen duten orrien hasieran dauden prolinak beharrezko malgutasuna ematen diete orri tarte hauei kupel egitura hau sortu ahal izateko. Malgutasun hau beharrezkoa da kupelaren toleste egokirako, ala ere, bi prolina bata bestearen ostean gehiegizko malgutasuna sortu dezakete egitura ezegonkortuz. Irudi hau, D) EGF-C domienuan aurkitzen den Pro685 beta kupelean aurkitzen diren aminoazido ezberdinekin lotura hidrofobikoak sortzen ditu. Serina batez ordezkatzerakoan, polaritate ezberdinaren ondorioz, elkarrekintza hauek ekidin ditzake. Irudi hauek, PyMOL software-a erabiliz egin dira. (DeLano scientifics) (PDB:1N7D) (PDB:3S06).

3.1.3 Eztabaida

Gaixotasun kardiobaskularra eritasun- eta heriotza- tasa handiena duen gaixotasuna da, hiltzen diren pertsonen herenaren kausa izanik [19–21]. FH pairatzen duten pertsonen kasuan, gaixotasun kardiobaskularra garatzeko arriskua askoz handiagoa da kolesterol maila jaisteko tratamendu goiztiar batekin ahalik eta lasterren hasten ez badira. Horretarako, ordea, ezinbestekoa da gaixotasunaren diagnostiko goiztiarra egitea. Gaur egun, FH diagnostikatzeko zenbait erizpide fenotipiko daude, hauek ordea ez dira nahikoak FH paziente guztiak identifikatzeko[22]. Hori dela eta, azken urteetan genoman oinarritutako teknikak aplikatzen hasi dira; hala ere, teknika hauek analisi funtzional baten beharra daukate diagnostiko definitibo eta fidagarri bat eman ahal izateko. Gaur egun, 1300 aldaera baino gehiago ezagutzen dira LDLR-n. Horietatik %80-90 inguru patogenoak izateko potentziala azaldu dute baina oso gutxi daude behar bezala funtzionalki karakterizatuta [3,10,23]. Gaixotasunaren diagnostiko goiztiar eta definitiboa pausu garrantzitsua da gaixotasunaren prognosia hobetzeko eta paziente gazteetan tratamendu egokia emateko [24], honek gainera, inbertsio handia aurreztuko lieke osasun zerbitzuei[25].

Gaur egun, LDLR-ren *ex vivo* analisi funtzionalak erradioaktibitatean oinarritutako teknikekin egiten dira, ^{125}I-LDL-ren barneraketa eta degradazioa neurtuz edo fluoreszentzian oinarritutako teknikak erabiliz. Urte askotan erradioaktibitate metodoak LDLR funtzionalki karakterizatzeko erreferentzia metodoak izan dira, hala ere, azken urteetan fluoreszentzian oinarritutako teknikak erabiltzen hasi dira hartzailearen aktibitatea testatzeko [11,14,26]. Erradioaktibitatean oinarritutako metodoek desabantaila ezberdinak aurkezten dituzte fluoreszentzian oinarritutakoekin alderatuz , batetik, erradioaktibitaterekin lan egiteak nahiko arriskutsua izan daiteke laginak manipulatzen

dituzten pertsonentzat, eta bestetik, hondakin erradiaktiboen prozesamenduak arazo etiko eta ekologiko ezberdinak ekar ditzake. Metodo fluorimetrikoak ordea, fluoroforo eta proteinaren arteko lotura kobalentean oinarritzen dira eta ondorioz erradiaktibitateak sortzen dituen arazoak ekiditen ditu. Gainera, FITC bidezko markaketa nahiko merkea da iodo erradiaktiboarekin alderatuz eta oso egonkorra.

Lan honetan, fluoreszentzia-tekniken baliogarritasuna (validez) aztertu da LDLR-ren aktibitatea neurtzerako orduan. Horretarako aurretiaz erradiaktibitate bidez karakterizatutako LDLR aldaera ezberdinen aktibitatea neurtu da fluxu zitometria erabiliz [27]. Hartzailearen aktibitatearen neurketan oso emaitza parekoak lortu dira sentsibilitatea eta emaitzen errepikakortasuna kontuan hartuta, bai ^{125}I-LDL-k zein FITC-LDL-k erabiliz (3.2 eta 3.4 Irudiak). Gainera, fluxu zitometriak mintzeko hartzaile kopurua eta batutako LDL-FITC kopuruaren kuantifikazioa baimendu du (3.4 eta 3.5 Irudiak) analisi eta karakterizazio hobea lortuz. Bestalde, zitometria bidez lortutako datuek mikroskopia konfokalez lortutako irudiekin osatuz LDLR aldaera ezberdinen sailkapena ahalbidetzen dute.

Lan honetan, fluxu zitometria eta FITC bidez markaturiko lipoproteinen erabilera, LDLR-ren aktibitatea determinatzeko teknika fidagarri eta egokia direla baieztatu dugu . Gainera, mikroskopia konfokalarekin konbinatuz, aldaera ezberdinen sailkapen egokia egiten lagundu dezake, gaixotasunaren diagnostiko fidagarriagoa ahalbidetuz. Fluoreszentzian oinarritutako metodologia hauek, beraz, aukera oso gomendagarria izango dira LDLR aldaera ezberdinen funtzionaltasuna determinatzeko, eta bereziki garrantzitsua izango da gaur egungo sekuentziazio metodologia berriek aurkitzen ari diren LDLR aldaera berrien kopuru handiagatik.

3.2 LDLR aldaeren analisi bateratuak familia-hiperkolesterolemiaren diagnostikoan duten erabilgarritasunaren azterketa

3.2.1 Sarrera

Familia-hiperkolesterolemia (FH) egun ezagutzen diren gaixotasun monogenikoen artean arrunt eta ezagunetarikoa da. Dentsitate baxuko lipoproteinaren hartzailean (ingelesetik, *Low Density Lipoprotein Receptor* edo *LDLR*) gertatzen diren mutazio ezberdinak gaixotasuna sortarazten duten kasuen % 90-aren atzean daude [6,28,29] . FH duten pertsonek gaixotasun kardiobaskularra garatzeko arrisku handiagoa daukate, besteak beste, odoleko LDL-kolesterol (LDL-C) maila altuengatik [30]. Horregatik, paziente hauen identifikazioak eta tratamendu goiztiarrak gaixotasun kardiobaskularra jasateko arriskua nabarmenki murriztu edo desagerrarazi dezakete [31]. Hau dela eta, Munduko Osasun Erakundeak (OMS) mundu mailako bilaketa gomendatu du, FH duten pazienteak era goiztiar batean identifikatu eta lipido maila gutxitzeko tratamendupean jartzeko, hau bait da onura gehien lortu dezaken biztanleria. Saiakera honetan, gaixotasuna diagnostikatzeko orain arte erabili den protokolo zabalduena FH izan zezaketen pertsonen parametro klinikoen azterketa izan da.. Hau ordea kasu askotan ez da nahikoa izaten diagnostiko zehatz eta definitibo bat eman ahal izateko[32]. Horregatik, protokolo eguneratuenetan test genetikoen erabilpena gomendatzen da[33].

LDLR-n dauden mutazioak deskribatzen hasi zirenetik, FH identifikatzeko teknikak asko hobetu dira eta ia egunero polimorfismo ezberdinak deskribatzen dira populazio ezberdinetan[3,34,35]. Hala ere, askotan eta askotan aldaera hauen funtzionaltasuna ez da aztertu eta, ondorioz, eskura egon daiteken informazio urriarekin medikuek diagnostiko ezegokiak eman ditzakete. Hori gutxi balitz, gaur egun garatu diren sekuentziazio- teknika berriak direla eta, inolako informazio klinikorik izango ez duten LDLR mutazio berri ugariren deskribapena espero da hurrengo urteetarako eta, ondorioz, bereziki garrantzitsua izango da hauen funtzionaltasunaren azterketa izatea. Gainera, FH datu-basearen arabera, *in silico* analisiek aurkitutako aldaeren %80-a soilik mutazio patogeno moduan sailkatu dituzte eta hauetatik erdiak baino gehiagok ez dauka inolako analisi osagarririk, hala nola, kosegregazio ikerketarik edo *in vitro* eginiko funtzio balioztapenik[36–38].

Kapitulu honetan FHz diagnostikatutako 55 familien deskribapen eta analisi fenotipiko eta genotipikoa burutu da. 55 familia hauek 5 aldaera funtzional eta 8 aldaera neutro aurkezten dituzte. Analisia era egokian egin ahal izateko karakterizatu gabeko 8 aldaeren balioztapen

funtzionala egin da. Azkenik, FH duten pazienteen diagnostiko egokirako parametro kliniko, molekular eta funtzionalen analisi bateratuaren garrantzia azpimarratu da.

3.2.2 Emaitzak

Portugalen egindako HF?FH ikerketan aurkitutako 35 aldaerek (totalaren % 30) funtzionaltasun eta patogenizitate ezezaguna dute. Ikerketa honetan 35 aldaera horietatik 8 aukeratu ziren karakterizazio funtzionala burutzeko. Karakterizatutako aldaerak hurrengo irizpideak jarraituz aukeratu ziren: (i) Portugaleko populazioan daukaten maiztasuna (1. Irudia), (ii) ko-segregazio eza, (iii) fenotipoaren larritasuna eta (iv) laginen eskuragarritasuna.

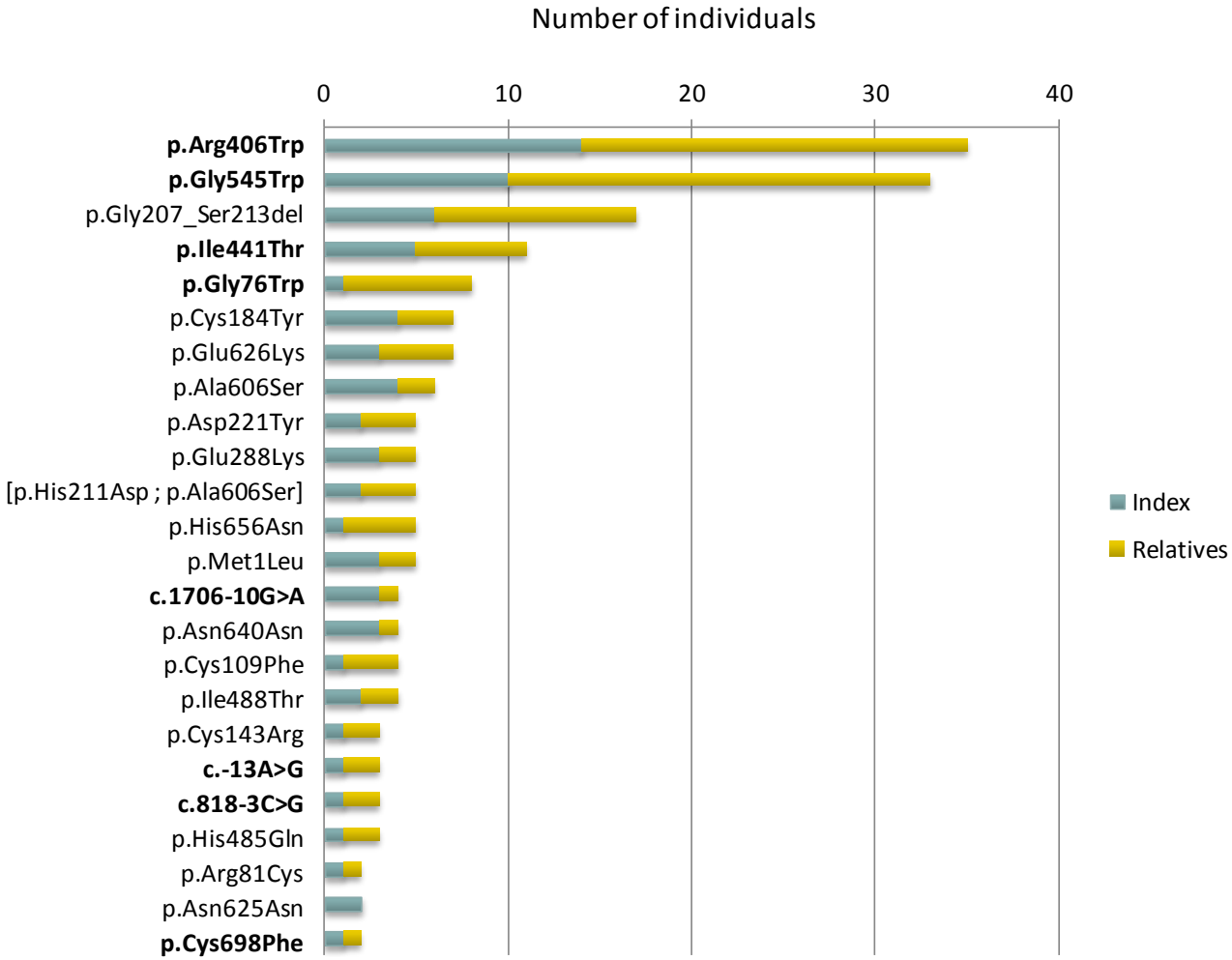

3.9 Irudia – Ikerketa funtzionala ez duten aldaeren artean, Portugaleko FH populazioan detektatutako aldaeren maiztasunak.

3.2.2.1 *In silico* analisia

Software ezberdinekin lortutako emaitzak bai 3.2 taulan bai 3.3 taulan ageri dira.

3.2 Taula. LDLR-an aurkitzen diren sentsu gabeko aldaeren in silico eta in vitro

Alteration			Frekuentziak			In silico analisia				Erreferentziak	
DNA osagarria	Proteina	Kosegregazioa (a)	1 KG(%)	ESP (%)	Normolipidemikoen panela (b)	Poliphen2	SIFT	Mutation Taster	Analaisi funtzionala	Deskribatua	Analisi funtzioanala
c.226G>C	p.Gly76Trp	3/3; 5/6	NF	NF	0/95	Probably	Deleterious	Disease causing	Benign	11	Lan honetan analizatua
c.806G>A	p.Gly269Asp	9/14; 2/2	0,1	0,008	0/95	Benign	Tolerated	Disease causing	Benign	34	27
c.829 G>A	p.Glu277Lys	2/2; 1/1	0,001	0,023	0/95	Benign	Tolerated	Disease causing	Benign	35	28
c.1216C>T	p.Arg406Trp	35/36; 0/2	NF	NF	0/95	Probably	Deleterious	Disease causing	Pathogenic	36	Lan honetan analizatua
c.1322T>C	p.Ile441Thr	11/12; 0/1	NF	NF	0/95	Probably	Deleterious	Disease causing	Pathogenic	2	Lan honetan analizatua
c.1633G>T	p.Gly545Trp	32/33; 0/4	NF	NF	0/95	Probably	Deleterious	Disease causing	Pathogenic	11	Lan honetan analizatua
c.2093G>T	p.Cys698Phe	2/0; 0/0	NF	NF	0/95	Probably	Deleterious	Disease causing	Pathogenic	3	Lan honetan analizatua
c.2575G>A	p.Val859Met	2/3; 1/1	0,001	0,008	0/95	Benign	Deleterious	Polimorphism	Benign	11	29

Letra lodiz markatuta ageri diren aldaerak 3 software ezberdinekin egoki analizatuak izan dira.
aKosegregazio balioak aldaera eramaile / FH edo aldaera eramaile /ez FH moduan ageri dira. bLipido maila normalak dituzten 95 pertsona (Normolipidemic) . 1Kg, 1000 Genomes Project; Esp, National Heart, Lung and Blood Insitutua GO Exome Sequencing Project; NF, ez da topatu.

3.3 Taula LDLR-an promoteore edo mozte itsasketa guneetan aurkitzen aldaeren in silico eta in vitro

Alteration			Frekuentziak			In silico analisia				Erreferentziak	
Introia	DNA osagarria	Kosegregazioa (a)	1 KG(%)	ESP (%)	Normolipidemic-oen panela (b)	Splice Port	NNSSO	NetGen2	Analaisi funtzionala	Deskribatua	Analisi funtzioanala
Promotorea	c.13A>G	3/5; 0/0	NF	0,008	0/95	60 (exon 1A)	0 (exon 1A)	100 (exon 1A)	Benign	9	37
5	c.818-3C>G	3/3; 0/1	NF	NF	0/95	0 (exon 6A)	0 (exon 6A)	0 (exon 6A)	Pathogenic	Novel	Lan honetan analizatua
7	1061-8T>C	12/13; 3/4	0,52	0,799	2/75	100 (exon 8A)	100 (exon 8A)	100 (exon 8A)	Benign	38	23
11	c.1706-10G>A	3/4; 1/1	0,08	0,146	0/95	100 (exon 12A)	100 (exon 12A)	100 (exon 12A)	Benign	Novel	Lan honetan analizatua
14	c.2140+5G>A	4/4; 0/0	0,28	0,889	ene-75	86 (exon 14D)	33 (exon 14D)	86 (exon 14D)	Benign	39	23

Letra lodiz markatuta ageri diren aldaerak 3 software ezberdinekin egoki analizatuak izan dira.z
aKosegregazio balioak aldaera eramaile/ FH edo aldaera eramaile /ez FH moduan ageri dira. bLipido maila normalak dituzten 95 pertsona. 1Kg, 1000 Genomes Project;
z Esp, National Heart, Lung and Blood Insitutua GO Exome Sequencing Project; NF, ez da topatu.

Mozte-Itsasketa guneetan eta promotorean ageri diren mutazioen karakterizazioa

c.-13A>G eta c.1706-10G>A aldaeren analisi funtzionala burutu zen da eta biak funtzionaltasun normala aurkeztu zuten (3.3 Taula) c.818-3C>G aldaerak ordea, bi nukleotido gehitzen ditu bostgarren exoian atxikituta (3.10. Irudia). Promotorean mutazioa duen aldaera berriz neutro moduan sailkatu da, LDLR-ren bi aleloak (T/C) RNA mezulari mailan ez bait dute inolako adierazpen diferentziarik. c.1706-10G>A aldaeraren kasuan bi aleloen osotasuna konprobatu eta ez da inolako ezberdintasunik topatu PCSK9 basatiarekin alderatzerakoan.

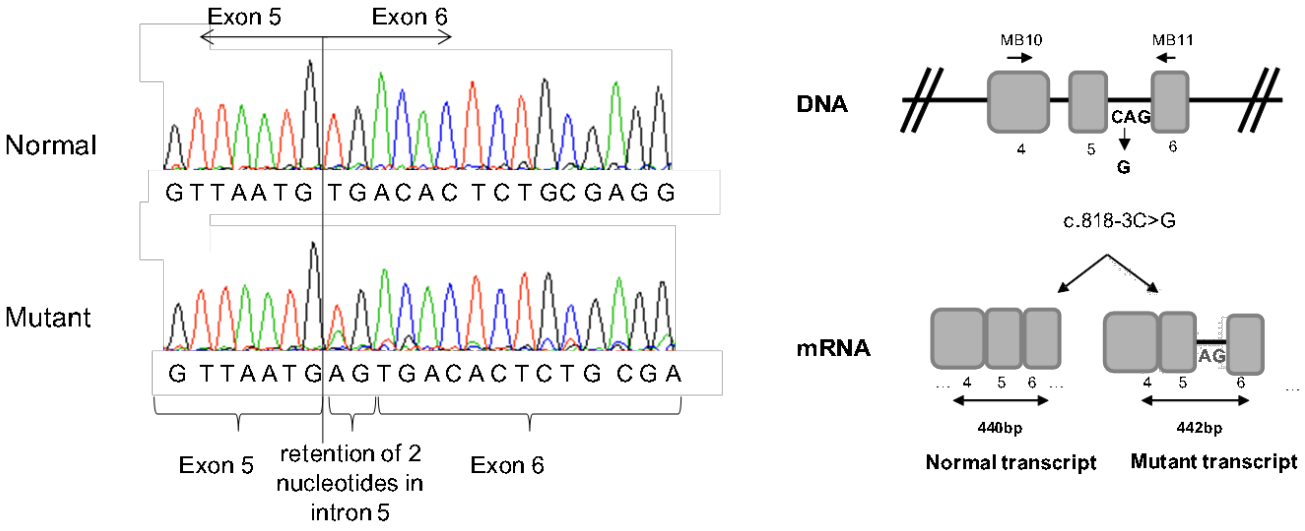

3.10 Irudia - c.818-3C>G aldaeraren efektua mRNA mailan. B irudian mRNA zati konkretu hau anplifikatzeko erabilitako hazleak eta aldaeraren kasuan exoian atxikituta geratu diren nukleotidoak ageri dira. 2 nukleotido hauek irakurtarauaren aldaketa sortzen dute irakurketa pauta aldatuz eta 274 aminoazidoan amaiera kodoi bat sartuz.

3.2.2.2 LDLR aldaera ezberdinen adierazpena CHO-*ldl*Δ7 zeluletan

LDLR aldaera ezberdinen adierazpena western plapaketa bidez aztertu zen. p.Gly76Trp aldaerak eta LDLR basatiak 130 kDa inguruan LDLR helduari dagokion banda bat ageri dute, (3.11A Irudia. 1. eta 2. kaleak). pArg406Trp aldaeraren kasuan, bi banda detektatu ziren, bata LDLR helduari dagokio, bestea LDLR heldugabeari dagokiolarik (3.11A Irudia. 3. Kalea). Azkenik p.Ile441Thr, p.Gly545 eta p.Cys698Phe aldaeretan LDLR heldugabeari dagokion banda bakarra detektatu zen (3.11A Irudia. 4., 5. eta 6. kaleak). Geleko kale ezberdinek proteina karga berdina zutela konprobatzeko GAPDH proteina konstitutiboaren aurkako antigorputza erabili genuen (3.11A Irudia). Proteina ezberdinen adierazpenak densitometria bidezko analisi bidez kuantifikatu ziren (3.11B Irudia), eta ez zen aldaeren artean ezberdintasun estatistikorik behatu.

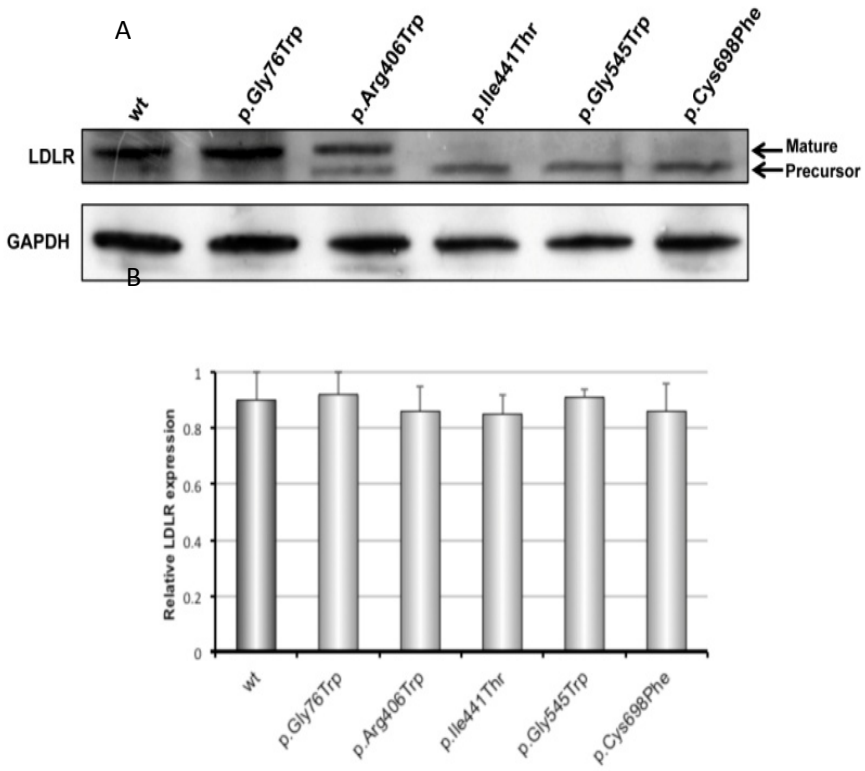

3.11 irudia. LDLR aldaeren adierazpen analisia western plapaketa bidez. A) western plapaketa; B) LDLR western plapaketaren analisi kuantitatiboa GAPDH proteinarekiko erlatibizatu ostean.

.

3.2.2.3 LDLR aldaeren fluxu zitometria bidezko funtzionaltasun analisia

p.Gly76Trp aldaerak LDLR basatiaren antzeko mintz mailako adierazpena erakutsi zuen (wt: 100±5; p.Gly76Trp:102±2). pArg406Trp, p.Ile441Thr, p.Gly545 eta p.Cys698Phe aldaerek aldiz adierazpen maila txikiagoa aurkeztu zuten LDLR basatiarekin alderatuz (p.Arg406Trp: 65±5; p.Ile441Thr: 7±5; p.Gly545Trp: 7±5; p.Cys698Phe: 8±6; P <0.01) (3.12A irudia). LDL eta hartzaile ezberdinen arteko batura-mailari dagokionez, adierazpen entseguan lortutako antzeko emaitzak ikusi ziren (wt:100±3; p.Gly76Trp: 90±3; p.Arg406Trp: 60±4; p.Ile441Thr: 5±3; p.Gly545Trp: 6±4; p.Cys698Phe: 3±1; P < 0.01) (3.12B Irudia). 3.12C irudian, aldaera berdinentzako LDL barneraketa datuak ageri dira (wt: 100±4; p.Gly76Trp: 95±5; p.Arg406Trp: 62±4;p.Ile441Thr: 10±3; p.Gly545Trp: 11±4; p.Cys698Phe: 8±5; P< 0.01). Lortutako emaitzak ikusita, esan daiteke p.Gly76Trp aldaerak ez duela inolako eraginik LDLR-ren aktibitatean. Beste lau aldaerek aldiz LDLR-ren aktibitatea partzialki murrizten dute (p.Arg406Trp) edo ia guztiz(p.Ile441Thr, p.Gly545 eta p.Cys698Phe).

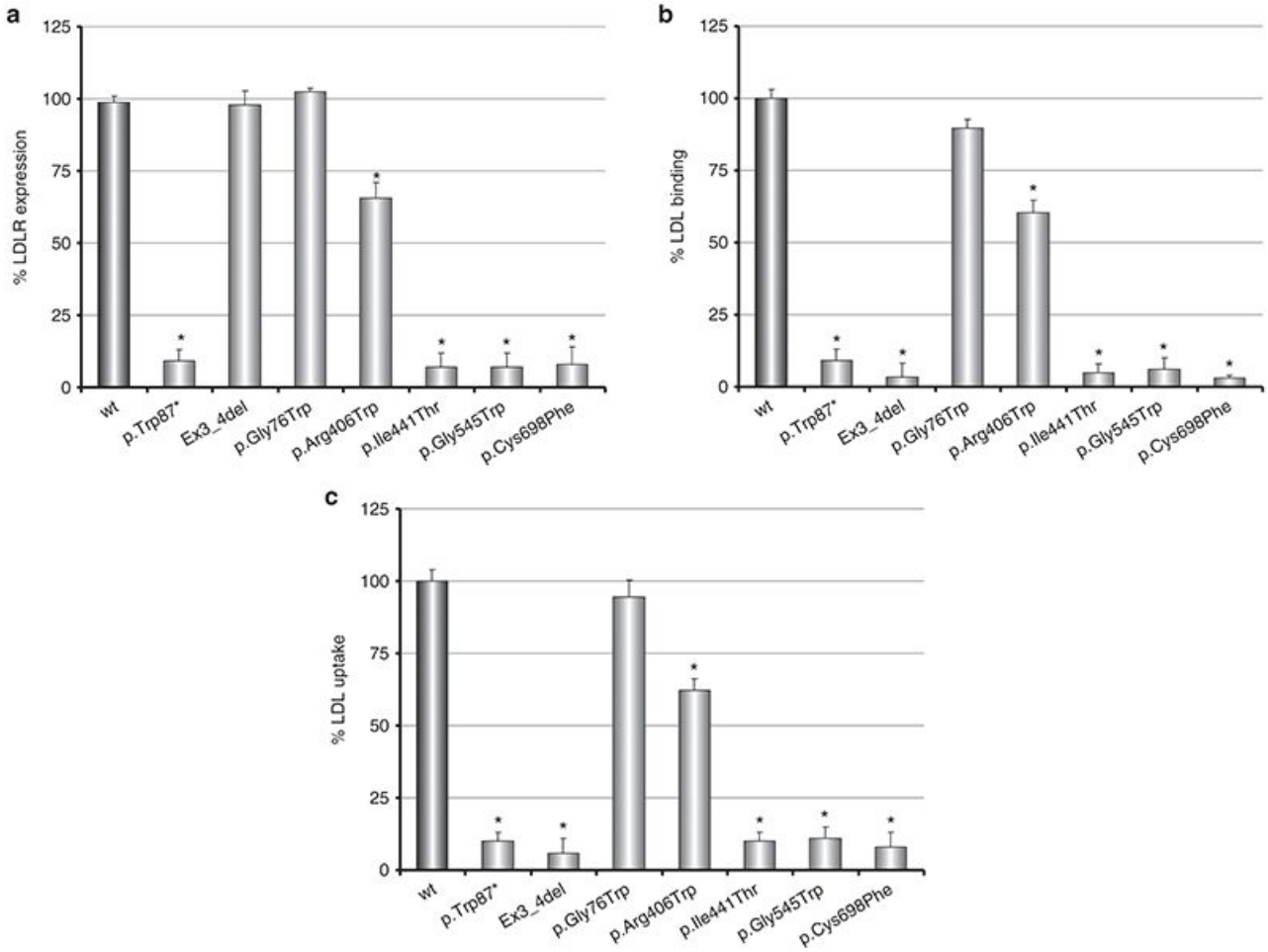

3.12 irudia LDLR aldaeren fluxu zitometria bidezko funtzionaltasun analisia. (A) LDLR-ren mintz-adierazpena. (B) LDLR-LDL batura 4 °C-tan 4 orduz inkubatu eta gero, ehunekotan adierazita. (C) LDL barneraketa, ehunekotan, 4 orduz 37 °C-tan inkubatu eta gero. Saio guztiak hiru aldiz errepikatu dira eta 10,000 zelulen intentsitatea neurtu da lagin bakoitzeko. Emaitzak esperimentu ezberdinen bataz besteko moduan adierazi dira ± desbiderapen estandarra (S.D., ingelesetik *standard deviation*). Esanguratasun estatistikoa Student t-testa ($p \leq 0.05$) erabiliz zehaztu da.

3.2.2.4 LDLR aldaera ezberdinen zelula-barneko kokapena eta mutazioen klasifikazioa

Fluxu zitometriaz lortutako emaitzen arabera, p.Arg406Trp aldaera erretikuluan partzialki atxikita geratu daiteke (2a klasea) edo birziklapen arazo bat izan dezake. Bestalde, p.Ile441Thr, p.Gly545 eta p.Cys698Phe aldaeren kasuan fluxu zitometriaz ez da LDLR-ren inolako mintz-adierazpenik detektatu hori dela eta bi klase ezberdinetan sailka daitezke, inolako barne adierazpenik aurkezten ez duten aldaerekin (1 klasea) edo erretikuluan erabat atxikita geratzen direnekin (2a klasea). 3.13 Irudian ikusten den moduan, p.Arg406Trp aldaerak kalrretikulinarekin kolokalizazio partziala dauka eta ondorioz 2b klasekoekin sailka daiteke. Beste hiru aldaerek ia guztiz kolokalizatzen dute erretikuluko kalrretikulina proteinarekin eta ondorioz 2a klasean sailkatzen dira.

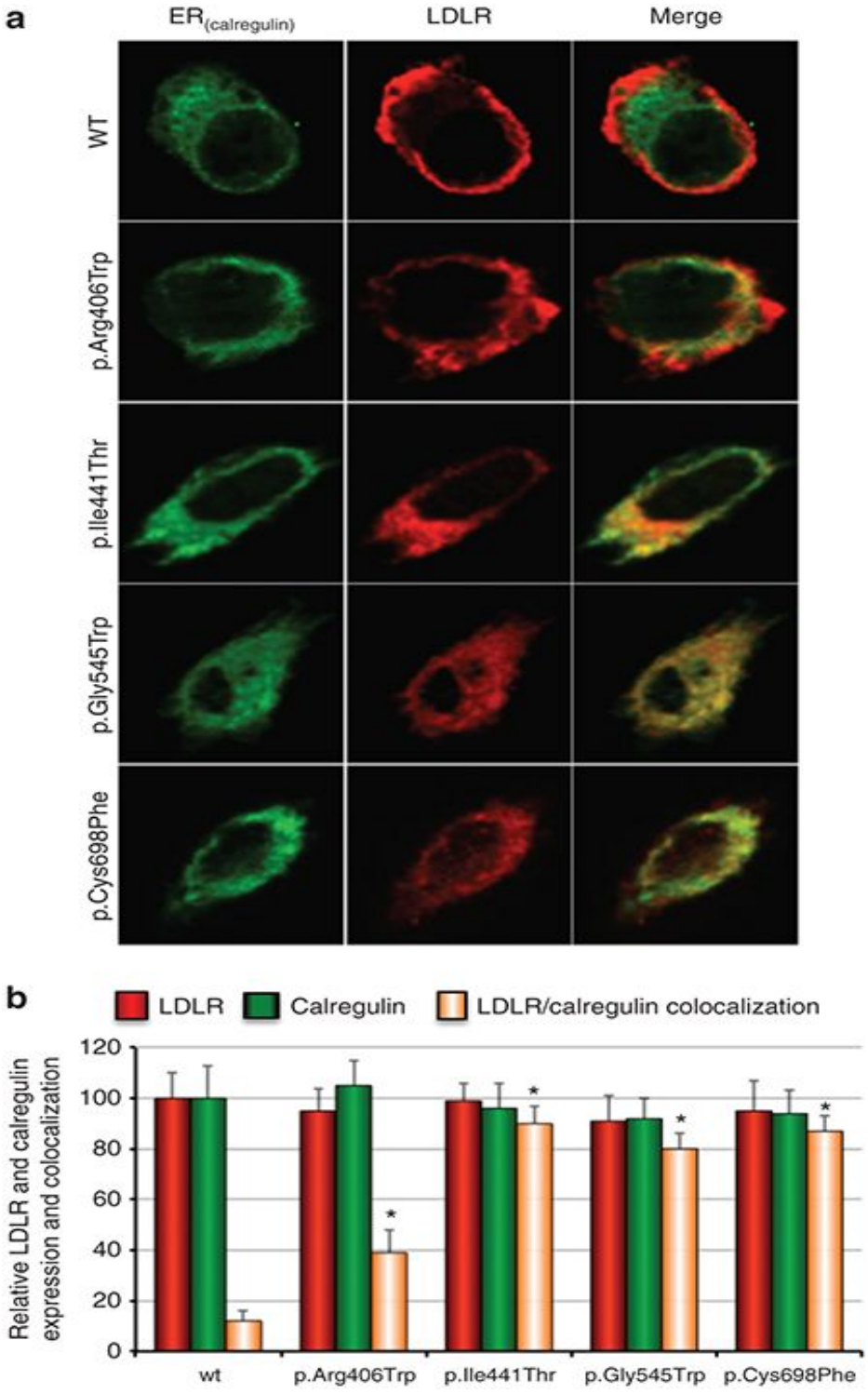

3.13 Irudia. Mikroskopia konfokal bidezko LDLR basatia, p.Arg406Thr, p.Ile441Thr, p.Gly545 eta p.Cys698Phe aldaeren analisia.(a) LDLR-aren adierazpena eta honek kalerretikulina proteinarekin daukan kolokalizazioa aztertu dira, 48 orduko trasnfekzioaren ostean . Proteina ezberdinen markaketa antigorputz espezifikoen bidez egin da. Texas Red eta Alexa 488 fluoroforoak LDLR eta kalerretikulina ikusteko erabili dira hurrenez hurren. Irudian erakusten diren zelulak 30 zelula ezberdinen irudien adierazgarriak dira. (b) Emaitzak irudi ezberdinetan lortutako intentsitateen bataz besteko moduan ageri dira ±SD. LDLR basatiarekiko esanguratasun estatistikoa Student testa ($p<0.001$) erabiliz kalkulatu da.

3.2.2.5 p.Arg406Trp aldaeraren birziklapen entseguak

p.Arg406Trp aldaerak birziklapen akatsik ez zuela ziurtatzeko, pH ezberdinetan lotzen duen LDL kopurua eta LDL-aren presentzian hartzaileak denboran zehar duen adierazpena kuantifikatu ziren fluxu zitometria bidez. 3.14A irudian aurkezten den moduan, LDL gehitu ondoren, LDLR-ren adierazpena ez zen murriztu denboran zehar ez LDLR basatian ez p.Arg406Trp aldaeraren kasuan. Bestalde ikus daiteke pH jaitsierak LDL-ren askapenean zuen eragina LDLR basatian zein p.Arg406Trp aldaeran oso antzekoa dela (3.14B). Bi kasuetan pH 5.5-ean daukaten LDL lotua pH 7.5-ean daukatenaren laurdena da. Bi esperimentu motetan p.Arg416Trp aldaera kontrol moduan erabili da.

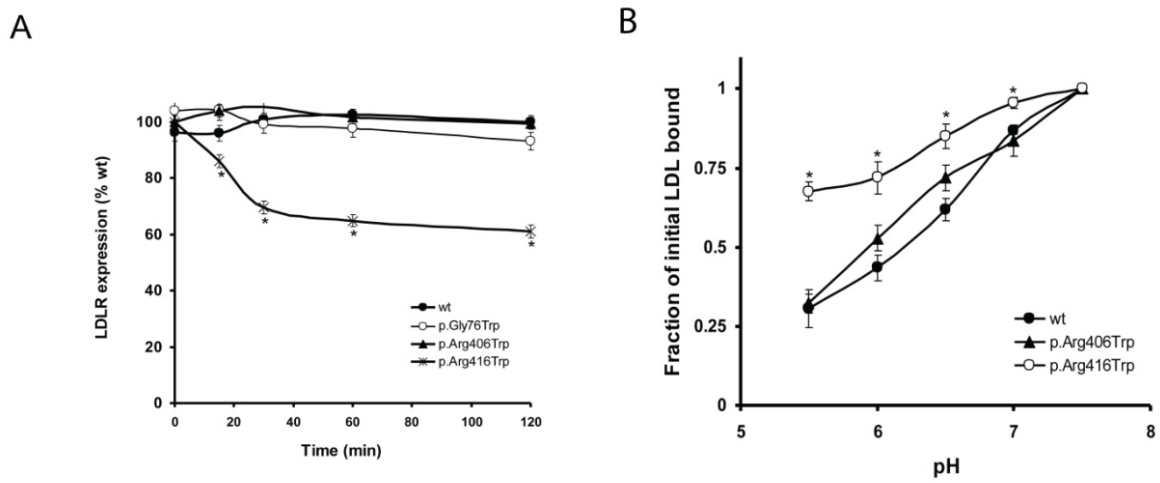

3.14 Irudia. p.Arg406Trp aldaeraren birziklapena. A) LDLR mintz adierazpena denboran zehar markatu gabeko 20μg/ml LDL gehitu ondoren; B) LDL-LDLR arteko mintz lotura pH ezberdina duten DMEM medioetan.

3.2.2.6 Lipido profila aldaera funtzional eta ez-funtzionaletan

diagnostikoaren fidagarritasuna hobetzeko aldaera patogenikoak dituzten pertsonen profil lipidikoak aldaera neutroak (funtzionalak) dituzten pertsonen profilekin alderatu ziren. Ikerketaren zati honetarako hurrengo bost aldaera neutroak dituzten pertsonen datu biokimikoak erabili ziren; p.Gly269Asp, p.Glu277Lys, c-1061-8T>C,c.2140+5G>A, eta p.Val859Met [11,26,39,40].

Bi talde hauen datuak konparatu ostean, aldaera ez funtzionalak dituzten pertsonek fenotipo larriago bat aurkezten zutela ikusi zen. Izan ere, adina, dentsitate altuko lipoproteina eta apoA1 ez diren beste parametro guztietan ezberdintasun esanguratsuak ikusi ziren. Esaterako, funtzionalak ez diren aldaerak dituzten pertsonak, LDL-C pertzentil altuagoetan aurkitzen dira (83.6±22.4 vs. 61.2 ±34.2 mg/dl; P = 0.002) (3.4 Taula).

Gaixotasun kardiobaskular goiztiarra ere askoz arruntagoa zela ikusi zen LDLR funtzio galera duten familietan (% 74.2) LDLR funtzio normala duten familiekin alderatuz gero (% 29.2). LDL-C mailak nahiko antzekoak izan ziren 75-eko pertzentiletik aurrerako taldeetan (%92 eta %61.1). 95-eko pertzentiletik aurrera ordea ez ziren diferentzia esanguratsurik ikusi (%75.9 eta %79.2 $P = 0.520$) (3.4 Taula).

p.Arg416Trp aldaerak duen funtzionaltasun galera txikia dela eta , aldaera hau duten pertsonen lipido profilak aldaera neutro eta aldaera ez funtzionalak dituzten pertsonen profilekin alderatu ziren. Aldaera neutrodun profilekin konparatuz gero fenotipo larriagoak ikusi ziren hurrengo parametroetan; kolesterol totala, LDL-C, apoB, apoB/apoA1 ratioa, eta LDL-C pertzentilen bataz besteko balioetan (333.9±78.5 vs. 278.2±59.23 mg/dl ($P = 0.02$); 237.7±112.4 vs. 168.2±53.0 mg/dl ($P = 0.002$);144.5±44.3 vs. 103.0±28.2 mg/dl ($P = 0.002$); 0.87±0.29 vs.0.63±0.28 mg/dl ($P = 0.027$); and 82.4±22.8 vs. 61.2±34.2 ($P =0.03$) hurrenez hurren). Bestalde, aldaera ez funtzionala duten pertsonen profilak p.Arg416Trp aldaera duten pertsonen profilekin konparatuz gero fenotipo larriagoak ikusi ziren baita ere kolesterol totala, LDL-C, apoB, apoB/apoA1 ratioa, eta LDL-C pertzentilen bataz besteko balioetan, kasu honetan ordea, ikusitako diferentziak ez ziren esanguratsuak izan; (333.9±78.5 vs. 322.2±68.2 mg/dl ($P = 0.82$); 237.7±112.4 vs. 230.7±94.1 mg/dl ($P = 0.96$); 144.5±44.3 vs. 117.4±35.4 mg/dl ($P = 0.19$); 0.87±0.29 vs. 0.79±0.21 mg/dl ($P = 0.492$); 82.4±22.8 vs. 84.4±22.4 ($P = 0.73$)). Triglizerido maila, HDL maila eta ApoA1 maila antzekoak ziren hiru taldeetan. Datu hauek bat datoz kosegregazio analisietan lortutakoekin, hauetan, bai funtzio galera aurkezten duten aldaerek, bai p.Arg416Trp aldaerak kosegregazio balio altuagoak aurkezten zituzten aldaera neutroekin alderatuz. LDL-C pertzentilak analizatzean, pertzentil baxuenak p.Arg416Trp aldaerak dituela ikusi zen (3.4 Taula).

3.4 Taula Aldaera neutro edo funtzionalak dituzten pertsonen eta p.Arg406Thr aldaera duten pertsonen datu biokimikoen konparaketa.

	p.Arg406 Trp	n	Funtzio galeradunak (a)	n	Funtzio normaldunak (a)	n	*P* balioa (b)	*P* balioa (c)
Adina	44.1 ± 12.0	20	43.0 ± 14.0	30	46.5 ± 14.0	40	0,970	0,512
Kolesterol totala	339.9 ± 78.5	19	322.2 ± 68.2	26	278.2 ± 59.23	31	0,818	**0,022**
LDL-C	247.8 ± 71.8	11	239.2 ± 69.5	18	185.3 ± 52.7	29	0,877	0,004
LDL-C cor (d)	237.7 ± 112.4	21	230.7 ± 94.1	31	168.2 ±53.0	42	0,963	**0,002**
High Density Lipoprotein	56.9 ± 12.4	12	57.0 ± 16.5	19	61.7 ± 26.2	29	0,734	0,944
Triglycerides	132.6 ± 54.9	12	108.4 ± 38.9	19	155.6 ± 66.8	29	0,220	0,300
Lipoprotein (a)	43.5 ± 72.1	21	88.6 ± 61.6	31	40.4 ± 50.6	41	0,001	0,732
Apolipoprotein B	144.5 ± 44.3	11	117.4 ± 35.4	7	103.0 ± 28.8	23	0,193	0,002
Apolipoprotein A1	172.7 ± 42.9	11	147.9 ± 13.3	7	188.9 ± 69.3	22	0,161	0,836
Apolipoprotein B								
Apolipoprotein A1 ratioa	0.87 ± 0.29	11	0.79 ± 0.21	7	0.63 ± 0.28	22	0,533	**0,027**
sdLDL	52.9 ± 10.1	3	45.74 ± 14.2	4	30.4 ± 12.4	7	0,492	0,067
LDL pertzentilak	82.4 ± 22.8	21	84.4 ± 22.4	31	61.2 ± 34.2	42	0,728	**0,029**
≥75 (%) partaideak	75%	12	100%	17	91,70%	24	0,060	0,53
≥95 (%) partaideak	66,70%	12	82,40%	17	79,20%	24	0,295	0,069
≥75 (%) familiarrak	95,70%	21	90,00%	31	61,50%	48	0,601	**0,001**
≥95 (%) familiarrak	52,20%	21	63,30%	31	44,20%	48	0,296	0,350
Kosegregazioa	35/36 (97.2%);0/2 (0%)		87/91 (95.6%); 0/9 (0%)		38/48 (79.2%); 12/16 (75%)		NA	NA

N/A, ez da aplikgarria

[a] Bataz besteko balioak ±SD. [b] pArg406Thr eta aldaera funtzionalen arteko konparaketaren *P* balioa. [c]pArg406Thr eta aldaera neutroen arteko konparaketaren *P* balioa. [d] LDL-C baloreak tratamenduaren arabera zuzenduta daude (1.3 estatinentzako eta 1.5 estatinak eta ezetimida konbinazioarentzako). [e] Tratamendu aurreko eta osteko baloreak. [f] Aldaera eramaileen artean.

Ikerketan ageri diren datu guztiak aldaera ezberdinak dituzten pertsona helduetatik lortu ziren.

3.2.3 Eztabaida

Lan honetan FH diagnostiko klinikoa duten 55 familien analisi fenotipiko eta genotipikoa aurkezten da, bertan, 13 mutazio ezberdin topatu dira. Lan honen bidez FH-ren diagnostikoa egiterakoan analisi bateratu bat egiteak izan dezaken garrantzia ebaluatu nahi izan dugu, izan ere datu kliniko, molekular eta funtzionaletaz baliatzeak zalantza gabeko diagnostiko definitibo bat ematen lagun bait dezake. Aurkitutako 13 mutazioetatik 11 aurretiaz deskribatuta zeuden eta gaixotasun- eragile moduan definitu izan dira, baina soilik bost aldaerek zeukaten analisi funtzional egoki bat eginda. Bi aldaera lan honetan deskribatu dira lehenengo aldiz. Beraz ikerketa honetan analisi funtzional egokia ez zeukaten 8 aldaerak sakonki aztertu dira. Aldaera hauetatik bostek funtzio galeraren bat aurkeztu dute eta beste hirurek LDLR basatiak duen antzeko aktibitatea . Gainera, aurretiaz beste populazio ezberdinetan deskribatutako beste 5 aldaera funtzionalen datuak ere sartu dira ikerketan emaitza zehatzagoak lortzeko asmoarekin.

Datu guztien azterketatik ondoriozta genezake aldaera funtzionalak dituzten partehartzaileen artean gaixotasun kardiobaskularren intzidentzia baxuagoa, lipoproteina aterogenikoen kontzentrazio txikiagoa eta LDL kolesterol pertzentil baxuagoak dituztela aldaera patogenikoak dituzten partehartzaileen datuekin konparatuz. Bai aldaeren patogenikoek zein aldaera neutroek FH-rekin duten kosegregazioa determinatzeko, aldaera neutroak eta aldaera patogenikoak dituzten familiak aztertu dira. Aldaera patogenikoen kasuan, hiperkolesterolemia zeukaten seniedeen artean %96.3 (36) aldaera funtzionalak zeuzkaten eta familia berdinetan kolesterol maila baxuak zeuzkatenenen artean (2) % 0 zeukaten aldaera patogenikoa. Aldaera neutroen kasuan, hiperkolesterolemia zeukaten seniedeen artean (48) % 79.2 aldaera funtzionalak zeuzkaten eta familia berdinetan kolesterol maila baxuak zeuzkatenenen artean (16) % 75 zeukaten aldaera patogenikoren bat. Aldaera baten funtzionaltasuna ikertzeko era ezberdinak daude baina egokiena kosegregazio analisia izango litzateke. Hau ordea ez da beti posible izaten, kosegregazio analisi egokia egiteko gutxienez aldaera berdina duten 50 pertsona behar bait dira [37]. Bestalde, parametro biokimikoen erabilera ez da aukera egokia patogenizitatea determinatzeko eta *in silico* analisiek ez dituzte beti emaitza fidagarriak ematen. Hau horrela, analisi funtzionala edukitzea aukera ezinhobea izan daitekela ondorioztatzen dugu bereziki kosegregazio analisiak ezinezkoak direnean, edo eta hauek posible izanik datu berriekin osatzeko. Izan ere, lan honetan aurkeztu diren moduko analisi funtzionalak biokimikako edozein laborategitan egin daitezke metodologia egokiak aplikatuz [41].

Analisi bateratu baten garrantzia argi geratzen da baita ere lan honetan lehenbiziko aldiz funtzionalki analizatu den p.Arg406Thr aldaerarekin. Kasu honetan datu kliniko, molekular eta

funtzionalak hartu dira kontuan zalantza gabeko konklusioetara iristeko.. p.Arg406Thr aldaera daukaten partehartzaileek funtzio- galera duten partehartzaileek lortutako antzeko emaitzak izan zituzten lipido profila eta kosegregazio analisiari dagokionez . Era berean, aldaera neutroak dauzkaten partehartzaileekin konparatzean diferentzia esanguratsuak ikusi ditugu dentsitate altuko lipoproteina, triglizerido eta apoA1 ez diren beste parametro guztietan. Datu guzti hauek aldaera honen patogenizitatea susmarazten dute. Hala ere, LDL-C pertzentilak analizatzerakoan zenbait emaitza arraro ikusi ditugu, hala nola, p.Arg406Thr aldaera duten kasuan arraroagoak direla LDL-C ≥75 pertzentiletik gora eta LDL-C ≥95 pertzentiletik gora dauden kasuak aldaera funtzionalak dituzten partehartzaileen artean baino (datuak ez daukate ezberdintasun estatistikorik). ;, Senitartekoen informazioa ikerketan kontutan hartu ezkero ordea, aldaera funtzionalak dauzkaten pertsonen LDL-C mailak baxuagoak direla ikus daiteke. Beraz, ondoriozta daiteke datu genotipiko/fenotipikoekin soilik ezin daitekela aldaera baten patogenizitatea zehatz definitu.. p.Arg406Thr aldaeraren funtzionaltasun-analisian LDL hartzaileak LDLR basatiaren aktibitatearen % 60 mantentzen duela erakutsi dugu. . Honek, % 80-ko aktibitate totala baimentzen du, beti ere beste aleloak mutazio kaltegarririk ez badauka. Beraz, esan genezake p.Arg406Thr aldaerak patogenizitate murriztua daukala, eta. ondorioz, aldaera hau daukaten pertsonen artean fenotipo ezberdinak aurkitzea ingurumen faktoreei egotzi dakioke, nahiz eta FH-dun pertsonak izan [42] Analizatutako 2a klaseko mutazioek (p.Ile441Thr, p.Gly545 eta p.Cys698Phe) ordea ez dute inolako hartzaile aktibitaterik eta ondorioz heterozigozian % 50 inguruko aktibitatea totala soilik ikus daiteke . . Momentuz ez da guztiz finkatu funtzio-galeraren zein portzentaitik aurrera kontsideratu behar den mutazio bat patogenoa, , edonola ere, zenbait publikazioren arabera % 20-30-eko funtzio galera suposatzen duen aldaera patogenotzat har daitekela proposatzen da.[6,11,26,43–45].

Karakterizazio funtzionalak aldaeren sailkapen egokiagoa egiteko aukera eskeintzen duen aldetik pazienteei gomendio eta tratamendu goiztiar eta egokiagoak emateko aukera ere ematen du. .Adibidez, aldaera funtzional eta limitean kokatzen diren kolesterol mailak dituzten pertsonek tratamendu ezberdinak beharko lituzketela aholka daiteke. p.Arg406Thr aldaerarekin lortutako emaitzek esaterako paziente hauen tratamendua zehatzago doitzeko aukera eskeintzen dute, dosi txikiagoekin efektu onak lortu ahal izango liratekela aurresan bait daiteke,tratamendu gogorragoak baztertuz. .

Laburbilduz, lan honetan aurkezten den analisi bateratuak FH-dun pazienteak era egokiago batean sailkatu, analizatu, diagnostikatu eta tratatzeko aukera ematen du. Pazienteen datu kliniko eta biokimikoei proteinaren analisi molekularra gehituz, gaixotasunaren informazio hobea eta sakonagoa lortu daiteke eta fenotipo ezberdinak ulertzeko posibilitatea zabaldu egiten da zalantza gabe.

3.3 Validation of LDLR Activity as a Tool to Improve Genetic Diagnosis of Familial Hypercholesterolemia: A Retrospective on Functional Characterization of LDLR Variants

3.3.1 LDL Receptor

The mature LDLR is a type I transmembrane protein of 839 amino acids which regulates cholesterol homeostasis in mammalian cells[46]. LDLR is mapped to 19p13.1–13.3 on the short arm of chromosome 19, spans 45 kb and consists of 18 exons and 17 introns that are transcribed and translated into five distinct domains which form the cell-surface LDL receptor[6]. The protein is encoded as a precursor of 860 amino acids comprising a 21-residues signal sequence at the N-terminus that is excised during protein translocation into the endoplasmic reticulum (ER)[47]. LDLR is synthesized on ribosomes of ER, then folded and partially glycosylated within ER and finally matured in the Golgi complex, where glycosylation is completed[48]. The mature protein is structured into functional domains organized in an ectodomain and intracellular domain. The ectodomain is encoded by exons 2–15 and harbours a ligand-binding domain, an epidermal growth factor (EGF) precursor homology domain and a C-terminal domain enriched in O-linked oligosaccharides (Figure 3.15A).

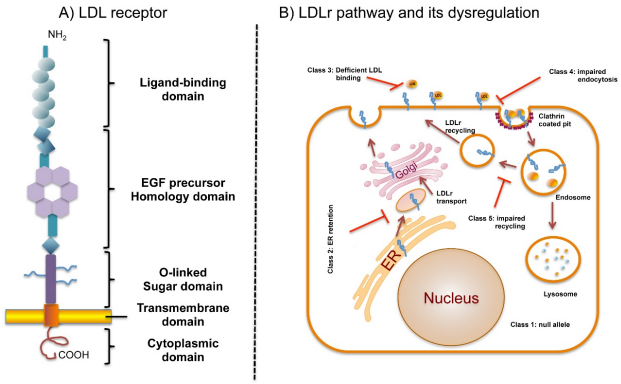

Figure 3.15 Domain organization of LDLR and LDLR pathway and its dysregulation by defective mutations. (**A**) Schematic representation of LDLR domains; (**B**) LDLR cycle. LDLR is synthesed at ER, transproted to Golgi where is further processed with glycosilations. Mature LDLR is transported to the plasma membrane, where the ligand-binding domain binds to the apo B100 moiety on LDL particles. The LDLR/LDL complex undergoes endocitosis and within the cell, LDL particle components are targeted for lysosomal degradation, whereas the LDLR is recycled to the cell surface. LDLR mutations affecting different LDLR cycle results in dysregulation of the cycle.

The ligand binding domain contains 7 cysteine-rich repeats (LR1 to LR7) of approximately 40 amino acids with three disulphide bridges each (CysI-III, CysII-V, CysIV-VI). In addition, an acidic residues cluster coordinates a Ca^{2+} ion which is required for correct folding of the

domain[49]. Binding of lipoproteins to the LDLR appears to be mediated by an interaction between acidic residues in the LDLR-binding domain and basic residues of apoE and apoB100[50,51]. The intracellular release of the cargo is driven by a low-pH-induced conformational change of LDLR from an open to a closed conformation[49,52,53]. Binding to different ligands appears to require different subsets of LR modules[49,51,54]. The LR modules are interspaced by a short linker sequence mostly formed by four residues ending in Thr with the sequence motif $XXC_6XXX\underline{\mathbf{T}}\mathbf{C}_1$-XX. Some linkers, however, are longer. It has been shown that O-glycans in the LR ligand-binding region of LDLR as well as VLDLR are important for high-affinity lipoprotein binding and uptake[55] .

The EGF precursor homology domain participates in the acid-dependent lipoprotein release in the endosome and consists of two EGF-like domains, six YWTD repeats that form a six-bladed β-propeller, and a third EGF-like repeat[18,56]. It has been shown that PCSK9, a secreted glycoprotein, promotes degradation of the LDLR, thereby preventing clearance of LDL-C by the cells[57] . It also interacts with the EGF-A domain of the LDLR at the cell surface and binds to the full-length receptor with a much higher affinity in the acidic environment of the endosome. Consequently, the receptor is transported from the endosome to the lysosome for degradation, rather than being recycled[57].

The C-terminal domain enriched in O-linked oligosaccharides contains 58 amino acids rich in threonine and serine residues. It is thought that this domain plays a role in the stabilization of the receptor[58]. This region shows minimal sequence conservation among six species analyzed and can be deleted without adverse effects on receptor function in cultured fibroblasts[59].

The intracellular domains are encoded by Exons 16–17 and together constitute the transmembrane domain. The TM domain contains 22 hydrophobic amino acids that are essential for anchoring the LDLR to the cell membrane. The cytoplasmic domain of LDLR, consists of 50 amino acid residues and contains two sequence signals for targeting the LDLR to the cell surface and localizing the receptor to coated pits[60]. Internalization of the LDLR also requires this cytoplasmic domain[61,62].

LDLR transcription is tightly regulated by the sterol-responsive element binding protein-2 (SREBP-2) through a feedback mechanism that responds to variations in intracellular sterol concentrations and cellular demand for cholesterol[63]. In addition to classical transcription regulators, a class of noncoding RNAs termed microRNAs (miRNAs), has emerged as critical regulators of gene expression acting predominantly at the post-transcriptional level[64]. In particular, miR-148a directly controls LDLR activity and is transcriptionally activated by SREBP1c in vitro and in vivo[65].

3.3.2 LDLR Pathway and Its Deregulation by Defective Mutations

Upon lipoprotein binding to LDLR at the cell surface, the complex is internalized through clathrin-coated pits into clathrin-coated vesicles[66] (Figure 1B). These vesicles fuse with early endosomes, and acidification of the endosomal pH promotes LDL release, which is later degraded in lysosomes. Normally, the LDLR is returned to the membrane and enters a new cycle[49].

This system maintains a constant level of cholesterol in hepatocytes and other cells by controlling both the rate of cholesterol uptake from LDL and the rate of cholesterol synthesis[67]. LDLR mutations affect different parts of this LDLR cycle leading to FH. *LDLR* mutations are thus classified depending on the phenotypic behaviour of the mutant protein (Figure 1B)[68,69]: Class 1. Synthesis alteration, known as "null alleles"; Class 2. Defective transport to Golgi or to the plasma membrane because the synthetized proteins do not have an adequate three-dimensional structure and are retained, completely or partially (2A and 2B, respectively) in the ER; Class 3. Deficient binding to ApoB, LDL binding activity is 2% to 30% of normal due to rearrangements in repeat cysteine residues in binding ligand domain or repeat deletions in EGFP-like domain; Class 4. Impaired endocytosis, LDLR is not recruited into clathrin-coated pits; Class 5. Alteration in the recycle mechanism as a consequence of an impaired LDL release in endosomes causing the receptor to be degraded in the lysosome. Recently, a sixth class of mutations in the *LDLR* that interfere with insertion of the LDLR into the cell membrane resulting in LDLR secretion has been described[70].

3.3.3 Determining the Pathogenicity of LDLR Variants

The majority of FH patients with positive genetic testing results have rare pathogenic variants in LDLR[71] which comprise 60% of the ~2000 *LDLR* genetic variants that have been submitted to the HGMD. Determining pathogenicity of LDLR is a key challenge in genomic medicine; therefore, several approaches including computer prediction algorithms, in vivo and in vitro experimental evidence, are used to gain information about variant effects[72].

3.3.3.1. In Silico Analysis

The revolution in DNA sequencing methodologies has tremendously increased the number of gene sequences over the last several years, and these technologies continue to evolve[73,74]. Next-generation sequencing (NGS) in combination with sequence target enrichment methods are useful in molecular diagnostics of FH[75]. Single-nucleotide polymorphisms (SNPs) are considered to be the most common genetic changes that result from alterations in a single nucleotide. Among SNPs, nonsynonymous SNPs (nsSNP) are associated with single amino acid substitution in the coding regions of a gene that may have a drastic effect on the structural and functional properties of the corresponding protein. These nsSNPs have been the subject of many recent studies and a large amount of data now exists in public repositories such as dbSNP[76],

HGVBase[77] and HGMD [78]. To manage the large amount of data produced, computational tools to predict the functional effects of sequence variations are under constant development to prioritize high-risk variants that should be experimentally characterized for pathogenicity. These tools have been developed based on features such as amino acid or nucleotide conservation and biochemical properties of the amino acid substitutions. Identification of single nucleotide polymorphisms in the coding region of a gene that have implications in inherited human diseases is the fundamental objective of research in medical genetics. The most used pathogenicity predictor open access software to assess the effect of *LDLR* variants are PolyPhen-2[79], Sorting Tolerant From Intolerant (SIFT)[80], Consensus Deleteriousness score of missense SNVs (Condel)[81], Mutation taster[82], Grantham Score[83] and PhyloP[84]. However, individual tools often disagree, in part because they utilize different predictive features. Understanding how amino acid substitutions affect protein functions is critical for the study of proteins and their implications in diseases. Another limitation is that prediction results are hard to interpret without physicochemical principles and biological knowledge. For this reason, there is a growing need for the development and evaluation of tools for predicting the pathogenicity of rare variants. Furthermore, functional validation of these *LDLR* variants must be conducted in order to identify which mutations lead to a functional loss of receptor activity.

3.3.3.2 Functional Characterization of LDLR Variants

Functional assays are a direct method to determine whether the activity of a mutant protein is altered by taking into account all the involved biological mechanisms. To date, functional studies of *LDLR* variants have been conducted using two major approaches: 1. ex vivo methods, using cells from FH patients; 2. in vitro methods using cell lines transfected with the *LDLR* mutant (Figure 3.16).

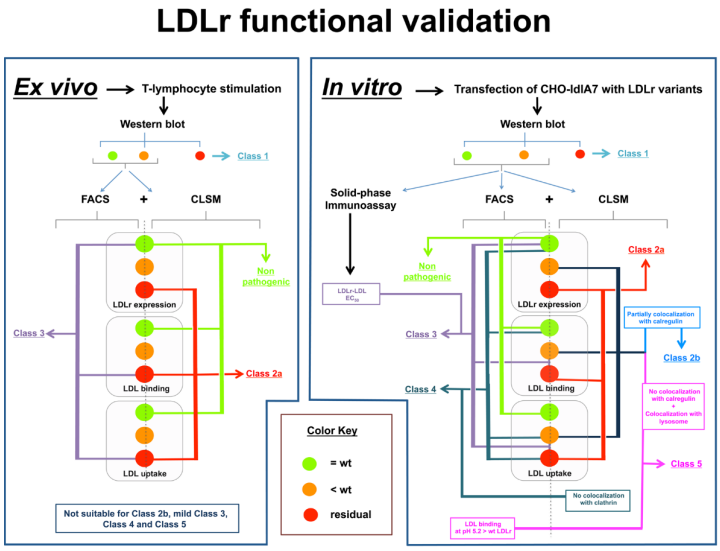

Figure 3.16 Flowchart of the used methodologies to functionally characterize LDLR variants ex vivo and in vitro. Functional studies of *LDLR* variants are mainly conducted using two major approaches: 1. ex vivo methods, using cells from Familial Hypercholesterolemia (FH) patients (left-hand panel); 2. in vitro methods using cell lines transfected with the LDLR variant (right-hand panel). LDLR activity determination is based in combination of different methodologies: Western blot to analyse LDLR expression followed by fluorescence-activated cell sorting (FACS) and Confocal Laser Scanning Microscopy (CLSM) that allow assessment of Class type mutation. The ex vivo approach is adequate for Class 1, Class 2a and Class 3 LDLR variants. In vitro characterization allows identification of Class 2b mutations by colocalizing the LDLR variants in the ER with calrgulin; using a solid-phase immunoassay it is possible to determine LDLR-LDL EC_{50} values for Class 3 mutations which is important to understand mild pathogenic variants; Class 4 variants are classified by complementing CLSM with a colocalization assay with clathrin and, identification of Class 5 mutants is performed by absence of LDLR colocalization with calregulin, LDLR colocalization with a lysosome marker complemented by a FACS analysis of LDL binding to LDLR at different pH (7.4-5.2).

Ex vivo Functional Validation

Since the first demonstration by Brown and Goldstein of the presence of a measurable LDL receptor pathway in cultured skin fibroblasts from FH-homozygotes and normolipidemic controls with ^{125}I-labeled LDL[85], research has focused on the development of new and less invasive methodologies for LDLR activity assessment. New strategies that use lymphocytes allow validation of LDLR functionality by immortalization mediated by Epstein–Barr virus[15,86,87], stimulation of LDLR expression in lymphocytes by incubation with statins[88,89], or treatment of cells with mitogens or CD3/CD28 beads to stimulate T-lymphocytes[15,90]. Comparative studies between results in fibroblasts with those obtained from immortalized lymphoblastoid cells from the same patient showed similar results[91]. T-lymphocyte stimulation by CD3/CD28 beads followed by determining LDLR activity through fluorescence-activated cell sorting (FACS) is a simple strategy used for functional assays. This technique requires

incubating cells from FH patients for 72 h with CD3/CD28 beads in a medium containing a lipoprotein deficient serum to upregulate the LDLR, and then they are incubated with labelled-LDL allowing the detection of the bound and/or internalized LDL amounts. Nowadays, LDL are normally labelled with fluorescent molecules that allow obtaining an accurate analysis by FACS [15,26]. Specifically, labelling LDLR with a fluorescent antibody or LDL with a fluorescent antibody allows determination of LDLR expression at the cell membrane and LDL-LDLR binding, respectively. LDL labelling is conducted by incubating cells for 4 h at 4 °C with fluorescent-labelled LDL [26,92]. A recent advance in determining LDL uptake was introduced by our group and consists of a combination of Fluorescein IsoTioCyanate labelled LDL (FITC-LDL) and Trypan-blue dye[26]. This method allows determination of LDL uptake in a single step because addition of Trypan blue to the cell suspension quenches external fluorescence from LDL bound to membrane receptors, allowing fluorescence quantification of internalized LDL exclusively [26]. Confocal microscopy with an anti-LDLR antibody is used to verify localization of the LDLR on the plasma membrane and of ApoB after endocytosis. The ex vivo approach is very suitable in assessment of Class 1, Class 2a and Class 3 LDLR variants in which LDL binding is highly impaired. However, ex vivo studies have the following limitations: because lymphocytes studies are from heterozygote patients, interference of the wild type allele has to be taken into account. Even in the presence of a null allele leading to a total absent protein, the activity of the LDLR synthesized from the normal allele is still detectable and the total measured activity is around 50%. If the variant under study is Class 2b, Class 3 (without a complete loss of binding capacity), Class 4 and Class 5 the activity data may range from 70–90% compared to activities of lymphocytes carrying wild type LDLR in both alleles. For this reason, ascertaining pathogenicity in these cases needs further analysis. Another limitation of ex vivo assays is that localization of LDLR to different subcellular compartments by confocal microscopy is difficult due to the extremely small cytoplasm of lymphocytes. Advantages and disadvantages between functional validation methodologies are shown in Table 3.5.

Table 3.5. Summary of advantages and disadvantages of radioactive and fluorescence-based methodologies used to characterize the activity of LDLR variants.

Differences between Functional Validation Methodologies	
Radioactivity	**Fluorescence**
Highly reproducible	**Highly reproducible**
Highly sensitive activity measurements	**Highly sensitive activity measurements**
Stable labeling	**Stable labeling**
Risk of exposure to radioisotopes	**Nonradioisotopes used**
Ethical considerations regarding waste elimination	**In combination with CLSM allow LDLR classification**
Noncompatible with CLSM	

Disadvantages are shown in red.

In Vitro Functional Validation

In vitro cell line model systems are particularly useful to help further our understanding of the mechanisms underlying pathogenicity of *LDLR* variants. The use of cell line models to study LDLR variant activities has many advantages: cell lines represent a renewable resource, are well-controlled systems and there is no need for clinical samples. The analyses performed on these cell lines to functionally validate *LDLR* variants are similar to those performed on ex vivo assays, including the use of FACS measurements with antibodies[93] or fluorescently-labeled LDL and confocal microscopy using antibodies for ApoB or markers for the endoplasmic reticulum[93]. Cells are transfected with an expression plasmid in which the *LDLR* carrying the studied mutation is cloned. The methodology used for that purpose is as follows:

Cell Transfection

LDLR-deficient Chinese hamster ovary (CHO) cell line ldlA7 (CHO-ldlA7) is transfected with plasmids carrying the *LDLR* variant of interest[11,41]]. Different methods of transfection are suitable depending on laboratory experience. Transfected cells are maintained in culture during 48 h to achieve maximal LDLR expression.

Western Blot Analysis

Usually the first step in functional characterization is to evaluate receptor expression. To do so, immunoblotting is used to test if the LDLR variant is able to go from the precursor to the mature form. Experimentally, cell lysates have to be prepared, protein concentration determined, and fractionated by electrophoresis. Then, for semiquantitative immunoblotting, proteins are transferred to nitrocellulose membranes which are immunostained using the appropriate antibodies. The signals are then developed and quantified. The relative LDLR expression for the LDLR variant is calculated as the ratio between the sum of band intensities corresponding to the mature and precursor form of LDLR protein to that of a constitutive protein such as GAPDH.

Quantification of LDLR Expression by Flow Cytometry

To determine LDLR cell surface expression by FACS, transfected CHO-ldlA7 cells are incubated with a primary antibody anti-LDLR for 1 h at room temperature, then washed with PBS-1% BSA and incubated with secondary antibody Alexa Fluor 488-conjugated antimouse IgG. Fluorescence is then acquired through FACS and compared with fluorescence obtained in cells expressing wild type LDLR.

3.3.3.2.2.4. Quantification of LDLR Activity by FACS

Transfected CHO-ldlA7 cells are incubated for 4 h at 37 °C or 4 °C with 20 μg/mL FITC–LDL to determine LDLR activity or LDL–LDLR binding, respectively. After incubation with FITC–LDL, CHO-ldlA7 cells are washed twice in PBS-1% BSA, fixed on 4% formaldehyde, and washed again. To determine the amount of internalized LDL, Trypan blue solution is added to a final concentration of 0.2% directly to the samples, eliminating the extracellular signal due to the noninternalized LDL–LDLR complexes.

Confocal Laser Scanning Microscopy

Confocal laser scanning microscopy is used to analyze LDL-LDLR binding, uptake, expression of LDLR, and enables determination of Class type mutation by testing LDLR colocalization with clathrin, lysosomes, or endoplasmic reticulum (ER). Cells are plated in coverslips and transfected with the LDLR containing plasmids. After 48 h, nonlabelled lipoproteins are added and cells, further incubated for a 4 h then stained with the appropriate primary antibodies for 16 h at 4 °C followed by incubation with fluorescent secondary antibodies. Cells are then visualized using a confocal microscope and images processed and fluorescence intensities quantified.

LDL–LDLR Binding at Different pH

To determine if the defect of an *LDLR* variant is due to defective LDLR recycling, an LDL binding assay is performed at different pH's to mimic the acidification process occurring in the endosome after LDL endocytosis. To do this, transfected cells are incubated with 20 μg/mL of LDL–FITC for 30 min in a 0.4-M sucrose medium at different pH's. Then, cells are washed three times to remove unbound LDL, fixed with 4% paraformaldehyde and the amount of bound LDL–FITC is quantified by FACS.

LDLR-LDL Affinity Assessment

In order to better classify Class 3 mutations from mild to severe pathogenic effect, a modified ELISA binding assay with purified soluble wt LDLR (sLDLR) or and the variant of interest can be performed. sLDLR variants are coated in 96-well and incubated with freshly purified human LDL for 2 h at RT, then samples are incubated with anti-Apolipoprotein B for 1 h followed by peroxidase-conjugated IgG for 1 h, and developed with a chromogenic substrate. After photometric quantification, EC_{50} values are calculated providing information about LDLR affinity to LDL[55].

In the recent years, our group has been actively using fluorescent-based methodologies to characterize and classify LDLR variants; the obtained results to date are shown in Table 3.6.

Table 3.6. LDLR variants characterized and classified by fluorescent-based methodologies at Instituto Biofisika (UPV/EHU, CSIC) and Departamento de Bioquímica, Universidad del País Vasco. In the table resume results from 8 different published articles (references 22,41,93,94,95,96,97,98) are shown. These results are part of the work performed during this thesis.

Functional Validated and Classified LDLR Variants	Classification	LDLR Activity	Reference
c.135C>G p.(Cys46Gly)	Class 3	60 %	94
p.(Asp47Asn)	Nonpathogenic	100 %	95
p.(Thr62Met)	Nonpathogenic	100 %	95
c.226G>T p.(Gly76Trp)	Nonpathogenic	100 %	22
c. 292G>A (p.Gly98Ser)	Nonpathogenic	100%	96
c.346T>C (p.Cys116Arg)	Class 3	25%	97
c.464G>A (p.Cys155Tyr)	Class 3	< 20%	93
c.502G>A (p.Asp168Asn)	Class 3	40%	97
c.514G>A (p.Asp172Asn)	Class 3	<2%	97
c.769C>T (p.Arg257Trp)	Nonpathogenic	100%	97
c.806G>A (p.Gly269Asp)	Nonpathogenic	100%	26
c.829G>A (p.Glu277Lys)	Nonpathogenic	100%	22
c.862G>A (p.Glu288Lys)	Class 3	60%	26
c. 890A>C (p.Asn297Thr)	Nonpathogenic	100%	96
c.895G>A (p.Ala299Thr)	Class 3	60%	26
c.898A>G (p.Arg300Gly)	Class 3	60%	97
c.902A>G (p.Asp301Gly)	Class 3	40%	97
c.1216C>T (p.Arg406Trp)	Class 2b or 5	60%	11
c.1246C>T (p.Arg416Trp)	Class 5	60%	93
c.1285G>C (p.Val429Leu)	Class 2a	<10%	41
c.1322T>C (p.Ile441Thr)	Class 2a	<10%	22
c.1336 C>G (p.Leu446Val)	Nonpathogenic	100%	98
c.1361C>A (p.Thr454Asn)	Class 5	60%	93
c.1468T>C (p.Trp490Arg)	Class 2a	<10%	41
c.1633G>T (p.Gly545Trp)	Class 2a	<10%	22
c.1723G>T (p.Leu575Phe)	Class 2	60%	99
c.1729T>G (p.Trp577Gly)	Class 2a	<10%	93
c.1744C>T (p.Leu582Phe)	Class 2	60%	99
c.1942T >C (p.Ser648Pro)	Class 2b	<25%	41
c.2053C>T (p.Pro685Ser)	Class 2b	<75%	41
c.2475C>A (p.Asn825Lys)	Class 4	60%	93
c.2575G>A (p.Val859Met)	Nonpathogenic	100%	22

3.3.6. ClinVar: Variant Pathogenicity Assignments based on LDLR Functional Characterization

The identification of many novel LDLR variants by NGS in clinical genetic testing has led to the need for storing data about variant classification in a clinically-applicable location. Thus, several general and gene-specific databases are available for use by investigators and clinicians, including the National Center for Biotechnology Information (NCBI) ClinVar database[100]. The ClinVar database at NCBI archives and aggregates submitted interpretations of the clinical and/or functional significance of variants for specified conditions, with opportunities to provide supporting evidence. Recently, the ClinVar database related to LDLR has been updated with variants stored in the LDLR—specific Leiden Open Variation Database (LOVD), increasing the size of the ClinVar LDLR database from 338 variants as of July 11, 2016, to 2248 variants as of April 30, 2018. Some research-oriented submissions may provide functional significance based on experimental evidence, which may inform the clinical interpretation of the same variant in patient encounters. To date there are 794 unique missense LDLR variants annotated in ClinVar identified by both research and clinical testing. Among them, the reported clinical significance is as follows: 2.02% benign/likely benign, 7.81 of uncertain significance, 62.80% pathogenic/ likely pathogenic and, 27.33% conflicting interpretations. The category "conflicting interpretations" includes variants with multiple submissions where the associated classifications were: benign/likely benign + uncertain significance; pathogenic/likely pathogenic + uncertain significance; or benign/likely benign + pathogenic/likely pathogenic.

As mentioned above, the most used methodologies to determine LDLR functionality ex vivo and in vitro are based on the use of radioactivity or fluorophores. LDL uptake and degradation of ^{125}I-labeled LDL has been commonly used in radioactivity-based methods, a methodology that is being replaced by the use of fluorescent-labeled LDL and antibodies for determining activity of LDLR[6,26,90,101]. Both methods have been used indistinctly, probably depending on the research laboratory facilities or continuation of the previously methodology in a specific laboratory. To date, 794 unique missense pathogenic LDLR variants have been annotated in ClinVar. Only a minority of these 794 variants have been proven pathogenic. Among them, the activity of 100 has been experimentally characterized (Table 3.7). Radioactive techniques have been used to functionally characterize 62 LDLR variants and fluorescence-based methodologies to characterize 33 variants. Two mutations have been assessed by both methodologies and three variants were characterized by other techniques (Western blot and RNA studies). Although the number of characterized variants may seem low (13% of the annotated missense variants), extensive work is being done by multiple laboratories to characterize the remaining variants. In the next few years the percentage of the functionally characterized variants will increase notably. In this respect, the use of fluorescence methodologies is increasing the number of validated variants because FACS allows easier quantification of LDLR expression at the cell surface and LDL uptake provides a better characterization of the defect associated with each mutation. In fact, FACS complementation

with confocal microscopy allows detection of the subcellular localization of the LDLR, which allows assignment of the class type of each variant studied[41].

Table 3.7 ClinVar annotated LDLR variants functionally characterized ex vivo or in vitro by radioactive, fluorescence-based or other techniques.

Ex Vivo			
Functional validated LDLR variants	**LDLR activity**	**Method**	**Reference**
c.1A>T (p.Met1Leu)	residual	Radioactivity	[102]
c.28T>A (p.Trp10Arg)	40%	Radioactivity	[103]
c.81C>G (p.Cys27Trp)	15–30%	Radioactivity	[6]
c.265T>C (p.Cys89Arg)	<5% Comp Htz	Radioactivity	[104]
c.268G>T (p.Asp90Tyr)	not determined	Radioactivity	[105]
c.407A>T (p.Asp136Val)	76% Htz	Fluorescence	[106]
c.418G>A (p.Glu140Lys)	30% Comp Htz	Radioactivity	[105]
c.443G>C (p.Cys148Ser)	2%	Radioactivity	[107]
c.530C>T (p.Ser177Leu)	<2%	Radioactivity	[108]
c.590G>T (p.Cys197Phe)	<2% Comp Htz	Radioactivity	[6]
c.590G>A (p.Cys197Tyr)	<2% Comp Htz	Radioactivity	[6]
c.662A>G (p.Asp221Gly)	<2% Comp Htz	Radioactivity	[6]
c.670G>A (p.Asp224Asn)	<2%	Radioactivity	[6]
c.676T>C (p.Ser226Pro)	<2%	Radioactivity	[6]
c.681C>G (p.Asp227Glu)	<2%	Radioactivity	[6]
c.682G>C (p.Glu228Gln)	2–5% Comp Htz	Radioactivity	[6]
c.796G>A (p.Asp266Asn)	<2%	Radioactivity	[107]
c.798T>A (p.Asp266Glu)	15–30%	Radioactivity	[6]
c.910G>A (p.Asp304Asn)	5–15%	Radioactivity	[6]
c.917C>T (p.Ser306Leu)	2–5% Comp Htz	Radioactivity	[6]
c.953G>A (p.Cys318Arg)	2–5%	Radioactivity	[6]
c.974G>A (p.Cys325Tyr)	<64%	Fluorescence	[15]
c.1003G>A (p.Gly335Ser)	30–40% Htz	Radioactivity	[6]
c.1013G>A (p.Cys338Tyr)	<10%	Radioactivity	[109]
c.1027G>A (p.Gly343Ser)	15–30% Comp Htz	Radioactivity	[6]
c.1055G>A (p.Cys352Tyr)	15–30% Comp htz	Radioactivity	[6]
c.1056C>G (p.Cys352Trp)	9%	Radioactivity	[104]
c.1090T>C (p.Cys364Arg)	15–30%	Radioactivity	[6]
c.1124A>G (p.Tyr375Cys)	<40%	Radioactivity	[110]
c.1135T>C (p.Cys379Arg)	15–30%	Radioactivity	[6]
c.1222G>A (p.Glu408Lys)	5–10%	Radioactivity	[111]
c.1252G>A (p.Glu418Lys)	<70 Comp Htz	Radioactivity	[112]
c.1285G>A (p.Val429Met)	<2%	Radioactivity	[113]
c.1291G>A (p.Ala431Thr)	5–15%	Radioactivity	[69]
c.1297G>C (p.Asp433His)	<10%	Radioactivity	[112]
c.1301C>A (p.Thr434Lys)	5–15% Comp Htz	Radioactivity	[6]
c.1432G>A (p.Gly478Arg)	2–5% Comp Htz	Radioactivity	[6]
c.1444G>A (p.Asp482Asn)	15% Comp Htz	Radioactivity	[111]
c.1567G>A (p.Val523Met)	15–30%	Radioac+Fluores	[69,104]
c.1618G>A (p.Ala540Thr)	<50%	Radioactivity	[16]
c.1637G>A (p.Gly546Asp)	<2%	Radioactivity	[6]

c.1646G>A (p.Gly549Asp)	<2%	Radioactivity	69
c.1694G>T (p.Gly565Val)	<2%	Radioactivity	6
c.1702C>G (p.Leu568Val)	25%	Radioactivity	112
c.1729T>C (p.Trp577Arg)	<5%	Fluorescence	114
c.1731G>A (p.Trp577Cys)	64%	Fluorescence	115
c.1735G>A (p.Asp579Asn)	<2% Comp Htz	Radioactivity	6
c.1775G>A (p.Gly592Glu)	<5% Comp Htz	Radioactivity	6
c.1796T>C (p.Leu599Ser)	5–15%	Radioactivity	6
c.2000G>A (p.Cys667Tyr)	<2%	Radioactivity	116
c.2054C>T (p.Pro685Leu)	15–30%	Radioactivity	117
c.2177C>T (p.Thr726Ile)	15–30% Comp Htz	Fluorescence	6
c.2389G>T (p.Val797Leu)	not determined	Other techniques	39
c.2389G>A (p.Val797Met)	not determined	Other techniques	118
c.2479G>A (p.Val827Ile)	15–30% Comp Htz	Radioactivity	6
	In vitro		
Functional validated LDLR variants	LDLR activity	Method	Reference
c.58G>A (p.Gly20Arg)	100%	Fluorescence	119
c.226G>T (p.Gly76Trp)	100%	Fluorescence	22
c.259T>G (p.Trp87Gly)	25–100%	Radioactivity	116
c.268G>A (p.Asp90Asn)	55%	Fluorescence	120
c.301G>A (p.Glu101Lys)	15–30%	Radioactivity	121
c.344G>A (p.Arg115His)	64%	Fluorescence	122
c.346T>C (p.Cys116Arg)	25%	Fluorescence	97
c.464G>A (p.Cys155Tyr)	<20%	Fluorescence	97
c.502G>A (p.Asp168Asn)	40%	Fluorescence	97
c.502G>C (p.Asp168His)	<2%	Radioactivity	123
c.514G > A (p.Asp172Asn)	40%	Fluorescence	97
c.589T>C (p.Cys197Arg)	<10%	fluorescence	124
c.665G>T (p.Cys222Phe)	33%	Fluorescence	125
c.769C>T (p.Arg257Trp)	100%	Fluorescence	97
c.782G>T (p.Cys261Phe)	<20%	Radioactivity	126
c.806G>A (p.Gly269Asp)	100%	Fluorescence	26
c.829G>A (p.Glu277Lys)	100%	Radioactivity	45
c.862G>A (p.Glu288Lys)	60%	Fluorescence	26
c.895G>A (p.Ala299Thr)	60%	Fluorescence	26
c.898A>G (p.Arg300Gly)	60%	Fluorescence	97
c.902A>G (p.Asp301Gly)	40%	Fluorescence	97
c.986G>A (p.Cys329Tyr)	31%	Fluorescence	120
c.1072T>C (p.Cys358Arg)	67–72%	Fluorescence	115
c.1136G>A (p.Cys379Tyr)	<40%	Radioactivity	127
c.1186G>A (p.Gly396Ser)	100%	Radioac+Fluores	128
c.1216C>T (p.Arg406Trp)	60%	Fluorescence	22
c.1246C>T (p.Arg416Trp)	60%	Fluorescence	93
c.1268T>C (p.Ile423Thr)	54%	Radioactivity	120
c.1285G>C (p.Val429Leu)	<10%	Radioactivity	11
c.1322T>C (p.Ile441Thr)	<10%	Fluorescence	22
c.1361C>A (p.Thr454Asn)	60%	Fluorescence	93
c.1468T>C (p.Trp490Arg)	<10%	Radioactivity	11
c.1633G>T (p.Gly545Trp)	<10%	Fluorescence	22
c.1664T>C (p.Leu555Pro)	<2%	Radioactivity	129

c.1690A>C (p.Asn564His)	**100%**	**Fluorescence**	[130]
c.1729T>G (p.Trp577Gly)	**<10%**	**Fluorescence**	[93]
c.1744C>T (p.Leu582Phe)	**60%**	**Fluorescence**	[99]
c.1747C>T (p.His583Tyr)	**<60%**	**Radioactivity**	[128]
c.1942T>C (p.Ser648Pro)	**<25%**	**Radioactivity**	[11]
c.2053C>T (p.Pro685Ser)	**<75%**	**Radioactivity**	[11]
c.2093G>T (p.Cys698Phe)	**<10%**	**Fluorescence**	[22]
c.2396T>G (p.Leu799Arg)	**residual**	**Other techniques**	[70]
c.2475C>A (p.Asn825Lys)	**60%**	**Fluorescence**	[93]
c.2483A>G (p.Tyr828Cys)	**<2% Comp Htz**	**Radioactivity**	[59]
c.2575G>A (p.Val859Met)	**100%**	**Radioactivity**	[11]

3.3.7. Conclusions

Recent advances in genetic sequencing technology have resulted in remarkable improvements in the speed, throughput and identification of LDLR variants occurring in FH patients. To date, more than 2000 LDLR variants associated with FH have been described but only a minority of them have been functionally validated and proven to be the cause of the disease. Awareness and identification of the pathogenic variants causing FH would provide a definitive diagnosis. Additionally, early diagnosis of FH can allow development of public health approaches to begin early treatment of FH and prevent of future cardiovascular events. In the last years, a big effort has been establishing new methodologies for assaying activity of these variants. Substitution of radioactivity for fluorescence based methodologies has lowered the cost and provided a feasible and accessible tool to characterize LDLR variants. Our group has been actively using and optimizing these fluorescent techniques to characterize and classify LDLR variants. In order to provide an accurate classification, we have also developed solid-phase immunoassays to determine LDLR binding affinity to LDL that will help to understand the phenotype of patients carrying Class 3 LDLR variants. In addition, these techniques allow the characterization of *APOB* and *APOE* pathogenic variants, as well as *PCSK9* gain and loss of function variants[98,131–134].

References

1. Goldstein, J. L. & Brown, M. S. History of Discovery : The LDL Receptor. *Arterioscler. Thromb.* **29,** 431–438 (2010).

2. Ned, R. M. & Sijbrands, E. J. G. Cascade Screening for Familial Hypercholesterolemia (FH). *PLoS Curr.* **3,** RRN1238 (2011).

3. Usifo, E. *et al.* Low-Density Lipoprotein Receptor Gene Familial Hypercholesterolemia Variant Database: Update and Pathological Assessment. *Ann. Hum. Genet.* **76,** 387–401 (2012).

4. Hobbs, H. H., Leitersdorf, E., Goldstein, J. L., Brown, M. S. & Russell, D. W. Multiple crm-mutations in familial hypercholesterolemia. Evidence for 13 alleles, including four deletions. *J. Clin. Invest.* **81,** 909–917 (1988).

5. Goldstein, J. L., Brown, M. S., Anderson, R. G. W., Russell, D. W. & Schneider, W. J. ENDOCYTOSIS : Concepts Receptor System. *Receptor* 1–39 (1985).

6. Hobbs et al. Molecular genetics of the LDL receptor gene in familial hypercholesterolemia. *Hum. Mutat.* **1,** 445–466 (1992).

7. Davis, C. G. *et al.* The J. D. mutation in familial hypercholesterolemia: Amino acid substitution in cytoplasmic domain impedes internalization of LDL receptors. *Cell* **45,** 15–24 (1986).

8. Lehrman, M. A., Goldstein, J. L., Brown, M. S., Russell, D. W. & Schneider, W. J. Internalization-defective LDL receptors produced by genes with nonsense and frameshift mutations that truncate the cytoplasmic domain. *Cell* **41,** 735–743 (1985).

9. Beglova, N., Jeon, H., Fisher, C. & Blacklow, S. C. Cooperation between fixed and low pH-inducible interfaces controls lipoprotein release by the LDL receptor. *Mol. Cell* **16,** 281–292 (2004).

10. Leigh, S. E. A., Foster, A. H., Whittall, R. A., Hubbart, C. S. & Humphries, S. E. Update and Analysis of the University College London Low Density Lipoprotein Receptor Familial Hypercholesterolemia Database. *Ann. Hum. Genet.* **72,** 485–498 (2008).

11. Silva, S. *et al.* In vitro functional characterization of missense mutations in the LDLR gene. *Atherosclerosis* **225,** 128–134 (2012).

12. KNIGHT, B. L. & SOUTAR, A. K. Changes in the Metabolism of Modified and Unmodified Low-Density Lipoproteins during the Maturation of Cultured Blood Monocyte-Macrophages from Normal and Homozygous Familial Hypercholesterolaemic Subjects. *Eur. J. Biochem.* **125,** 407–413 (1982).

13. Leren, T. P. *et al.* Molecular genetics of familial hypercholesterolaemia in Norway. *J Intern Med* **241,** 185–194 (1997).

14. Ranheim, T., Kulseth, M. A., Berge, K. E. & Leren, T. P. Model system for phenotypic characterization of sequence variations in the LDL receptor gene. *Clin. Chem.* **52,** 1469–1479 (2006).

15. Romano, M. *et al.* An improved method on stimulated T-lymphocytes to functionally

characterize novel and known LDLR mutations. *J. Lipid Res.* **52,** 2095–2100 (2011).

16. Sun, X. M., Patel, D. D., Knight, B. L. & Soutar, A. K. Comparison of the genetic defect with LDL-receptor activity in cultured cells from patients with a clinical diagnosis of heterozygous familial hypercholesterolemia. The Familial Hypercholesterolaemia Regression Study Group. *Arterioscler. Thromb. Vasc. Biol.* **17,** 3092–101 (1997).

17. Tada, H. *et al.* A novel method for determining functional LDL receptor activity in familial hypercholesterolemia: Application of the CD3/CD28 assay in lymphocytes. *Clin. Chim. Acta* **400,** 42–47 (2009).

18. Jeon, H. *et al.* Implications for familial hypercholesterolemia from the structure of the LDL receptor YWTD-EGF domain pair. *Nat. Struct. Biol.* **8,** 499–504 (2001).

19. Miniño, A. M., Xu, J., Kochanek, K. D. & Tejada-Vera, B. Death in the United States, 2007. *NCHS Data Brief* 1–8 (2009).

20. Terzic, A. & Waldman, S. Chronic diseases: The emerging pandemic. *Clin. Transl. Sci.* **4,** 225–226 (2011).

21. Waldman, S. A. & Terzic, A. Cardiovascular Health: The Global Challenge. *Clin. Pharmacol. Ther.* **90,** 483–485 (2011).

22. Benito-Vicente, A. *et al.* The importance of an integrated analysis of clinical, molecular, and functional data for the genetic diagnosis of familial hypercholesterolemia. *Genet. Med.* **17,** 980–988 (2015).

23. Haase, A. & Goldberg, A. C. Identification of people with heterozygous familial hypercholesterolemia. *Curr. Opin. Lipidol.* **23,** 282–9 (2012).

24. Nordestgaard, B. G. *et al.* Familial hypercholesterolaemia is underdiagnosed and undertreated in the general population: Guidance for clinicians to prevent coronary heart disease. *Eur. Heart J.* **34,** 3478–3490 (2013).

25. Brice, P., Burton, H., Edwards, C. W., Humphries, S. E. & Aitman, T. J. Familial hypercholesterolaemia: A pressing issue for European health care. *Atherosclerosis* **231,** 223–226 (2013).

26. Etxebarria, A. *et al.* Functional characterization of splicing and ligand-binding domain variants in the LDL receptor. *Hum. Mutat.* **33,** 232–243 (2012).

27. Brown, M. S. & Goldstein, J. L. Regulation of the activity of the low density lipoprotein

receptor in human fibroblasts. *Cell* **6,** 307–16 (1975).

28. Fouchier, S. W., Defesche, J. C., Umans-Eckenhausen, M. A. & Kastelein, J. J. The molecular basis of familial hypercholesterolemia in The Netherlands. *Hum. Genet.* **109,** 602–615 (2001).

29. Humphries, S. E. *et al.* Mutational analysis in UK patients with a clinical diagnosis of familial hypercholesterolaemia: relationship with plasma lipid traits, heart disease risk and utility in relative tracing. *J. Mol. Med.* **84,** 203–214 (2006).

30. Goldstein, J. L., Hobbs, H. H. & Brown, M. S. *Familial Hipercholesterolemia.* (Macgraw Hills, 1995). doi:10.1036/ommbid.149

31. K, D. *et al. Clinical Guidelines and Evidence Review for Familial hypercholesterolaemia: the identification and management of adults and children with familial hypercholesterolaemia*. (2008).

32. Alves, A. C. *et al.* Molecular diagnosis of familial hypercholesterolemia: an important tool for cardiovascular risk stratification. *Rev. Port. Cardiol.* **29,** 907–21 (2010).

33. Catapano, A. L. *et al.* ESC / EAS Guidelines for the management of dyslipidaemias The Task Force for the management of dyslipidaemias of the European Society of Cardiology (ESC) and the European Atherosclerosis Society (EAS) □ , □□. **217,** 3–46 (2011).

34. Medeiros, A. M., Alves, A. C., Francisco, V. & Bourbon, M. Update of the Portuguese Familial Hypercholesterolaemia Study. *Atherosclerosis* **212,** 553–558 (2010).

35. Kusters, D. M. *et al.* Founder mutations in the Netherlands: geographical distribution of the most prevalent mutations in the low-density lipoprotein receptor and apolipoprotein B genes. *Netherlands Hear. J.* **19,** 175–182 (2011).

36. Bourbon, M., Alves, A. C., Medeiros, A. M., Silva, S. & Soutar, A. K. Familial hypercholesterolaemia in Portugal. *Atherosclerosis* **196,** 633–642 (2008).

37. Huijgen, R., Kindt, I., Defesche, J. C. & Kastelein, J. J. P. Cardiovascular risk in relation to functionality of sequence variants in the gene coding for the low-density lipoprotein receptor: A study among 29 365 individuals tested for 64 specific low-density lipoprotein-receptor sequence variants. *Eur. Heart J.* **33,** 2325–2330 (2012).

38. Fouchier, S. W., Kastelein, J. J. P. & Defesche, J. C. Update of the molecular basis of familial hypercholesterolemia in The Netherlands. *Hum. Mutat.* **26,** 550–556 (2005).

39. Bourbon, M. *et al.* Genetic diagnosis of familial hypercholesterolaemia: the importance of functional analysis of potential splice-site mutations. *J. Med. Genet.* **46,** 352–357 (2009).

40. Ekström, U., Abrahamson, M., Sveger, T., Lombardi, P. & Nilsson-Ehle, P. An efficient screening procedure detecting six novel mutations in the LDL receptor gene in Swedish children with hypercholesterolemia. *Hum. Genet.* **96,** 147–50 (1995).

41. Etxebarria, A. *et al.* Advantages and versatility of fluorescence-based methodology to characterize the functionality of LDLR and class mutation assignment. *PLoS One* **9,** (2014).

42. Pimstone, S. N. *et al.* Phenotypic variation in heterozygous familial hypercholesterolemia: a comparison of Chinese patients with the same or similar mutations in the LDL receptor gene in China or Canada. *Arterioscler. Thromb. Vasc. Biol.* **18,** 309–15 (1998).

43. Løhne, K., Urdal, P., Leren, T. P., Tonstad, S. & Ose, L. Standardization of a flow cytometric method for measurement of low-density lipoprotein receptor activity on blood mononuclear cells. *Cytometry* **20,** 290–295 (1995).

44. Urdal, P., Leren, T. P., Tonstad, S., Lund, P. K. & Ose, L. Flow cytometric measurement of low density lipoprotein receptor activity validated by DNA analysis in diagnosing heterozygous familial hypercholesterolemia. *Cytometry* **30,** 264–8 (1997).

45. Ekström, U. *et al.* Expression of an LDL receptor allele with two different mutations (E256K and I402T). *Mol. Pathol.* **53,** 31–6 (2000).

46. Brown, M. & Goldstein, J. A receptor-mediated pathway for cholesterol homeostasis. *Science (80-.).* **232,** 34–47 (1986).

47. Strøm, T. B. *et al.* The cytoplasmic domain is not involved in directing Class 5 mutant LDL receptors to lysosomal degradation. *Biochem. Biophys. Res. Commun.* **408,** 642–6 (2011).

48. Brown, M. S., Herz, J. & Goldstein, J. L. LDL-receptor structure. Calcium cages, acid baths and recycling receptors. *Nature* **388,** 629–30 (1997).

49. Rudenko, G. *et al.* Structure of the LDL receptor extracellular domain at endosomal pH. *Science (80-.).* **298,** 2353–2358 (2002).

50. Esser, V., Limbird, L. E., Brown, M. S., Goldstein, J. L. & Russell, D. W. Mutational

analysis of the ligand binding domain of the low density lipoprotein receptor. *J. Biol. Chem.* **263,** 13282–90 (1988).

51. Russell, D. W., Brown, M. S. & Goldstein, J. L. Different combinations of cysteine-rich repeats mediate binding of low density lipoprotein receptor to two different proteins. *J. Biol. Chem.* **264,** 21682–8 (1989).

52. Beglova, N. & Blacklow, S. C. The LDL receptor: how acid pulls the trigger. *Trends Biochem. Sci.* **30,** 309–17 (2005).

53. Surdo, P. Lo *et al.* Mechanistic implications for LDL receptor degradation from the PCSK9/LDLR structure at neutral pH. *EMBO Rep.* **12,** 1300–1305 (2011).

54. Daly, N. L., Scanlon, M. J., Djordjevic, J. T., Kroon, P. A. & Smith, R. Three-dimensional structure of a cysteine-rich repeat from the low-density lipoprotein receptor. *Proc. Natl. Acad. Sci.* **92,** 6334–6338 (1995).

55. Wang, S. *et al.* Site-specific O-glycosylation of members of the low-density lipoprotein receptor superfamily enhances ligand interactions. *J. Biol. Chem.* **293,** 7408–7422 (2018).

56. Davis, C. G. *et al.* Acid-dependent ligand dissociation and recycling of LDL receptor mediated by growth factor homology region. *Nature* **326,** 760–5

57. Zhang, D.-W. *et al.* Binding of proprotein convertase subtilisin/kexin type 9 to epidermal growth factor-like repeat A of low density lipoprotein receptor decreases receptor recycling and increases degradation. *J. Biol. Chem.* **282,** 18602–12 (2007).

58. Goldstein J.L., Hobbs H.H., Brown M.S. Familial hypercholesterolemia. In: Scriver C.R., Beaudet A.L., Sly W.S., Valle D., editors. The Metabolic and Molecular Bases of Inherited Disease. McGraw-Hill; New York, NY, USA: 2001.

59. Davis, C. G. *et al.* Deletion of clustered O-linked carbohydrates does not impair function of low density lipoprotein receptor in transfected fibroblasts. *J. Biol. Chem.* **261,** 2828–38 (1986).

60. Yokode, M. *et al.* Cytoplasmic sequence required for basolateral targeting of LDL receptor in livers of transgenic mice. *J. Cell Biol.* **117,** 39–46 (1992).

61. Davis, C. G. *et al.* The J.D. mutation in familial hypercholesterolemia: amino acid substitution in cytoplasmic domain impedes internalization of LDL receptors. *Cell* **45,** 15–24 (1986).

62. Lehrman, M. A., Goldstein, J. L., Brown, M. S., Russell, D. W. & Schneider, W. J. Internalization-defective LDL receptors produced by genes with nonsense and frameshift mutations that truncate the cytoplasmic domain. *Cell* **41,** 735–43 (1985).

63. Dawson, P. A. *et al.* Sterol-dependent repression of low density lipoprotein receptor promoter mediated by 16-base pair sequence adjacent to binding site for transcription factor Sp1. *J. Biol. Chem.* **263,** 3372–9 (1988).

64. Ambros, V. The functions of animal microRNAs. *Nature* **431,** 350–5 (2004).

65. Goedeke, L. *et al.* MicroRNA-148a regulates LDL receptor and ABCA1 expression to control circulating lipoprotein levels. *Nat. Med.* **21,** 1280–1288 (2015).

66. Chen, W. J., Goldstein, J. L. & Brown, M. S. NPXY, a sequence often found in cytoplasmic tails, is required for coated pit-mediated internalization of the low density lipoprotein receptor. *J. Biol. Chem.* **265,** 3116–23 (1990).

67. Goldstein, J. L. & Brown, M. S. The LDL receptor and the regulation of cellular cholesterol metabolism. *J. Cell Sci. Suppl.* **3,** 131–7 (1985).

68. Hobbs, H. H., Russell, D. W., Brown, M. S. & Goldstein, J. L. The LDL receptor locus in familial hypercholesterolemia: mutational analysis of a membrane protein. *Annu. Rev. Genet.* **24,** 133–70 (1990).

69. Tolleshaug, H., Goldstein, J. L., Schneider, W. J. & Brown, M. S. Posttranslational processing of the LDL receptor and its genetic disruption in familial hypercholesterolemia. *Cell* **30,** 715–24 (1982).

70. Strøm, T. B., Laerdahl, J. K. & Leren, T. P. Mutation p.L799R in the LDLR, which affects the transmembrane domain of the LDLR, prevents membrane insertion and causes secretion of the mutant LDLR. *Hum. Mol. Genet.* **24,** 5836–44 (2015).

71. Futema, M. *et al.* Whole exome sequencing of familial hypercholesterolaemia patients negative for LDLR/APOB/PCSK9 mutations. *J. Med. Genet.* **51,** 537–44 (2014).

72. MacArthur, D. G. *et al.* Guidelines for investigating causality of sequence variants in human disease. *Nature* **508,** 469–476 (2014).

73. Khafizov, K., Madrid-Aliste, C., Almo, S. C. & Fiser, A. Trends in structural coverage of the protein universe and the impact of the Protein Structure Initiative. *Proc. Natl. Acad. Sci.* **111,** 3733–3738 (2014).

74. Levitt, M. Nature of the protein universe. *Proc. Natl. Acad. Sci. U. S. A.* **106,** 11079–84 (2009).

75. Vandrovcova, J. *et al.* The use of next-generation sequencing in clinical diagnosis of familial hypercholesterolemia. *Genet. Med.* **15,** 948–57 (2013).

76. Smigielski, E. M., Sirotkin, K., Ward, M. & Sherry, S. T. dbSNP: a database of single nucleotide polymorphisms. *Nucleic Acids Res.* **28,** 352–5 (2000).

77. Fredman, D. *et al.* HGVbase: a human sequence variation database emphasizing data quality and a broad spectrum of data sources. *Nucleic Acids Res.* **30,** 387–91 (2002).

78. Stenson, P. D. *et al.* Human Gene Mutation Database (HGMD ®): 2003 update. *Hum. Mutat.* **21,** 577–581 (2003).

79. Adzhubei, I. A. *et al.* A method and server for predicting damaging missense mutations. *Nat. Methods* **7,** 248–9 (2010).

80. Ng, P. C. SIFT: predicting amino acid changes that affect protein function. *Nucleic Acids Res.* **31,** 3812–3814 (2003).

81. González-Pérez, A. & López-Bigas, N. Improving the assessment of the outcome of nonsynonymous SNVs with a consensus deleteriousness score, Condel. *Am. J. Hum. Genet.* **88,** 440–449 (2011).

82. Schwarz, J. M., Rödelsperger, C., Schuelke, M. & Seelow, D. MutationTaster evaluates disease-causing potential of sequence alterations. *Nat. Methods* **7,** 575–576 (2010).

83. Grantham, R. Amino Acid Difference Formula to Help Explain Protein Evolution Amino Acid Difference Formula to Help Explain Protein Evolution. *Science (80-.).* **185,** 862–864 (1974).

84. Pollard, K. S., Hubisz, M. J., Rosenbloom, K. R. & Siepel, A. Detection of nonneutral substitution rates on mammalian phylogenies. *Genome Res.* **20,** 110–121 (2010).

85. Goldstein, J. L. & Brown, M. S. Binding and degradation of low density lipoproteins by cultured human fibroblasts. *J. Biol. Chem.* **249,** 5153–5162 (1974).

86. Holla, Ø. L. *et al.* Effects of intronic mutations in the LDLR gene on pre-mRNA splicing: Comparison of wet-lab and bioinformatics analyses. *Mol. Genet. Metab.* **96,** 245–52 (2009).

87. Chan, P., Jones, C., Lafrenière, R. & Parsons, H. G. Surface expression of low density

lipoprotein receptor in EBV-transformed lymphocytes: characterization and use for studying familial hypercholesterolemia. *Atherosclerosis* **131,** 149–60 (1997).

88. Chan, P. C., Lafrenière, R. & Parsons, H. G. Lovastatin increases surface low density lipoprotein receptor expression by retarding the receptor internalization rate in proliferating lymphocytes. *Biochem. Biophys. Res. Commun.* **235,** 117–22 (1997).

89. Sakuma, N., Iwata, S., Ichikawa, T. & Fujinami, T. Assessment of functional low-density-lipoprotein receptors on lymphocytes by a simplified method using culture medium with lipoprotein-free fetal calf serum and pravastatin. *Clin. Biochem.* **25,** 368–70 (1992).

90. Tada, H. *et al.* A novel method for determining functional LDL receptor activity in familial hypercholesterolemia: application of the CD3/CD28 assay in lymphocytes. *Clin. Chim. Acta.* **400,** 42–7 (2009).

91. van der Westhuyzen, D. R. *et al.* Low density lipoprotein receptor mutations in South African homozygous familial hypercholesterolemic patients. *Arteriosclerosis* **4,** 238–47

92. Raungaard, B., Heath, F., Brorholt-Petersen, J. U., Jensen, H. K. & Faergeman, O. Flow cytometric assessment of LDL receptor activity in peripheral blood mononuclear cells compared to gene mutation detection in diagnosis of heterozygous familial hypercholesterolemia. *Cytometry* **36,** 52–9 (1999).

93. Etxebarria, A. & Benito-Vicente, A. Functional Characterization and Classification of Frequent Low-Density Lipoprotein Receptor Variants. *Hum. ...* (2015).

94. Benito-Vicente, A. *et al.* Replacement of cysteine at position 46 in the first cysteine-rich repeat of the LDL receptor impairs apolipoprotein recognition. *PLoS One* **13,** e0204771 (2018).

95. Benito-Vicente, A. *et al.* p.(Asp47Asn) and p.(Thr62Met): non deleterious LDL receptor missense variants functionally characterized in vitro. *Sci. Rep.* **8,** 16614 (2018).

96. Jiang, L. *et al.* Analysis of LDLR variants from homozygous FH patients carrying multiple mutations in the LDLR gene. *Atherosclerosis* **263,** 163–170 (2017).

97. Etxebarria, A. *et al.* Activity-associated effect of LDL receptor missense variants located in the cysteine-rich repeats. *Atherosclerosis* **238,** 304–312 (2015).

98. Di Taranto, M. D. *et al.* Identification and in vitro characterization of two new PCSK9 Gain of Function variants found in patients with Familial Hypercholesterolemia. *Sci.*

Rep. **7,** 1–9 (2017).

99. Jiang, L. *et al.* The use of targeted exome sequencing in genetic diagnosis of young patients with severe hypercholesterolemia. *Sci. Rep.* **6,** 36823 (2016).

100. Landrum, M. J. *et al.* ClinVar: public archive of interpretations of clinically relevant variants. *Nucleic Acids Res.* **44,** D862-8 (2016).

101. Knight, B. L. & Soutar, A. K. Changes in the metabolism of modified and unmodified low-density lipoproteins during the maturation of cultured blood monocyte-macrophages from normal and homozygous familial hypercholesterolaemic subjects. *Eur. J. Biochem.* **125,** 407–13 (1982).

102. Langenhoven, E. *et al.* Two novel point mutations causing receptor-negative familial hypercholesterolemia in a South African Indian homozygote. *Atherosclerosis* **125,** 111–9 (1996).

103. Cassanelli, S. *et al.* A 'de novo' point mutation of the low-density lipoprotein receptor gene in an Italian subject with primary hypercholesterolemia. *Clin. Genet.* **53,** 391–5 (1998).

104. Bertolini, S. *et al.* Analysis of LDL receptor gene mutations in Italian patients with homozygous familial hypercholesterolemia. *Arterioscler. Thromb. Vasc. Biol.* **19,** 408–18 (1999).

105. Rubinsztein, D. C., Jialal, I., Leitersdorf, E., Coetzee, G. A. & van der Westhuyzen, D. R. Identification of two new LDL-receptor mutations causing homozygous familial hypercholesterolemia in a South African of Indian origin. *Biochim. Biophys. Acta* **1182,** 75–82 (1993).

106. Romano, M. *et al.* Identification and functional characterization of LDLR mutations in familial hypercholesterolemia patients from Southern Italy. *Atherosclerosis* **210,** 493–6 (2010).

107. Slimane, M. N. *et al.* CYS127S (FH-Kairouan) and D245N (FH-Tozeur) mutations in the LDL receptor gene in Tunisian families with familial hypercholesterolaemia. *J. Med. Genet.* **39,** e74 (2002).

108. Hobbs, H. H. *et al.* Evidence for a dominant gene that suppresses hypercholesterolemia in a family with defective low density lipoprotein receptors. *J. Clin. Invest.* **84,** 656–64 (1989).

109. Nauck, M. S. *et al.* FH-Freiburg: a novel missense mutation (C317Y) in growth factor repeat A of the low density lipoprotein receptor gene in a German patient with homozygous familial hypercholesterolemia. *Atherosclerosis* **151,** 525–34 (2000).

110. Assouline, L. *et al.* Identification of two novel LDL receptor gene defects in French-Canadian pediatric population: mutational analysis and biochemical studies. *Hum. Mutat.* **9,** 555–62 (1997).

111. Webb, J. C. *et al.* Characterization of mutations in the low density lipoprotein (LDL)-receptor gene in patients with homozygous familial hypercholesterolemia, and frequency of these mutations in FH patients in the United Kingdom. *J. Lipid Res.* **37,** 368–81 (1996).

112. Miyake, Y. *et al.* Update of Japanese common LDLR gene mutations and their phenotypes: Mild type mutation L547V might predominate in the Japanese population. *Atherosclerosis* **203,** 153–60 (2009).

113. Leitersdorf, E., Van der Westhuyzen, D. R., Coetzee, G. A. & Hobbs, H. H. Two common low density lipoprotein receptor gene mutations cause familial hypercholesterolemia in Afrikaners. *J. Clin. Invest.* **84,** 954–61 (1989).

114. Schmidt, H. H.-J. *et al.* Liver transplantation in a subject with familial hypercholesterolemia carrying the homozygous p.W577R LDL-receptor gene mutation. *Clin. Transplant.* **22,** 180–4 (2008).

115. Hattori, H. *et al.* Eight novel mutations and functional impairments of the LDL receptor in familial hypercholesterolemia in the north of Japan. *J. Hum. Genet.* **47,** 80–7 (2002).

116. Leitersdorf, E., Tobin, E. J., Davignon, J. & Hobbs, H. H. Common low-density lipoprotein receptor mutations in the French Canadian population. *J. Clin. Invest.* **85,** 1014–23 (1990).

117. Soutar, A. K., Knight, B. L. & Patel, D. D. Identification of a point mutation in growth factor repeat C of the low density lipoprotein-receptor gene in a patient with homozygous familial hypercholesterolemia that affects ligand binding and intracellular movement of receptors. *Proc. Natl. Acad. Sci. U. S. A.* **86,** 4166–4170 (1989).

118. Mak, Y. T. *et al.* Mutations in the low-density lipoprotein receptor gene in Chinese familial hypercholesterolemia patients. *Arterioscler. Thromb. Vasc. Biol.* **18,** 1600–5 (1998).

119. Pavloušková, J., Réblová, K., Tichý, L., Freiberger, T. & Fajkusová, L. Functional analysis of the p.(Leu15Pro) and p.(Gly20Arg) sequence changes in the signal sequence of LDL receptor. *Atherosclerosis* **250,** 9–14 (2016).

120. Chang, J.-H. *et al.* Identification and characterization of LDL receptor gene mutations in hyperlipidemic Chinese. *J. Lipid Res.* **44,** 1850–8 (2003).

121. Webb, J. C. *et al.* Characterization of two new point mutations in the low density lipoprotein receptor genes of an English patient with homozygous familial hypercholesterolemia. *J. Lipid Res.* **33,** 689–98 (1992).

122. Khoo, K. L., Van Acker, P., Tan, H. & Deslypere, J. P. Genetic causes of familial hypercholesterolaemia in a Malaysian population. *Med. J. Malaysia* **55,** 409–18 (2000).

123. Leitersdorf, E. *et al.* A missense mutation in the low density lipoprotein receptor gene causes familial hypercholesterolemia in Sephardic Jews. *Hum. Genet.* **91,** 141–7 (1993).

124. Thormaehlen, A. S. *et al.* Systematic cell-based phenotyping of missense alleles empowers rare variant association studies: a case for LDLR and myocardial infarction. *PLoS Genet.* **11,** e1004855 (2015).

125. Wang, H. *et al.* Functional characterization of two low-density lipoprotein receptor gene mutations in two Chinese patients with familial hypercholesterolemia. *PLoS One* **9,** e92703 (2014).

126. Ekström, U. *et al.* An individual with a healthy phenotype in spite of a pathogenic LDL receptor mutation (C240F). *Clin. Genet.* **55,** 332–9 (1999).

127. Martín de Llano, J. J. *et al.* A single point mutation in the low-density lipoprotein receptor switches the degradation of its mature protein from the proteasome to the lysosome. *Int. J. Biochem. Cell Biol.* **38,** 1340–51 (2006).

128. Zhao, Z. & Michaely, P. Role of an intramolecular contact on lipoprotein uptake by the LDL receptor. *Biochim. Biophys. Acta* **1811,** 397–408 (2011).

129. Sun, X. M. *et al.* Familial hypercholesterolemia in China. Identification of mutations in the LDL-receptor gene that result in a receptor-negative phenotype. *Arterioscler. Thromb. a J. Vasc. Biol.* **14,** 85–94 (1994).

130. Jensen, H. K. *et al.* Two mutations in the same low-density lipoprotein receptor allele act in synergy to reduce receptor function in heterozygous familial hypercholesterolemia. *Hum. Mutat.* **9,** 437–44 (1997).

131. Alves, A. C. *et al.* Characterization of the First PCSK9 Gain of Function Homozygote. *J. Am. Coll. Cardiol.* **66,** 2152–2154 (2015).

132. Cenarro, A. *et al.* The p.Leu167del mutation in APOE gene causes autosomal dominant hypercholesterolemia by down-regulation of LDL receptor expression in hepatocytes. *J. Clin. Endocrinol. Metab.* **101,** 2113–2121 (2016).

133. Fernández-Higuero, J. A. *et al.* Structural analysis of APOB variants, p.(Arg3527Gln), p.(Arg1164Thr) and p.(Gln4494del), causing Familial Hypercholesterolaemia provides novel insights into variant pathogenicity. *Sci. Rep.* **5,** 1–8 (2015).

134. Fernández-Higuero, J. A. *et al.* Structural changes induced by acidic pH in human apolipoprotein B-100. *Sci. Rep.* **6,** 1–10 (2016).

Chapter 4

Functional analysis of PCSK9 variants

Publications extracted from this chapter:

1. Alves, A. C. Etxebarria A, Medeiros AM, Benito-Vicente A et al. Characterization of the First PCSK9 Gain of Function Homozygote. J. Am. Coll. Cardiol. 66, 2152–2154 (2015).

2. Di Taranto, M. D. Benito-Vicente A., et al. Identification and in vitro characterization of two new PCSK9 Gain of Function variants found in patients with Familial Hypercholesterolemia. Sci. Rep. 7, 1–9 (2017).

3. Sánchez-Hernández R.M., Di Taranto M.D., Benito-Vicente A. *et al*. A novel gain-of-function PCSK9 mutation in the C-terminal domain. Under Revision. BBA Moleular and Cell biology of Lipids

4. Increasing the leucine stretch length of the PCSK9 signal peptide promotes autosomal dominant hypercholesterolaemia. Benito-Vicente A. *et al.* Under Review. Atherosclerosis Thrombosis and Vascular Biology.

4.1 Introduction

PCSK9 is one of the major genes implicated in autosomal dominant hypercholesterolemia (ADH), along with the Low-Density Lipoprotein Receptor (*LDLR*), the Apolipoprotein B (*APOB*), and the recently described p.Leu167del mutation in *APOE*[1–4]. *PCSK9* encodes the pro-protein convertase subtilisin/kexin type 9, a circulating protein that regulates plasma cholesterol levels by shortening the half-life of the LDLR protein[5]. PCSK9 is synthesized predominantly in the liver. Once secreted, PCSK9 binds to the EGFA domain of the LDLR[6–8], undergoes endocytosis, and targets LDLR for lysosomal degradation[8]. Two different types of pathogenic variants have been identified in this gene: a) loss of function (LOF) variants producing an hipofunctional protein, which causes an increase of LDLR amounts on the cell membrane and, consequently, hypocholesterolemia; b) gain of function (GOF) variants producing an hyperfunctional protein which degrades LDLR more efficiently, decreasing its levels and causing autosomal dominant hypercholesterolemia (ADH) and premature cardiovascular disease. The PCSK9-D374Y mutant is the most severe known GOF variant. This particular mutation increases the affinity of PCSK9 for the LDLR more than 10 fold. PCSK9-D374Y carriers have extremely elevated LDL cholesterol (LDL-C) levels (around 10 mmol/L)[9]. In contrast, loss-of-function (LOF) mutations in PCSK9 are associated with lifelong reductions in LDL-C levels that confer athero- protection[10].

PCSK9 is a 692-amino acid glycoprotein, synthetized as a 72 kDa soluble zymogen (proPCSK9), which contains a signal peptide (SP), a N-terminal peptide and a pro-domain region followed by a catalytic domain with the catalytic triad of serin proteases, aspartate (D), histidine (H) and serine (S), and a cysteine/histidine-rich-C-terminal domain (CTD). The pro-PCSK9 undergoes autocatalytic processing in the endoplasmic reticulum (ER), generating a ~62 kDa mature protein and a ~14 kDa pro-peptide. The pro-domain remains non-covalently attached to the rest of the protein along the secretory pathway[11]. The SP of PCSK9 contains 30 amino acids and directs the nascent protein to the ER where it is cleaved co-translationally[12–14]. PCSK9 SP encompasses a characteristic tandem repeat sequence of nine leucines[15].

Discovery of PCSK9 as a player of LDL uptake opened new therapeutic avenues. In fact PCSK9 has become the target of several therapies administered in case of failure of traditional therapies or in the most severe cases. Nowadays, the most promising therapy is based in the use of anti-PCSK9 monoclonal antibodies[16,17].

An accurate evaluation of each variant identified during any genetic screening is essential to define its pathogenic role. Although several bioinformatics tools are available [18], *in silico* predictions are not sufficiently effective to reliably assess the pathogenicity of variants and in particular, of GOF variants [19]. Therefore, *in vitro* functional characterization is the most effective and reliable method to evaluate the pathogenic role of *PCSK9*. Recent guidelines

support this concept and suggest that, among different criteria, functional assays can provide strong evidence of pathogenicity [20]. Several methods have been proposed to functionally characterize FH causative variants [21–23].

Base on all aforementioned considerations, the objectives of the present chapter were:

1) To functionally analyze two PCSK9 variants p.(Ala62Asp) and p.(Pro467Ala) present in a double heterozygous Portuguese child.
2) Functional assessment of 5 new PCSK9 variants (p.(Pro331Ala), p.(Arg357Cys), p.(Ser636Arg), p.(His643Arg) and p.(Arg499His)) found in Italian population that were not previously characterized.
3) Functional characterization of two frequent *PCSK9* variants (c.63_65delGCT (p.Leu23del, L8) and c.60_65dupGCTGCT (p.Leu22_Leu23dup, L11)) in Spanish population located in the signal peptide of PCSK9.

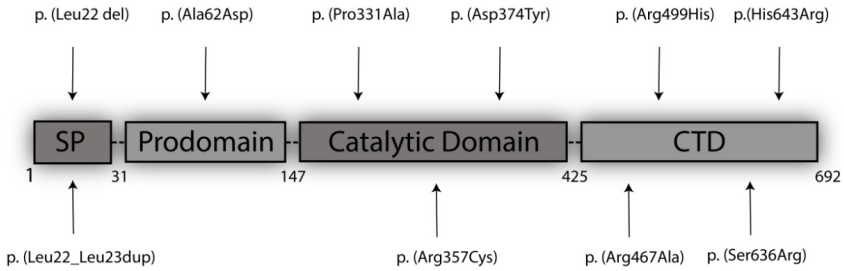

Figure 4.1. Protein sequence location of PCSK9 variants analyzed in this work.

4.2. Characterization of the First *PCSK9* Gain of Function Homozygote

GOF mutations in *PCSK9* are a rare cause of FH. We characterized two novel putative *PCSK9* GOF missense variants identified in a double heterozygous child with a clinical diagnosis of FH and no mutation in the *LDLR* and in *APOB* genes. The identified *PCSK9* variants were (p.[(Ala62Asp)]; [(Pro467Ala)]).

4.2.1 Results

4.2.1.1 p.(Ala62Asp), or p.(Pro467Ala) expression and secretion pattern is similar to wt PCSK9

For functional characterization, HEK293 cells (which do not endogenously produce PCSK9 were transfected with either wt, p.(Ala62Asp), or p.(Pro467Ala) *PCSK9* expression vectors. The

GOF p.(Asp374Tyr) PCSK9 was used as positive control. Cellular expression and secretion patterns of wt and all 3 mutants were similar (Figure 4.2).

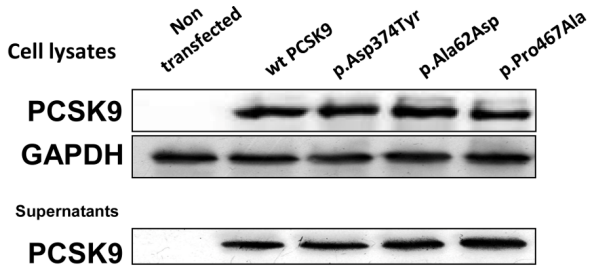

Figure 4.2. Expression and secretion of PCSK9 variants in stably transfected HEK293 cells.

4.2.1.2 p.(Ala62Asp) and p.(Pro467Ala) PCSK9 enhances PCSK9 function in HepG2

We next transfected HepG2 cells with these vectors and assessed cell surface LDLR expression as well as fluorescent LDL uptake by flow cytometry. Compared with nontransfected cells (baseline), cells expressing wt PCSK9 had reduced LDLR (-30%; $p<0.05$), and cells expressing either p.(Asp374Tyr), p.(Ala62Asp), or p.(Pro467Ala) PCSK9 had further reduced LDLR cell surface expression (-52%, -46%, and -56%, respectively; $p< 0.05$ vs. wt, all) (Figure 4.3 A). Likewise, fluorescent LDL uptake was significantly lower (-35% vs. baseline) in cells expressing any of the 3 PCSK9 variants compared with cells expressing wt PCSK9 (-20% vs. baseline) (Figure 4.3 B). These data indicate that p.(Ala62Asp) and p.(Pro467Ala) are genuine PCSK9 GOF variants.

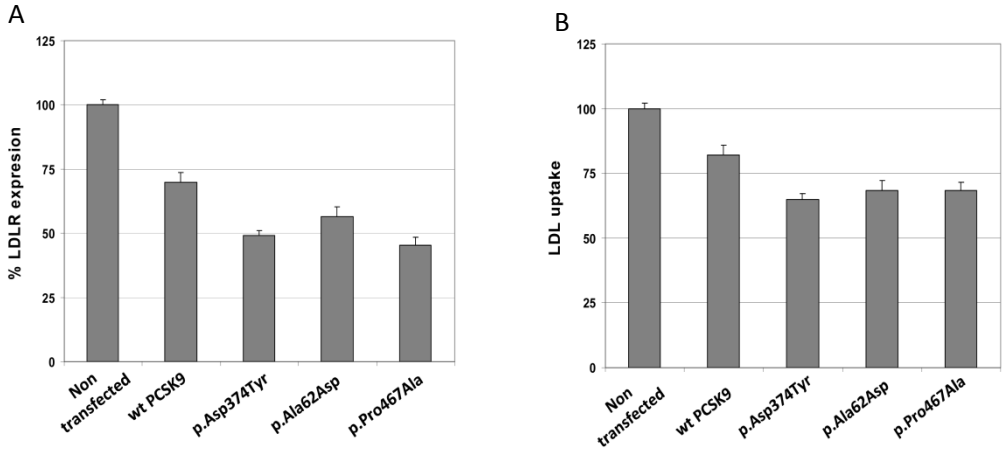

Figure 4.3: LDLR expression and LDL uptake in transiently transfected HepG2. A) LDLR expression at cellular membrane in HepG2 cells transiently transfected with PCSK9. B) LDL internalization after 4 h incubation at 37 °C in HepG2 cells transiently transfected with PCSK9. 10,000 cells were acquired in a Facscalibur. The values represent the mean of triplicate determinations (n = 3); error bars represent ±SD. *P < 0.001 compared to the wt using a Student's t-test.

4.2.2 Discussion

Homozygous carriers of *PCSK9* GOF mutations present a milder phenotype compared to *LDLR* homozygous FH patients[24] and, a similar phenotype than *APOB* or *LDLRAP*1 HoFH patients [25].

In this work the characterization of two novel PCSK9 variants; p.(Asp62Ala) and p.(Pro467Ala) is shown. Both mutations were found in different alleles of a young Portuguese child that to our knowledge represents the first case of a characterized double heterozygous FH patient. Although the *in silico* analyses predicts both variants to be non pathogenic, the *in vitro* characterization of these new variants demonstrated that they were both pathogenic (more active than wt PCSK9 at reducing cell surface LDLR expression) and as such genuine GOF PCSK9 variants. However, the mechanisms by which these two missense mutations affects LDLR function remain to be elucidated. Ongoing experiments are currently being carried out to determine the binding affinities of the variants towards LDLR and structural differences compared to wt PCSK9.

Further investigation will be needed to fully understand the GOF mechanisms of p.(Asp62Ala) and p.(Pro467Ala) PCSK9 variants in order to predict their effect onto LDL-C levels and the impact that PSCK9 inhibitor therapy could have in these particular cases.

4.3 *In vitro* characterization of three new *PCSK9* GOF variants found in patients with FH

Two hundred sixty nine Italian patients with a clinical suspect of FH were screened for variants in *LDLR* and the patients without pathogenic variants were screened for mutations in *PCSK9* and *APOB*. Functional characterization of *PCSK9* variants was performed by assessment of protein secretion, of LDLR activity in presence of the PCSK9 variants as well as LDLR-PCSK9 variants affinity. Among 81 patients without mutation in *LDLR*, 8 *PCSK9* variant in heterozygosis were found, 5 of which were carriers of variants whose role in FH pathogenesis is still unknown. Functional characterization revealed that three variants (p.(Arg357Cys), p.(Arg499His) and p.(Ser636Arg)) were GOF variants. The study highlights the important role played by functional characterization in integrating diagnostic procedures when the pathogenicity of new variants has not been previously demonstrated.

4.3.1 Results

4.3.1.1 Secretion of p.(Asp374Tyr), p.(Pro331Ala), p.(Arg357Cys), p.(Ser636Arg) p.(His643Arg) and p.(Arg499His) PCSK9 variants to the extracellular medium

HEK293 cells were transfected with DNA constructs encoding for wt, p.(Asp374Tyr), p.(Pro331Ala), p.(Arg357Cys), p.(Ser636Arg), p.(His643Arg) and p.(Arg499His) PCSK9 variants. PCSK9 secretion efficiency was analyzed by ELISA by comparing secreted PCSK9

with intracellular PCSK9 (Table x and Figure 4.4). Following PCSK9 secretion analysis, HEK293 medium was recovered and PCSK9 purified by nickel affinity chromatography. Purified PCSK9 were analyzed by western blot (figura 4.4 B).

A

	ng secreted PCSK9 / total PCSK9
PCSK9 wt	16.2 ± 0.8
P.(Asp374Tyr)	15.5 ± 0.1
p.(Pro331Ala)	16.3 ± 0.5
p.(Arg357Cys)	15.7 ± 0.5
p.(Ser636Arg)	15.1 ± 0.9
p.(His643Arg)	15.7 ±0.7

B

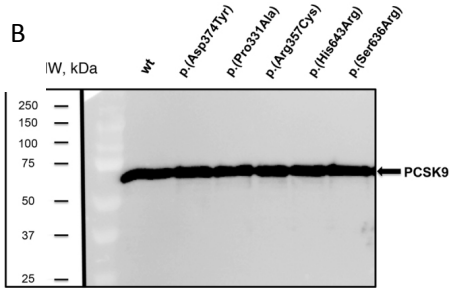

Figure 4.4. A) Extent of PCSK9 secretion analysed by ELISA. B) A representative Western blot analysis of purified PCSK9. A representative experiment from three independently performed assays is shown.

4.3.1.2 p.(Arg357Cys), p.(Ser636Arg) and p.(Arg499His) *PCSK9* variants diminish LDL uptake activity

In the first experimental approach to determine the activity of the PCSK9 variants, HEK293 cells were transiently transfected with wt, p.(Pro331Ala), p.(Arg357Cys), p.(Ser636Arg), p.(His643Arg) and p.(Arg499His) expression vectors (GOF p.(Asp374Tyr) PCSK9 variant was used as a positive internal control of the method). The efficiency of fluorescent LDL (FITC-LDL) uptake by the cells was measured as described in materials and methods. As shown in figure 4.5 A and C, LDL uptake was significantly reduced upon expression of p.(Arg357Cys), p.(Ser636Arg) and p.(Arg499His) PCSK9 variants, compared to wt PCSK9 whereas the uptake of p.(Pro331Ala) and p.(His643Arg) variants was similar to wt PCSK9 (Figure 4.5 A). This approach provides information on both intracellular and extracellular effects of PCSK9 variants. In order to deeply investigate the action mechanism of PCSK9 variants and to test only their extracellular action, the LDLR assay was performed incubating cells in a culture medium and adding recombinant purified PCSK9 variants exogenously. For that purpose, HepG2 cells (to test the PCSK9 behaviors in a hepatic cell line), figure 4.5 B and D, respectively, were treated with 5 µg/mL PCSK9 variants. Then, cells were incubated with 20 µg/mL FITC-LDL to determine the extent of LDL uptake. As shown in figure 4.5 B p.(Arg357Cys) and p.(Ser636Arg) showed a GOF activity in HEK293 and HepG2 cells, respectively, in which LDL uptake was diminished significantly when compared to wt PCSK9. Interestingly, and as shown in figure 4.5 D, exogenous activity of the p.(Arg499His) PCSK9 variant was similar to wt PCSK9 both in in HEK293 and in HepG2 cells.

Activities of p.(Pro331Ala) and p.(His643Arg) PCSK9 variants were similar to wt PCSK9. The p.(Asp374Tyr) GOF variant was used as internal control of the assay, and caused the expected reduction of LDL uptake already described.

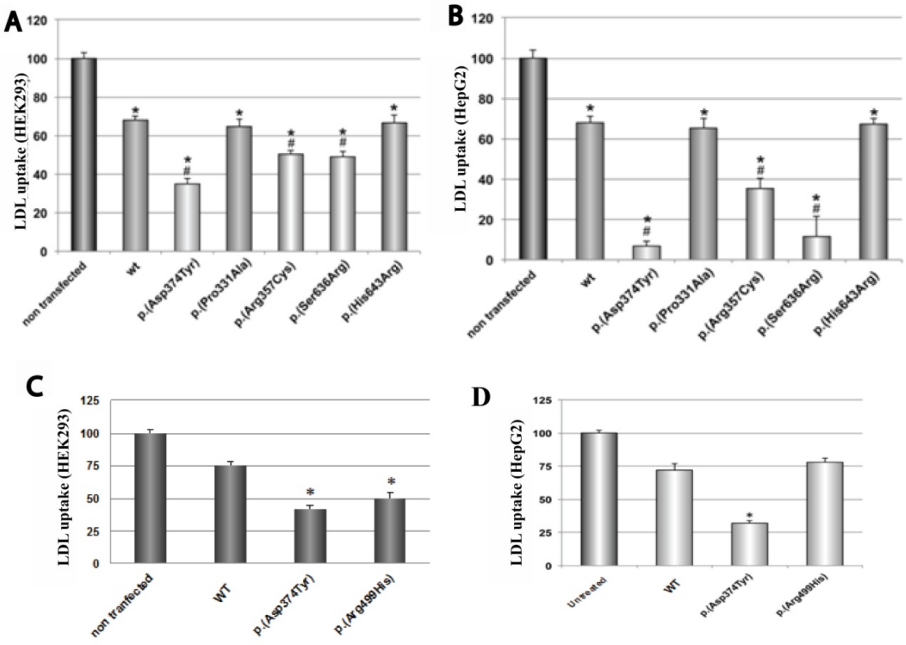

Figure 4.5. Effect of wt, p.(Asp374Tyr) p.(Pro331Ala), p.(Arg357Cys), p.(Ser636Arg) and p.(Arg499His) *PCSK9* variants on LDL uptake. A and C) LDL uptake in transiently transfected HEK293. B and D) LDL uptake in HepG2 cells treated with 2 µg/mL of purified PCSK9. HepG2 cells were incubated with the purified *PCSK9* variants at 2 µg/mL for 2 h prior FITC-LDL addition. LDL internalization was determined after 4 h incubation at 37 °C as described in Materials and Methods. Values represent the mean ± standard deviation of 3 independent experiments performed by triplicate. *$p < 0.01$ versus non transfected cells; #<0.01 versus wt *PCSK9* in A and B. The p.(Asp374Tyr) GOF mutant was used as internal control. *$p < 0.01$ versus wt *PCSK9* in C and D.

4.3.1.3 p.(Arg357Cys) and p.(Ser636Arg) PCSK9 variants show higher affinity for LDLR than wt PCSK9.

Next, we tested binding affinities of wt PCSK9, p.(Pro331Ala), p.(Arg357Cys), p.(Ser636Arg), p.(Arg499His) and p.(His643Arg) PCSK9 variants for LDLR at both pH 7.2 and pH 5.5 using a solid phase binding immunoassay. The calculated EC_{50} values for each variant are shown in Table 2. Affinity values of p.(Pro331Ala) and p.(Arg499His) variants to LDLR were similar to those found for WT PCSK9 both at pH 7.2 and pH 5.2. These results indicate that the GOF effect of p.(Asp499His) variant is not due to increased affinity for LDLR.

In contrast, for p.(His643Arg) variant, only the value at pH 7.2 is similar to the wt, being its EC_{50} at pH 5.5 higher than the wt (44.2 nM vs. 23.2 nM, respectively) (Table 2). However, EC_{50} values for wt LDLR of p.(Arg357Cys) and p.(Ser636Arg) variants were 50.9 and 47.4 nM, respectively, thus showing a higher affinity for LDLR and confirming the GOF activity. In addition and as internal control for method validation, EC_{50} value of p.(Asp374Tyr) GOF was

determined, and as expected, this variant showed a higher affinity to LDLR compared to wt PCSK9 (19.3 nM vs. 112.2 nM, respectively) (Table 4.1).

Table 4.1. EC_{50} values for the binding of PCSK9 variants to LDLR, as determined by solid-phase immunoassay at pH 7.2 and pH 5.5.

	EC_{50} (nM)*	
	pH 7.2	**pH 5.5**
wt	112 ± 16.8	23.2 ± 3.7
p.(Asp374Tyr)	19.3 ± 9.4	7.4 ± 1.7
p.(Pro331Ala)	97.6 ± 21.7	25.5 ± 7.7
p.(Arg357Cys)	50.9 ± 13.6	13.3 ± 6.7
p.(Ser636Arg)	47.4 ± 7.1	13.9 ± 5.5
p.(His643Arg)	93.7 ±13.4	44.2 ± 3.2
p.(Arg499His)	110.6 ± 23.5	33.2 ± 3.1

*Data are reported as mean±standard deviation.

4.3.1.4 Intracellular expression of LDLR is reduced when co-expressed with p.(Arg499His) PCSK9 variant

In order to corroborate the results obtained by FACS showing that cells expressing p.(Arg499His) *PCSK9* variant have reduced LDLR expression at cell surface and reduced LDL uptake (Figures 4.5 A and 4.5 B, respectively), HEK293 cells were transiently cotransfected with LDLR-GFP and with wt, GOF variant p.(Asp374Tyr) or p.(Arg499His) *PCSK9* variant. This procedure improves detection of the intracellular amounts of LDLR in the presence of PCSK9. The amount of intracellular LDLR-GFP was determined in cell lysates by western blot analysis 48 h post-transfection. As shown in figure 4.6 intracellular levels of LDLR-GFP were significantly lower in cells transfected with p.(Arg499His) *PCSK9* variant than in cells transfected with wt PCSK9, confirming the results obtained by FACS.

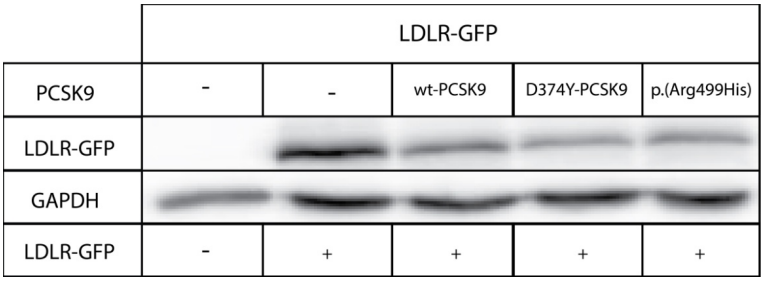

Figure 4.6. Effect of wt, p.(Asp374Tyr) and p.(Arg499His) *PCSK9* variants in LDLR intracellular amounts. Stably *PCSK9* transfected HEK293 cells were transiently co-transfected with GFP-LDLR plasmid. The amount of intracellular GFP-LDLR was determined in cell lysates by Western blot analysis. Three separate Western blot analyses were performed, of which one representative is shown.

4.3.1.5 p.(Arg499His) PCSK9 variant drives LDLR to intracellular degradation

To study whether PCSK9 affects intracellular LDLR levels and the transport of LDLR towards the cell membrane, stably transfected HEK293 cells with wt or p.(Arg499His) PCSK9 were co-transfected with a plasmid containing cDNA of the LDLR ectodomain (ED-LDLR). The amounts of ED-LDLR in the medium were quantified by Western blot analysis (Figure 4.7). The results show that the medium of cells co-transfected with ED-*LDLR* and p.(Arg499His) *PCSK9* variant contained 2-fold less ED-LDLR than those transfected with wt PCSK9 (Figure 4.7) indicating that LDLR is being degraded intracellularly.

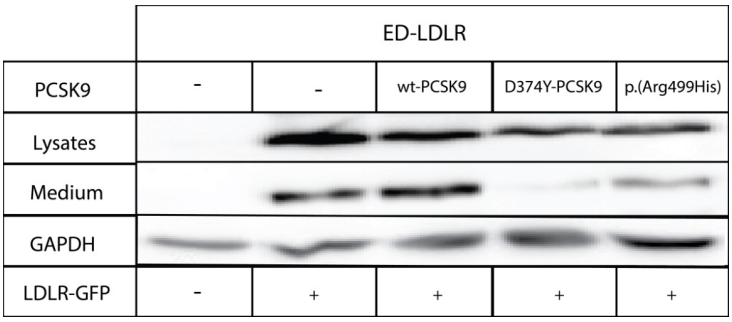

Figure 4.7. Effect of p.(Arg499His) *PCSK9* variant on the secretion of ED-LDLR. Stably *PCSK9* transfected HEK293 cells were transiently co-transfected with ED-LDLR plasmid. The amount of the ED-LDLR was determined in lysates and in media by Western blot analysis. A representative experiment from three independently performed assays is shown.

4.3.2 Discussion

Variants in the *PCSK9* gene are responsible for about 1% of FH cases, whereas the *LDLR* variants account for most of cases. The action mechanism of PCSK9 is at the basis of the dual effect of its variants, LOF variants causing hypocholesterolemia and GOF variants causing FH. The rare variants in the PCSK9 gene should be correctly evaluated before claiming their role as LOF or GOF. According to recent guidelines, a strict pathogenic classification is needed to correctly define the role of variants identified during re-sequencing studies. Functional studies are qualified as "strong" criteria for assessing variant pathogenicity[20].

PCSK9 GOF mutations have different mechanisms of action depending on the protein domain involved. The majority of them appear in the prodomain or in the catalytic domain, whereas the CTD GOF variants are less frequent[27]. The variants located in the prodomain have a broad mechanism of action; most frequently they increase LDLR degradation by both intracellular and extracellular effects[27–29]. Hence, some of them increase intracellular activity and LDLR degradation independently of autocatalytic activity[29], others show a decreased autocatalytic cleavage while increasing intracellular LDLR degradation[28,30,31] and finally, in some prodomain variants, the extracellular affinity of PCSK9 for LDLR is increased[28,29] . The catalytic domain is involved in the autocatalytic cleavage and the extracellular binding of

PCSK9 to the LDLR and, consequently, the mutations located in this domain lead to partial or complete resistance to furin cleavage, increasing PCSK9 activity[32].

The CTD of *PCSK9* has three repeat modules called M1, M2, M3[33], which are necessary to induce PCSK9-mediated degradation of the PCSK9-LDLR complex. The best-characterized function of the *PCSK9* CTD is to increase the affinity between PCSK9 and LDLR at the low pH of the endosomes, although this domain does not directly interact with the EGF-A domain of the LDLR[34]. Some variants in CTD increasing external degradation of LDLR are p.(Asn425Ser) and p.(Arg496Trp)[28]. Other variants in the CTD could lead to misfolding of *PCSK9* and generate more stable extracellular unions[33]. Other intracellular mechanisms of the interaction between *PCSK9* and LDLR have been described[35], and a possible role of the CTD for proper intracellular sorting of the PCSK9-LDLR complex has been suggested, although it still remains puzzling how *PCSK9* CTD governs LDLR degradation. Some data suggest that once the PCSK9-LDLR complex reaches the trans-Golgi network (TGN), PCSK9 possibly interacts with a co-receptor through its CTD, which would lead LDLR to the lysosomes[36].

In this study, 5 rare variants in the PCSK9 gene (2.6% of total examined patients) whose role in FH pathogenesis had never been previously were identified. In order to test the effect of PCSK9 rare variants in LDLR, functional characterization was performed by assessing protein secretion, LDLR activity in the presence of PCSK9 variant proteins as well as LDLR affinity of PCSK9 variants. Although the amounts of secreted PCSK9 appeared to be similar among the studied variants and the wt protein, we observed different behaviors of the LDLR regulation: 3 variants were GOF (p.(Arg357Cys), p.(Ser636Arg) and p.(Arg499His)), 2 variants (p.(Pro331Ala) and p.(His643Arg)) did not show any alteration compared to wt PCSK9. The effect of PCSK9 variants on LDLR was first tested on HEK293 transiently transfected with each PCSK9 variant, and then on HEK293 and HepG2 incubated with purified PCSK9 variants. These two approaches were used to test both intracellular and extracellular action of PCSK9 variants, showing concordant results for p.(Arg357Cys) and p.(Ser636Arg) but not for p.(Arg499His) which when added extracellularly did not have any effect. The measurement of LDLR affinity of the 5 variants evaluated in solid phase at both neutral and acid pH confirmed the GOF effect of the p.(Arg357Cys) and p.(Ser636Arg) variants which almost doubled affinity compared to wt. However, p.(Arg499His) variant did not show any affinity difference when compared to wt.

For p.(Arg499His) GOF carriers, the phenotype is indistinguishable from FH caused by *LDLR* mutations with almost complete penetrance[37]. Most p.(Arg499His) GOF carriers have LDL-C concentrations in the range of FH secondary to *LDLR* mutations; and some p.(Arg499His) GOF carriers presented with ASCVD, corneal arcus and tendon xanthomas in a frequency similar to the *LDLR*-caused FH[38]. Our study shows that p.(Arg499His) *PCSK9* variant is efficiently produced and secreted, which, together with the similar affinities and

activities of purified recombinant WT and p.(Arg499His) *PCSK9* variant, indicates that the observed GOF activity is not mediated by an extracellular effect. More interestingly, expression of this *PCSK9* variant negatively affects both extracellular and intracellular LDLR levels (determined by FACS and by cotransfection with LDLR-GFP, respectively), pointing out that an intracellular effect underlies its GOF activity.

We also detected a reduced amount of LDLR-GFP due to mutant *PCSK9* that can be interpreted as a consequence of increased proteasomal degradation. Therefore, p.(Arg499His) variant located in the CTD could present GOF mechanism of action by increasing mobility of the LDLR-PCSK9 complex from ER to trans-Golgi network and reducing thus intracellular LDLR concentration.

In conclusion, in our study 5 PCSK9 variants with an unknown effect on FH pathogenesis were identified. After extensive functional evaluation, we demonstrated a GOF effect of the p.(Arg357Cys) and p.(Ser636Arg) variants with an increased affinity by the receptor that promotes LDLR extracellular degradation. In contrast, p.(Arg499His) is a new GOF *PCSK9* mutation that reduces LDLR membrane expression through an intracellular effect, demonstrating the important role of CTD domain in the intracellular metabolism of the LDLR/PCSK9 complex.

1. Abifadel, M. *et al.* Mutations in PCSK9 cause autosomal dominant hypercholesterolemia. *Nat. Genet.* **34,** 154–156 (2003).
2. Allard, D. *et al.* Novel mutations of thePCSK9 gene cause variable phenotype of autosomal dominant hypercholesterolemia. *Hum. Mutat.* **26,** 497–497 (2005).
3. Leren, T. P. Mutations in the PCSK9 gene in Norwegian subjects with autosomal dominant hypercholesterolemia. *Clin. Genet.* **65,** 419–22 (2004).
4. Cenarro, A. *et al.* The p.Leu167del mutation in APOE gene causes autosomal dominant hypercholesterolemia by down-regulation of LDL receptor expression in hepatocytes. *J. Clin. Endocrinol. Metab.* **101,** 2113–2121 (2016).
5. Maxwell, K. N., Fisher, E. A. & Breslow, J. L. Overexpression of PCSK9 accelerates the degradation of the LDLR in a post-endoplasmic reticulum compartment. *Proc. Natl. Acad. Sci.* **102,** 2069–2074 (2005).
6. Bottomley, M. J. *et al.* Structural and Biochemical Characterization of the Wild Type PCSK9-EGF(AB) Complex and Natural Familial Hypercholesterolemia Mutants. *J. Biol. Chem.* **284,** 1313–1323 (2009).
7. Chen, Y. *et al.* Role of ubiquitination in PCSK9-mediated low-density lipoprotein receptor degradation. *Biochem. Biophys. Res. Commun.* **415,** 515–518

(2011).

8. Zhang, D. W. *et al.* Binding of proprotein convertase subtilisin/kexin type 9 to epidermal growth factor-like repeat A of low density lipoprotein receptor decreases receptor recycling and increases degradation. *J. Biol. Chem.* **282,** 18602–18612 (2007).
9. Hopkins, P. N. *et al.* Characterization of Autosomal Dominant Hypercholesterolemia Caused by PCSK9 Gain of Function Mutations and Its Specific Treatment With Alirocumab, a PCSK9 Monoclonal AntibodyCLINICAL PERSPECTIVE. *Circ. Cardiovasc. Genet.* **8,** 823–831 (2015).
10. Cohen, J. C., Boerwinkle, E., Mosley, T. H. & Hobbs, H. H. Sequence variations in PCSK9, low LDL, and protection against coronary heart disease. *N. Engl. J. Med.* **354,** 1264–72 (2006).
11. Benjannet, S. *et al.* NARC-1/PCSK9 and its natural mutants: zymogen cleavage and effects on the low density lipoprotein (LDL) receptor and LDL cholesterol. *J. Biol. Chem.* **279,** 48865–75 (2004).
12. Görlich, D., Hartmann, E., Prehn, S. & Rapoport, T. A. A protein of the endoplasmic reticulum involved early in polypeptide translocation. *Nature* **357,** 47–52 (1992).
13. Blobel, G. & Dobberstein, B. Transfer of proteins across membranes. I. Presence of proteolytically processed and unprocessed nascent immunoglobulin light chains on membrane-bound ribosomes of murine myeloma. *J. Cell Biol.* **67,** 835–51 (1975).
14. Gilmore, R. Protein translocation across the endoplasmic reticulum: a tunnel with toll booths at entry and exit. *Cell* **75,** 589–92 (1993).
15. Abifadel, M. *et al.* A PCSK9 variant and familial combined hyperlipidaemia. *J. Med. Genet.* **45,** 780–6 (2008).
16. Robinson, J. G. *et al.* Efficacy and Safety of Alirocumab in Reducing Lipids and Cardiovascular Events. *N. Engl. J. Med.* **372,** 1489–1499 (2015).
17. Sabatine, M. S. *et al.* Efficacy and Safety of Evolocumab in Reducing Lipids and Cardiovascular Events. *N. Engl. J. Med.* **372,** 1500–1509 (2015).
18. Camastra, F., Di Taranto, M. D. & Staiano, A. Statistical and Computational Methods for Genetic Diseases: An Overview. *Comput. Math. Methods Med.* **2015,** 1–8 (2015).

19. Flanagan, S. E., Patch, A.-M. & Ellard, S. Using SIFT and PolyPhen to Predict Loss-of-Function and Gain-of-Function Mutations. *Genet. Test. Mol. Biomarkers* **14,** 533–537 (2010).
20. Richards, S. *et al.* Standards and guidelines for the interpretation of sequence variants: a joint consensus recommendation of the American College of Medical Genetics and Genomics and the Association for Molecular Pathology. *Genet. Med.* **17,** 405–423 (2015).
21. Romano, M. *et al.* An improved method on stimulated T-lymphocytes to functionally characterize novel and known LDLR mutations. *J. Lipid Res.* **52,** 2095–2100 (2011).
22. Di Taranto, M. D., D'Agostino, M. N. & Fortunato, G. Functional characterization of mutant genes associated with autosomal dominant familial hypercholesterolemia: Integration and evolution of genetic diagnosis. *Nutr. Metab. Cardiovasc. Dis.* **25,** 979–987 (2015).
23. Alves, A. C. atarina, Etxebarria, A., Soutar, A. K. atherine, Martin, C. & Bourbon, M. Novel functional APOB mutations outside LDL-binding region causing familial hypercholesterolaemia. *Hum. Mol. Genet.* **23,** 1817–1828 (2014).
24. Cuchel, M. *et al.* Homozygous familial hypercholesterolaemia: New insights and guidance for clinicians to improve detection and clinical management. A position paper fromthe Consensus Panel on Familial Hypercholesterolaemia of the European Atherosclerosis Society. *Eur. Heart J.* **35,** 2146–2157 (2014).
25. Fellin, R., Arca, M., Zuliani, G., Calandra, S. & Bertolini, S. The history of Autosomal Recessive Hypercholesterolemia (ARH). From clinical observations to gene identification. *Gene* **555,** 23–32 (2015).
26. Dron, J. S. & Hegele, R. A. Complexity of mechanisms among human proprotein convertase subtilisin-kexin type 9 variants. *Curr. Opin. Lipidol.* **28,** 161–169 (2017).
27. Fasano, T., Sun, X.-M., Patel, D. D. & Soutar, A. K. Degradation of LDLR protein mediated by 'gain of function' PCSK9 mutants in normal and ARH cells. *Atherosclerosis* **203,** 166–171 (2009).
28. Abifadel, M. *et al.* Identification and characterization of new gain-of-function mutations in the PCSK9 gene responsible for autosomal dominant hypercholesterolemia. *Atherosclerosis* **223,** 394–400 (2012).

29. Cunningham, D. *et al.* Structural and biophysical studies of PCSK9 and its mutants linked to familial hypercholesterolemia. *Nat. Struct. Mol. Biol.* **14,** 413–419 (2007).
30. Cameron, J. *et al.* Effect of mutations in the PCSK9 gene on the cell surface LDL receptors. *Hum. Mol. Genet.* **15,** 1551–1558 (2006).
31. Naoumova, R. P. *et al.* Severe hypercholesterolemia in four British families with the D374Y mutation in the PCSK9 gene: long-term follow-up and treatment response. *Arterioscler. Thromb. Vasc. Biol.* **25,** 2654–60 (2005).
32. Susan-Resiga, D. *et al.* The Proprotein Convertase Subtilisin/Kexin Type 9-resistant R410S Low Density Lipoprotein Receptor Mutation. *J. Biol. Chem.* **292,** 1573–1590 (2017).
33. Holla, Ø. L. *et al.* Role of the C-terminal domain of PCSK9 in degradation of the LDL receptors. *J. Lipid Res.* **52,** 1787–1794 (2011).
34. Poirier, S. *et al.* Dissection of the endogenous cellular pathways of PCSK9-induced low density Lipoprotein receptor degradation. Evidence for an intracellular route. *J. Biol. Chem.* **284,** 28856–28864 (2009).
35. Poirier, S., Hamouda, H. A., Villeneuve, L., Demers, A. & Mayer, G. Trafficking Dynamics of PCSK9-Induced LDLR Degradation: Focus on Human PCSK9 Mutations and C-Terminal Domain. *PLoS One* **11,** e0157230 (2016).
36. Francke, U., Brown, M. S. & Goldstein, J. L. Assignment of the human gene for the low density lipoprotein receptor to chromosome 19: synteny of a receptor, a ligand, and a genetic disease. *Proc. Natl. Acad. Sci. U. S. A.* **81,** 2826–30 (1984).
37. Soutar, A. K. & Naoumova, R. P. Mechanisms of disease: Genetic causes of familial hypercholesterolemia. *Nat. Clin. Pract. Cardiovasc. Med.* **4,** 214–225 (2007).

Chapter 5

Study of ApoB100: effects of the endosome acidification on protein structure and characterization of ApoB100 variants.

Publications extracted from this chapter:

Fernández-Higuero JA, Etxebarria A, **Benito-Vicente A**, Alves AC, Arrondo JLR, Ostolaza H, et al. Structural analysis of APOB variants, p.(Arg3527Gln), p.(Arg1164Thr) and p.(Gln4494del), causing Familial Hypercholesterolaemia provides novel insights into variant pathogenicity. Sci Rep. Nature Publishing Group; 2015;5: 1–8. doi:10.1038/srep18184

Fernández-Higuero JA, **Benito-Vicente A**, Etxebarria A, Milicua JCG, Ostolaza H, Arrondo JLR, et al. Structural changes induced by acidic pH in human apolipoprotein B-100. Sci Rep. Nature Publishing Group; 2016;6: 1–10. doi:10.1038/srep36324

Alves AC, **Benito-Vicente A**, Medeiros AM, Kaajal R, Martin C, Bourbon M. Further evidence of novel APOB mutations as a cause of Familial Hypercholesterolaemia. Atherosclerosis. 2018; doi:10.1016/j.atherosclerosis.2018.06.819

5.1 Introduction

Lipoproteins play important physiologic roles in cellular function and regulation of lipid metabolic pathways. LDLs are the major natural transporter of cholesterol and phospholipids, acting as a constant supply of cholesterol for peripheral tissues and cells [1]. ApoB100, the scaffold of LDL particles, contains multiple lipid-associating regions [2] to adopt the required structure for binding to the LDLR which is responsible for the uptake of LDL particles into cells [3]. Once internalized, the LDLR-lipoprotein complex traffics to endosomes, where the lipoprotein cargo is released and the receptor is recycled back to the cell surface [4,5]. ApoB100-LDLR interaction is disrupted in the late endosome as a consequence of its acidification [6]. Dissociation of LDL from LDLR in the endosome is a key process that enables receptor recycling and LDL degradation in the lysosome [4,5].

Many studies related to LDLR have been conducted to understand the mechanism of pH-dependent LDL release. It was shown that endosome acidification promotes lipoprotein release by inducing a conformational change in the receptor from an extended conformation at neutral pH to a compact conformation at acidic enviroment [5,6]. Elongated stick-like LDLR structures have been observed in reconstituted vesicles at neutral pH [6], whereas crystallographic studies at acidic pH show a closed conformation with intramolecular contacts between cysteine-rich LR4–LR5 repeats of the ligand-binding domain and the β-propeller [5]. The closed conformation adopted by the LDLR at acidic pH leads to a weakened interaction with lipoproteins [7]. Although knowledge on LDLR conformational changes occurring in the cargo-releasing process has increased considerably, structural changes occurring in LDL particles have not been explored so far. In fact, acidic pH might affect ApoB100 conformation, the characteristics of LDL particle or both, and thus contributes, as well, to the cargo-releasing process. It has been suggested that ApoB100 is composed of globular domains connected by flexible segments that would stabilize the overall structure of the protein-lipid complex. Secondary structure predictions suggest that ApoB100 contains five distinct alternating α-helical and β-sheet domains: NH_2- βα1-β1-α2-β2-α3-COOH with different lipid binding affinities [8–11]. Some regions of the ApoB100 rich in β-structures are embebded in the phospholipid monolayer of the particle [12,13], while the residues involved in LDLR binding are exposed to the medium [12]. A low resolution structure of LDL at extracellular pH showing the localization of ApoB100 α-helix and β-sheet-rich domains across the LDL surface was determined by electron cryomicroscopy (cryoEM), a technique that preserves the native structure of the particles [14]. The extraordinary size of ApoB100, which is a monomeric protein constituted by 4,536 amino acids [15], represents a great challenge for structural studies. Currently, no high-resolution image of any ApoB100 domains is available. Different attempts have also been made to elucidate LDL:ApoB100 structure. Among them are, small angle

neutron scattering of lipid-free ApoB100 which describes the modular architecture of the protein with ordered domains connected by flexible linkers [16]; small-angle X-ray scattering which models the LDL core at low-resolution [17], and cryomicroscopy for single particle reconstruction[18]. Infrared (IR) is a low-resolution technique that can complement the information obtained by other biophysical techniques with higher resolution, providing information related to size and density of LDL and, also about the secondary structure content of ApoB100 under different conditions [13,19].

So far, only few variants have been reported and characterized as functionally defective in *APOB* gene [20–25]. The most common mutation found in *APOB* is a single amino acid substitution of arginine by glutamine at position 3527 (p.(Arg3527Gln)), which markedly reduces the affinity for the LDLR [24,25]. It has been described that the highly conserved receptor binding-site is stabilized by the interaction of Arg3527 with Trp4396, and as mentioned above, replacement of Arg3527 by a Gln impairs receptor recognition [20,23]. The mutation spectrum of *APOB* has notably increased in the recent years due to next generation sequencing (NGS) techniques that allow the study of all 29 APOB exons without increasing the laboratory work [21,26,27]. However, because *APOB* is a very polymorphic gene, these variants need to be functionally assessed [21]. Traditionally, for molecular diagnosis of FH the whole *LDLR* and *PCSK9* genes have been sequenced, as well as fragments of exons 26 and 29 of *APOB*, since these exons are known to contain variants associated with FH [28–32]. With new technological advances, the entire *APOB* [21,26] gene can now be sequenced easily using NGS panels, thereby increasing the identification of a greater number of putative pathogenic variants in this gene [21,26,33,34]. However, this adds a new concern for FH diagnosis, the necessity of a pathogenicity validation of these new variants. NGS has revolutionized research in genetics as well as improved and widened genetic diagnosis of the FH disease [21,26,34–38]. However, a faithful validation of the pathogenicity of these variants becomes more necessary than never.

Based on the all these considerations, the objectives of the present chapter were:

1) To explore possible structural changes in ApoB100 and LDL under acidic pH conditions, mimicking the endosome environment. We used dynamic light scattering (DLS) and electron microscopy to analyze morphology of wt LDL particles. Infrared (IR) spectroscopy was used to determine, both secondary structure content of ApoB100 and LDL stability at two different pHs.
2) To analyze the aforementioned characteristics of LDL particles from heterozygous patients carrying p.(Arg3527Gln) (c.10580G>A), p.(Arg1164Thr) (c.3491G>C) and p.(Gln4494del) (c.13480_13482delCAG) variants.
3) To perform a functional study for 2 rare *APOB* variants, p.(Pro994Leu) and p.(Thr3826Met) that reside out from the consensus LDLR binding site.

5.2 Structural changes induced by acidic pH in human ApoB100

Acidification in the endosome causes lipoprotein release by promoting a conformational change in LDLR allowing its recycling and degradation of LDL. Notwithstanding knowledge on conformational changes occurring in LDLR has considerably increased lastly, posible structural changes in LDL particles have not been fully explored yet. This led us the possibility to explore ApoB100 structure by different techniques: infrared (IR) spectroscopy, dynamic light scattering (DLS) and electron microscopy (EM) to assess changes in different parameters induced by an acidic pH mimicking the edosome environment.

5.2.1 Results5.2.1.1 LDL morphology and size are not affected by acidic pH

LDL size was analyzed by DLS at pH 7.4 and pH 5.0 as representative of physiological and endosomal enviroments, respectively. The mean particle diameter obtained at neutral pH was 29.4±0.2 nm in concordance with previous reports[39]. Figure 5.1 A shows that there was no alteration of the mean particle diameter at pH 5.0 compared to pH 7.4. Moreover, size distribution was similar for both experimental conditions, which discards possible aggregation or degradation of LDL particle induced by acidic pH. LDL morphology was examined by NS-EM at pH 7.4 and pH 5.0, all examined particles were approximately circular, consistent with a spherical shape (Figure 5.1 B and C). For LDL at both pHs, the peak population of the selected 1400 particles was in the diameter range of 28-30 nm corroborating the values obtained by DLS (Figure 5.1D)

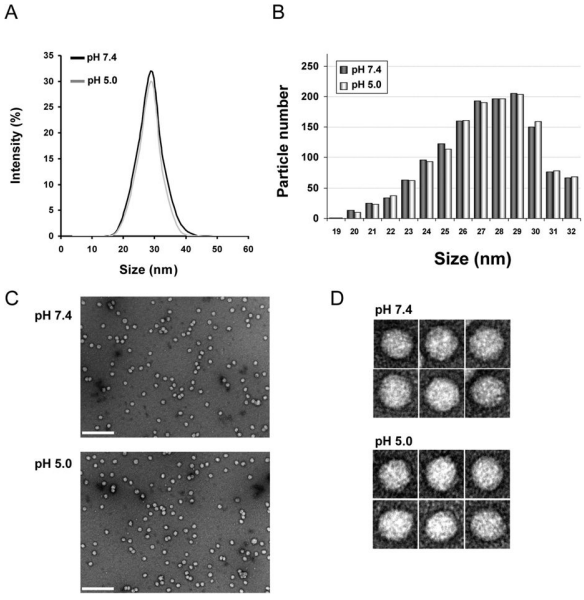

Figure 5.1. **Acidic pH does not affect LDL morphology and size.** (A) Size distribution of LDL at pH 7.4 and 5.0 determined by DLS; (B) Frequency histograms showing particle size distribution of LDL at pH 7.4 and pH 5.0. (C) electron-micrographs of LDL at pH 7.4 and 5.0 at low resolution showing a homogeneous particle population; (D) selected individual LDL particles at higher magnification. Particle size was determined as described in Materials and Methods. LDL size distribution in (D) was measured as Feret diameter calculated from 1600 particles.

5.2.1.2 pH acidification promotes changes in the secondary structure of ApoB100

To test possible changes in the secondary structure of ApoB100 induced by acidification of the medium, infrared spectra were recorded taking spectra every 0.5 pH units in the interval of 7.4 to 5.0. As shown in figure 5.2, a mayor transition from β-sheet to α-helix structure content occurs between pH 7 and 6.5 observing a slight increment in α-helix content in detriment of the β-sheet content. Below this pH the percentages of secondary structure remained practically unchanged. The percentages values of β-sheet/α-helix structure contents illustrating the transition at pH interval (7.4-5.0) are shown in figure 5.2.

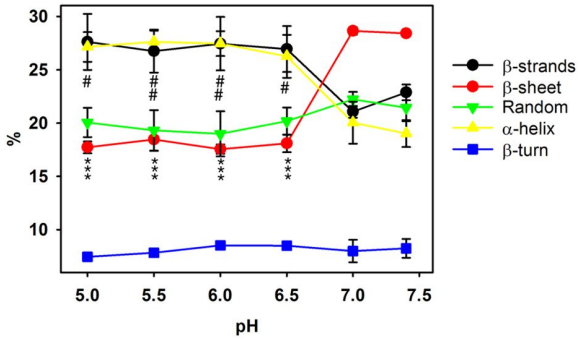

Figure 5.2. **pH acidification promotes changes in the secondary structure of ApoB100.** The spectra were obtained in D_2O buffer at 37 °C and data processed as described in Materials and Methods. Data are mean ± S.D. (n = 3). All measurements were performed independently 3 times and levels of significance were determined by a two-tailed Student's t-test. ***P < 0.001 when compared β -sheet percentage content at different pH with data obtained at pH 7.4. #P < 0.05; ##P < 0.01 when compared α -helix percentage content at different pH with data obtained at pH 7.4.

5.2.2 Discussion

It is well established that ApoB100 binds with high affinity to LDLR via a ligand-binding domain consisting of seven cysteine-rich repeats (LR1–LR7) [40]. In the acidic environment of the endosome, the affinity of the LDLR β-propeller for LDLR cysteine-rich repeats domain is higher than for LDL and the β -propeller functions as an alternative substrate for the LDLR ligand-binding domain[7] Consequently, a conformational switch from an open (ligand-active) to a closed (ligand-inactive) LDLR conformation occurs, with a concomitant LDL release [5,41]. Molecular mechanisms occurring in LDLR at acidic pH are well known [5–7], however, little attention has been paid so far to changes occurring in LDL, mainly because its structural complexity and the huge molecular size of ApoB100. This limitations have led to assume that LDL would have a mere passive role in the dissociation process, mainly driven by conformational changes in LDLR at acidic pH [5,42,43]

However, it seems reasonable to hypothesize that acidification of the pH may also influence the structure of ApoB100 and this, in turn, might affect the dissociation of the LDL/LDLR complex promoting or assisting a faster dissociation from LDLR. Here we show that acidification of the pH promotes changes in secondary structural elements of ApoB100, increasing the α-helix content in detriment of the β-sheet content. Further studies will be necessary to further to elucidate if LDL conformational changes at endosomal milieu are sufficient or not for the dissociation of the LDL/LDLR complex or act coordinately with those

occurring in LDLR. It may be postulated that changes in ApoB100 structure might influence such dissociation, facilitating adoption by LDLR of the closed conformation required for recycling. It was previously reported that pH lowering favours dissociation of LDL/LDLR complex by reducing the affinity of LDLR-LR5 for ApoB100 [44]. Binding analysis of LR5 repeat to mimicking peptides of LDL site B (exposed residues 3356–3368 located on the LDL surface) [45] or LDL site A (an additional proposed binding site comprising residues 3143–3155) [20,45,46] leads to consider a sequential binding model in which site B binds first to LDL [47]. Then, re-organization in the LDL leads to a greater exposure of site A, allowing recognition of this site by another LR in the receptor [47]. In accordance with this model, it can be speculated that the structural changes in ApoB100 upon acidification determined in this work might affect somehow or directly modify one of the recognition sites in ApoB100 displacing the equilibrium towards dissociation of LDL/LDLR complex. Alternatively, the whole ApoB100 ligand binding domain may be affected by the structural rearrangement occurring at acidic pH, leading to the same effects described above.

Here we have also analyzed the effect of pH acidification on lipoprotein particle size and morphology by DLS and electron microscopy. LDL particles consist of a single copy of ApoB100 wrapped around the surface of the lipid particle composed of a monolayer of phospholipids, sphingomyelin and unesterified cholesterol molecules [11,48]. In the proposed belt-and-bow model, ApoB100 makes a full turn around the particle, with a loose C-terminal part crossing over and forming a bow [49] following a meandering path[10]. ApoB100 also penetrates partially the phospholipids monolayer reaching the outer core of the particle and interacts with the lipids of the deeper layer of LDL as well [10,50]. In addition, ApoB100 is by necessity very flexible, as it must continually adapt its conformation and length to decreasing particle size during the lipolytic cascade from VLDL to LDL [51]. It was previously shown that at different pHs, the topology of loops and turns is altered leading to changes in the forces that stabilize the strands and the tertiary structure of the proteins[52]. However, we show here that neither particle size and morphology, nor lipidic microenvironment of LDL is modified by pH acidification, indicating that the obsreved structural changes occurring in ApoB100 upon acidification do not greatly alter the mayor physical properties of the particle.

There is strong evidence that the acidic microenvironment in the arterial intima has a direct role in the development of atherosclerosis, characterized by the extra- and intra-cellular accumulation of lipoprotein-derived lipids. Acidity enhances processes such as proteolytic, lipolytic, and oxidative modifications of LDL and other apoB-containing lipoproteins [53,54]. Therefore, the conformational changes induced on apoB structure by acidic environment showed in this work could have special relevance in the pathophysiology of atherosclerosis as the association with LDLR would be reduced, what would increase LDL time residence in acidic compartment favouring modifications occurring within the atherosclerotic lesions [55]. It

would be interesting to know possible changes occurring in other ApoB100 containing lipoproteins such as VLDL and IDL. IR spectroscopy cannot discriminate among the apoproteins contained in these lipoproteins and consequently structural information can not be specifically assigned to apoE, apoCII, apoCIII or apoB-100.

In conclusion, the data presented here show that pH acidification results in a different secondary structure content of ApoB100 suggesting a more active role of apolipoprotein in the LDLR/LDL releasing process that occurs upon endosomal acidification. It is also remarkable the reversibility of the structural modifications determined after neutral pH restitution, which indicates, that ApoB100 conformation is pH specific. The obtained results emphasize a more dynamic LDL/LDLR dissociation process than previous ascertained and provide new structural insights into the LDL/LDLR interactions than can occur at endosomal low-pH milieu.

5.3 Structural analysis of *APOB* variants, p.(Arg3527Gln), p.(Arg1164Thr) and p.(Gln4494del), causing Familial Hypercholesterolemia

Recently, p.(Arg1164Thr) and p.(Gln4494del) *APOB* variants showing impaired LDLR binding capacity, and diminished LDL uptake have been described[21]. The objective of this work was to analyse the structure of these two variants to gain insight into their pathogenicity. Therefore, secondary structure of the human ApoB100 has been investigated by IR spectroscopy and LDL particle size both by dynamic light scattering (DLS) and electron microscopy.

5.3.1 Results

5.3.1.1 Analysis of the binding capacity of p.(Arg1164Thr) and p.(Gln4494del) ApoB100 variants to LDLR

Previously, Alves and colleagues[21] had reported that binding of p.(Arg3527Gln), p.(Arg1164Thr) and p.(Gln4494del) to LDLR in lymphocytes resulted diminished relative to wt ApoB100. Here we determined that the uptake by lymphocytes of the pathogenic *APOB* variants was reduced about 50% compared to wt ApoB-containing lipoproteins (Figure 5.3), thus corroborating the data obtained by Alves and cols. Deficient LDL uptake of LDL containing ApoB100 variants was also confirmed using by HepG2 cell line, with uptake values similar to the determined in human lymphocytes (Figure 5.3).

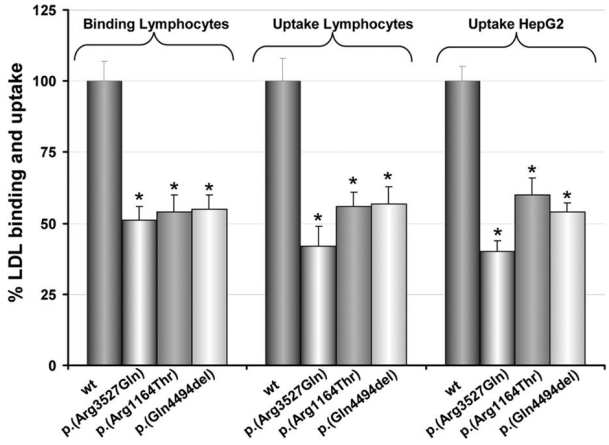

Figure 5.3. **Binding and uptake capacity of p.(Arg1164Thr) and p.(Gln4494del) ApoB100 variants.** Binding of FITC-LDL was assessed by incubation of lymphocytes with 20 µg/mL labelled-LDL for 4 h at 4 °C. For analysis of FITC-LDL uptake, lymphocytes or HepG2 cells were incubated for 4 h at 37 °C with 20 µg/mL FITC-LDL. 10,000 cells were acquired in a FACScalibur. The values represent the mean of triplicate determinations (n = 3); error bars represent ± SD. *p < 0.025 compared with wt ApoB100 (Student's t-test, two tailed).

Binding capacity of p.(Arg3527Gln), p.(Arg1164Thr) and p.(Gln4494del) variants to LDLR was checked with the U937 cells proliferation assay, which is a reference method to determine functional assays in *APOB*[56]. Cells growing in the presence of LDL carrying p.(Arg3527Gln), p.(Arg1164Thr) or p.(Gln4494del) variants showed ~1/3 growth compared with wt LDL (Figure 5.4) suggesting that the binding capacity of the variants to LDLR was affected.

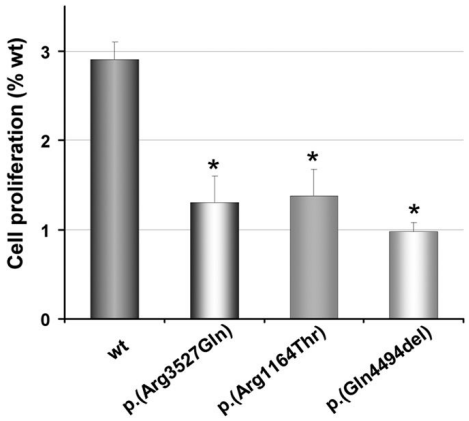

Figure 5.4. U937 cells proliferation assay the presence of LDL carrying p.(Arg3527Gln), p.(Arg1164Thr) or p.(Gln4494del) variants. Cells were incubated for 48 h with LDL and proliferation was assessed by CellTiter 96wAQueous Non-Radioactive Cell Proliferation Assay. The values represent the mean of triplicate determinations (n = 3); error bars represent ± SD. *p < 0.025 compared with wt ApoB100 (Student's t-test, two tailed).

5.3.1.2 Analysis of the size of LDL variants

Peak diameters of LDL particle carrying wt ApoB100, p.(Arg3527Gln), p.(Arg1164Thr) and p.(Gln4494del) were determined by DLS (Figure 5.5 A). The mean LDL diameter of the wt ApoB100-LDL was 29.1 ± 0.2 nm and, the diameters of p.(Arg3527Gln),

p.(Arg1164Thr) and p.(Gln4494del) -LDL were 27.8 ± 0.3 nm, 27.9 ± 0.6 nm and 25.2 ± 0.9 nm, respectively.

Particle morphology and size stimation of the LDLs carrying wt ApoB100, p.(Arg3527Gln), p.(Arg1164Thr) or p.(Gln4494del) variants were examined by NS-EM. All particles examined were approximately circular, consistent with a spherical shape (Figure 5.5 B and C). For wt LDL, 75% of the selected 1600 particles were in the diameter range of 27–31 nm, with the peak population (21%) at 29 nm (Fig. 3D). However, electron micrographs of LDL particles from patients with *APOB* variants p.(Arg3527Gln), p.(Arg1164Thr) and p.(Gln4494del) showed smaller diameters. For p.(Arg3527Gln) and p.(Arg1164Thr) variants most of the particles (~78%) were in the diameter range of 25–29 nm, with the peak population (~ 20%) at 27 nm (Fig. 3D). However, electron micrographs of p.(Gln4494del)-LDL showed that most (81%) of the selected particles were between 24–27 nm in diameter with the peak population (77%) at 25.5 nm (Figure 5.5 D).

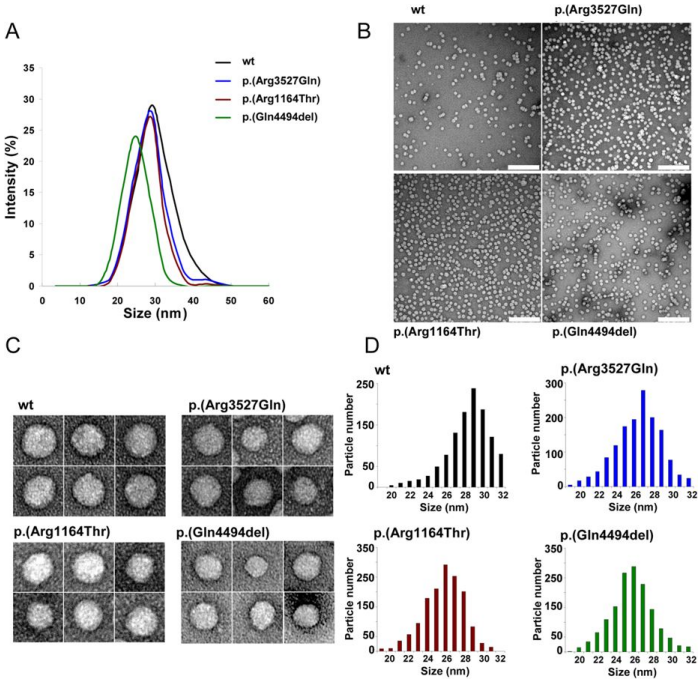

Figure 5.5. size of LDL variants. (A) Size distribution of isolated LDL carrying wt, p.(Arg3527Gln), p.(Arg1164Thr) and p.(Gln4494del) variants determined by DLS; (B) electron-micrographs of wt, p.(Arg3527Gln), p.(Arg1164Thr) and p.(Gln4494del) variants at low resolution showing a homogeneus particle population; (C) selected individual LDL particles at higher magnification showing and (D) Frequency histograms showing particle size distribution of wt, p.(Arg3527Gln), p.(Arg1164Thr) and p.(Gln4494del) variants. Particle size was determined as described in Materials and Methods. LDL size distribution in (D) was measured as Feret diameter calculated from 1600 particles.

5.3.1.3 Analysis of the secondary structure of the *APOB* variants

To determine possible changes in secondary structure of *APOB* p.(Arg3527Gln), p.(Arg1164Thr) and p.(Gln4494del) variants we used IR spectroscopy. The amide I band of each sample was individually fitted considering the component band position obtained from

Fourier derivation and deconvolution, as previously described[13]. These component bands have been assigned to several secondary structures as α-helix, β-turns, sheets or strands, and other unordered structures, usually called random, that typically appear around 1656, 1670, 1630, 1617 and 1642 cm^{-1} in deuterated media, respectively[13,57]. In LDL, β-strands are defined as segments embedded inside the particle monolayer, which are characterized by a band at a lower frequency than canonical extended structure[12]. The mean secondary structure composition obtained for wt ApoB100 was characterized by a high content in β-structures (>50%) with α-helix content of about 20% (Table 5.1), in agreement with previous IR studies [13,19], ApoB100 p.(Arg3527Gln) variant showed a reduced content in β-strands (around 3%) with slight increase in α-helixes (2%), similarly to that occurring in p.(Gln4494del) variant in which deletion of Gln at 4494 position produced a clear change in amide I band shape (Figure 5.6) mainly resulting in a decrease of β-strands, from 22% to 15%, and in approximately 4% increase in α-helix contribution (Table 1). In contrast, p.(Arg1164Thr) variant showed an amide I band decomposition similar to wt (Table 5.1), as expected from the similarity of their band shapes (Figure 5.6).

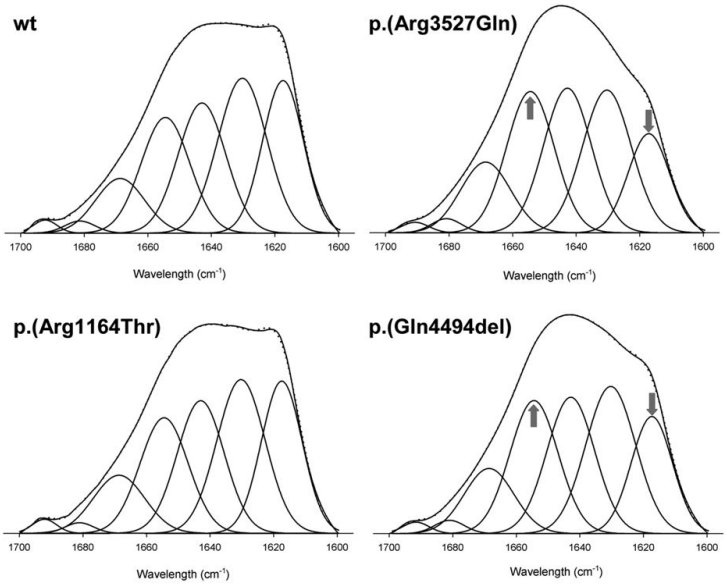

Figure 5.6. **Secondary structure of the *APOB* variants.** The spectra were obtained in D_2O buffer at 37 °C as described in Materials and Methods.

Table 5.1

Structure	wt ApoB100	p.(Arg3527Gln)	p.(Arg1164Thr)	p.(Gln4494del)
β-Turn	11.0 ± 0.7	12.0 ± 0.8	11.3 ± 0.5	13.4 ± 0.7
α-helix	19.8 ± 1.1	21.6 ± 1.4*	19.2 ± 0.5	24.2 ± 1.4*
Random	21.7 ± 0.4	22.4 ± 0.6	21.6 ± 0.2	23.6 ± 0.5
β Sheet	25.8 ± 0.3	25.5 ± 0.2	25.3 ± 0.4	24.3 ± 2.1
β Strand	21.7 ± 1.8	18.6 ± 1.7*	22.6 ± 1.0	14.5 ± 2.3*

Values shown represent the mean ± standard deviation. *$p < 0.01$ compared with wt ApoB100.

5.3.2 Discussion

FH is one of the most prevalent genetically inherited disorders that leads to greatly increased LDL levels along lifetime and development of early coronary artery disease [3]. The mechanisms underlying the process of atherosclerotic changes of the vessel wall have been extensively addressed both clinically and experimentally and, searching the *APOB* gene for new pathogenic variants has disclosed few alterations reported as functionally defective [20–24,27].

In the present work we sought to understand the loss of functionality previously shown for p.(Arg1164Thr) and p.(Gln4494del) *APOB* variants[21]. We have used a biophysical approach to determine LDL binding, uptake, particle size and secondary structure of LDL containing p.(Arg3527Gln), p.(Arg1164Thr) and p.(Gln4494del) ApoB variants. A major limitation in the present study is that LDL characterization is based on samples obtained from heterozygous mutation carriers. Nevertheless, the validity of this work is strengthened by previous *in vivo* studies showing that in heterozygous patients, particles carrying functional-defective ApoB100 accumulate in plasma, for example, p.(Arg3527Gln) mutant:wild-type LDL ratio was shown to be ~70:30 [58] and p.(Arg50Trp) mutant:wild-type ratio ~75:25 [27]. In this study, the ~50% decreased binding and uptake of LDL together with the ~2/3 reduced proliferation of U937 cells when incubated with LDL from heterozygous patients containing p.(Arg1164Thr) or p.(Gln4494del) variants shows an impaired LDL/LDLR recognition in saturable conditions.

It has been suggested that in patients carrying p.(Arg3527Gln) variant, the impaired removal of LDL from plasma promotes the formation of small dense LDL particles (sdLDL) [23]. In the present work, LDL particles obtained from heterozygous patients carrying p.(Arg3527Gln) or p.(Arg1164Thr) variants show a main population of particles of ~27 nm, significantly smaller than the ones carrying wt ApoB100 (~29 nm) and furthermore, the reduced size is even more pronounced in LDL harbouring p.(Gln4494del) ApoB100, with a mean diameter of ~25 nm. Thus, the smaller size found in LDL carrying p.(Arg1164Thr) and p.(Gln4494del) raises the possibility that delipidation processes may occur *in vivo*. It has been shown that the longer residence of LDL in blood allows an extensive activity of certain enzymes such as hepatic lipase (HL) and, cholesterol ester transfer protein (CETP) [59,60]. In fact, *in vitro* studies reveal that lipoprotein lipase (LPL) and HL induce alterations in LDL composition mainly characterized by a substantial reduction in the core triglyceride content [61]. It has also been shown that the sequential effects of lipid transfer and lipolysis promote dramatic changes in the mean size of plasma LDL favouring the formation of sdLDL [62].

In addition, the mutation itself can distort the structure of ApoB100 binding domain as described for p.(Arg3527Gln) mutation [63]. The belt conformation of ApoB100 that surrounds the LDL particle is maintained by interaction of Arg3527 with Trp4396 [64], which stabilizes two clusters of basic amino acids ensuring the binding of ApoB100 to LDLR [65]. It has been proposed that replacement of the Arg3527 promotes a conformational change in ApoB100

causing a rearrangement of a number of charged residues rather than loss of a single receptor-interactive residue [66]. The maintenance of these clusters could also be hampered in the case of p.(Gln4494del) variant because the amino acid deletion moves forward one position into the following amino acid. Therefore, the distortion introduced by p.(Gln4494del) may have a central role in the defective binding and the formation of smaller LDL particles. The analysis of these LDL by IR spectroscopy shows marked differences in the secondary structure of p.(Arg3527Gln) and p.(Gln4494del) compared with wt, their β-strands content being lower while their random and α-helix structure contributions slightly higher. It has been described that the reduced content of β-strands may be related with smaller LDLs [67] and that changes in the intensity and width of the β-strands band detected by IR spectroscopy might be related to more atherogenic LDL [68]. Although, the differences in the % structure may seem small, considering the big size of ApoB100, these results imply a huge structural rearrangement that likely affects the affinity for LDLR. Therefore, these structural changes may account for the impaired affinity of LDL carrying p.(Arg3527Gln) or p.(Gln4494del).

The diameter of the LDL particle and the ApoB100 conformation have implications for the binding affinity of ApoB100 to the receptors [69] thus the observed differences in one of these parameters, if not both, explain the defective activity of the ApoB100 variants characterized in this work. It is noteworthy that p.(Arg1164Thr) mutation barely modifies ApoB100 structure despite the reduced uptake of this lipoprotein, suggesting that Arg 1164 residue is important for LDL interaction with LDLR.

We conclude that changes found in particle size and/or secondary structure composition of ApoB100 underlie the defective binding and uptake of p.(Arg3527Gln), p.(Arg1164Thr) and p.(Gln4494del) variants. The structural analysis of these LDL carrying ApoB variants helps to understand their defective binding to LDLR, and remarks the importance of residues outside the postulated LDLR binding domain for ApoB100 to adopt a correct structure. *In vitro* experiments mimicking delipidation processes of lipoproteins are still in progress in our laboratory to elucidate how these processes affect both particle size and ApoB100 structure and will help to correlate these factors with LDL binding capacity.

5.4 Further evidence of novel *APOB* mutations as a cause of Familial Hypercholesterolemia

APOB mutations are a rare cause of FH and, until recently, routine genetic diagnosis only included the study of two small *APOB* fragments (exons 26 and 29). In previous years, five novel functional mutations have been described in *APOB* fragments not routinely studied.

Among them, our group has functionally characterized two novel variants, p.(Pro994Leu) and p.(Thr3826Met), in order to determine the genetic cause of hypercholesterolemia in patients with a clinical diagnosis of FH.

5.4.1 Results

5.4.1.1 Functional characterization of p.(Pro994Leu) and p.(Thr3826Met) *APOB* variants

Recently new 11 putative pathogenic *APOB* variants were described in the Portuguese population[70]. Due to sample availavility, only two of the variants, namely (p.(Pro994Leu) and p.(Thr3826Met)) have been functionally characterized. Functional characterization of those two ApoB100 variants was performed by isolating LDL particles from patients and relatives, carriers and non-carriers of the variants under study. Control samples obtained from an individual with wt *APOB* or from an individual with p.(Arg3527Gln) *APOB* variant were also included in the studies. *In vitro* LDL assays were performed in lymphocytes and U937 cells as described in Methods.

5.4.1.2 *In vitro* analysis of p.(Pro994Leu) *APOB* variant

The p.(Pro994Leu) *APOB* variant was previously identified by the group of Dr. Bourbon[21]. Figure 5.7 A shows the pedigree of the family carrying p.(Pro994Leu) variant. Plasma samples for functional characterization analysis were obtained from III:1 and IV:1 individuals. *In vitro* functional characterization of this *APOB* variant showed a similar LDL binding compared to wt ApoB100 containing LDL and similar growth of U937 cells than in the presence of wt ApoB100 containing LDL (Figure 5.7 B and C). The functional validation of this *APOB* variant shows a neutral effect on the protein function (Figure 5.7 B and C), the ACMG classification [4] for this variant is likely benign.

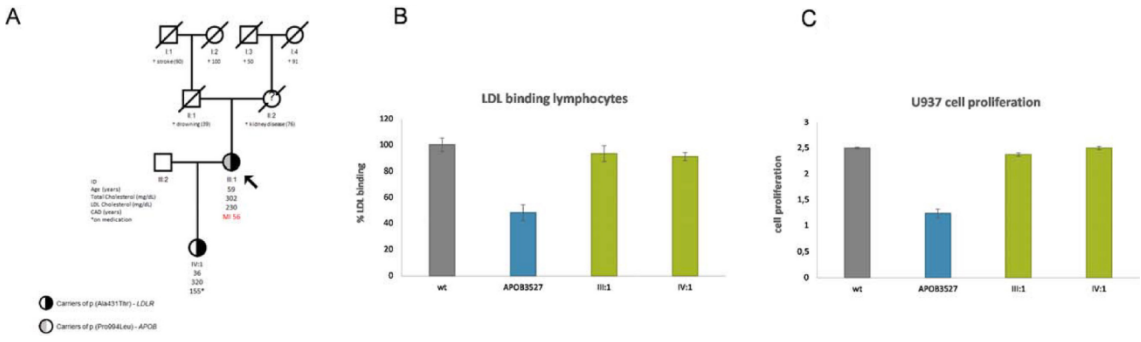

Figure 5.7. Functional characterization of p.(Pro994Leu) *ApoB100* variant. (A) Pedigree of the family carrying p.(Pro994Leu) variant. Index case is indicated by an arrow. (B) LDL-binding capacity after 4 h incubation at 4 °C in lymphocytes (C) U937 cell proliferation assay after 48 h incubation with LDL, presented as fold induction with respect to control without added LDL. The values represent the mean from at least 3 experiments; wt represents the experiment with wt ApoB100 carrying LDL; error bars represent ±SD. *$p < 0.05$ (Student *t*-test, one-tailed).

5.4.1.3 *In vitro* analysis of p.(Thr3826Met) *APOB* variant

The p.(Thr3826Met) *APOB* variant was previously identified by the group of Dr. Bourbon [7]. Figure 5.8 A shows the pedigree of the family carrying p.(Thr3826Met) variant. Plasma samples for functional characterization analysis were obtained from II:1, II:2 and IV:1 individuals. III:1 individual is a child with hypercholesterolemia but negative for mutations in *LDLR, PCSK9* and *APOB*. *In vitro* analysis of p.(Thr3826Met) *APOB* variant showed decreased LDL binding and reduced growth in U937, showing a similar effect as p.(Arg3527Gln) *APOB* variant (Figure 5.8 B and C). These results provide evidence that p.(Thr3826Met) is a pathogenic variant affecting ApoB100 binding capacity and therefore can be considered causative of FH. ACMG classification for this variant[35] is likely pathogenic.

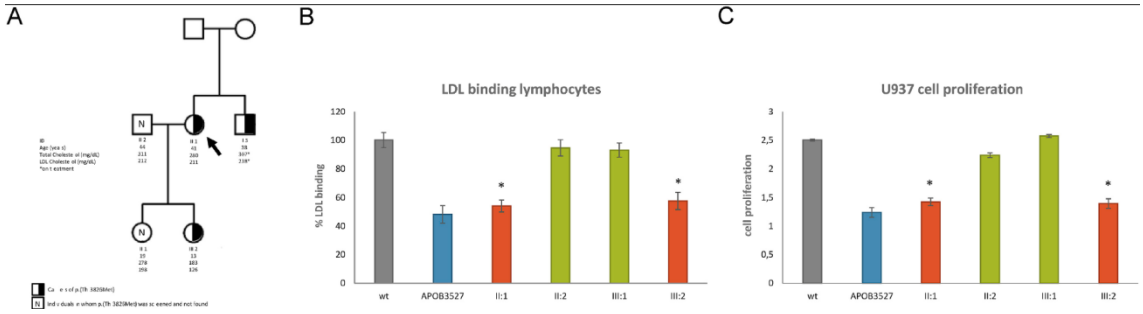

Figure 5.8. Functional characterization of p.(Thr3826Met) *ApoB100* variant. (A) Pedigree of the family with p.(Thr3826Met) variant, index case is indicated by an arrow. (B) LDL-binding capacity after 4 h incubation at 4 °C in lymphocytes (C) U937 cell proliferation assay after 48 h incubation with LDL, presented as fold induction with respect to control without addition of LDL. The values represent the mean from at least 3 experiments; wt represents the experiment with wt ApoB100 carrying LDL; error bars represent ±SD. *$p < 0.05$ (Student *t*-test, one-tailed).

5.4.2 Discussion

It is estimated that in FH cohorts worldwide, approximately 40-60% of clinical FH patients have an identified causative mutation[37,71–75]. The remaining patients may have defects in genes associated with FH, but in regions that have no yet been included in routine analysis or in other novel or even known dislipidemia genes. In order to obtain a correct molecular diagnosis it is important to functionally characterize the putative pathogenic variants to prove that the defect is causative of FH. This is important for all FH related gene variants but mainly for *APOB* variants, since only a small part of this gene has traditionally been analyzed. Functional characterization is scientifically much more demanding than DNA sequencing[76], however, a few labs, including ours, are currently doing it.

In vitro analysis of p.(Thr3826Met) *APOB* variant shows a decreased LDL binding as well as reduced growth of U937 cells, showing a similar effect as p.(Arg3527Gln) *APOB* variant (Figure 5.8B, C). A single individual showed incomplete penetrance as described before

for other *APOB* variants carriers[21,26]. In fact, the most common *APOB* variant, p.(Arg3527Gln), and several other novel functional *APOB* variants, have shown incomplete penetrance in at least one member of all families[21,24,26,27,77]. This demonstrates that although it is not common to observe a lack of penetrance with *LDLR* variants, a lack of penetrance with *APOB* variants is common.

Functional studies are the gold standard for assessing variant pathogenicity and the assays presented in this work follow the same principles as Brown and Goldstein studies[4,78]. This variant was identified in 2 unrelated cases (and 3 relatives) without another putative pathogenic variant in the 6 genes studied. The functional studies showed that p.(Thr3826Met) *APOB* variant is responsible for a reduced binding of apoB-LDL to LDLR similar to the well-known p.(Arg3527Gln) variant. Following ACMG guidelines, p.(Thr3826Met) variant is classified as likely pathogenic. Although this variant has a minor allele frequency (MAF) higher than any other variants causing FH, it is still considered rare. For all the reasons presented above we think this variant is the cause of disease for the described patients. However, as performed in this study, it is advisedable that all other known causes of the FH phenotype should be ruled out before attributing a diagnosis of FH solely based in the presence of this variant.

It is expected that a further 5-10% of all clinical FH patients considered mutation negative until now will have FH due to a novel *APOB* mutation. The low penetrance of *APOB* variants together with the high rate of common variants in *APOB* lead to a requirement of functional characterization of all novel variants to prove their pathogenicity. However, this is a challenge, since functional studies have to be carried out with patient sample, not always easy to obtain, and the studies are labour intensive. Among the nearly 300 variants with functional studies in genes associated with FH, only 6% are variants on *APOB*[35]. However, *APOB* variants are the second major cause of FH and so the identification of novel variants should be sought and in *vitro* studies should be performed to confirm their pathogenicity.

Our present study has thous contribute to increase the list of pathogenic *APOB* variants causing FH, and provides the functional study for two rare *APOB* variants.

References

1. Oram, J. F. & Heinecke, J. W. ATP-Binding Cassette Transporter A1: A Cell Cholesterol Exporter That Protects Against Cardiovascular Disease. *Physiol. Rev.* **85,** 1343–1372 (2005).

2. Chen, P. F. *et al.* Primary sequence mapping of human apolipoprotein B-100 epitopes. Comparisons of trypsin accessibility and immunoreactivity and implication for apoB

conformation. *Eur. J. Biochem.* **175,** 111–8 (1988).

3. Goldstein, J. L., Hobbs, H. H. & Brown, M. S. *Familial Hipercholesterolemia.* (Macgraw Hills, 1995). doi:10.1036/ommbid.149

4. Brown, M. & Goldstein, J. A receptor-mediated pathway for cholesterol homeostasis. *Science (80-.).* **232,** 34–47 (1986).

5. Rudenko, G. *et al.* Structure of the LDL receptor extracellular domain at endosomal pH. *Science (80-.).* **298,** 2353–2358 (2002).

6. Jeon, H. & Shipley, G. G. Vesicle-reconstituted Low Density Lipoprotein Receptor. *J. Biol. Chem.* **275,** 30458–30464 (2000).

7. Zhao, Z. & Michaely, P. Role of an intramolecular contact on lipoprotein uptake by the LDL receptor. *Biochim. Biophys. Acta - Mol. Cell Biol. Lipids* **1811,** 397–408 (2011).

8. Chen, G. C. *et al.* Structural domains of human apolipoprotein B-100. Differential accessibility to limited proteolysis of B-100 in low density and very low density lipoproteins. *J. Biol. Chem.* **264,** 14369–75 (1989).

9. Yang, C. Y. *et al.* Structure and conformational analysis of lipid-associating peptides of apolipoprotein B-100 produced by trypsinolysis. *J. Protein Chem.* **8,** 689–99 (1989).

10. Hevonoja, T., Pentikäinen, M. O., Hyvönen, M. T., Kovanen, P. T. & Ala-Korpela, M. Structure of low density lipoprotein (LDL) particles: basis for understanding molecular changes in modified LDL. *Biochim. Biophys. Acta* **1488,** 189–210 (2000).

11. Segrest, J. P., Jones, M. K., De Loof, H. & Dashti, N. Structure of apolipoprotein B-100 in low density lipoproteins. *J Lipid Res* **42,** 1346–1367 (2001).

12. Goormaghtigh, E., Cabiaux, V., De Meutter, J., Rosseneu, M. & Ruysschaert, J. M. Secondary structure of the particle associating domain of apolipoprotein B-100 in low-density lipoprotein by attenuated total reflection infrared spectroscopy. *Biochemistry* **32,** 6104–10 (1993).

13. Bañuelos, S., Arrondo, J. L., Goñi, F. M. & Pifat, G. Surface-core relationships in human low density lipoprotein as studied by infrared spectroscopy. *J. Biol. Chem.* **270,** 9192–6 (1995).

14. Ren, G. *et al.* Model of human low-density lipoprotein and bound receptor based on CryoEM. *Proc. Natl. Acad. Sci.* **107,** 1059–1064 (2010).

15. Yang, C.-Y. *et al.* Sequence, structure, receptor-binding domains and internal repeats of human apolipoprotein B-100. *Nature* **323,** 738–742 (1986).

16. Johs, A. *et al.* Modular Structure of Solubilized Human Apolipoprotein B-100. *J. Biol. Chem.* **281,** 19732–19739 (2006).

17. Baumstark, M. W., Kreutz, W., Berg, A. & Keul, J. Symmetry of the surface, and structure of the central core of human LDL particles, analyzed by X-ray small angle scattering. *Adv. Exp. Med. Biol.* **285,** 123–30 (1991).

18. Lund-Katz, S., Laplaud, P. M., Phillips, M. C. & Chapman, M. J. Apolipoprotein B-100 Conformation and Particle Surface Charge in Human LDL Subspecies: Implication for LDL Receptor Interaction †. *Biochemistry* **37,** 12867–12874 (1998).

19. Fernández-Higuero, J. A., Salvador, A. M., Martín, C., Milicua, J. C. G. & Arrondo, J. L. R. Human LDL Structural Diversity Studied by IR Spectroscopy. *PLoS One* **9,** e92426 (2014).

20. Borén, J. *et al.* Identification of the principal proteoglycan-binding site in LDL. A single-point mutation in apo-B100 severely affects proteoglycan interaction without affecting LDL receptor binding. *J. Clin. Invest.* **101,** 2658–2664 (1998).

21. Alves, A. C. atarina, Etxebarria, A., Soutar, A. K. atherine, Martin, C. & Bourbon, M. Novel functional APOB mutations outside LDL-binding region causing familial hypercholesterolaemia. *Hum. Mol. Genet.* **23,** 1817–1828 (2014).

22. Gaffney, D. *et al.* Independent mutations at codon 3500 of the apolipoprotein B gene are associated with hyperlipidemia. *Arterioscler. Thromb. Vasc. Biol.* **15,** 1025–9 (1995).

23. Innerarity, T. L. *et al.* Familial defective apolipoprotein B-100: low density lipoproteins with abnormal receptor binding. *Proc. Natl. Acad. Sci. U. S. A.* **84,** 6919–23 (1987).

24. Myant, N. B. Familial defective apolipoprotein B-100: a review, including some comparisons with familial hypercholesterolaemia. *Atherosclerosis* **104,** 1–18 (1993).

25. Pullinger, C. R. *et al.* The apolipoprotein B R3531C mutation. Characteristics of 24 subjects from 9 kindreds. *J. Lipid Res.* **40,** 318–27 (1999).

26. Motazacker, M. M. *et al.* Advances in genetics show the need for extending screening strategies for autosomal dominant hypercholesterolaemia. *Eur. Heart J.* **33,** 1360–1366 (2012).

27. Thomas, E. R. A. *et al.* Identification and biochemical analysis of a novel APOB mutation that causes autosomal dominant hypercholesterolemia. *Mol. Genet. Genomic Med.* **1,** 155–161 (2013).

28. Soutar, A. K. & Naoumova, R. P. Mechanisms of disease: Genetic causes of familial hypercholesterolemia. *Nat. Clin. Pract. Cardiovasc. Med.* **4,** 214–225 (2007).

29. Lombardi, P. *et al.* Mutations in the low density lipoprotein receptor gene of familial hypercholesterolemic patients detected by denaturing gradient gel electrophoresis and direct sequencing. *J. Lipid Res.* **36,** 860–7 (1995).

30. Palacios, L. *et al.* Molecular characterization of familial hypercholesterolemia in Spain. *Atherosclerosis* **221,** 137–142 (2012).

31. Taylor, A. *et al.* Mutation detection rate and spectrum in familial hypercholesterolaemia patients in the UK pilot cascade project. *Clin. Genet.* **77,** 572–580 (2010).

32. Kusters, D. M. *et al.* Founder mutations in the Netherlands: geographical distribution of the most prevalent mutations in the low-density lipoprotein receptor and apolipoprotein B genes. *Netherlands Hear. J.* **19,** 175–182 (2011).

33. Radovica-Spalvina, I. *et al.* Next-generation-sequencing-based identification of familial hypercholesterolemia-related mutations in subjects with increased LDL–C levels in a latvian population. *BMC Med. Genet.* **16,** 86 (2015).

34. Grenkowitz, T. *et al.* Clinical characterization and mutation spectrum of German patients with familial hypercholesterolemia. *Atherosclerosis* **253,** 88–93 (2016).

35. Chora, J. R., Medeiros, A. M., Alves, A. C. & Bourbon, M. Analysis of publicly available LDLR, APOB, and PCSK9 variants associated with familial hypercholesterolemia: application of ACMG guidelines and implications for familial hypercholesterolemia diagnosis. *Genet. Med.* **20,** 591–598 (2018).

36. Futema, M., Plagnol, V., Whittall, R. A., Neil, H. A. W. & Humphries, S. E. Use of targeted exome sequencing as a diagnostic tool for Familial Hypercholesterolaemia. *J. Med. Genet.* **49,** 644–649 (2012).

37. Iacocca, M. A. *et al.* Use of next-generation sequencing to detect LDLR gene copy number variation in familial hypercholesterolemia. *J. Lipid Res.* **58,** 2202–2209 (2017).

38. Johansen, C. T. *et al.* LipidSeq: a next-generation clinical resequencing panel for monogenic dyslipidemias. *J. Lipid Res.* **55,** 765–772 (2014).

39. Bourbon, M., Alves, A. C., Medeiros, A. M., Silva, S. & Soutar, A. K. Familial hypercholesterolaemia in Portugal. *Atherosclerosis* **196,** 633–642 (2008).

40. Goldstein, J. L. & Brown, M. S. The LDL Receptor. *Arterioscler. Thromb. Vasc. Biol.* **29,** 431–438 (2009).

41. Rudenko, G. & Deisenhofer, J. The low-density lipoprotein receptor: ligands, debates and lore. *Curr. Opin. Struct. Biol.* **13,** 683–9 (2003).

42. Arias-Moreno, X., Velazquez-Campoy, A., Rodríguez, J. C., Pocoví, M. & Sancho, J. Mechanism of Low Density Lipoprotein (LDL) Release in the Endosome. *J. Biol. Chem.* **283,** 22670–22679 (2008).

43. Zhao, Z. & Michaely, P. The Epidermal Growth Factor Homology Domain of the LDL Receptor Drives Lipoprotein Release through an Allosteric Mechanism Involving H190, H562, and H586. *J. Biol. Chem.* **283,** 26528–26537 (2008).

44. Arias-Moreno, X., Arolas, J. L., Aviles, F. X., Sancho, J. & Ventura, S. Scrambled Isomers as Key Intermediates in the Oxidative Folding of Ligand Binding Module 5 of the Low Density Lipoprotein Receptor. *J. Biol. Chem.* **283,** 13627–13637 (2008).

45. Chen, Z., Saffitz, J. E., Latour, M. A. & Schonfeld, G. Truncated apo B-70.5–containing lipoproteins bind to megalin but not the LDL receptor. *J. Clin. Invest.* **103,** 1419–1430 (1999).

46. Law, A. & Scott, J. A cross-species comparison of the apolipoprotein B domain that binds to the LDL receptor. *J. Lipid Res.* **31,** 1109–20 (1990).

47. Martínez-Oliván, J., Arias-Moreno, X., Velazquez-Campoy, A., Millet, O. & Sancho, J. LDL receptor/lipoprotein recognition: endosomal weakening of ApoB and ApoE binding to the convex face of the LR5 repeat. *FEBS J.* **281,** 1534–1546 (2014).

48. Steim, J. M., Edner, O. J. & Bargoot, F. G. Structure of human serum lipoproteins: nuclear magnetic resonance supports a micellar model. *Science* **162,** 909–11 (1968).

49. Chatterton, J. E. *et al.* Immunoelectron microscopy of low density lipoproteins yields a ribbon and bow model for the conformation of apolipoprotein B on the lipoprotein surface. *J. Lipid Res.* **36,** 2027–37 (1995).

50. Prassl, R. & Laggner, P. Molecular structure of low density lipoprotein: current status and future challenges. *Eur. Biophys. J.* **38,** 145–158 (2009).

51. McNamara, J. R., Small, D. M., Li, Z. & Schaefer, E. J. Differences in LDL subspecies involve alterations in lipid composition and conformational changes in apolipoprotein B. *J. Lipid Res.* **37,** 1924–35 (1996).

52. Chehín, R. *et al.* Thermal and pH-Induced Conformational Changes of a β-Sheet Protein Monitored by Infrared Spectroscopy †. *Biochemistry* **38,** 1525–1530 (1999).

53. Lähdesmäki, K. *et al.* Acidity and lipolysis by group V secreted phospholipase A2 strongly increase the binding of apoB-100-containing lipoproteins to human aortic proteoglycans. *Biochim. Biophys. Acta - Mol. Cell Biol. Lipids* **1821,** 257–267 (2012).

54. Öörni, K. *et al.* Acidification of the intimal fluid: the perfect storm for atherogenesis. *J. Lipid Res.* **56,** 203–214 (2015).

55. Oörni, K., Pentikäinen, M. O., Ala-Korpela, M. & Kovanen, P. T. Aggregation, fusion, and vesicle formation of modified low density lipoprotein particles: molecular mechanisms and effects on matrix interactions. *J. Lipid Res.* **41,** 1703–14 (2000).

56. Van den Broek, A. J. *et al.* Screening for familial defective apolipoprotein B-100 with improved U937 monocyte proliferation assay. *Clin. Chem.* **40,** 395–9 (1994).

57. Tybjaerg-Hansen, A. Rare and common mutations in hyperlipidemia and atherosclerosis. With special reference to familial defective apolipoprotein B-100. *Scand. J. Clin. Lab. Invest. Suppl.* **220,** 57–76 (1995).

58. Pullinger, C. R. *et al.* Familial ligand-defective apolipoprotein B. Identification of a new mutation that decreases LDL receptor binding affinity. *J. Clin. Invest.* **95,** 1225–1234 (1995).

59. Deckelbaum, R. J. *et al.* Reversible modification of human plasma low density lipoproteins toward triglyceride-rich precursors. A mechanism for losing excess cholesterol esters. *J. Biol. Chem.* **257,** 6509–17 (1982).

60. Homma, Y., Nakaya, N., Nakamura, H. & Goto, Y. Increase in the density of lighter low density lipoprotein by hepatic triglyceride lipase. *Artery* **13,** 19–31 (1985).

61. Aviram, M., Bierman, E. L. & Chait, A. Modification of low density lipoprotein by lipoprotein lipase or hepatic lipase induces enhanced uptake and cholesterol accumulation in cells. *J. Biol. Chem.* **263,** 15416–22 (1988).

62. Lagrost, L., Gambert, P. & Lallemant, C. Combined effects of lipid transfers and lipolysis on gradient gel patterns of human plasma LDL. *Arterioscler. Thromb. a J.*

Vasc. Biol. **14,** 1327–36 (1994).

63. März, W. *et al.* Accumulation of 'small dense' low density lipoproteins (LDL) in a homozygous patients with familial defective apolipoprotein B-100 results from heterogenous interaction of LDL subfractions with the LDL receptor. *J. Clin. Invest.* **92,** 2922–2933 (1993).

64. Schumaker, V. N., Phillips, M. L. & Chatterton, J. E. Apolipoprotein B and low-density lipoprotein structure: implications for biosynthesis of triglyceride-rich lipoproteins. *Adv. Protein Chem.* **45,** 205–48 (1994).

65. Milne, R. *et al.* The use of monoclonal antibodies to localize the low density lipoprotein receptor-binding domain of apolipoprotein B. *J. Biol. Chem.* **264,** 19754–60 (1989).

66. Lund-Katz, S., Innerarity, T. L., Arnold, K. S., Curtiss, L. K. & Phillips, M. C. 13C NMR evidence that substitution of glutamine for arginine 3500 in familial defective apolipoprotein B-100 disrupts the conformation of the receptor-binding domain. *J. Biol. Chem.* **266,** 2701–4 (1991).

67. Tanfani, F., Galeazzi, T., Curatola, G., Bertoli, E. & Ferretti, G. Reduced beta-strand content in apoprotein B-100 in smaller and denser low-density lipoprotein subclasses as probed by Fourier-transform infrared spectroscopy. *Biochem. J.* **322 (Pt 3,** 765–9 (1997).

68. Fernández-Higuero, J. A., Salvador, A. M., Martín, C., Milicua, J. C. G. & Arrondo, J. L. R. Human LDL structural diversity studied by IR spectroscopy. *PLoS One* **9,** (2014).

69. Miserez, A. R. & Keller, U. Differences in the phenotypic characteristics of subjects with familial defective apolipoprotein B-100 and familial hypercholesterolemia. *Arterioscler. Thromb. Vasc. Biol.* **15,** 1719–29 (1995).

70. Alves, A.C., Benito-Vicente, A., Medeiros, A.M., Reeves, K., Martin, C., Bourbon, M. Further evidence of novel APOB mutations as a cause of familial hypercholesterolaemia. *Atherosclerosis* (2018).

71. Nordestgaard, B. G. *et al.* Familial hypercholesterolaemia is underdiagnosed and undertreated in the general population: Guidance for clinicians to prevent coronary heart disease. *Eur. Heart J.* **34,** 3478–3490 (2013).

72. Fouchier, S. W., Defesche, J. C., Umans-Eckenhausen, M. A. & Kastelein, J. J. The molecular basis of familial hypercholesterolemia in The Netherlands. *Hum. Genet.* **109,**

602–615 (2001).

73. Futema, M. *et al.* Whole exome sequencing of familial hypercholesterolaemia patients negative for LDLR/APOB/PCSK9 mutations. *J. Med. Genet.* **51,** 537–44 (2014).

74. Bourbon, M. *et al.* Mutational analysis and genotype-phenotype relation in familial hypercholesterolemia: The SAFEHEART registry. *Atherosclerosis* **262,** 8–13 (2017).

75. Santos, R. D. *et al.* Clinical and molecular aspects of familial hypercholesterolemia in Ibero-American countries. *J. Clin. Lipidol.* **11,** 160–166 (2017).

76. Soutar, A. K. Rare genetic causes of autosomal dominant or recessive hypercholesterolaemia. *IUBMB Life* NA-NA (2010). doi:10.1002/iub.299

77. Vrablík, M., Ceska, R. & Horínek, A. Major apolipoprotein B-100 mutations in lipoprotein metabolism and atherosclerosis. *Physiol. Res.* **50,** 337–43 (2001).

78. Etxebarria, A. *et al.* Advantages and versatility of fluorescence-based methodology to characterize the functionality of LDLR and class mutation assignment. *PLoS One* **9,** (2014).

Annexes

Annex I

Increasing the leucine stretch length of the PCSK9 signal peptide promotes autosomal dominant hypercholesterolemia

Increasing the leucine stretch length of the PCSK9 signal peptide promotes autosomal dominant hypercholesterolemia. **Benito-Vicente A**, Uribe KB, Palacios L', Cenarro A, Calle X, et al. Increasing the leucine stretch length of the PCSK9 signal peptide promotes autosomal dominant hypercholesterolaemia. ATVB. Under Revision.

4.4. Introduction

The SP of PCSK9 contains 30 amino acids and directs the nascent protein to the ER where it is cleaved co-translationally. PCSK9 SP encompasses a characteristic tandem repeat sequence of nine leucines. Interestingly, the presence of eleven leucine residues (c.60_65dupGCTGCT, p.Leu22_Leu23dup, L11) instead of nine in the SP of PCSK9 has recently been associated with high LDL-C levels[1], whereas PCSK9 variants with a SP containing eight (c.63_65delGCT, p.Leu23del, L8) or ten leucines (L10) have been found in individuals with low plasma lipid levels. Unlike mutations found on secreted PCSK9, mutations located within the SP should not augment PCSK9 function when secreted to the extracellular medium, as the SP is cleaved co-translationally by the signal-peptidase complex[2–4]. The molecular pathway(s) by which the L11 variant promotes hypercholesterolemia therefore remains to be investigated. Therefore, L8 and L11 PCSK9 variants have been functionally characterized *in vitro*.

4.4.1 Results

4.4.1.1 The L8 PCSK9 variant is secreted normally whereas the L11 variant is secreted less efficiently than wt PCSK9

We transfected HEK293 cells with DNA constructs encoding for wt, L8, L11 or D347Y PCSK9 variants and examined the effects of those mutations on PCSK9 synthesis and auto-processing. Wild type, L8, L11 and D347Y PCSK9 variants were expressed to similar extents in cells with no apparent difference in auto-processing as shown by Western Blot (Figure 4.8 A). The extent of protein expression was determined by quantitative densitometric analysis. The relative band intensity of mature PCSK9 protein expression was calculated as the ratio of 62 kDa PCSK9 band intensity to that of GAPDH (Figure 4.8 B). However, the amount of secreted L11 PCSK9 variant was diminished significantly by approximately 20 % compared to wt PCSK9 as ascertained by the relative protein amount of PCSK9 determined by ELISA to total PCSK9 mRNA at different incubation times (4-24 h) (Figure 4.8 C).

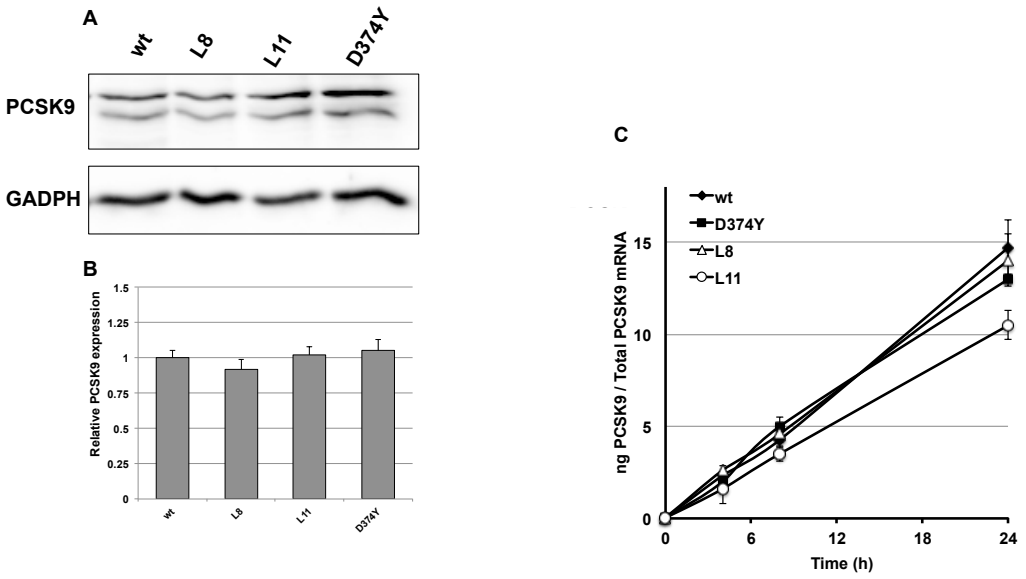

Figure 4.8. Expression of PCSK9 variants in stably transfected HEK293 cells. A)intracellular expression; B) relative amount of mature PCSK9 expression to GAPDH; C) secretion of PCSK9 was determined by ELISA and relativized to total PCSK9 mRNA of stably transfected cells.

4.4.1.2 The Leu22-Leu23 duplication within PCSK9 signal peptide (L11) variably enhances PCSK9 function in transfected cells

HEK293 and HepG2 cells were transiently transfected with wt, L8, L11 and D374Y PCSK9 expression vectors, and the levels of cell surface LDLR were measured 48 h later. Compared to wt PCSK9, the L11 variant significantly decreased cell surface LDLR expression (by approximately 20%), whereas the L8 variant did not. The PCSK9-D374Y GOF variant was used as positive control and reduced LDLR expression by more than 50%, under the same experimental conditions (Figure 4.9 A and 4.9 B). We next measured fluorescent LDL uptake in those cells. Paralleling LDLR expression patterns, LDL uptake was significantly reduced upon expression of the L11 PCSK9 variant in both cell lines (≈20%), compared to wt PCSK9 (Figure 4.9 C and 4.9 D). The D374Y variant was the most potent at reducing LDL uptake in those cells (≈50%), whereas wt and L8 PCSK9 promoted similar LDL uptake.

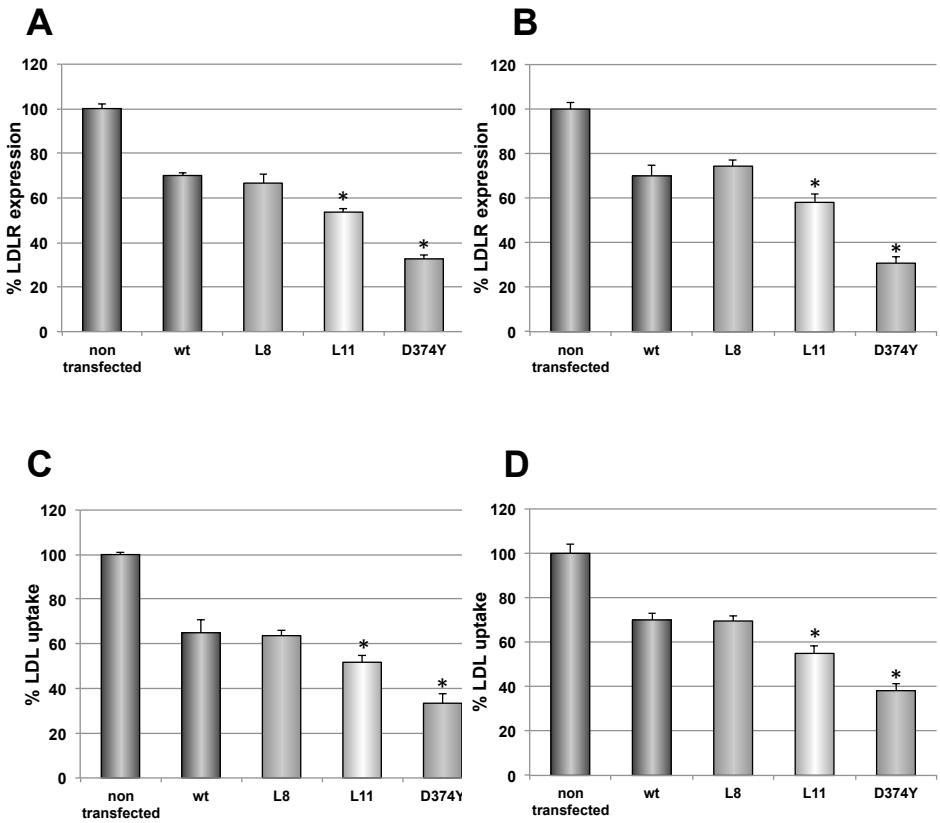

Figure 4.9: LDL uptake and LDLR expression in stably transfected HEK293 and transiently transfected HepG2. A) LDLR expression at cellular membrane in Hek293 cells stably transfected with PCSK9. B) LDLR expression at cellular membrane in HepG2 cells transiently transfected with PCSK9. C) LDL internalization after 4 h incubation at 37 °C in Hek293 cells transiently transfected with PCSK9. D) LDL internalization after 4 h incubation at 37 °C in HepG2 cells transiently transfected with PCSK9. 10,000 cells were acquired in a Facscalibur. The values represent the mean of triplicate determinations (n = 3); error bars represent ±SD. *P < 0.001 compared to the wt using a Student's t-test.

4.4.1.3 Purified L8 and L11 PCSK9 addition to HepG2 cell media do not alter LDLR expression or LDL uptake

We also purified wt, L8, L11 and D374Y PCSK9 from the supernatant of stably transfected HEK293 cells and added similar concentrations of these recombinant proteins in the culture medium of HepG2 cells for 2 h prior to fluorescent LDL uptake assay. Under these experimental conditions, neither L8 nor L11 significantly altered cellular LDL uptake, compared to wt PCSK9. We ascertained that recombinant PCSK9-D374Y sharply reduced LDL uptake in those cells (Fig. 4.10 A). Levels of cell surface LDLR were also measured 2 h after PCSK9 (wt, L8, L11 and D374Y) addition to the culture mediums. In agreement with LDL uptake determination, neither L8 nor L11 significantly altered extracellular LDLR

expression, compared to wt PCSK9. As expected, recombinant PCSK9-D374Y reduced very significantly LDLR amount at plasma membrane in both HEK293 and HepG2 cells (Fig. 4.10 B).

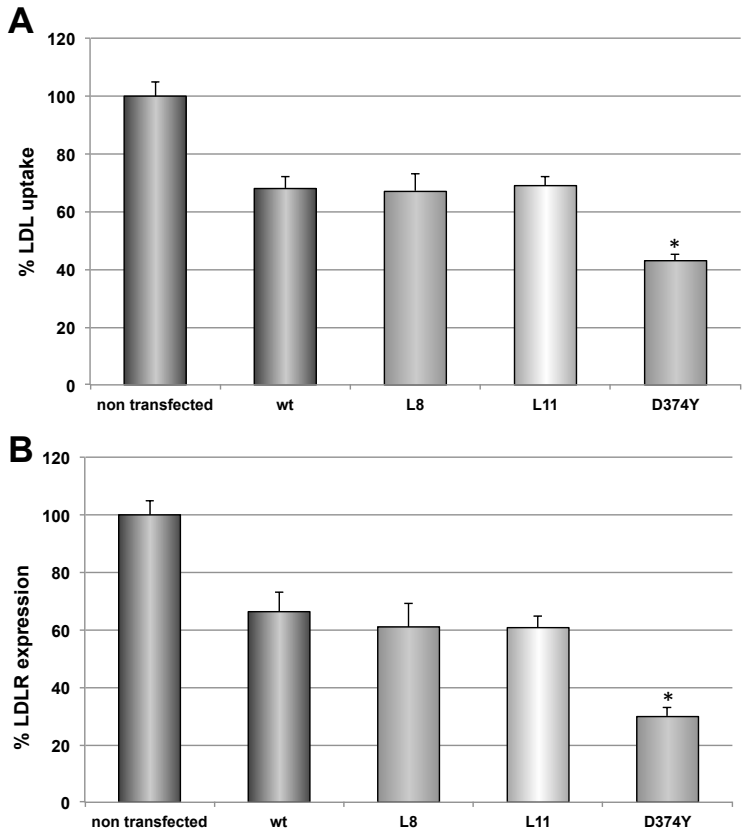

Figure 4.10. LDL uptake and LDLR expression in HepG2 cells incubated with purified PCSK9 variants. A) LDL internalization after 2 h incubation with 5 µM PCSK9 followed by 4 h incubation with labeled LDL at 37 °C. B) Cell membrane LDLR expression after 2 h incubation with 5 µM PCSK9 in HepG2. 10,000 cells were acquired using a Facscalibur. The values represent the mean of triplicate determinations (n = 3); error bars represent ±SD. *P < 0.001 compared to wt using a Student's t-test.

4.4.1.4 LDLR-PCSK9 affinity measurements by solid-phase immunoassay

Next, we tested binding affinities of wt PCSK9 and L8, L11 and D374Y variants for LDLR using a solid phase binding immunoassay. Assuming an interaction model where the ligand has a unique and homogeneous binding site in the receptor (Langmuir isotherm model), the non-linear regression calculation of the binding curves indicates an EC_{50} for wt LDLR of 88.4 nM, in agreement with previously reported values [18]. No affinity differences were found between L8, L11 and wt for the LDLR (Table 1). In contrast, the D374Y GOF variant was used as a positive control, and as expected, its affinity for the LDLR was significantly higher

than that of wt PCSK9 (Table 4.2).

Table 4.2: EC_{50} values for the binding of wt, L8, L11 and D374Y PCSK9 variants to LDLR, as determined by solid-phase immunoassay at pH 7.4.

	pH 7.4	
	EC_{50} (nM)	S.D.
wt	88.4	± 9.5
L8	84.9	± 5.9
L11	94.6	± 10.6
D374Y	16.6	± 4.5

Data are reported as mean ±standard deviation of 3 independent experiments performed by triplicate

4.4.1.5 Bioinformatics analysis predicts physical and structural modifications in the L11 signal peptide

We conducted *in silico* analyses to evaluate the impact of Leu22-Leu23 duplication and Leu23 deletion on the hydrophobicity and secondary structure of the signal peptide. The predicted ΔG_{app} for wt PCSK9 SP was 0.226 kcal/mol and for L8-PCSK9 1.154 kcal/mol, indicating that deletion of Leu23 contributes to a lower hydrophobicity of the SP. In contrast, the insertion of two leucines in L11-PCSK9 variants increases the hydrophobicity of the SP with a predicted ΔG_{app} of -1.005 kcal/mol, indicating that insertion of two additional leucines increases the thermodynamic stability of the SP.

We also modelled the secondary structure of wt, L8 and L11 PCSK9-SP. As shown in Figure 4.11, the predicted secondary structures of wt and L8 PCSK9-SP did not differ substantially. However, the Leu22-Leu23 duplication in the PCSK9-SP appeared to induce a conformational change around the SP cleavage site (Figure 4.11 C).

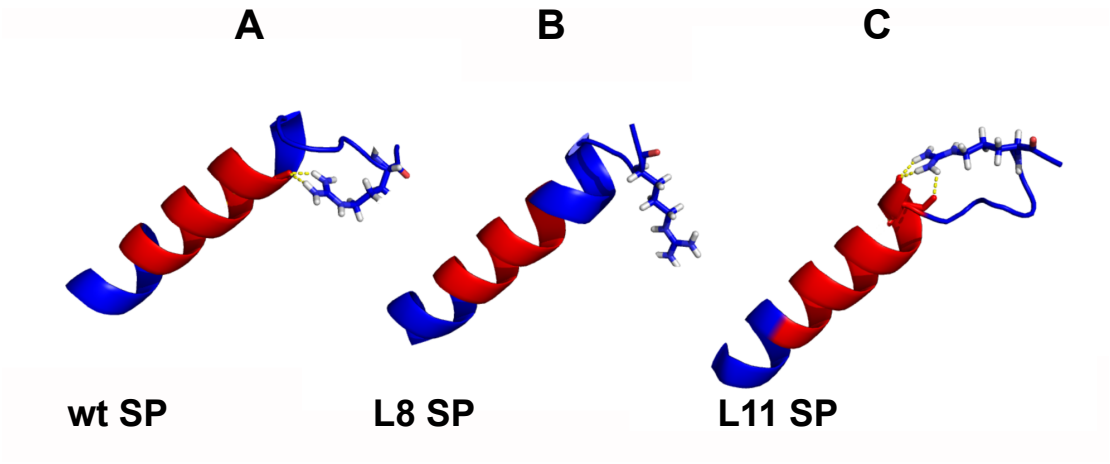

Figure 4.11. Prediction of secondary structure of wt, L8 and L11 signal peptides. Secondary structures of the wt, L8 and L11 signal peptides were modeled using the Iterative Threading Assembly Refinement (I-TASSER) online server [26].

4.4.1.6 The L11 PCSK9 variant is partially retained in the ER

Given the apparent discrepancy observed with the L11 variant on LDLR expression and function when expressed endogenously or added exogenously in cultured cells, together with the information obtained by informatics tools, we next investigated whether Leu22-Leu23 duplication could modulate processing of the SP *in vitro*. Immunoblot analyses of endoplasmic reticulum extracts isolated from HEK293 cells transfected with either wt, L8, or L11 PCSK9 variants were performed. The results shown in Figure 4.12 A indicate that L11 variant displayed a reduced SP cleavage compared to wt PCSK9 as indicated by the higher molecular weight band detected by Western blot. On the other hand, no differences between the SP cleavage were detected with L8 PCSK9 variant when compared to wt (Figure 4.12 A).

To further corroborate retention of L11-PCSK9 in the ER, confocal microscopy was performed to analyse co-localization of PCSK9 with calreticulin, a specific ER marker. As show in Figure 4.12 B, co-localization of L11-PCSK9 with calreticulin was higher than that of wt-PCSK9, indicating accumulation in the ER. Co-localization of L8-PCSK9 in the ER was similar than that of wt-PCSK9 (Figure 4.12 B)

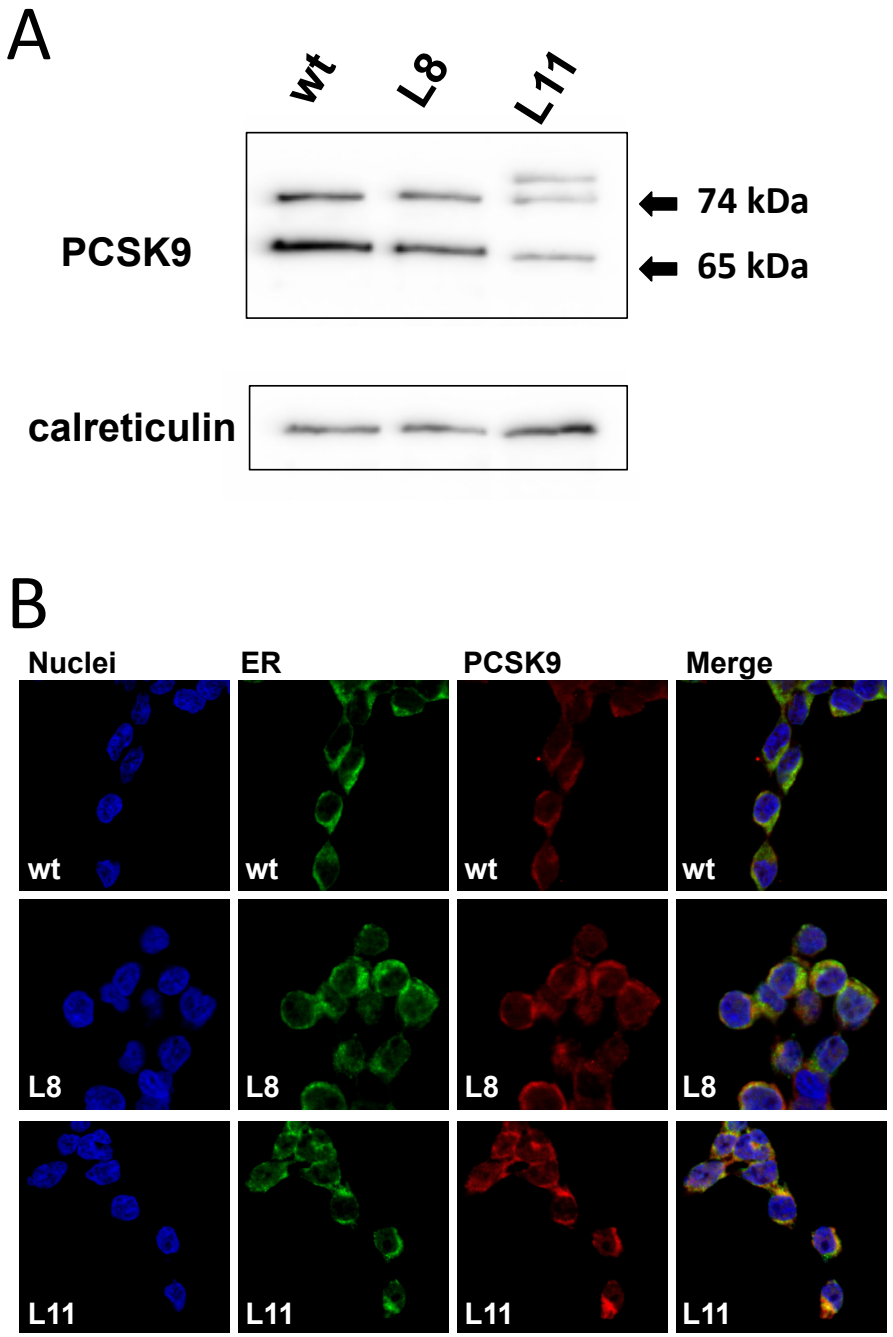

Figure 4.12. PCSK9 cleavage in the ER and colocalization with calreticulin. **A)** PCSK9 stably transfected HEK293 cells lysates were centrifuged to purify the ER. Reticulum fractions were analyzed by Western blot. Processed and not processed PCSK9 were quantified and relativized to calreticulin signal. B) PCSK9 and calreticulin co-localization in cells transfected with wt, L8 and L11 PCSK9 variants. Cells were analyzed by confocal microscopy as described in Materials and Methods.

4.4.2 Discussion

It has been previously reported that the leucine stretch in exon 1 of *PCSK9* is a heterogeneous sequence, and protein activity is differently affected depending on the number of Leu residues in the SP, leading to a GOF protein if two Leu are inserted or to a LOF if only one Leu is inserted[1].

In the sequencing analysis of a large cohort including 6597 unrelated ADH subjects we found that approximately 1% and 0.4% of them carried the L11 and L8 mutation, respectively. This is the largest screening of these mutations published so far. Interestingly, only the L11 mutation was overrepresented among subjects without any other mutation causing ADH. This difference clearly indicates that the L11 mutation is causative of hypercholesterolemia in these subjects. Furthermore, the L11 mutation is not homogeneously present in all ADH groups. L11 is rare among definite phenotypes and more common among those subjects with probable FH. Since the clinical classification is predominantly based on LDL-C concentration[5], this distribution suggests that the L11 mutation contributes more to a milder hypercholesterolemia phenotype than that observed in subjects with *LDLR* or *APOB* mutations. This is in agreement with most other exon 1 GOF PCSK9 mutations in which LDL-C levels and prevalence of cardiovascular disease appear to be lower than those resulting from *LDLR* or *APOB* mutations[6]. Here, we assessed the functionality of the L8 PCSK9 variant by analysing expression and LDL uptake in HEK293 and HepG2 transfected cells as well as by characterizing the activity of purified recombinant PCSK9 in HepG2 cells. The L8 variant has been previously associated with low levels of plasma cholesterol and triglycerides, however, these results remain inconclusive considering the small number of L8 carriers included in that study[7]. The data obtained in the present work indicate that L8 PCSK9 variant is not associated with increased LDLR activity. L8 is indeed expressed and secreted to the extracellular medium similarly to wt PCSK9 and its activity is similar to that of wt PCSK9 both in terms of LDLR expression and LDL uptake. Similar results have been obtained when LDLR expression and LDL uptake were obtained when the L8 variant was added exogenously onto HepG2 cells (Fig. 4.10), demonstrating that p.Leu23del mutation in the signal peptide does not modify the activity of PCSK9.

The L11 allele was first described by Chen et al.[8], and has been associated with ADH by cosegregation studies[1]. L11 variant seems to moderately increase total cholesterol and LDL-C levels and might also be observed in Familial Combined hyperlypidemia (FCHL), where it contributes with other genetic and environmental factors to the onset of the phenotype characterized by elevated levels of plasma cholesterol, triglycerides or both. We show here that when LDLR activity is assayed in cells expressing this variant, L11 behaves as a mild GOF variant with an activity approximately reduced by 20%. However, when purified recombinant

L11 variant is added exogenously to HepG2 cells, this variant shows similar activity than wt PCSK9.

A detailed bioinformatics analysis using *in silico* tools indicates that insertion of 2 leucines occurring in L11 PCSK9 variant significantly contributes to a higher hydrophobicity of the SP that is in the range within the cleavable hydrophobicity predicted from model signal peptides harbouring 8-17 Leu residues stretches[9]. In addition, L11 SP seems to be energetically more favourable for accessing to the ER lipid bilayer compared to wt PCSK9[10] and thermodynamically more stable (wt ΔG_{app}: 0.226 kcal/mol *vs.* L11-PCSK9 ΔG_{app}: -1.005 kcal/mol). It is likely that the longer hydrophobic region resulting from two Leu insertion combined with the negatively charged residues positioned immediately after the cleavage site sequence in PCSK9 (QEDEDGDY) is unfavourable for signal peptide cleavage, which occurs with other proteins[10]. In addition, the insertion of 2 Leu in the L11 variant would induce a local conformational rearrangement just before the cleavage site that may affect peptidase activity. Because signal peptide cleavage is a co-translational event, a slow cleavage rate might also impede correct folding of PCSK9 thus affecting its chaperone function towards LDLR described by Strom et al[11]. According to this model, PCSK9 interacts with the LDLR EGF-A domain in the ER and in post-ER compartments thereby altering the transport of the LDLR to the cell membrane[11]. Although not being critical for LDLR transport, PCSK9 may prevent LDLR proteasomal degradation by assisting LDLR folding in the ER. Furthermore, the hydrophobic interaction at the interface between PCSK9 and the EGF-A repeat supports the notion that PCSK9 prevents the exposure of hydrophobic residues within the EGF-A repeat[12].

The findings, together with our experimental data allow classifying L11 PCSK9 variant as pathogenic. The data presented here indicate that the lower amount of LDLR in L11 PCSK9 expressing cells would be a consequence of a diminished transport rate of LDLR to the cellular membrane rather than different activity of the mature PCSK9. In fact once the SP is cleaved, mature protein resulting from both wt and L11 PCSK9 have identical primary sequences; besides their affinity constants determined by solid-phase immunoassays are similar (Table 4.2), being therefore similar their extracellular activities, as shown in Figure 4.10.

In conclusion, we have determined that L8 is a non-pathogenic variant and that L11 PCSK9 variant reduces LDLR activity by a non-canonical mechanism, in which as a consequence of an impaired cleavage of the signal peptide, LDLR is less efficiently transported to the cell membrane. Therefore, LDL uptake is also reduced and the moderately increment of the LDL-C causes the FH phenotype in patients carrying L11 PCSK9 variant. These findings highlight the importance of a deep *in vitro* characterization of PCSK9 genetic variants in order to assign pathogenicity and to improve clinical diagnosis and therapy of inherited FH disease.

1. Abifadel, M. *et al.* A PCSK9 variant and familial combined hyperlipidaemia. *J. Med. Genet.* **45,** 780–6 (2008).

2. Görlich, D., Hartmann, E., Prehn, S. & Rapoport, T. A. A protein of the endoplasmic reticulum involved early in polypeptide translocation. *Nature* **357,** 47–52 (1992).

3. Gilmore, R. Protein translocation across the endoplasmic reticulum: a tunnel with toll booths at entry and exit. *Cell* **75,** 589–92 (1993).

4. Blobel, G. & Dobberstein, B. Transfer of proteins across membranes. I. Presence of proteolytically processed and unprocessed nascent immunoglobulin light chains on membrane-bound ribosomes of murine myeloma. *J. Cell Biol.* **67,** 835–51 (1975).

5. Nordestgaard, B. G. *et al.* Familial hypercholesterolaemia is underdiagnosed and undertreated in the general population: Guidance for clinicians to prevent coronary heart disease. *Eur. Heart J.* **34,** 3478–3490 (2013).

6. Hopkins, P. N. *et al.* Characterization of Autosomal Dominant Hypercholesterolemia Caused by PCSK9 Gain of Function Mutations and Its Specific Treatment With Alirocumab, a PCSK9 Monoclonal AntibodyCLINICAL PERSPECTIVE. *Circ. Cardiovasc. Genet.* **8,** 823–831 (2015).

7. Slimani, A. *et al.* PCSK9 polymorphism in a Tunisian cohort: Identification of a new allele, L8, and association of allele L10 with reduced coronary heart disease risk. *Mol. Cell. Probes* **29,** 1–6 (2015).

8. Chen, S. N. *et al.* A common PCSK9 haplotype, encompassing the E670G coding single nucleotide polymorphism, is a novel genetic marker for plasma low-density lipoprotein cholesterol levels and severity of coronary atherosclerosis. *J. Am. Coll. Cardiol.* **45,** 1611–9 (2005).

9. Nilsson, I., Whitley, P. & von Heijne, G. The COOH-terminal ends of internal signal and signal-anchor sequences are positioned differently in the ER translocase. *J. Cell Biol.* **126,** 1127–32 (1994).

10. Amaya, Y., Nakai, T. & Miura, S. Evolutionary well-conserved region in the signal peptide of parathyroid hormone-related protein is critical for its dual localization through the regulation of ER translocation. *J. Biochem.* **159,** 393–406 (2016).

11. Strøm, T. B., Tveten, K. & Leren, T. P. PCSK9 acts as a chaperone for the LDL receptor in the endoplasmic reticulum. *Biochem. J.* **457,** 99–105 (2014).

12. Kwon, H. J., Lagace, T. A., McNutt, M. C., Horton, J. D. & Deisenhofer, J. Molecular basis for LDL receptor recognition by PCSK9. *Proc. Natl. Acad. Sci. U. S. A.* **105,** 1820–1825 (2008).

Annex I I

miR-27b modulates insulin resistance in hepatocytes by targeting insulin receptor and repressing insulin signaling pathway

- miR-27b modulates insulin resistance in hepatocytes by targeting insulin receptor and repressing insulin signaling pathway. Benito-Vicente A, Uribe KB, Rotllan N, Jebari S, Canfrán-Duque A, Galicia U, Saenz De Urturi D, Aspichueta P, Ostolaza H, Fernández-Hernando C, Martín C. Manuscript in preparation

6.1 Introduction

Obesity is a global epidemic that has nearly tripled since 1975, with more than 1.9 billion overweight adults and 650 million obese people in 2016[1]. Obesity constitutes the main risk of cardiovascular disease, type 2 diabetes mellitus (T2DM), hypertension and coronary heart disease. Among them, T2DM is the most strongly associated with obesity; prevalence of obesity-related diabetes is expected to double up to 300 million by 2025[2]. Insulin resistance (IR) is one of the key factors in the development of T2DM. Although the molecular mechanism leading to disease is still unclear, common features in obese individuals with T2DM include elevation of TG, reduction in HDL-C, increased concentration of ApoB-100, small dense LDL and HDL. Plasma lipid accumulation promotes an excessive lipid uptake by peripheral tissues such as heart, pancreas or liver[3]. In the particular case of the liver, the unbalance between lipid input and output leads to their accumulation in the liver due to its incapacity for processing the excessive lipid income[4]. As a consequence of liver lipid accumulation, resident macrophages (kupffer cells) and recruited extra-hepatic macrophages change their fate, and increase their proinflamatory molecule production, that along with the already existing lipid accumulation promote liver IR[5,6]. IR is a common feature in metabolic syndrome characterized by impaired insulin signaling in which insulin exerts a lower biological effect than the expected[7]. IR has been described as one of the mayor factors for T2DM development, and is commonly linked with non alcoholic fatty acid disease (NAFLD) or cardiovascular disease (CVD)[7–9]. Indeed, it has been associated with changes in lipid and lipoprotein metabolism that could promote both pathogenic situations[10]. In normal conditions, insulin binds to insulin receptor (INSR) which triggers dimerization and autophosphorylation of the receptor molecules. These events lead to the phosphorylation of INRS substrates (IRS), as well as other proteins that, in turn, can activate multiple intracellular signaling intermediates. In particular, the normal metabolic signaling pathway is activated by IRS1/IRS2 interaction with phosphatidylinositol 3-kinase (PI3K), which subsequently phosphorylates and activates Akt kinase. This event is determinant in the mechanism of insulin action on glucose uptake[11] and glycogen synthesis activation[12] along with gluconeogenesis inhibition[13 14] (Fig. 6.1 A).

Activation of insulin signaling *via* the IRS/PI3- kinase pathway is less efficient in insulin-resistant animals and *in vitro* models[15] and as consequence insulin target tissues show reduced glucose uptake, glycogen synthesis, and enhanced glucose *de novo* synthesis[16] (Figure 6.1 B). Besides, pancreatic β-cells have a decreased glucose transport , which, in turn, increases insulin secretionto compensate the diminished glucose uptake. Under these circumstances, the impossibility to produce enough insulin by pancreatic β-cells leads to hyperglycemia, which is a hallmark of IR to T2DM transition[17]

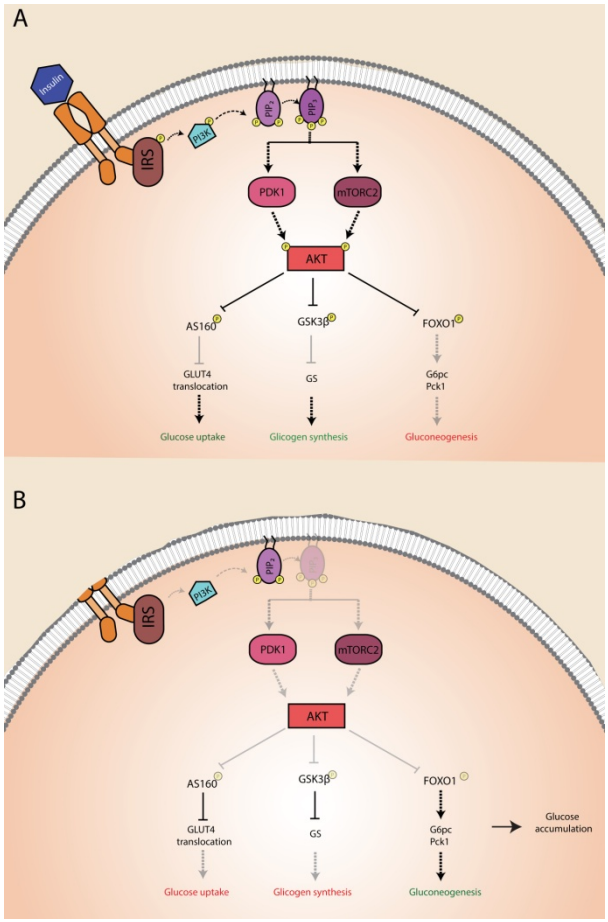

Figure 6.1. Insulin signaling pathway and its alteration in insulin resistance. A) Insulin binding to its receptor activates IRS/PI3-Kinase pathway, which in turn leads to GLUT4 translocation and subsequent glucose uptake upon AS160 inhibition, glycogen synthase (GS) activation by GSK3β inhibition and the inhibition of gluconeogenic enzymes upon FOXO1 phosphorylation. B) Insulin signaling impairment produces an increased hepatic glucose production and impaired glucose uptake and storage.

Although several key processes of the molecular mechanism for IR have been identified[8,18], including polymorphisms in insulin cascade-related genes, post-transcriptional mechanisms remain less characterized. The implication of microRNAs (miRNA; miR) in the pathophysiology of multiple cardiometabolic pathologies, including obesity, IR, atherosclerosis and heart failure, has emerged as a major focus of interest in recent years [19–23]. miRNA are ≈22 nucleotide-long highly conserved non-coding RNAs. These short RNAs are able to regulate many biological functions by interacting primarily with the 3' untranslated region (UTR) of their targeted messenger RNA (mRNA)[24,25]. miRNAs are normally encoded within the introns of protein-coding genes and share common promoters; even in some cases they can have their own promoter[26]. They are transcribed as primary-miRNA (pri-miRNA) consisting on 33-35 bp double stranded RNA with a terminal loop and single stranded RNA at both 3'- and 5'-sides. Once transcribed, the pri-miRNAs are rapidly processed by a protein complex called

microprocessor, which is composed by the nuclear RNAse III Drosha and its cofactor DGCR8. The microprocessor cleaves the pri-miRNA ≈22 bp away from the terminal loop generating the miRNA precursor (pre-miRNA) which can be translocated from the nucleus to the cytosol through exportin 5. In the cytosol, pre-miRNA terminal loop is cleaved by Dicer-TAR RNA-binding protein (TRBP) complex and the resulting double stranded RNA is loaded into AGO protein. Once there, the passenger strand is rapidly degraded while the guide strand forms the RNA-induced silencing complex (RISC)[27] (Figure 6.2).

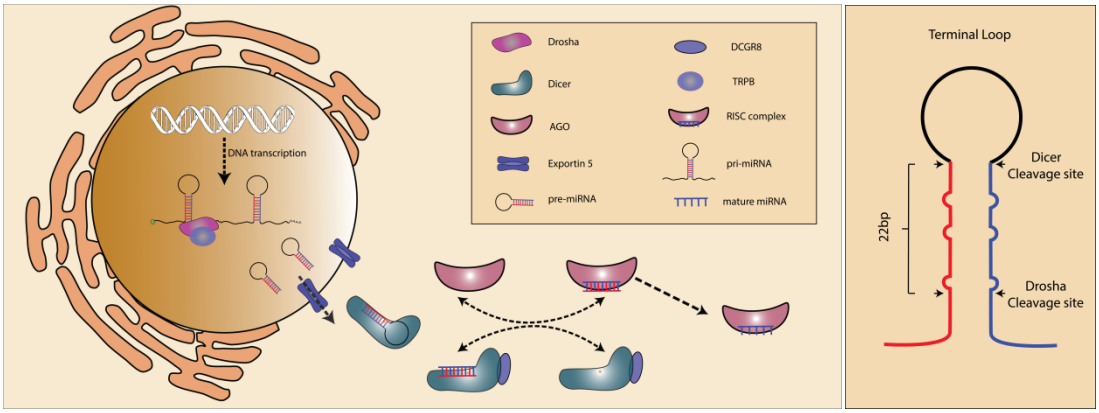

Figure 6.2. miRNA processing. The miRNA are transcribed by RNA polymerase II (RNA Pol II/III). The synthesized pri-miRNA is processed by Drosa/DGCR8 complex generating the pre-miRNA that is transported out from the nucleus by exportin 5. Once in the cytoplasm the terminal loop is cleaved by Dicer/TRPB and the RNA product is loaded into AGO proteins where the guide RNA along with AGO protein forms the RISC complex once passenger strand has been degraded.

There is evidence that a coordinated action of multiple miRNas is in regulation of pathways leading to IR[28–32], T2DM and also in the development of CVD[33–35]. Therefore, to gain insight into miRNAs-regulated IR mechanisms will provide enormous potential in the prevention and early diagnosis of disease. Upregulation of several miRNAs has been associated to obesity and IR, among them, it has been shown that miR-27b is overexpressed in liver of obese people, but its role in IR has not deeply explored. The main objective of the present work has been to investigate the possible role of miR-27b in insulin signaling pathway regulation in hepatocytes, both *in vitro* and *in vivo*, its implications in IR development in the liver, and the expression profile of miR-27b in hepatocytes from obese mice *in vivo*.

6.2 Materials and Methods

6.2.1 Bioinformatics

hsa-miR-27b predicted target genes were indentified using miRWalk database (http://www.umm.uni-heidelberg.de/apps/zmf/mirwalk/) which summarizes target interactions from 12 prediction algorithms. For this work, miRWalk, miRanda, RNA22 and TargetScan were specifically used. Only genes matching for the 4 algorithms were introduced in the next step. PANTHER database (http://www.pantherdb.org) was used to classify those genes into different gene/protein families. The 5 genes with the best score among the insulin pathway genes where introduced in STRING (http://string-db.org) to visualize functional interactions.

6.2.2 Cell culture

Huh7 hepatocarcinoma cell line was kindly given by Dr. Jose Ignacio Ruiz-Sanz (UPV/EHU). The cells were maintained in Dulbecco´s Modified Eagle Medium (DMEM) containing %10 (v/v) fetal bovine serum (FBS) (Lonza, Belgium), 100 U/mL penicillin, 100 µg/mL streptomycin and 4 mM glutamine (Pen Strep Glutamine, Invitrogen) at 37°C and 5 % CO_2. For RNA and protein analysis cells where treated as described below.

6.2.3 *In vitro* miRNA transfections

For miR-27b mimic and miR-27b inhibitor transfection, Huh7 cells were plated in 6 well culture plates (1 x 10^6 cells/well) and transfected using Lipofectamine™ RNAiMAX Transfection Reagent following manufactured instructions. Briefly, 10 minutes before transfection Huh7 cells were washed with PBS and culture medium was replaced with 500 µL serum- and antibiotic free Opti-MEM culture medium. Then, 300 µL transfection mixture was added and plates were incubated during 8 h at 37°C and 5 % CO_2. Finally 800 µL of Opti-MEM containing 10% FBS were added to the culture plates. Cells were maintained in transfection medium for 48 h to achieve maximum effect. Both miR-27b mimic (Dharmacon, C-300589-05) and miR-27b inhibitor (Dharmacon, IH-300589-07) were transfected to achieve 40 nM final concentration. All experimental control samples were transfected either with non-targeting control mimic (Dharmacon, CN 001000-01-20) or non-targeting control inhibitor (Dharmacon, IN-001005-01-05).

6.2.4 RNA isolation and quantitative PCR analysis

For mRNA analysis, total RNA was extracted from miR-27b mimic, inhibitor and the non-targeting controls transfected Huh7 cells using TRIzol reagent (Invitrogen) according to manufacturer´s instructions. 1 µg of extracted RNA was reverse-transcribed using iScript™ Reverse Transcription Supermix (BioRad, 1708841). Quantitative real-time PCR (qRT-PCR)

was performed in triplicate using iQ SYBR green Supermix (Bio-Rad) on a Real-Time Detection System (Bio-Rad). The mRNA level was normalized to ribosomal RNA 18S as a housekeeping gene. Mature miR-27b expression was detected using TaqMan miRNA Assay kit (Life Technologies) according to the manufacturer's instructions. qRT-PCR was performed using TaqMan Universal Master Mix, U6 RNA was used for normalization. Primer information is detailed in table 6.1.

Table 6.1. List of primers used for qRT-PCT analysis in Huh7 cells

Gene	Forward Primer Sequence (5' -> 3')	Reverse Primer Sequence (5' -> 3')
INSR	AGTTTGAGGACATGGAGAATGTG	ATAGGAACGATCTCTGAACTCCAC
IRS1	ACAAACGCTTCTTCGTACTGC	AGTCAGCCCGCTTGTTGATG
GSK3B	GGCAGCATGAAAGTTAGCAGA	GGCGACCAGTTCTCCTGAATC
FOXO1	TCGTCATAATCTGTCCCTACACA	CGGCTTCGGCTCTTAGCAAA
AKT2	ACCACAGTCATCGAGAGGACC	GGAGCCACACTTGTAGTCCA
ABCA1	ACCCACCCTATGAACAACATGA	GAGTCGGGTAACGGAAACAGG
GAPDH	GGAGCGAGATCCCTCCAAAAT	GGCTGTTGTCATACTTCTCATGG

6.2.5 Western blot analysis

For Western blot analysis, Huh7 cells transfected with miR-27b mimic, miR-27b inhibitor and the non-targeting miR-control were lysed using ice-cold buffer containing 50 mM Tris–HCl, 125 mM NaCl, 1% Nonidet P-40, 5.3 mM NaF, 1.5 mM NaP, 1 mM orthovanadate, 1 mg/mL protease inhibitor cocktail (Roche), and 0.25 mg/mL Pefabloc, 4-(2-aminoethyl)-benzenesulfonyl fluoride hydrochloride (AEBSF; Roche), pH 7.5. Cells were rotated for 1 h and centrifuged at 12,000 x g for 10 minutes. Proteins from the supernanants were resolved by 8.5% Tris-Glycine SDS-PAGE. The gels were blotted onto nitrocellulose membranes (Protran BA 83, Whatman™, GE Healthcare, Germany), blocked for 1 h in TBS-T (50 mM Tris-HCl, 150 mM NaCl, pH 7.5, 0.1% Tween 20) containing 5% bovine serum albumine and immunoblotted for 16 h at 4°C with the following antibodies: ABCA1 (1:1000), INSR (1:1000), IRS1 (1:500), AKT2 (1:1000), GSK3β (1:1000), FOXO1 (1:1000) and HSP90 (1:1000) for 16 h at 4°C (Table 6.2). Protein bands were visualized using the Odyssey Infrared Imaging System (LI-COR Biotechnology). Densitometric analysis of the gels was carried out using ImageJ software from the NIH (http://rsbweb.nih.gov/ij/).

Table 6.2. List of antibodies used for Western blot analysis

Gene	Antibody	Product details		Dilution	Host
INSR	INSRβ (C18C4)	Novus	NBP1-19192	1/1000	Mouse
IRS1	IRS1	Novus	NB100-58837	1/1000	Rabbit
GSK3B	GSK-3-β (27C10)	Cell Signaling	9454S	1/1000	Rabbit
FOXO1	FOXO1 (L27)	Cell Signaling	9315S	1/500	Rabbit
AKT2	AKT2 (5B5)	Cell Signaling	2965S	1/1000	Rabbit
ABCA1	ABCA1	Abcam	ab18180	1/1000	Mouse
HSP90	HSP90	Bd Pharmigen	610419	1/1000	Mouse

6.2.6 Mice studies

Eight-week-old male C57BL/6 mice were purchased from Jackson Laboratories (Bar Harbor, ME, USA) and kept under constant temperature and humidity in a 12h controlled dark/light cycle. Mice were fed a high-fat diet (HFD) containing 0.3% cholesterol and 21% (wt/wt) fat (Dyets, Inc) for three weeks in order to upregulate miR-27b expression[36]. Liver samples were collected as previously described[37] and stored at−80°C.

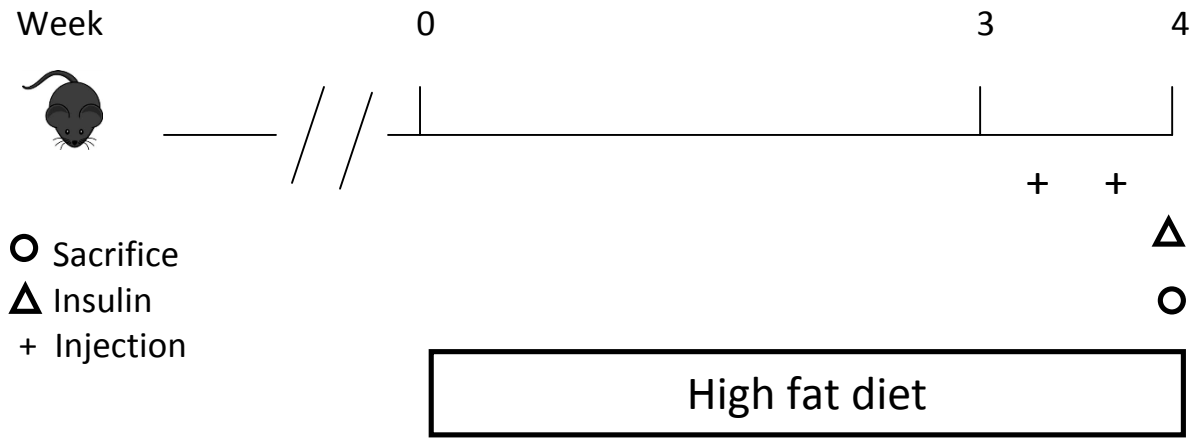

Figure 6.3. Experimental outline followed.

6.2.6.1 miR-27b overexpression studies in mice

mu-pre-miR-27b (accession MI000142) was subcloned into an AAV8 vector and its expression was regulated under the control of a liver-specific thyroxine-binding globulin (TBG) promoter. After 3 weeks at HFD, mice were divided into 2 groups: non-targeting AAV8 (AAV-Null, *n*=5) and pre-miR-27b AAV8 (AAV- 27b, *n*=5 per group). Each group was then treated with 5×10^{12}GC (genome copies) per kg AAV Null or 5×10^{12}GC/kg pre-miR-27b AAV in PBS by retro-orbital injection. Two weeks after treatment, mice were sacrificed and hepatic gene expression was analyzed by Western blot and qRT-PCR using the antibodies and primers described in tables 6.2 and 6.3, respectively.

Table 6.3. List of primers used for QRT-PCT analysis in mice tissue

Gene	Forward Primer Sequence (5' -> 3')	Reverse Primer Sequence (5' -> 3')
INSR	ATGGGCTTCGGGAGAGGAT	CTTCGGGTCTGGTCTTGAACA
IRS1	CGATGGCTTCTCAGACGTG	CAGCCCGCTTGTTGATGTTG
GSK3B	ATGGCAGCAAGGTAACCACAG	TCTCGGTTCTTAAATCGCTTGTC
FOXO1	CCCAGGCCGGAGTTTAACC	GTTGCTCATAAAGTCGGTGCT
AKT2	ACGTGGTGAATACATCAAGACC	GGGCCTCTCCTTATACCCAAT
ABCA1	GGTTTGGAGATGGTTATACAATAGTTGT	CCCGGAAACGCAAGTCC
18S	TTCCGATAACGAACGAGACTCT	TGGCTGAACGCCACTTGTC

6.2.6.2 miR-27b inhibition studies

Eight-week-old male C57BL/6 were fed a HFD for 3 weeks and divided into 2 groups: LNA control and LNA anti-miR-27b. During the fourth week, both groups were injected twice with 2.5 mg/kg of either LNA control (5′-ACGTGCTATACGCCCA-3′) (n=8) or LNA anti-miR-27b (5′-AACTTAGCCACTGTGA-3′) (n=8) by retro-orbital injection. One week after treatment mice were sacrificed and hepatic gene expression was analyzed by Western blot and qRT-PCR using the antibodies and primers described in tables 6.2 and 6.3.

To determine anti-miR-27b treatment effect on insulin signaling, 10 minutes before sacrifice; mice were intraperitoneally injected with 1 U/kg of insulin. Finally, hepatic AKT phosphorylation was analyzed by Western blot and the signal was normalized to total AKT and HSP90. The antibodies used for Western blot analysis are described in table 6.4.

Table 6.4. List of antibodies used for AKT phosphorylation studies.

Gene	Antibody	Product details		Dilution	Host
AKT2	AKT2 (5B5)	Cell Signaling	2965S	1/1000	Rabbit
pAKT	pAKT Ser473	Cell Signaling	9271S	1/1000	Rabbit
HSP90	HSP90	Bd Pharmigen	610419	1/1000	Mouse

6.3 Results

6.3.1 Identification of miR-27b as a potential regulator of the insulin signaling pathway

miR-27b is a conserved miRNA encoded within the 14 intron of *C9orf3* gene (figure 6.4 A). It is known to regulate lipid-related processes and is involved in cancer regulation. However, the role of miR-27b in other type of pathologies is less known. In order to gain insight on processes regulated by hsa-miR-27b, a bioinformatic analysis was carried out and predicted target genes were indentified using miRWalk database. These genes were classified according to the pathways in which they are involved (figure 6.4 B). Interestingly, insulin pathway was one of the pathways overrepresented. It has been described that miR-27b is overexpressed under high lipid environment and insulin resistance is also a common feature at increased lipid levels[16,36]. Accordingly, the five genes participating in insulin pathway showing the highest miR-27b score were selected for a deeper analysis (figure 6.4 C). The predicted miR-27b binding sites are shown in figure 6.4 D.

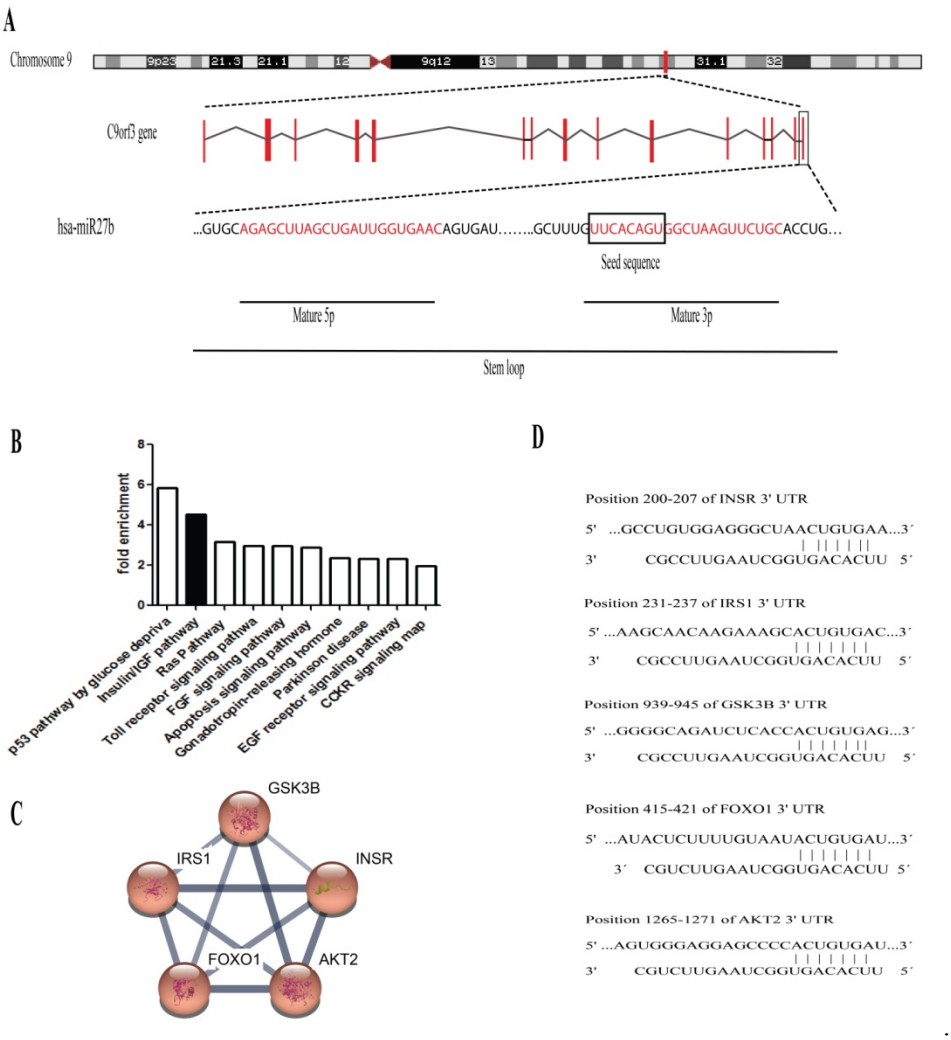

Figure 6.4. miR-27b is predicted to target many genes involved in insulin signaling pathway. (A) Schematic representation of miR-27b genomic location. (B) Pathway enrichment of validated targets of miR-27b. (C) Interaction gene sequences of the five genes selected in this study with miR-27b. (D) Genetic representation of miR-27b interactions with the 3´UTR of the selected genes.

6.3.2 miR-27b regulates hepatic INSR in Huh7 cells

Insulin signaling plays an important role in glucose homeostasis and its malfunctioning leads to glucose metabolism unbalance. To assess the role of miR-27b on hepatic insulin signaling, Huh7 cells were transiently transfected with either miR-27b mimics (Figure 6.5A) or inhibitors (Figure 6.5B). In both cases, miRNA, mRNA and protein expression analysis were conducted for the five selected genes. In both set of experiments a non-targeting miRNA was used as control. As shown in figure 6.5C and 6.5E, overexpression of miR-27b caused a significant decrease of INSR and IRS1 expression, both at mRNA and protein levels. However, mRNA levels and expression of FOXO1, AKT2 or GSK3β proteins were not modified (Figure 6.5C and 6.5E). ABCA1, previously described as a miR-27b target, was used as positive control and as

expected, both mRNA levels determined by qRT-PCR and protein expression determined by Western blot were downregulated (figure 6.5C and 6.5E). On the other hand, inhibition of miR-27b significantly increased INSR and ABCA1 expression. Values of IRS1 expression were also increased, but differences relative to control were not significant. (Figure6.5D and 6.5E). Levels of FOXO1, AKT2 and GSK3β were not modified by the inhibition of the miRNA suggesting that they are not regulated by miR-27b (Figure 6.5D and 6.5E).

To determine the role of miR-27b on insulin pathway regulation in Huh7 cells, insulin-induced signaling was studied. As shown in figure 6.5F, transfection with miR-27b mimic significantly reduced AKT phosphorylation compared to control miRNA. Conversely, inhibition of the endogenous miR-27b significantly increased AKT phosphorylation (Figure 6.5F). These results clearly demonstrate that miR-27b affects negatively insulin signaling when miR-27b is over-expressed and positively upon miR-27b inhibition.

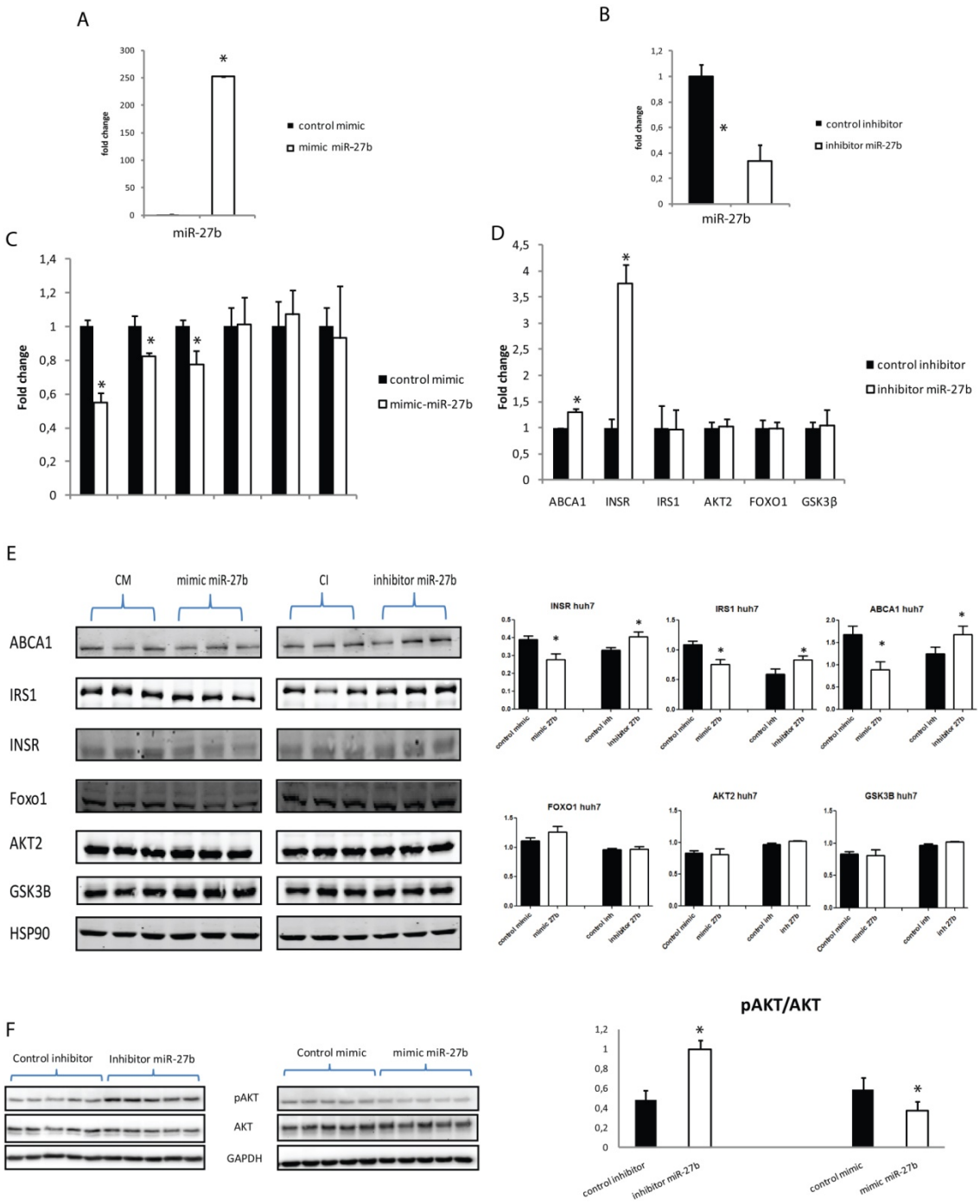

Figure 6.5. miR-27b modulation affects insulin signaling in Huh7 cell line. (A-B) miR-27b qRT-PCR in Huh7 cells transfected with (A) 40 nM control mimic and mimic miR-27b. (B) 40 nM control inhibitor and inhibitor miR-27b. (C-D) mRNA expression of ABCA1, INSR, IRS1, AKT2, FOXO1 and GSK3β in Huh7 cells transfected with 40nM control mimic and mimic miR-27b (C) or 40nM control inhibitor and inhibitor miR-27b (D). (E) Western blot analysis of ABCA1, INSR, IRS1, AKT2, FOXO1 and GSK3β protein expression in Huh7 cell transfected with miR-27b mimic or miR-27b inhibitor and their respective

controls. (F) Western blot analysis of AKT phosphorylation in Huh7 cells treated with miR-27b mimic or miR-27b inhibitor and their respective controls.

6.3.3 miR-27b regulates hepatic INSR *in vivo* in wild type mice

Insulin signaling deregulation together with miR-27b up-regulation, among others, has been described in mice fed with HFD[36]. Our previous results showing INSR targeting by miR-27b followed by inhibition of insulin signaling in Huh7 cells, raise the possibility that miR-27b might be involved in insulin resistance in mice fed a HFD. To address this hypothesis, mice fed HFD were treated with either AAV miR-27b or LNA anti-miR-27b, and then, ABCA1, INSR, INS1, AKT2, FOXO1 and GSK3β mRNA levels and protein expression was determined. In all cases, non-targeting AAV or non-targeting LNA were used as controls. The extent of miR-27b over-expression or inhibition was confirmed by qRT-PCR, being as expected, up- or down-regulated, respectively. In experiments using AAV miR-27b, mature miR-27b resulted enriched two fold compared with non-targeting miRNA, whereas transfection with LNA anti-miR-27b completely abolished miR-27b levels (Figure 6.6 A and B). Surprisingly, down-regulation of miR-27b with LNA anti-miR-27b only caused up-regulation of INSR mRNA (Figure 6.6 3D). mRNA expression of the remaining genes was similar to LNA-control values. On the other hand, overexpression of miR-27b with AAV miR-27b did not modified mRNA level of any of the genes under study compared to AVV control (Figure 6.6 C). Not even ABCA1 mRNA, which was used as internal control of the assay, showed any variation compared to AVV control (Figure 6.6 C). However, when determining protein expression by Western blot, significant differences among protein expression levels were found (Figure 6.6 D and E). So, ABCA1 protein levels resulted significantly diminished in AAV miR-27b- treated mice, according to previously described results[38]. Similarly, INSR protein levels were significantly diminished in AVV miR-27b- treated mice and, as expected, significantly augmented in presence of LNA anti-miR-27b, both compared to their respective controls (Figure 6.6 D and E). It is noteworthy that, in contrast with the results obtained in human Huh7 cells, IRS1 expression was not modified in any of the experimental approaches (mice treated with AAV miR-27b or with LNA anti-miR-27b) (Figure 6.6 D and E). It was previously demonstrated that miR-27b affects INSR expression in wild type mice[39]. In order to confirm the role of miR-27b in insulin resistance, insulin signaling was assessed following the previously described methodology. So, the effect of miR-27b inhibition by LNA anti-miR-27b treatment was determined by analysis of AKT phosphorylation in wild type mice after 1 U/Kg of insulin intraperitoneal administration. Figure 6.6 F shows that phosphorylated AKT levels are significantly higher in mice treated with LNA anti-miR-27b comparing with control mice.

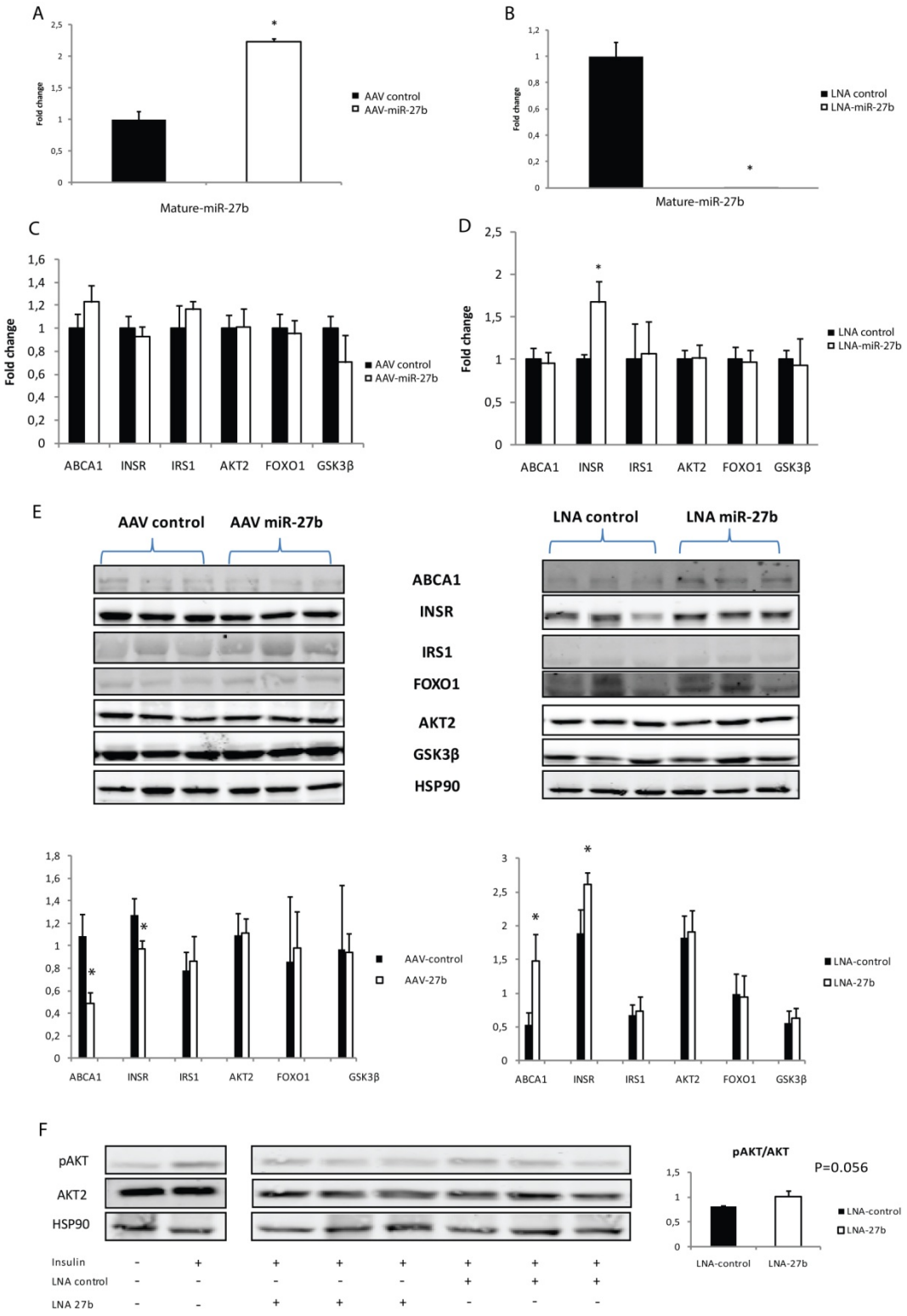

Figure 6.6. miR-27b modulation affects insulin signaling in wild type mice. (A-B) miR-27b qRT-PCR in wild type mice treated with null AAV or AAV miR-27b (A) or LNA control or LNA miR-27b inhibitor (B). (C-D) mRNA expression of ABCA1, INSR, IRS1, AKT2, FOXO1 and GSK3β in wild type mice treated with null AAV or AAV miR-27b (C) or LNA control or LNA miR-27b inhibitor (D). (E) Western blot analysis of ABCA1, INSR, IRS1, AKT2, FOXO1 and GSK3β protein expression in wild type mice treated either with AAV miR-27b or LNA miR-27b inhibitor and their respective controls. (F)

Western blot analysis of AKT phosporylation in wild type mice treated with LNA miR-27b inhibitor and its respective control.

6.4 Discussion

Overweight and obesity are the main driving forces of T2DM progression[40], which has been continuously rising in developed countries, and therefore, predicted to reach epidemic dimensions in the next decades[41]. Obesity is linked to the development of T2DM and cardiovascular diseases possibly through detrimental effects on insulin and glucose metabolism[42]. Indeed, sustained high FFA plasma concentration coming from excessive accumulation in adipose tissue in obese people[43] leads to lipid accumulation within hepatocytes, an event that is causally related to deregulation of insulin sensitivity in liver[44] .

One of the most relevant pathological characteristics of T2DM is an impaired response to insulin due to disruption of insulin signaling pathway, in which, among other mechanisms, involvement of several miRNAs has been described[29,45,46]. Epigenetic studies have emerged as promising candidates to understand the link between obesity and diabetes. Multiple miRNAs acting in concert have been associated with IR in skeletal muscle[47]. However, the role of miRNAs regulating liver insulin signaling is less known. It has been described that in liver, high plasma lipid levels or high fat diet induces a 3 fold upregulation of miR-27b[36], a well known regulator of lipid energy homeostasis[38,48,49]. However, there is a gap of information regarding miR-27b implication in liver insulin signaling, even though it has been demonstrated to be upregulated in the liver of obese people[50].

The main focus of interest of the present study has been to elucidate the implication of miR-27b in insulin-dependent liver signaling. miR-27b is encoded in human chromosome 19, specifically in the intron 14 of the *C9orf3* gene as part of the miR-23b-27b-24-1 cluster [36]. The bioinformatics analysis performed in this work points out insulin pathway as an enriched target for miR-27b with many proteins potentially regulated by this miRNA. The high interaction score showed by miR-27b for INSR, IRS1, AKT2, FOXO1 and GSK3β led us next to deeply assess both *in vitro* and *in vivo* the interaction between miR-27b and its *in silico* predicted targets. Hence, Our analysis of insulin signaling reveals an inverse correlation between miR-27b expression and both INSR mRNA and protein levels, thus indicating that miR-27b regulates directly INSR in Huh7 cells (Figure 6.5). Our finding is fully consistent with a recent report showing the targeting of miR-27b to the 3' UTR of INSR[39] Similarly to our findings in Huh7 cells, they observed a direct downregulation of INSR in chronic hyperinsulinemia-induced IR adipocytes[39].

In addition, we show as well that miR-27b regulates IRS1 mRNA and protein expression *in vitro*, while AKT2, FOXO1 and GSK3β were not modified when miR-27b was either up- or downregulated (Figure 6.5). IRS1 downregulation is normally associated with a mild insulin resistance due to independent IRS2 compensatory signaling[51]. However, we find here that the combination of IRS1 and INSR inhibitions in Huh7 cells generates a strong insulin signaling impairment, as it is shown in Figure 6.5 where AKT phosporylation is significantly impaired[52].

Direct regulation of INSR by miR-27b was also confirmed *in vivo* in hepatocytes from mice fed HFD treated with either AAV miR-27b or LNA anti-miR-27b. Corroborating the results obtained in Huh7 cells, miR-27b overexpression showed a reduced INSR protein expression in mice liver, while downregulation of miR-27b caused an increase of INSR expression at protein level. In contrast, expression of IRS1 was not modified in mice, neither by miR-27b overexpression nor by its downregulation. The differences observed between the *in vitro* and *in vivo* models could be explained by sequence conservation among IRS1 3' UTR, while in mice there is only one predicted miR-27b binding site, human IRS1 3' UTR has two additional predicted miRNA binding sites that could be responsible of a more efficient interaction with miR-27b. Nonetheless, we show that INSR downregulation is enough to reduce insulin signaling *in vivo* as demonstrated by results shown in figure xxx.

Hepatic IR is a common feature in obese patients, in which lipid accumulation and chronic inflammation favours its development[5,44]. It is also well established that miRNAs can modulate insulin signaling in the body, although the interplay of different miRNAs leading to IR remains to be elucidated. *In vitro* and *in vivo* model systems are the basis for the understanding and control of off-target effects of miRNA and, modulating the miRNA activities may provide exciting opportunities for obesity and T2DM therapy. To date, several miRNAs have been demonstrated to be involved in the development of IR through interfering with insulin signaling pathway. For instance, obesity-induced miR-15b and miR-195 overexpression is linked to the pathogenesis of IR in liver by INSR targeting[45,46]. Similarly to the miR-27b effects described in this work, miR-15b and miR-195 target INSR 3'UTR directly, and downregulate INSR expression at the translational level. This direct targeting of INSR 3'UTR by different miRNAs that are upregulated in a HFD, suggests that a synergistic effect may potentiate the development of hepatic IR, which may in turn lead to T2DM. As occurring in our mice model in which miR-27b does not target IRS1, saturated fatty acid diet-induced [45]overexpression of miR-15b does not supress IRS1[45]. In the case of miR-15b, its targeting to INSR results in a drastic repression of protein expression, and eventually causes impaired insulin signaling and insulin-stimulated synthesis of glycogen in hepatocytes[45].

There is evidence that certain diabetes-related miRNA may also play a role in the development of cardiovascular disease and other diabetic complications[53,54] . This suggests that miRNAs may

be involved in the interaction between IR and development of additional characteristic cardiometabolic disease traits[55]. miR-128-1, another miRNAs affecting insulin pathway, also targets directly the 3' UTR of the *LDLR* and *ABCA1*, and its inhibition in mice caused a significant drop in circulating cholesterol and TAG levels, improved homeostasis and insulin sensitivity by enhancing the expression of INSR and IRS[56]. In other tissues, additional miRNAs are involved in IR development, for example, miR-375 regulates β-cell function and pancreatic insulin secretion[57], miR-135 promotes IR in muscle cells[29] and miR-146a impairs insulin signaling downregulating IRS2 *in vitro*[28].

The complexity of the miRNA network that links obesity with T2DM progression led us to focus this study on the effect caused by miR-27b modulation into hepatic insulin signaling. Therefore, INSR was confirmed as metabolic target of miR-27b both in human hepatocarcinome cell line and in mice thus showing its capacity of leading to IR generation at an early stage by modulating INSR expression. Moreover, we found that IRS1 is targeted by miR-27b in human cell line but not in mice probably due to a lack of conservation in several of the predicted miR-27b binding sites in mice, this indicates that in humans miR-27b affects also modulating IR downstream insulin signaling. This work emphasizes the importance of miRNA modulation studies to determine their functional effects. In fact, our study demonstrates the direct effect of miR-27b on INSR and IRS1 expression and its potential role as insulin signaling regulator.

References

1. World Health Organization. Obesity and Overweight. Available online: http://www.who.int/mediacentre/factsheets/fs311/en/ (accesed on 21october 2018).

2. Dyson, P. A. The therapeutics of lifestyle management on obesity. *Diabetes. Obes. Metab.* **12,** 941–6 (2010).

3. Dirkx, E., Schwenk, R. W., Glatz, J. F. C., Luiken, J. J. F. P. & van Eys, G. J. J. M. High fat diet induced diabetic cardiomyopathy. *Prostaglandins, Leukot. Essent. Fat. Acids* **85,** 219–225 (2011).

4. Tarantino, G., Savastano, S. & Colao, A. Hepatic steatosis, low-grade chronic inflammation and hormone/growth factor/adipokine imbalance. *World J. Gastroenterol.* **16,** 4773–83 (2010).

5. Prieur, X., Roszer, T. & Ricote, M. Lipotoxicity in macrophages: evidence from diseases associated with the metabolic syndrome. *Biochim. Biophys. Acta - Mol. Cell Biol. Lipids*

1801, 327–337 (2010).

6. Koyama, Y., Brenner, D. A., Koyama, Y. & Brenner, D. A. Liver inflammation and fibrosis Find the latest version : Liver inflammation and fibrosis. **127,** 55–64 (2017).

7. Ormazabal, V. *et al.* Association between insulin resistance and the development of cardiovascular disease. *Cardiovasc. Diabetol.* 1–14 (2018). doi:10.1186/s12933-018-0762-4

8. Perry, R. J., Samuel, V. T., Petersen, K. F. & Shulman, G. I. The role of hepatic lipids in hepatic insulin resistance and type 2 diabetes. *Nature* **510,** 84–91 (2014).

9. Qi, Y. *et al.* Myocardial loss of IRS1 and IRS2 causes heart failure and is controlled by p38α MAPK during insulin resistance. *Diabetes* **62,** 3887–900 (2013).

10. Grundy, S. M. Small LDL, atherogenic dyslipidemia, and the metabolic syndrome. *Circulation* **95,** 1–4 (1997).

11. Leto, D. & Saltiel, A. R. Regulation of glucose transport by insulin: Traffic control of GLUT4. *Nat. Rev. Mol. Cell Biol.* **13,** 383–396 (2012).

12. Kaidanovich, O. & Eldar-Finkelman, H. The role of glycogen synthase kinase-3 in insulin resistance and type 2 diabetes. *Expert Opin. Ther. Targets* **6,** 555–61 (2002).

13. Oh, K.-J., Han, H.-S., Kim, M.-J. & Koo, S.-H. CREB and FoxO1: two transcription factors for the regulation of hepatic gluconeogenesis. *BMB Rep.* **46,** 567–74 (2013).

14. Guo, S. Insulin signaling, resistance, and metabolic syndrome: Insights from mouse models into disease mechanisms. *J. Endocrinol.* **220,** (2014).

15. Zhang, D. *et al.* Resistance to High-Fat Diet-Induced Obesity and Insulin Resistance in Mice with Very Long-Chain Acyl-CoA Dehydrogenase Deficiency. *Cell Metab.* **11,** 402–411 (2010).

16. Jung, U. & Choi, M.-S. Obesity and Its Metabolic Complications: The Role of Adipokines and the Relationship between Obesity, Inflammation, Insulin Resistance, Dyslipidemia and Nonalcoholic Fatty Liver Disease. *Int. J. Mol. Sci.* **15,** 6184–6223 (2014).

17. Paternostro, G. *et al.* Cardiac and skeletal muscle insulin resistance in patients with coronary heart disease. A study with positron emission tomography. *J. Clin. Invest.* **98,** 2094–9 (1996).

18. Petersen, M. C. *et al.* Insulin receptor Thr1160 phosphorylation mediates lipid-induced hepatic insulin resistance. *J. Clin. Invest.* **126,** 4361–4371 (2016).

19. Vegter, E. L., van der Meer, P., de Windt, L. J., Pinto, Y. M. & Voors, A. A. MicroRNAs in heart failure: from biomarker to target for therapy. *Eur. J. Heart Fail.* **18,** 457–68 (2016).

20. Fernández-Hernando, C. & Moore, K. J. MicroRNA modulation of cholesterol homeostasis. *Arterioscler. Thromb. Vasc. Biol.* **31,** 2378–82 (2011).

21. Fernández-Hernando, C., Suárez, Y., Rayner, K. J. & Moore, K. J. MicroRNAs in lipid metabolism. *Curr. Opin. Lipidol.* **22,** 86–92 (2011).

22. Singh, A. K. *et al.* Posttranscriptional regulation of lipid metabolism by non-coding RNAs and RNA binding proteins. *Semin. Cell Dev. Biol.* **81,** 129–140 (2018).

23. Price, N. L. & Fernández-Hernando, C. miRNA regulation of white and brown adipose tissue differentiation and function. *Biochim. Biophys. Acta* **1861,** 2104–2110 (2016).

24. Huntzinger, E. & Izaurralde, E. Gene silencing by microRNAs: contributions of translational repression and mRNA decay. *Nat. Rev. Genet.* **12,** 99–110 (2011).

25. Ghildiyal, M. & Zamore, P. D. Small silencing RNAs: an expanding universe. *Nat. Rev. Genet.* **10,** 94–108 (2009).

26. Monteys, A. M. *et al.* Structure and activity of putative intronic miRNA promoters. *RNA* **16,** 495–505 (2010).

27. Ha, M. & Kim, V. N. Regulation of microRNA biogenesis. *Nat. Rev. Mol. Cell Biol.* **15,** 509–524 (2014).

28. Liu, H., Ren, G., Zhu, L., Liu, X. & He, X. The upregulation of miRNA-146a inhibited biological behaviors of ESCC through inhibition of IRS2. *Tumor Biol.* **37,** 4641–4647 (2016).

29. Honardoost, M., Arefian, E., Soleimani, M., Soudi, S. & Sarookhani, M. R. Development of Insulin Resistance through Induction of miRNA-135 in C2C12 Cells. *Cell J.* **18,** 353–61 (2016).

30. Landgraf, P. *et al.* A mammalian microRNA expression atlas based on small RNA library sequencing. *Cell* **129,** 1401–14 (2007).

31. Jeong, H.-J., Park, S.-Y., Yang, W.-M. & Lee, W. The induction of miR-96 by

mitochondrial dysfunction causes impaired glycogen synthesis through translational repression of IRS-1 in SK-Hep1 cells. *Biochem. Biophys. Res. Commun.* **434,** 503–508 (2013).

32. Chen, T., Ding, G., Jin, Z., Wagner, M. B. & Yuan, Z. Insulin ameliorates miR-1-induced injury in H9c2 cells under oxidative stress via Akt activation. *Mol. Cell. Biochem.* **369,** 167–74 (2012).

33. Melkman-Zehavi, T. *et al.* miRNAs control insulin content in pancreatic β-cells via downregulation of transcriptional repressors. *EMBO J.* **30,** 835–845 (2011).

34. Zhou, K. *et al.* Interpreting the various associations of MiRNA polymorphisms with susceptibilities of cardiovascular diseases. *Medicine (Baltimore).* **97,** e10712 (2018).

35. Kong, L. *et al.* Significance of serum microRNAs in pre-diabetes and newly diagnosed type 2 diabetes: a clinical study. *Acta Diabetol.* **48,** 61–69 (2011).

36. Vickers, K. C. *et al.* MicroRNA-27b is a regulatory hub in lipid metabolism and is altered in dyslipidemia. *Hepatology* **57,** 533–542 (2013).

37. Rayner, K. J. *et al.* MiR-33 Contributes to the Regulation of Cholesterol Homeostasis. *Science (80-.).* **328,** 1570–1573 (2010).

38. Goedeke, L. *et al.* miR-27b inhibits LDLR and ABCA1 expression but does not influence plasma and hepatic lipid levels in mice. *Atherosclerosis* **243,** 499–509 (2015).

39. Srivastava, A. *et al.* Chronic hyperinsulinemia induced miR-27b is linked to adipocyte insulin resistance by targeting insulin receptor. *J. Mol. Med.* **96,** 315–331 (2018).

40. Chen, L., Magliano, D. J. & Zimmet, P. Z. The worldwide epidemiology of type 2 diabetes mellitus--present and future perspectives. *Nat. Rev. Endocrinol.* **8,** 228–36 (2011).

41. Shaw, J. E., Sicree, R. A. & Zimmet, P. Z. Global estimates of the prevalence of diabetes for 2010 and 2030. *Diabetes Res. Clin. Pract.* **87,** 4–14 (2010).

42. Bergman, R. N. & Ader, M. Free fatty acids and pathogenesis of type 2 diabetes mellitus. *Trends Endocrinol. Metab.* **11,** 351–6 (2000).

43. Oh, Y. S., Bae, G. D., Baek, D. J., Park, E.-Y. & Jun, H.-S. Fatty Acid-Induced Lipotoxicity in Pancreatic Beta-Cells During Development of Type 2 Diabetes. *Front. Endocrinol. (Lausanne).* **9,** (2018).

44. Birkenfeld, A. L. & Shulman, G. I. Nonalcoholic fatty liver disease, hepatic insulin resistance, and type 2 diabetes. *Hepatology* **59,** 713–23 (2014).

45. Yang, W.-M., Jeong, H.-J., Park, S.-W. & Lee, W. Obesity-induced miR-15b is linked causally to the development of insulin resistance through the repression of the insulin receptor in hepatocytes. *Mol. Nutr. Food Res.* **59,** 2303–2314 (2015).

46. Yang, W.-M., Jeong, H.-J., Park, S.-Y. & Lee, W. Saturated fatty acid-induced miR-195 impairs insulin signaling and glycogen metabolism in HepG2 cells. *FEBS Lett.* **588,** 3939–46 (2014).

47. Zhou, T. *et al.* Regulation of Insulin Resistance by Multiple MiRNAs via Targeting the GLUT4 Signaling Pathway. *Cell. Physiol. Biochem.* **38,** 2063–2078 (2016).

48. Hu, X. *et al.* MiR-27b Impairs Adipocyte Differentiation of Human Adipose Tissue-Derived Mesenchymal Stem Cells by Targeting LPL. *Cell. Physiol. Biochem.* **47,** 545–555 (2018).

49. Shirasaki, T. *et al.* MicroRNA-27a Regulates Lipid Metabolism and Inhibits Hepatitis C Virus Replication in Human Hepatoma Cells. *J. Virol.* **87,** 5270–5286 (2013).

50. Collares, R. V. A., Salgado, W., Da Cunha Tirapelli, D. P. & Dos Santos, J. S. The expression of LEP, LEPR, IGF1 and IL10 in obesity and the relationship with microRNAs. *PLoS One* **9,** 1–6 (2014).

51. Kubota, T., Kubota, N. & Kadowaki, T. Imbalanced Insulin Actions in Obesity and Type 2 Diabetes: Key Mouse Models of Insulin Signaling Pathway. *Cell Metab.* **25,** 797–810 (2017).

52. Cho, H. Insulin Resistance and a Diabetes Mellitus-Like Syndrome in Mice Lacking the Protein Kinase Akt2 (PKBbeta). *Science (80-.).* **292,** 1728–1731 (2001).

53. Ślusarz, A. & Pulakat, L. The two faces of miR-29. *J. Cardiovasc. Med.* **16,** 480–490 (2015).

54. Kato, M., Castro, N. E. & Natarajan, R. MicroRNAs: potential mediators and biomarkers of diabetic complications. *Free Radic. Biol. Med.* **64,** 85–94 (2013).

55. Wang, R. *et al.* Elevated circulating microRNA-122 is associated with obesity and insulin resistance in young adults. *Eur. J. Endocrinol.* **172,** 291–300 (2015).

56. Wagschal, A. *et al.* Genome-wide identification of microRNAs regulating cholesterol

and triglyceride homeostasis. *Nat. Med.* **21,** 1290–1297 (2015).

57. Eliasson, L. The small RNA miR-375 - a pancreatic islet abundant miRNA with multiple roles in endocrine beta cell function. *Mol. Cell. Endocrinol.* **456,** 95–101 (2017).

Conclusions

According to the obtained results we propose the following conclusions:

- **Functional characterization of LDLR variants studies:**

1. Flow cytometry using FITC-labelled LDL is a reliable and accurate methodology to determine LDLR activity. This method combined with the use of confocal microscopy offers the possibility of class type assignment for LDLR mutants, thus contributing to improve the diagnosis of FH.
2. Solid-phase immunoassays to determine LDLR-ApoB100 binding affinity allows an accurate classification of *LDLR* variants and contributes significantly to the understanding of the phenotype of patients carrying Class 3 LDLR variants. In addition, this technique allows the characterization of *APOB* and *APOE* pathogenic variants, as well as *PCSK9* gain and loss of function variants.
3. Integrated analysis of clinical, molecular, and functional data is important for the correct assessment of patients with FH who might otherwise be misdiagnosed. A detailed analysis of the protein at molecular level, together with clinical and molecular data already obtained routinely, provides relevant information to understand the phenotype observed in these patients that can be translated into clinical management improvements.
4. The methodology used in this work has allowed us to characterize 30 LDLR variants.

- **Functional characterization of *PCSK9* variants studies:**

1. We characterize the first case of a double heterozygous FH patient by *in vitro* demonstration that p.(Asp62Ala) and p.(Pro467Ala) PCSK9 variants are pathogenic.
2. The increased affinity of p.(Arg357Cys) and p.(Ser636Arg) PCSK9 variants for LDLR is the cause of GOF activity that promotes LDLR extracellular degradation. In contrast, p.(Arg499His) GOF PCSK9 activity is mediated by an intracellular effect which promotes LDLR degradation.
3. p.(Leu22_Leu23dup) PCSK9 variant reduces LDLR activity by a non-canonical mechanism, in which as a consequence of an impaired cleavage of the signal peptide, LDLR is less efficiently transported to the cell membrane. Therefore, LDL uptake is also

reduced and the moderately increment of the LDL-C causes the FH phenotype. In contrast, p.(Leu23del) is a non-pathogenic variant.

4. The methodology used in this work has allowed us to characterize 10 PCSK9 variants

- ***APOB* studies:**

1. pH acidification promotes changes in the secondary structure of ApoB100 suggesting a more active role of apolipoprotein in the LDLR/LDL releasing process in endosomes than previously anticipated, providing new clues for therapeutic intervention in the future.
2. Changes in particle size and/or secondary structure composition of ApoB100 may explain the defective binding and uptake of p.(Arg3527Gln), p.(Arg1164Thr) and p.(Gln4494del) variants to LDLR, highlighting the relevance of residues outside the postulated LDLR binding domain for ApoB100.
3. p.(Thr3826Met) ApoB100 is a pathogenic variant that causes reduced LDL binding to LDLR despite the mutation is located outside of the consensus LDLR binding site. p.(Pro994Leu) is instead a benign ApoB100 variant.

- **miR-27b study:**

1. The direct effect of miR-27b on INSR and IRS1 expression highlights its potential role as insulin signalling regulator. The upregulation of miR-27b in HFD mice could underlie T2DM progression.

Publications

1. Etxebarria A, **Benito-Vicente A**, Alves AC, Ostolaza H, Bourbon M, Martin C. Advantages and versatility of fluorescence-based methodology to characterize the functionality of LDLR and class mutation assignment. PLoS One. 2014;9. doi:10.1371/journal.pone.0112677

2. Etxebarria A, **Benito-Vicente A,** Palacios L, Stef M, Cenarro A, Civeira F, et al. Functional characterization and classification of frequent low-density lipoprotein receptor variants. Hum Mutat. 2015;36: 129–141. doi:10.1002/humu.22721

3. **Benito-Vicente A**, Alves AC, Etxebarria A, Medeiros AM, Martin C, Bourbon M. The importance of an integrated analysis of clinical, molecular, and functional data for the genetic diagnosis of familial hypercholesterolemia. Genet Med. IOP Publishing; 2015;17: 980–988. doi:10.1038/gim.2015.14

4. Alves AC, Etxebarria A, Medeiros AM, **Benito-Vicente A**, Thedrez A, Passard M, et al. Characterization of the First PCSK9 Gain of Function Homozygote. J Am Coll Cardiol. American College of Cardiology Foundation; 2015;66: 2152–2154. doi:10.1016/j.jacc.2015.08.871

5. Fernández-Higuero JA, Etxebarria A, **Benito-Vicente A**, Alves AC, Arrondo JLR, Ostolaza H, et al. Structural analysis of APOB variants, p.(Arg3527Gln), p.(Arg1164Thr) and p.(Gln4494del), causing Familial Hypercholesterolaemia provides novel insights into variant pathogenicity. Sci Rep. Nature Publishing Group; 2015;5: 1–8. doi:10.1038/srep18184

6. Etxebarria A, **Benito-Vicente A**, Stef M, Ostolaza H, Palacios L, Martin C. Activity-associated effect of LDL receptor missense variants located in the cysteine-rich repeats. Atherosclerosis. Elsevier Ltd; 2015;238: 304–312. doi:10.1016/j.atherosclerosis.2014.12.026

7. Fernández-Higuero JA, **Benito-Vicente A**, Etxebarria A, Milicua JCG, Ostolaza H, Arrondo JLR, et al. Structural changes induced by acidic pH in human apolipoprotein B-100. Sci Rep. Nature Publishing Group; 2016;6: 1–10. doi:10.1038/srep36324

8. Cenarro A, Etxebarria A, De Castro-Orós I, Stef M, Bea AM, Palacios L, Mateo-Gallego R, **Benito-Vicente A** et al. The p.Leu167del mutation in APOE gene causes autosomal

dominant hypercholesterolemia by down-regulation of LDL receptor expression in hepatocytes. J Clin Endocrinol Metab. 2016;101: 2113–2121. doi:10.1210/jc.2015-3874

9. Jiang L, Wu W-F, Sun L-Y, Chen P-P, Wang W, **Benito-Vicente A**, et al. The use of targeted exome sequencing in genetic diagnosis of young patients with severe hypercholesterolemia. Sci Rep. Nature Publishing Group; 2016;6: 36823. doi:10.1038/srep36823

10. Jiang L, **Benito-Vicente A**, Tang L, Etxebarria A, Cui W, Uribe KB, et al. Analysis of LDLR variants from homozygous FH patients carrying multiple mutations in the LDLR gene. Atherosclerosis. Elsevier Ltd; 2017;263: 163–170. doi:10.1016/j.atherosclerosis.2017.06.014

11. Di Taranto MD, **Benito-Vicente A**, Giacobbe C, Uribe KB, Rubba P, Etxebarria A, et al. Identification and in vitro characterization of two new PCSK9 Gain of Function variants found in patients with Familial Hypercholesterolemia. Sci Rep. 2017;7: 1–9. doi:10.1038/s41598-017-15543-x

12. Wang S, Mao Y, Narimatsu Y, Ye Z, Tian W, Goth CK, Lira-Navarrete E, Pedersen NB, **Benito-Vicente A,** et al. Site-specific O-glycosylation of members of the low-density lipoprotein receptor superfamily enhances ligand interactions. J Biol Chem. 2018;293: 7408–7422. doi:10.1074/jbc.M117.817981

13. Alves AC, **Benito-Vicente A**, Medeiros AM, Kaajal R, Martin C, Bourbon M. Further evidence of novel APOB mutations as a cause of Familial Hypercholesterolaemia. Atherosclerosis. 2018; doi:10.1016/j.atherosclerosis.2018.06.819

14. **Benito-Vicente A**, Uribe K, Jebari S, Galicia-Garcia U, Ostolaza H, Martin C. Validation of LDLr Activity as a Tool to Improve Genetic Diagnosis of Familial Hypercholesterolemia: A Retrospective on Functional Characterization of LDLr Variants. Int J Mol Sci. 2018;19: 1676. doi:10.3390/ijms19061676

15. **Benito-Vicente A**, Uribe KB, Siddiqi H, Jebari S, Galicia-Garcia U, Larrea-Sebal A, et al. Replacement of cysteine at position 46 in the first cysteine-rich repeat of the LDL receptor impairs apolipoprotein recognition. Aspichueta P, editor. PLoS One. 2018;13: e0204771. doi:10.1371/journal.pone.0204771

16. **Benito-Vicente A**, Siddiqi H , Uribe KB, Jebari S, Galicia-Garcia U, Larrea-Sebal A, Stef M, Ostolaza H , Palacios L, Martín C. p.(Asp47Asn) and p.(Thr62Met): non deleterious LDL receptor missense variants functionally characterized in vitro. Scientific Reports. 2018;8. Doi: 10.1038/s41598-018-34715-x

17. **Benito-Vicente A**, Uribe KB, Jebari S, Galicia-Garcia U, Ostolaza H, Martin M.Familial Hypercholesterolemia: The Most Frequent Cholesterol Metabolism Disorder Caused Disease. Int J Mol Sci. 2018 Nov 1;19(11). pii: E3426. doi: 10.3390/ijms19113426.

Benito-Vicente A, Uribe KB, Palacios L', Cenarro A, Calle X, et al. Increasing the leucine stretch length of the PCSK9 signal peptide promotes autosomal dominant hypercholesterolaemia. ATVB. Under Revision.

First author of the paper

CSIC

Instituto
Biofisika
Institutua